NBS

Technical Note No. 101

TRANSMISSION LOSS PREDICTIONS FOR TROPOSPHERIC COMMUNICATION CIRCUITS

VOLUME 2

P. L. RICE, A. G. LONGLEY, K. A. NORTON, AND A. P. BARSIS

U. S. DEPARTMENT OF COMMERCE
NATIONAL BUREAU OF STANDARDS

THE NATIONAL BUREAU OF STANDARDS

The National Bureau of Standards is a principal focal point in the Federal Government for assuring maximum application of the physical and engineering sciences to the advancement of technology in industry and commerce. Its responsibilities include development and maintenance of the national standards of measurement, and the provisions of means for making measurements consistent with those standards; determination of physical constants and properties of materials; development of methods for testing materials, mechanisms, and structures, and making such tests as may be necessary, particularly for government agencies; cooperation in the establishment of standard practices for incorporation in codes and specifications; advisory service to government agencies on scientific and technical problems; invention and development of devices to serve special needs of the Government; assistance to industry, business, and consumers in the development and acceptance of commercial standards and simplified trade practice recommendations; administration of programs in cooperation with United States business groups and standards organizations for the development of international standards of practice; and maintenance of a clearinghouse for the collection and dissemination of scientific, technical, and engineering information. The scope of the Bureau's activities is suggested in the following listing of its four Institutes and their organizational units.

Institute for Basic Standards. Electricity. Metrology. Heat. Radiation Physics. Mechanics. Applied Mathematics. Atomic Physics. Physical Chemistry. Laboratory Astrophysics.* Radio Standards Laboratory: Radio Standards Physics; Radio Standards Engineering.** Office of Standard Reference Data.

Institute for Materials Research. Analytical Chemistry. Polymers. Metallurgy. Inorganic Materials. Reactor Radiations. Cryogenics.** Office of Standard Reference Materials.

Central Radio Propagation Laboratory.** Ionosphere Research and Propagation. Troposphere and Space Telecommunications. Radio Systems. Upper Atmosphere and Space Physics.

Institute for Applied Technology. Textiles and Apparel Technology Center. Building Research. Industrial Equipment. Information Technology. Performance Test Development. Instrumentation. Transport Systems. Office of Technical Services. Office of Weights and Measures. Office of Engineering Standards. Office of Industrial Services.

---

* NBS Group, Joint Institute for Laboratory Astrophysics at the University of Colorado.
** Located at Boulder, Colorado.

NATIONAL BUREAU OF STANDARDS

Technical Note 101

Issued May 7, 1965

TRANSMISSION LOSS PREDICTIONS FOR TROPOSPHERIC COMMUNICATION CIRCUITS

VOLUME 2

P. L. Rice, A. G. Longley, K. A. Norton, and A. P. Barsis
Central Radio Propagation Laboratory
National Bureau of Standards
Boulder, Colorado

For sale by the Superintendent of Documents, U. S. Government Printing Office
Washington, D.C. 20402
Price: $1.00

FOREWORD

A short history of the development of the prediction methods in this Technical Note will permit the reader to compare them with earlier procedures. Some of these methods were first reported by Norton, Rice and Vogler [1955]. Further development of forward scatter predictions and a better understanding of the refractive index structure of the atmosphere led to changes reported in an early unpublished NBS report and in NBS Technical Note 15 [Rice, Longley and Norton, 1959]. The methods of Technical Note 15 served as a basis for part of another unpublished NBS report which was incorporated in Air Force Technical Order T.O. 31Z-10-1 in 1961. A preliminary draft of the current technical note was submitted as a U.S. Study Group V contribution to the CCIR in 1962.

Technical Note 101 uses the metric system throughout. For most computations both a graphical method and formulas suitable for a digital computer are presented. These include simple and comprehensive formulas for computing diffraction over smooth earth and over irregular terrain, as well as methods for estimating diffraction over an isolated rounded obstacle. New empirical graphs are included for estimating long-term variability for several climatic regions, based on data that have been made available to NBS.

For paths in a continental temperate climate, these predictions are practically the same as those published in 1961. The reader will find that a number of graphs have been simplified and that many of the calculations are more readily adaptable to computer programming. The new material on time availability and service probability in several climatic regions should prove valuable for areas other than the U.S.A.

Note: This Technical Note consists of two volumes as indicated in the Table of Contents.

TABLE OF CONTENTS

Volume 1

		PAGE NO.
1.	INTRODUCTION	1-1
2.	THE CONCEPTS OF SYSTEM LOSS, TRANSMISSION LOSS, PATH ANTENNA GAIN, AND PATH ANTENNA POWER GAIN	2-1
	2.1 System Loss and Transmission Loss	2-1
	2.2 Available Power from the Receiving Antenna	2-3
	2.3 Antenna Directive Gain and Power Gain	2-6
	2.4 Polarization Coupling Loss and Multipath Coupling Loss	2-8
	2.5 Path Loss, Basic Transmission Loss, Path Antenna Gain, and Attenuation Relative to Free Space	2-10
	2.6 Propagation Loss and Field Strength	2-13
3.	ATMOSPHERIC ABSORPTION	3-1
	3.1 Absorption by Water Vapor and Oxygen	3-1
	3.2 Sky-Noise Temperature	3-3
	3.3 Attenuation by Rain	3-4
	3.4 Attenuation in Clouds	3-6
4.	DETERMINATION OF AN EFFECTIVE EARTH'S RADIUS	4-1
5.	TRANSMISSION LOSS PREDICTION METHODS FOR WITHIN-THE-HORIZON PATHS	5-1
	5.1 Line-of-Sight Propagation Over a Smooth or Uniformly Rough Spherical Earth	5-1
	5 1.1 A curve-fit to terrain	5-5
	5.1.2 The terrain roughness factor, σ_h	5-6
	5.2 Line-of-Sight Propagation Over Irregular and Cluttered Terrain	5-7
6.	DETERMINATION OF ANGULAR DISTANCE FOR TRANSHORIZON PATHS	6-1
	6.1 Plotting a Great Circle Path	6-1
	6.2 Plotting a Terrain Profile and Determining the Location of Radio Horizon Obstacles	6-3
	6.3 Calculation of Effective Antenna Heights for Transhorizon Paths	6-4
	6.4 Calculation of the Angular Distance, θ	6-5
7.	DIFFRACTION OVER A SINGLE ISOLATED OBSTACLE	7-1
	7.1 Single Knife Edge, No Ground Reflections	7-1
	7.2 Single Knife Edge with Ground Reflections	7-3

PAGE NO.

7.3 Isolated Rounded Obstacle, No Ground Reflections 7-4

7.4 Isolated Rounded Obstacle with Ground Reflections 7-6

8. DIFFRACTION OVER SMOOTH EARTH AND OVER IRREGULAR TERRAIN 8-1

8.1 Diffraction Attenuation Over a Smooth Earth 8-1

8.2 Diffraction Over Irregular Terrain 8-3

8.2.1 Diffraction over paths where $d_{st} \cong d_{sr}$ 8-4

8.2.2 For horizontal polarization 8-4

8.3 Single-Horizon Paths, Obstacle not Isolated. 8-5

9. FORWARD SCATTER 9-1

9.1 The Attenuation Function, $F(\theta d)$. 9-2

9.2 The Frequency Gain Function, H_o. 9-3

9.3 The Scattering Efficiency Correction, F_o. 9-5

9.4 Expected Values of Forward Scatter Multipath Coupling Loss . . . 9-6

9.5 Combination of Diffraction and Scatter Transmission Loss 9-7

10. LONG-TERM POWER FADING 10-1

10.1 The Effective Distance, d_e 10-7

10.2 The Functions $V(50, d_e)$ and $Y(p, d_e)$ 10-8

10.3 Continental Temperate Climate 10-9

10.4 Maritime Temperate Climate 10-12

10.5 Other Climates 10-13

10.6 Variability for Knife-Edge Diffraction Paths 10-13

11. REFERENCES 11-1

12. LIST OF SYMBOLS AND ABBREVIATIONS. 12-1

TABLE OF CONTENTS

Volume 2

PAGE NO.

ANNEX I: AVAILABLE DATA AND STANDARD CURVES I-1

I.1 Available Data as a Function of Path Length I-1

I.2 Standard Point-to-Point Transmission Curves I-3

ANNEX II: BEAM ORIENTATION, POLARIZATION, AND MULTIPATH COUPLING LOSS II-1

II.1 Representation of Complex Vector Fields II-1

II.2 Principal and Cross-Polarization Components II-4

II.3 Unit Complex Polarization Vectors II-6

II.4 Power Flux Densities II-8

II.5 Polarization Efficiency II-10

II.6 Multipath Coupling Loss. II-12

II.7 Idealized Theoretical Antenna Patterns. II-15

II.8 Conclusions II-23

ANNEX III: FORMULAS, COMPUTER METHODS, AND SAMPLE CALCULATIONS III-1

III.1 Line-of-Sight III-2

III.2 Diffraction Over a Single Isolated Obstacle III-15

III.3 Diffraction Over a Single Isolated Obstacle with Ground Reflections III-17

III.4 Parameters K and b° for Smooth Earth Diffraction III-23

III.5 Forward Scatter III-24

III.6 Transmission Loss with Antenna Beams Elevated or Directed Out of the Great Circle Plane III-37

III.7 Long-Term Power Fading III-44

III.7.1 Diurnal and seasonal variability in a continental temperate climate III-45

III.7.2 To mix distributions III-50

III.8 Examples III-69

III.8.1 Line of sight predictions III-69

III.8.2 Transmission loss prediction for a rounded isolated obstacle III-73

III.8.3 Predicted transmission loss for a transhorizon path . . . III-77

PAGE NO.

ANNEX IV: FORWARD SCATTER IV-1

ANNEX V: PHASE INTERFERENCE FADING AND SERVICE PROBABILITY . . . V-1

V.1 The Two Components of Fading V-3

V.2 The Nakagami-Rice Distribution V-5

V.3 Noise-Limited Service V-11

V.4 Interference-Limited Service V-13

V.5 The Joint Effect of Several Sources of Interference Present Simultaneously V-17

V.6 The System Equation for Noise-Limited Service V-18

V.7 The Time Availability of Interference-Limited Service V-20

V.8 The Estimation of Prediction Error V-21

V.9 The Calculation of Service Probability Q for a Given Time Availability p V-23

V.10 Optimum Use of the Radio Frequency Spectrum V-29

AVAILABLE DATA AND STANDARD CURVES

The simplest way to predict long-term median transmission loss values would be to use a best-fit curve drawn through measured data (represented by their overall median values), plotted as a function of path length. Such a method ignores essentially all of our understanding of the physics of tropospheric propagation, is subject to especially large errors over rough terrain, and such empirical curves represent only the conditions for which data are available.

Curves that may be useful for establishing preliminary allocation plans are presented in section I.2 of this annex. These "standard" curves were prepared for a fixed combination of antenna heights and assume propagation over a smooth earth. The curves are not suitable for use on particular point-to-point paths, since they make no allowance for the wide range of propagation path profiles or atmospheric conditions that may be encountered over particular paths.

I.1 Available Data as a Function of Path Length

Period-of-record median values of attenuation relative to free space are plotted vs. distance in figures I.1 to I.4 for a total of 750 radio paths, separating the frequency ranges 40-150 MHz, 150-600 MHz, 600-1000 MHz, and 1-10 GHz. Major sources of data other than those referenced by Herbstreit and Rice [1959] are either unpublished or are given by Bray, Hopkins, Kitchen, and Saxton [1955], Bullington [1955], duCastel [1957b], Crysdale [1958], Crysdale, Day, Cook, Psutka, and Robillard [1957], Dolukhanov [1957], Grosskopf [1956], Hirai [1961a, b], Josephson and Carlson [1958], Jowett [1958], Joy [1958a, b], Kitchen and Richmond [1957], Kitchen, Richards, and Richmond [1958], Millington and Isted [1950], Newton and Rogers [1953], Onoe, Hirai, and Niwa [1958], Rowden, Tagholm, and Stark [1958], Saxton [1951], Ugai [1961], and Vvedenskii and Sokolov [1957].

Three straight lines were determined for each of the data plots shown in figures I.1 to I.4. Near the transmitting antenna, $A = 0$ on the average. Data for intermediate distances, where the average rate of diffraction attenuation is approximately $0.09\, f^{\frac{1}{3}}$ db per kilometer, determine a second straight line. Data for the greater distances, where the level of forward scatter fields is reached, determine the level of a straight line with a slope varying from 1/18 to 1/14 db per kilometer, depending on the frequency.

The dashed curves of figures I.1-I.3 show averages of broadcast signals recorded at 2500 random locations in six different areas of the United States. The data were normalized to 10-meter and 300-meter antenna heights, and to frequencies of 90, 230, and 750 MHz. For this data sample [TASO 1959], average fields are low mainly because the receiver locations were not carefully selected, as they were for most other paths for which data are shown.

The extremely large variance of long-term median transmission loss values recorded over irregular terrain is due mainly to differences in terrain profiles and effective antenna

heights. For a given distance and given antenna heights a wide range of angular distances is possible, particularly over short diffraction and extra-diffraction paths. Angular distance, the angle between radio horizon rays from each antenna in the great circle plane containing the antennas, is a very important parameter for transmission loss calculations, (see section 6). Figure I. 5 shows for a number of paths the variability of angular distance relative to its value over a smooth spherical earth as a function of path distance and antenna heights.

Most of the "scatter" of the experimental long-term medians shown in figures I. 1 - I. 4 is due to path-to-path differences. A small part of this variation is due to the lengths of the recording periods. For all data plotted in the figures the recording period exceeded two weeks, for 630 paths it exceeded one month, and for 90 paths recordings were made for more than a year.

An evaluation of the differences between predicted and measured transmission loss values is discussed briefly in annex V. In evaluating a prediction method by its variance from observed data, it is important to remember that this variance is strongly influenced by the particular data sample available for comparison. Thus it is most important that these data samples be as representative as possible of the wide range of propagation path conditions likely to be encountered in the various types of service and in various parts of the world.

To aid in deciding whether it is worthwhile to use the point-to-point prediction method outlined in sections 4 - 10, instead of simpler methods, figure I. 6 shows the cumulative distribution of deviations of predicted from observed long-term median values. The dash-dotted curve shows the cumulative distribution of deviations from the lines drawn in figures I. 1 - I. 4 for all available data. The solid and dashed curves compare predictions based on these figures with ones using the point-to-point method for the same paths. Note that the detailed point-to-point method could not be used in many cases because of the lack of terrain profiles.

Figure I. 6 shows a much greater variance of data from the "empirical" curves of figures I. 1 - I. 4 for the sample of 750 paths than for the smaller sample of 217 paths for which terrain profiles are available. The wide scatter of data illsutrated in figure I. 4 for the frequency range 1 - 10 GHz appears to be mainly responsible for this. Figure I. 4 appears to show that propagation is much more sensitive to differences in terrain profiles at these higher frequencies, as might be expected. The point-to-point prediction methods, depending on a number of parameters besides distance and frequency, are also empirical, since they are made to agree with available data, but estimates of their reliability over a period of years have not varied a great deal with the size of the sample of data made available for comparison with them.

I.2 Standard Point-to-point Transmission Loss Curves

A set of standard curves of basic transmission loss versus distance is presented here. Such curves may be useful for establishing preliminary allocation plans but they are clearly not suitable for use on particular point-to-point paths, since they make no allowance for the wide range of propagation path terrain profiles or atmospheric conditions which may be encountered. Similar curves developed by the CCIR [1963g; 1963h] are subject to the same limitations.

The standard curves show basic transmission loss versus path distance for $p = 0.01$ to 99.99 percent of the time. These curves were obtained using the point-to-point predictions for a smooth earth, $N_s = 301$, antenna heights of 30 meters, and estimates of oxygen, water vapor, and rain absorption explained in section 3. Cumulative distributions of hourly median transmission loss for terrestrial links may be read from figures I.7 to I.17 for distances from 0 to 1000 kilometers and for 0.1, 0.2, 0.5, 1, 2, 5, 10, 22, 32.5, 60 and 100 GHz. The same information may be obtained from figures I.18 to I.20.

For earth-space links, it is important to know the attenuation relative to free space, A, between the earth station and space station as a function of distance, frequency, and the angle of elevation, θ_h, of the space station relative to the horizontal at the earth station [CCIR 1963i; 1963j]. Using the CCIR basic reference atmosphere*, [CCIR Report 231, 1963e] standard propagation curves providing this information for 2, 5, 10, 22, 32.5, 60 and 100 GHz, for values of p ranging from 0.01 to 99.99 percent, and for $\theta_h = 0$, 0.03, 0.1, 0.3, 1.0, and $\pi/2$ radians are shown in figures I.21 - I.26, where $A_m(p)$ is plotted against the straight-line distance, r, between antennas. The relationship between A_m and L_b is given by

$$L_{bm}(p) + A_m(p) + L_{bf} = A_m(p) + 32.446 + 20 \log f + 20 \log r \quad \text{db} \qquad \text{(I.1)}$$

where f is the radio frequency in megahertz and r is the straight-line distance between antennas, expressed in kilometers.

The curves in figures I.7 - I.26 provide long-term cumulative distributions of hourly median values. Such standard propagation curves are primarily useful only for general qualitative analyses and clearly do not take account of particular terrain profiles or particular climatic effects. For example, the transmission loss at the 0.1% and 0.01% levels will be substantially smaller in maritime climates where ducting conditions are more common.

---

*The transmission loss predictions for this atmosphere are essentially the same as predictions for $N_s = 301$.

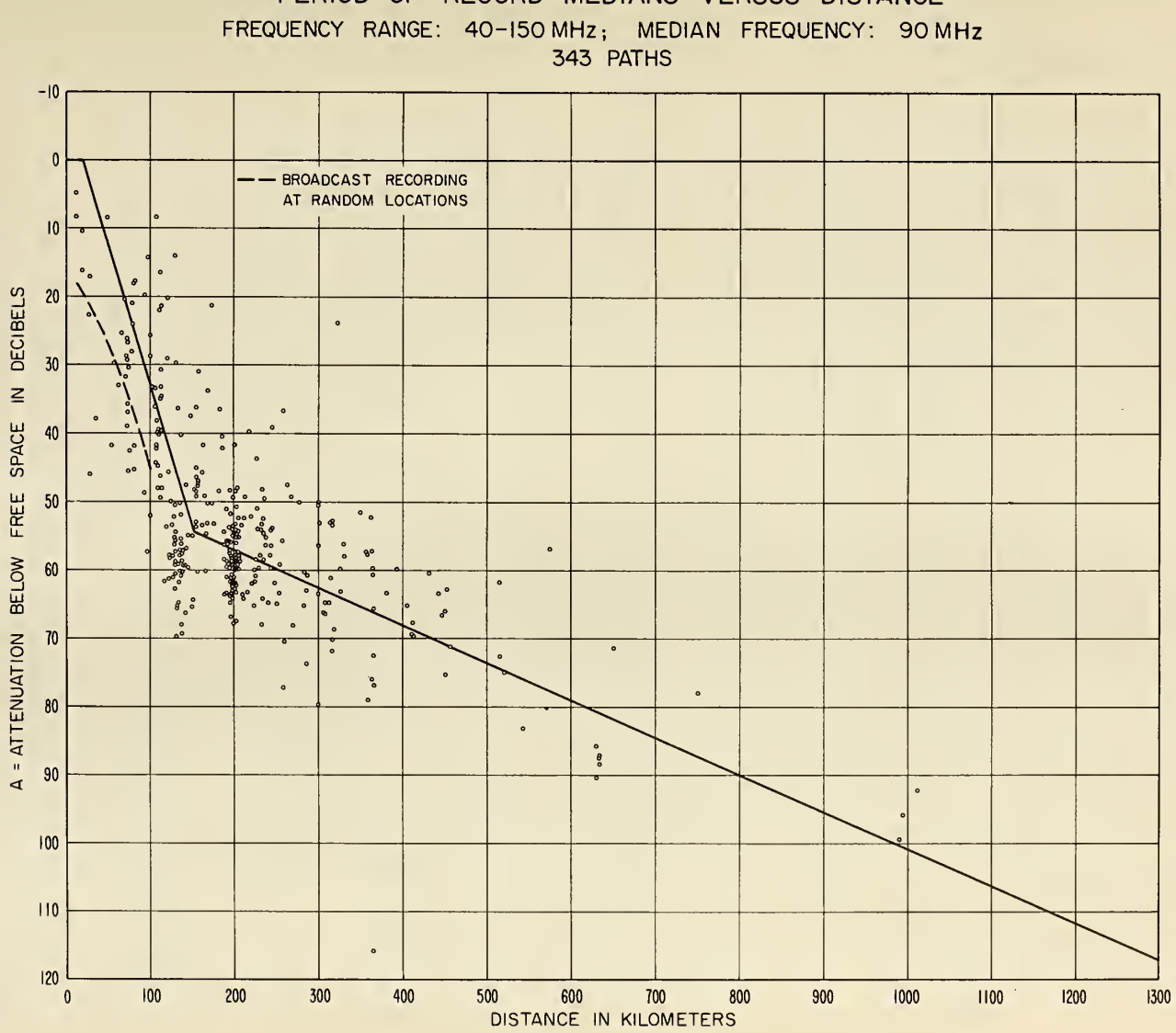
PERIOD OF RECORD MEDIANS VERSUS DISTANCE
FREQUENCY RANGE: 40-150 MHz; MEDIAN FREQUENCY: 90 MHz
343 PATHS
BROADCAST RECORDING
AT RANDOM LOCATIONS
A = ATTENUATION BELOW FREE SPACE IN DECIBELS
DISTANCE IN KILOMETERS
-10
0
10
20
30
40
50
60
70
80
90
100
110
120
0
100
200
300
400
500
600
700
800
900
1000
1100
1200
1300

Figure I.1

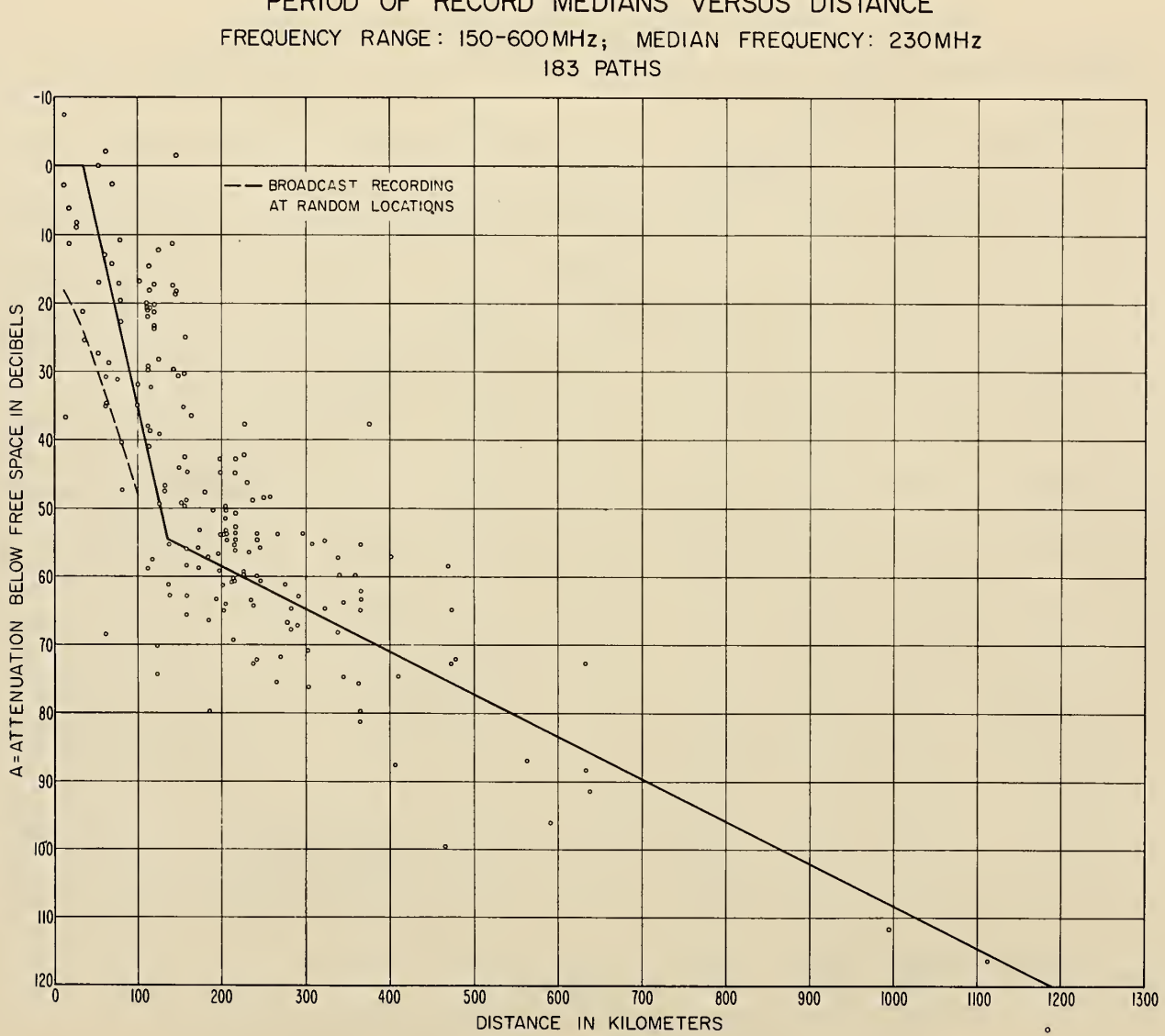
PERIOD OF RECORD MEDIANS VERSUS DISTANCE
FREQUENCY RANGE: 150-600 MHz; MEDIAN FREQUENCY: 230 MHz
183 PATHS
BROADCAST RECORDING
AT RANDOM LOCATIONS
A=ATTENUATION BELOW FREE SPACE IN DECIBELS
-10
0
10
20
30
40
50
60
70
80
90
100
110
120
0
100
200
300
400
500
600
700
800
900
1000
1100
1200
1300
DISTANCE IN KILOMETERS

Figure I.2

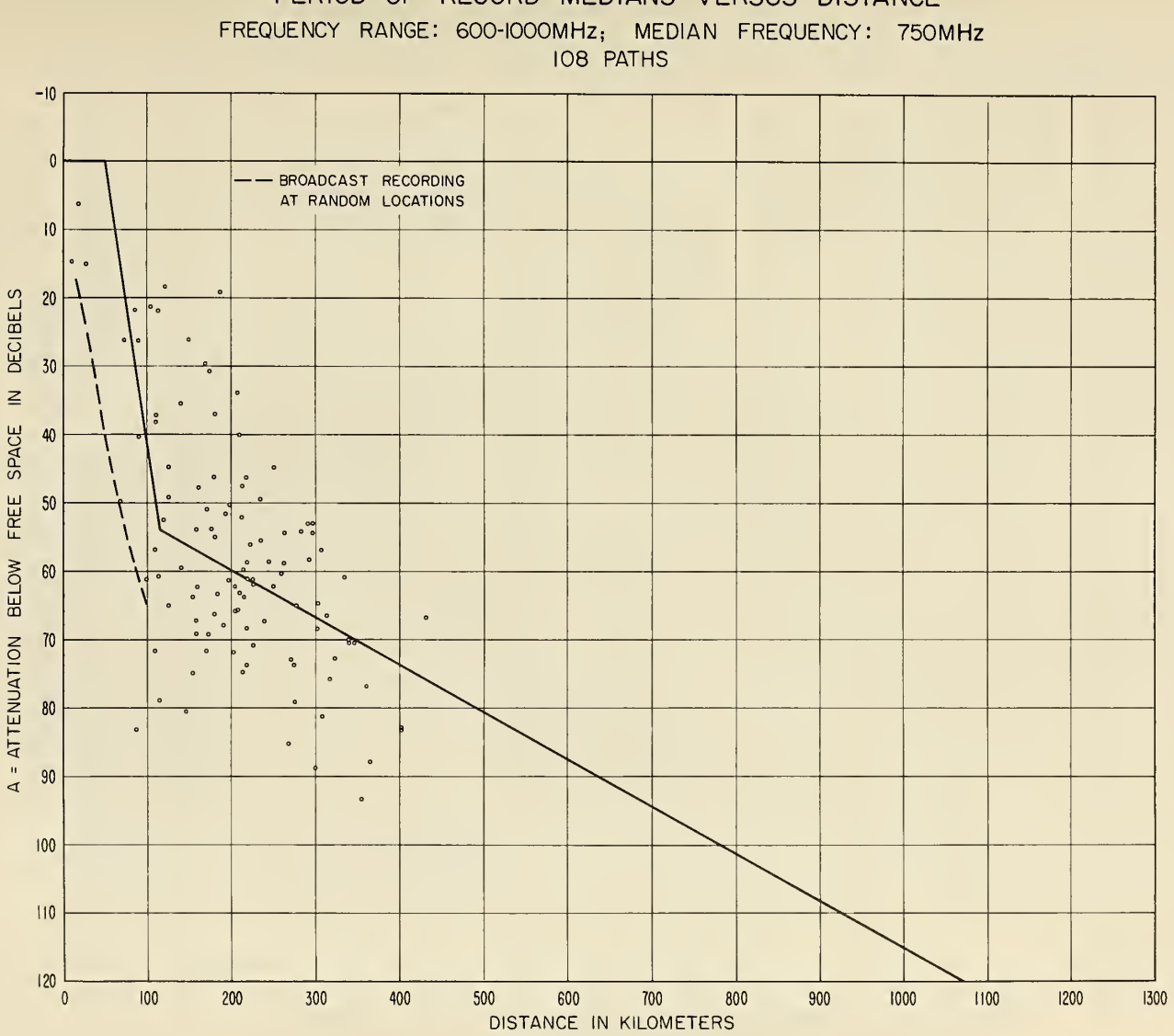
PERIOD OF RECORD MEDIANS VERSUS DISTANCE
FREQUENCY RANGE: 600-1000MHz; MEDIAN FREQUENCY: 750MHz
108 PATHS
BROADCAST RECORDING
AT RANDOM LOCATIONS
A = ATTENUATION BELOW FREE SPACE IN DECIBELS
DISTANCE IN KILOMETERS
-10
0
10
20
30
40
50
60
70
80
90
100
110
120
0
100
200
300
400
500
600
700
800
900
1000
1100
1200
1300

Figure I.3

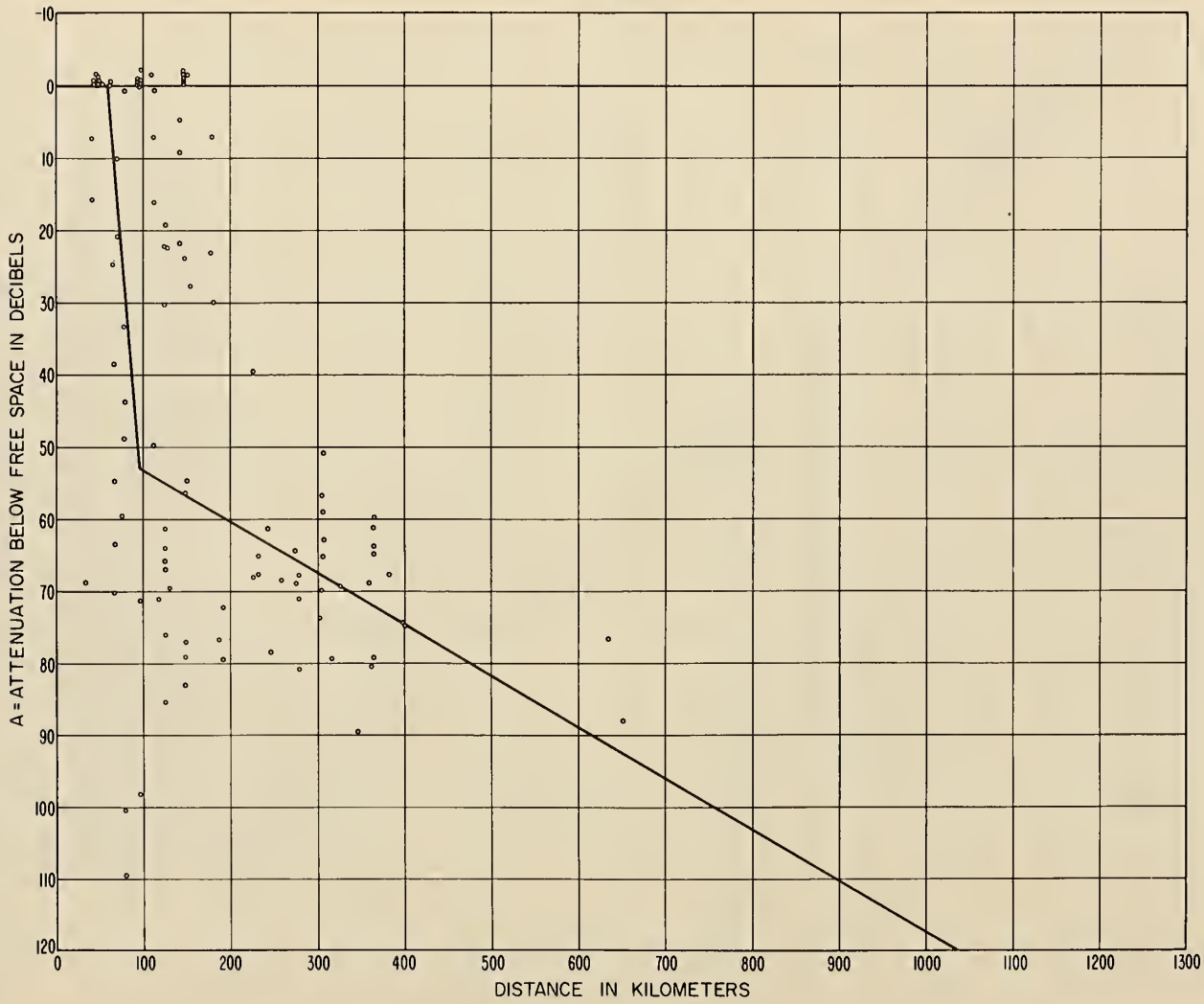
PERIOD OF RECORD MEDIANS VERSUS DISTANCE
FREQUENCY RANGE: 1000-10,000 MHz; MEDIAN FREQUENCY: 3500 MHz
110 PATHS
A = ATTENUATION BELOW FREE SPACE IN DECIBELS
-10
0
10
20
30
40
50
60
70
80
90
100
110
120
0
100
200
300
400
500
600
700
800
900
1000
1100
1200
1300
DISTANCE IN KILOMETERS

Figure I.4

ANGULAR DISTANCE VERSUS DISTANCE FOR THE 290 PATHS FOR WHICH TERRAIN PROFILES ARE AVAILABLE

THE CURVES SHOW ANGULAR DISTANCE, θ, AS A FUNCTION OF DISTANCE OVER A SMOOTH EARTH OF EFFECTIVE RADIUS = 9000 KILOMETERS

THE WIDE SCATTER OF THE DATA ON THIS FIGURE ARISES ALMOST ENTIRELY FROM DIFFERENCES IN TERRAIN PROFILES, AND ILLUSTRATES THE IMPORTANCE OF ANGULAR DISTANCE AS A PREDICTION PARAMETER

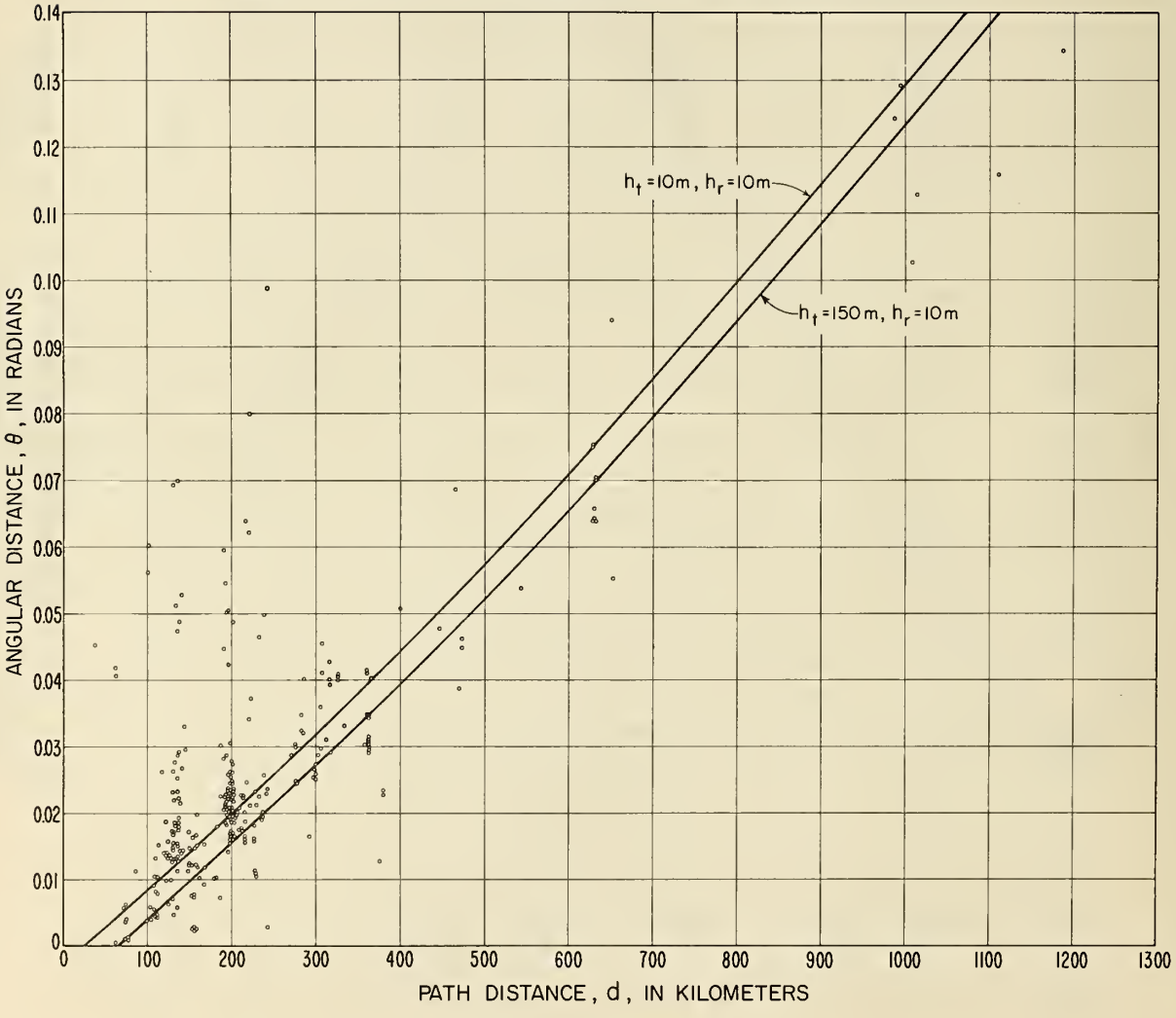

Figure I.5

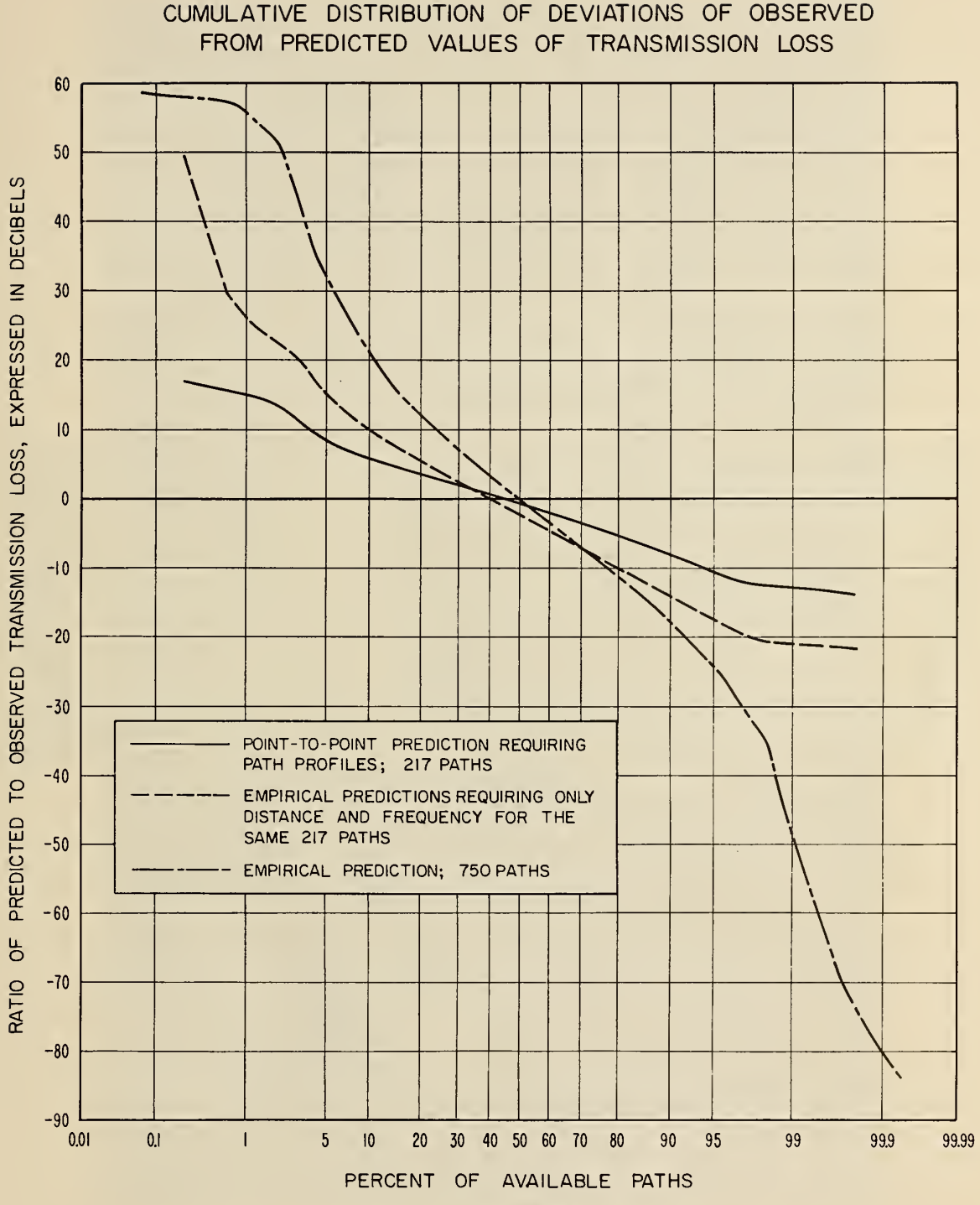
CUMULATIVE DISTRIBUTION OF DEVIATIONS OF OBSERVED FROM PREDICTED VALUES OF TRANSMISSION LOSS
RATIO OF PREDICTED TO OBSERVED TRANSMISSION LOSS, EXPRESSED IN DECIBELS
60
50
40
30
20
10
0
-10
-20
-30
-40
-50
-60
-70
-80
-90
0.01
0.1
1
5
10
20
30
40
50
60
70
80
90
95
99
99.9
99.99
PERCENT OF AVAILABLE PATHS
POINT-TO-POINT PREDICTION REQUIRING PATH PROFILES; 217 PATHS
EMPIRICAL PREDICTIONS REQUIRING ONLY DISTANCE AND FREQUENCY FOR THE SAME 217 PATHS
EMPIRICAL PREDICTION; 750 PATHS

Figure I.6

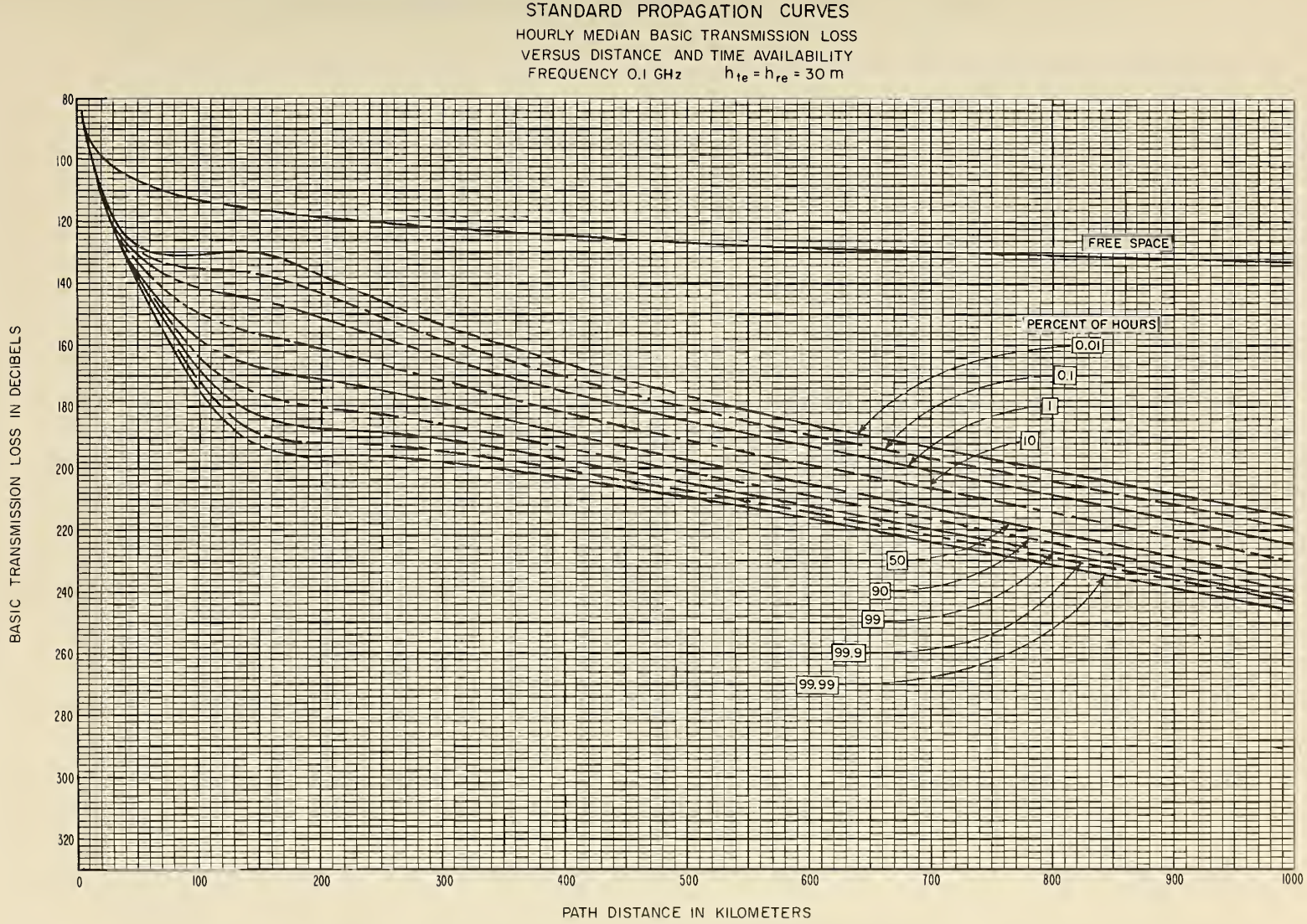
STANDARD PROPAGATION CURVES
HOURLY MEDIAN BASIC TRANSMISSION LOSS
VERSUS DISTANCE AND TIME AVAILABILITY
FREQUENCY 0.1 GHz $h_{te} = h_{re} = 30$ m
BASIC TRANSMISSION LOSS IN DECIBELS
80
100
120
140
160
180
200
220
240
260
280
300
320
FREE SPACE
PERCENT OF HOURS
0.01
0.1
1
10
50
90
99
99.9
99.99
0
100
200
300
400
500
600
700
800
900
1000
PATH DISTANCE IN KILOMETERS

Figure I.7

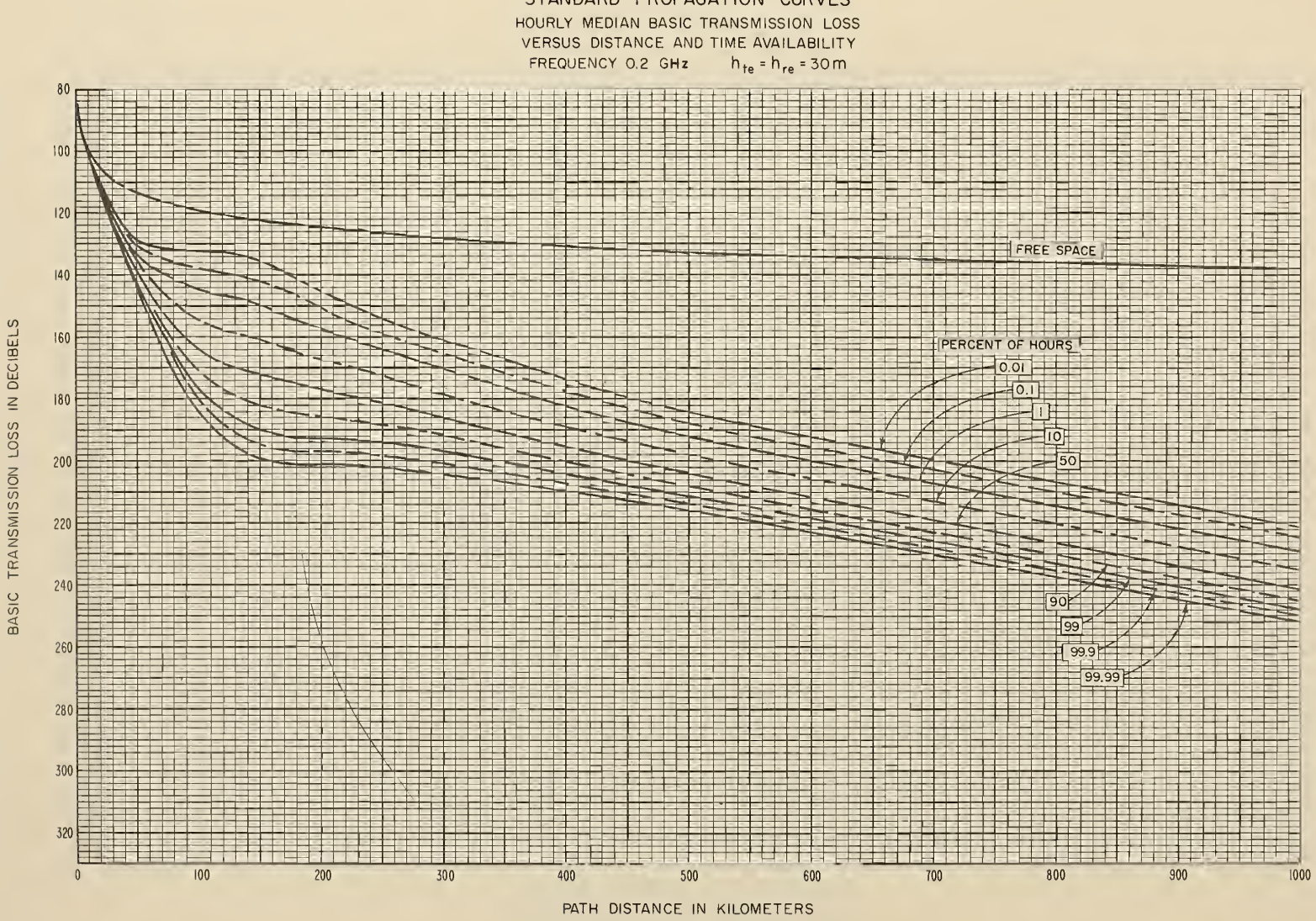
STANDARD PROPAGATION CURVES
HOURLY MEDIAN BASIC TRANSMISSION LOSS
VERSUS DISTANCE AND TIME AVAILABILITY
FREQUENCY 0.2 GHz $h_{te} = h_{re} = 30$ m
BASIC TRANSMISSION LOSS IN DECIBELS
80
100
120
140
160
180
200
220
240
260
280
300
320
FREE SPACE
PERCENT OF HOURS
0.01
0.1
1
10
50
90
99
99.9
99.99
0
100
200
300
400
500
600
700
800
900
1000
PATH DISTANCE IN KILOMETERS

Figure I.8

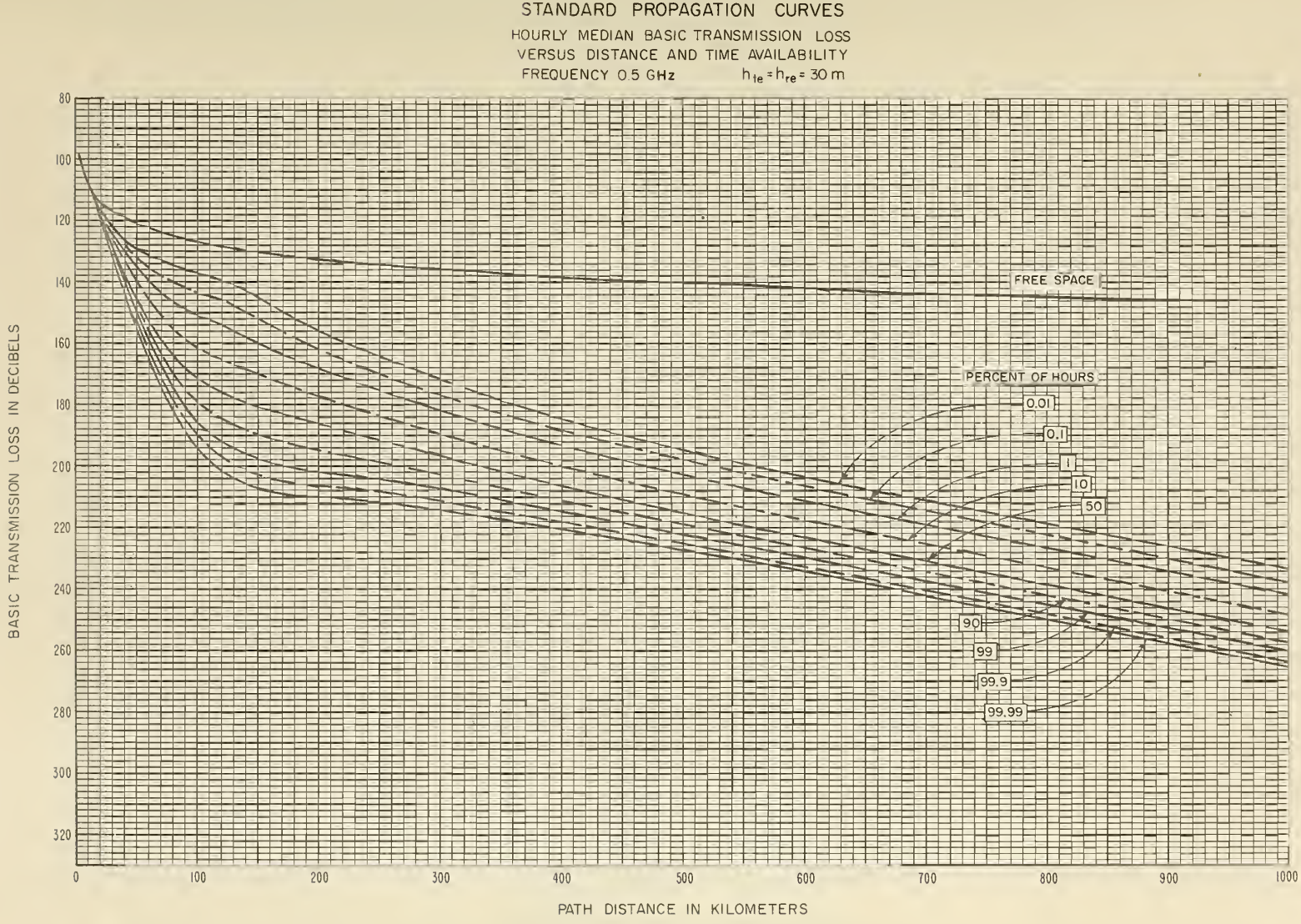
STANDARD PROPAGATION CURVES
HOURLY MEDIAN BASIC TRANSMISSION LOSS
VERSUS DISTANCE AND TIME AVAILABILITY
FREQUENCY 0.5 GHz $h_{te} = h_{re} = 30$ m
BASIC TRANSMISSION LOSS IN DECIBELS
80
100
120
140
160
180
200
220
240
260
280
300
320
FREE SPACE
PERCENT OF HOURS
0.01
0.1
1
10
50
90
99
99.9
99.99
0
100
200
300
400
500
600
700
800
900
1000
PATH DISTANCE IN KILOMETERS

Figure I.9

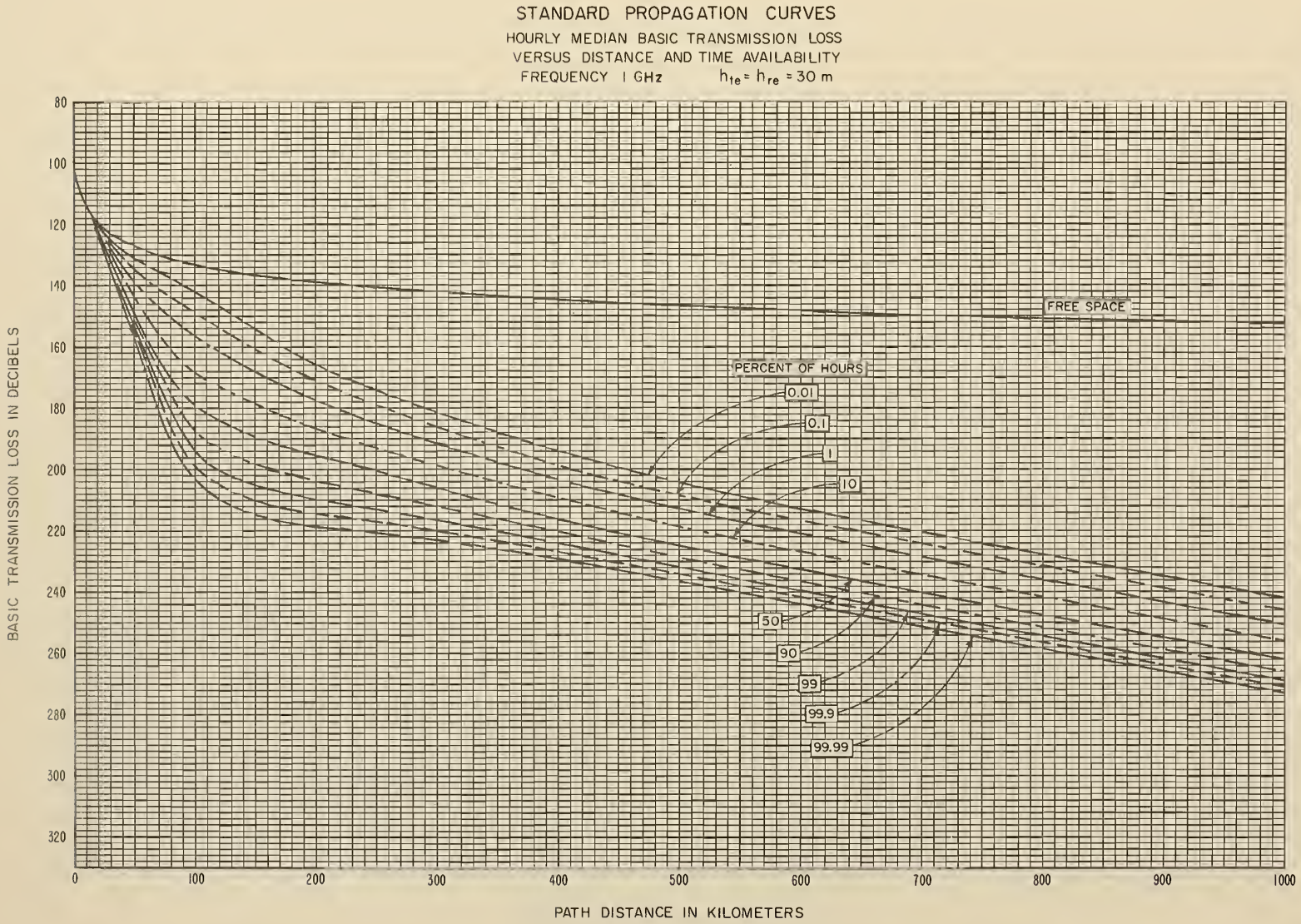
STANDARD PROPAGATION CURVES
HOURLY MEDIAN BASIC TRANSMISSION LOSS
VERSUS DISTANCE AND TIME AVAILABILITY
FREQUENCY 1 GHz $h_{te} = h_{re} = 30$ m
BASIC TRANSMISSION LOSS IN DECIBELS
80
100
120
140
160
180
200
220
240
260
280
300
320
FREE SPACE
PERCENT OF HOURS
0.01
0.1
1
10
50
90
99
99.9
99.99
0
100
200
300
400
500
600
700
800
900
1000
PATH DISTANCE IN KILOMETERS

Figure I.10

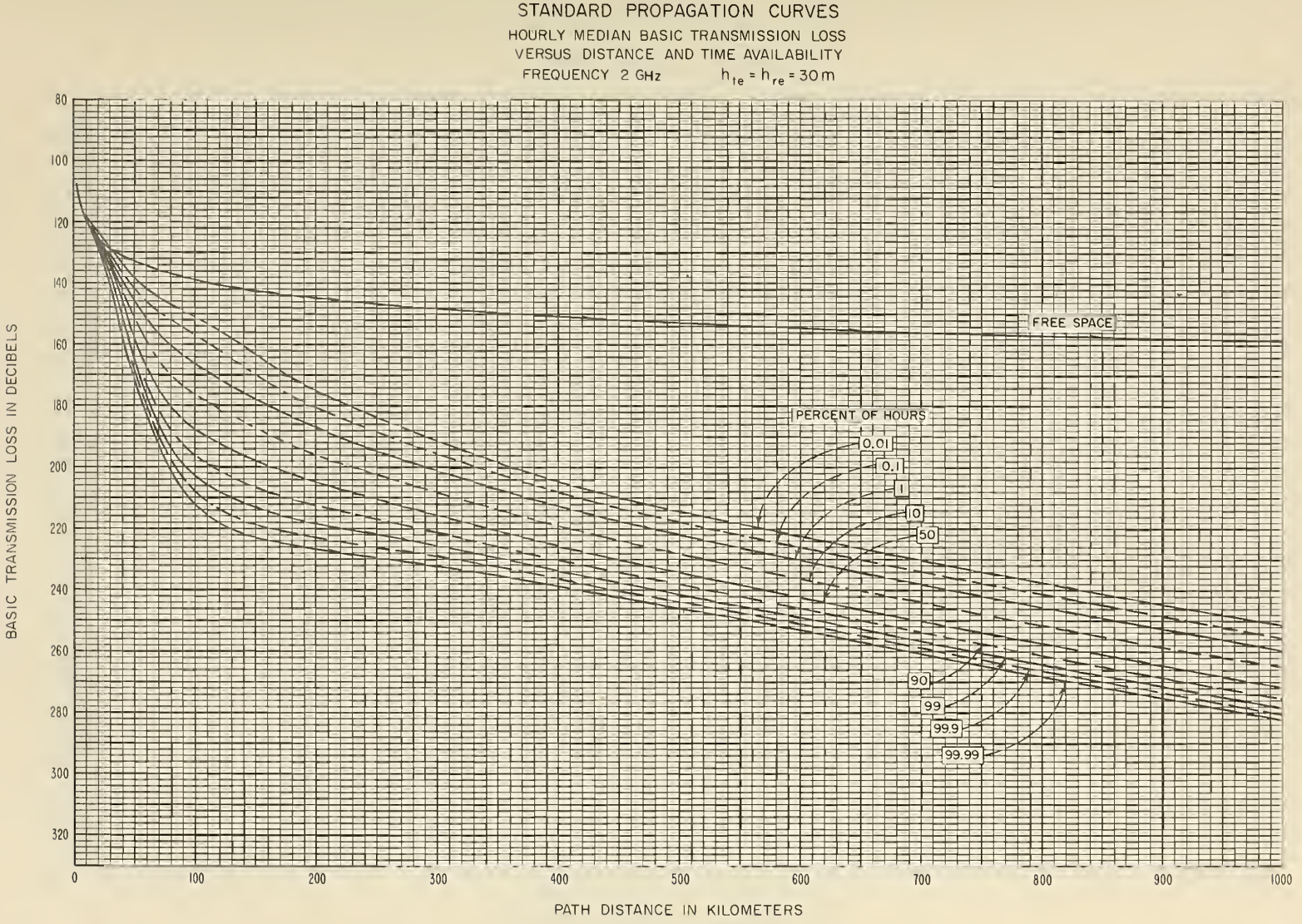
STANDARD PROPAGATION CURVES
HOURLY MEDIAN BASIC TRANSMISSION LOSS
VERSUS DISTANCE AND TIME AVAILABILITY
FREQUENCY 2 GHz
$h_{te} = h_{re} = 30$ m
BASIC TRANSMISSION LOSS IN DECIBELS
80
100
120
140
160
180
200
220
240
260
280
300
320
FREE SPACE
PERCENT OF HOURS
0.01
0.1
1
10
50
90
99
99.9
99.99
0
100
200
300
400
500
600
700
800
900
1000
PATH DISTANCE IN KILOMETERS

Figure I.11

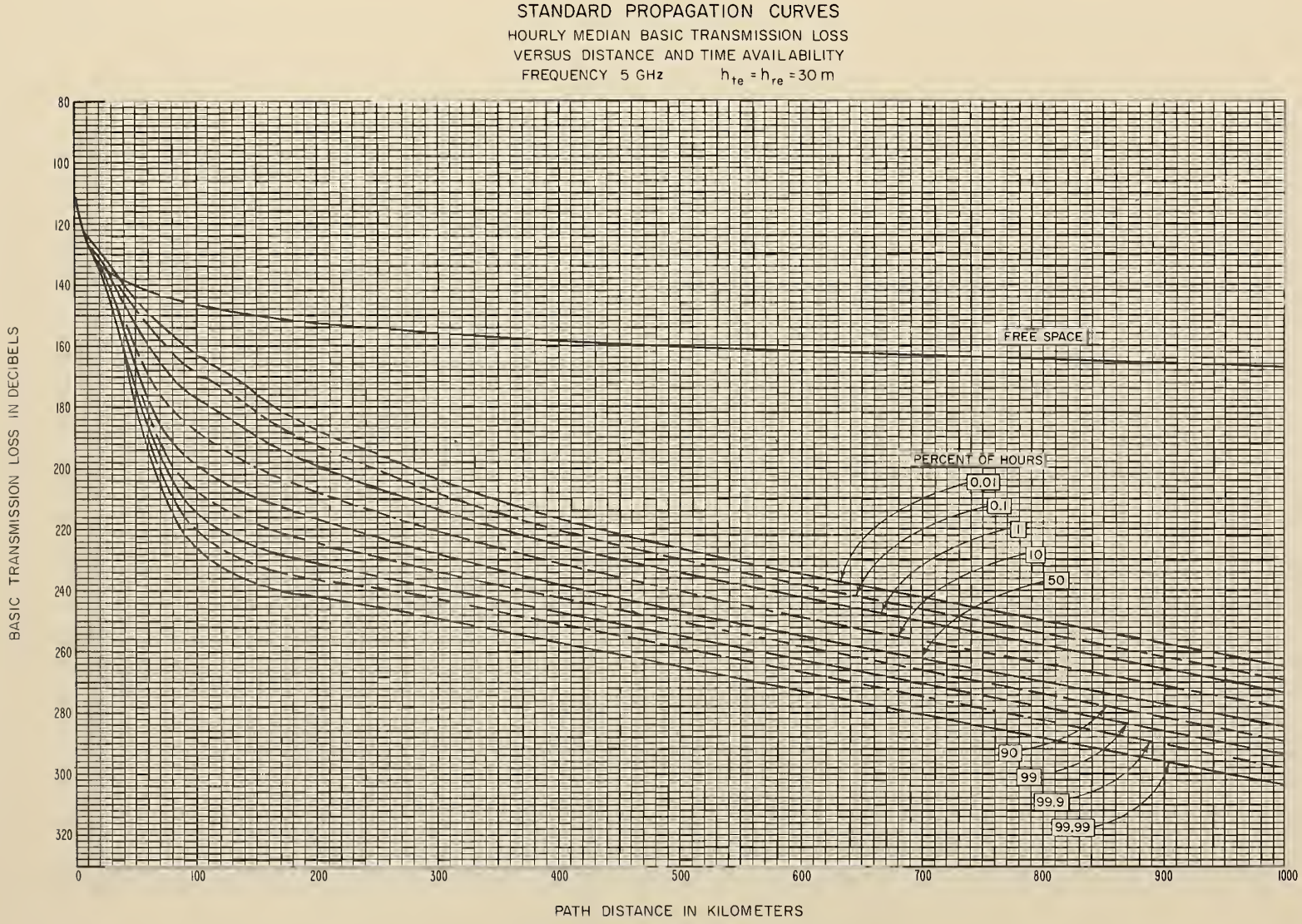
STANDARD PROPAGATION CURVES
HOURLY MEDIAN BASIC TRANSMISSION LOSS
VERSUS DISTANCE AND TIME AVAILABILITY
FREQUENCY 5 GHz $h_{te} = h_{re} = 30$ m
BASIC TRANSMISSION LOSS IN DECIBELS
80
100
120
140
160
180
200
220
240
260
280
300
320
FREE SPACE
PERCENT OF HOURS
0.01
0.1
1
10
50
90
99
99.9
99.99
0
100
200
300
400
500
600
700
800
900
1000
PATH DISTANCE IN KILOMETERS

Figure I.12

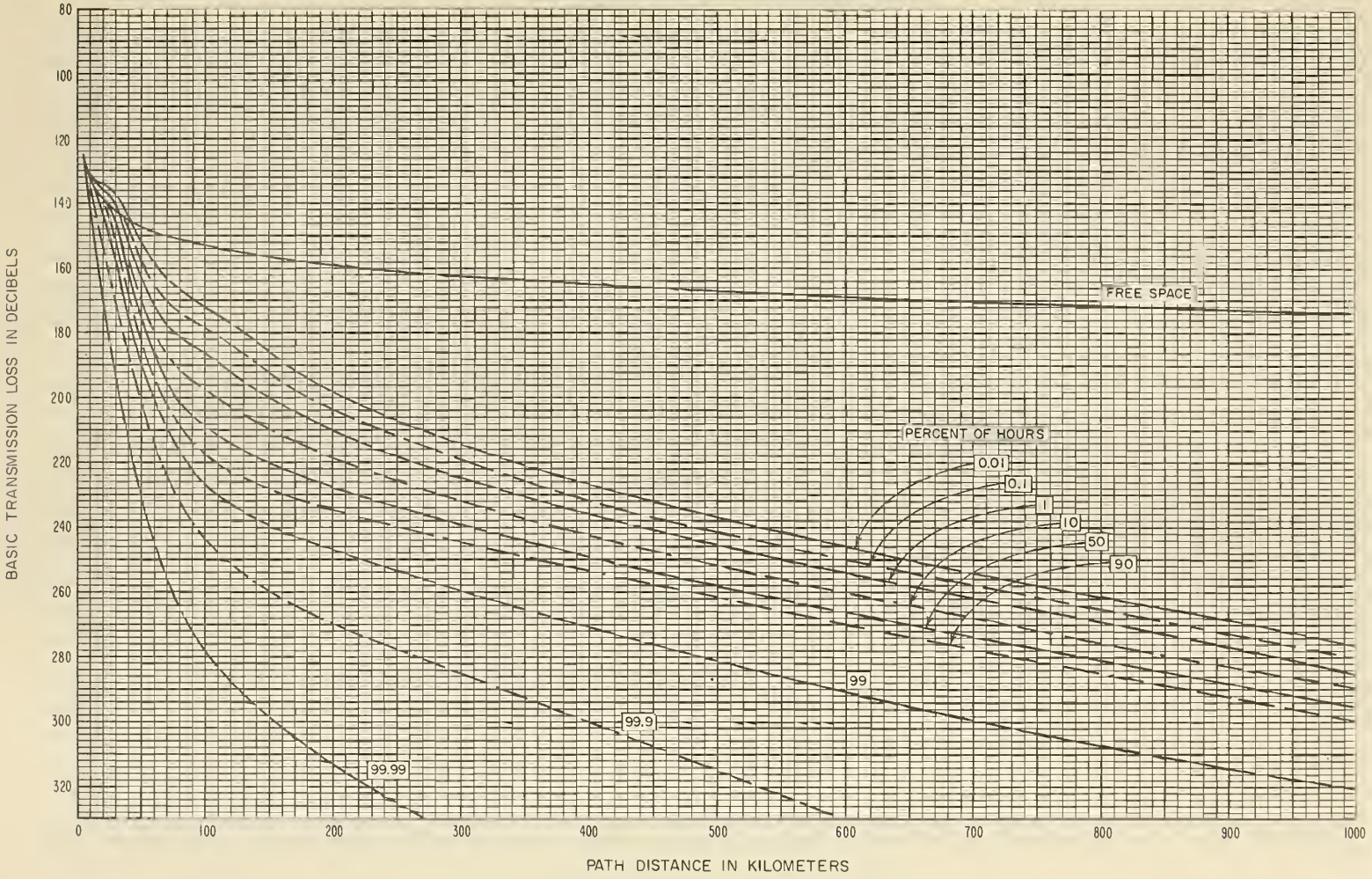
STANDARD PROPAGATION CURVES
HOURLY MEDIAN BASIC TRANSMISSION LOSS
VERSUS DISTANCE AND TIME AVAILABILITY
FREQUENCY 10 GHz $h_{te} = h_{re} = 30$ m
BASIC TRANSMISSION LOSS IN DECIBELS
80
100
120
140
160
180
200
220
240
260
280
300
320
FREE SPACE
PERCENT OF HOURS
0.01
0.1
1
10
50
90
99
99.9
99.99
0
100
200
300
400
500
600
700
800
900
1000
PATH DISTANCE IN KILOMETERS

Figure I.13

STANDARD PROPAGATION CURVES

HOURLY MEDIAN BASIC TRANSMISSION LOSS
VERSUS DISTANCE AND TIME AVAILABILITY
FREQUENCY 22.2 GHz $h_{te} = h_{re} = 30m$

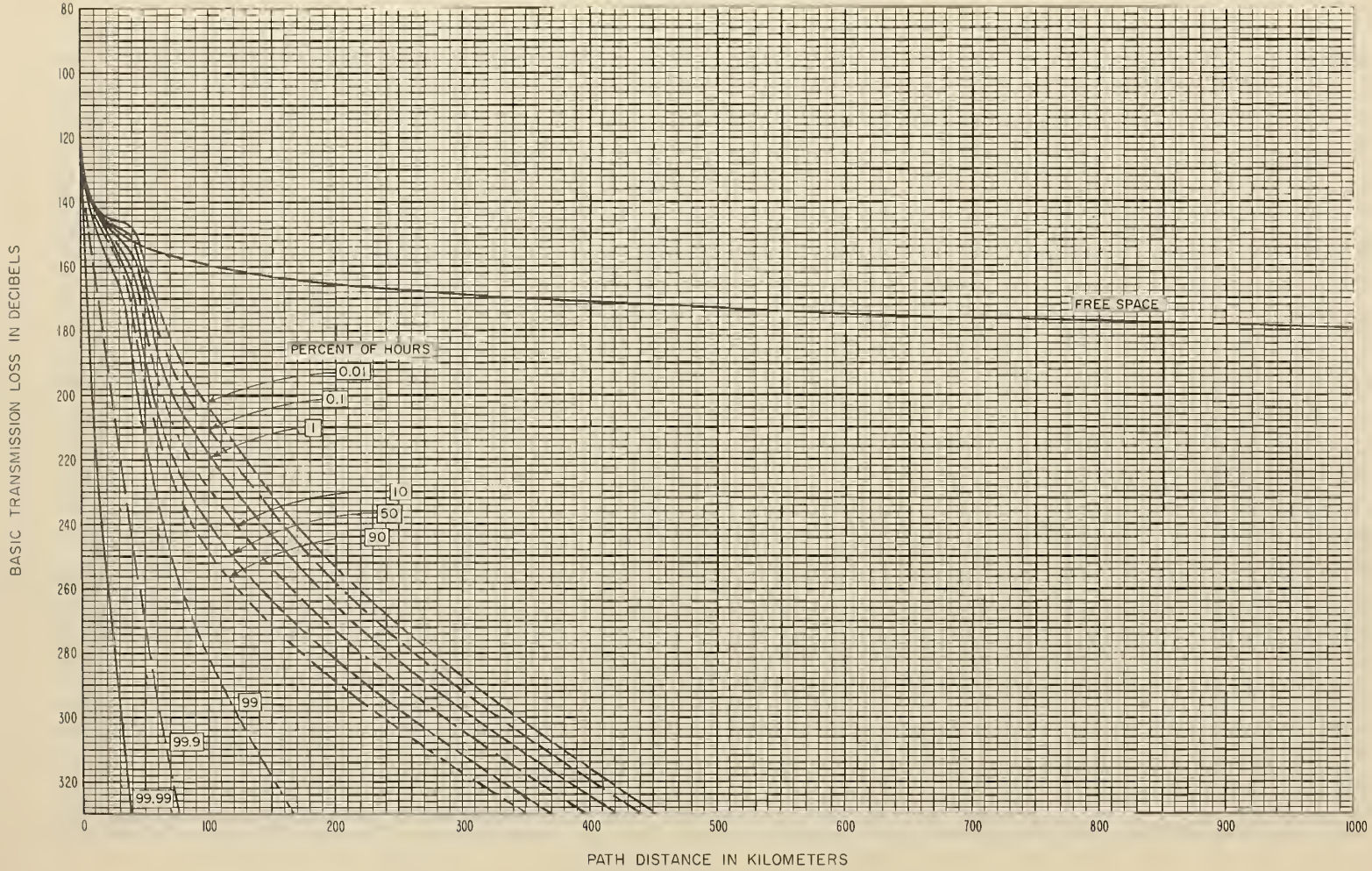

Figure I.14

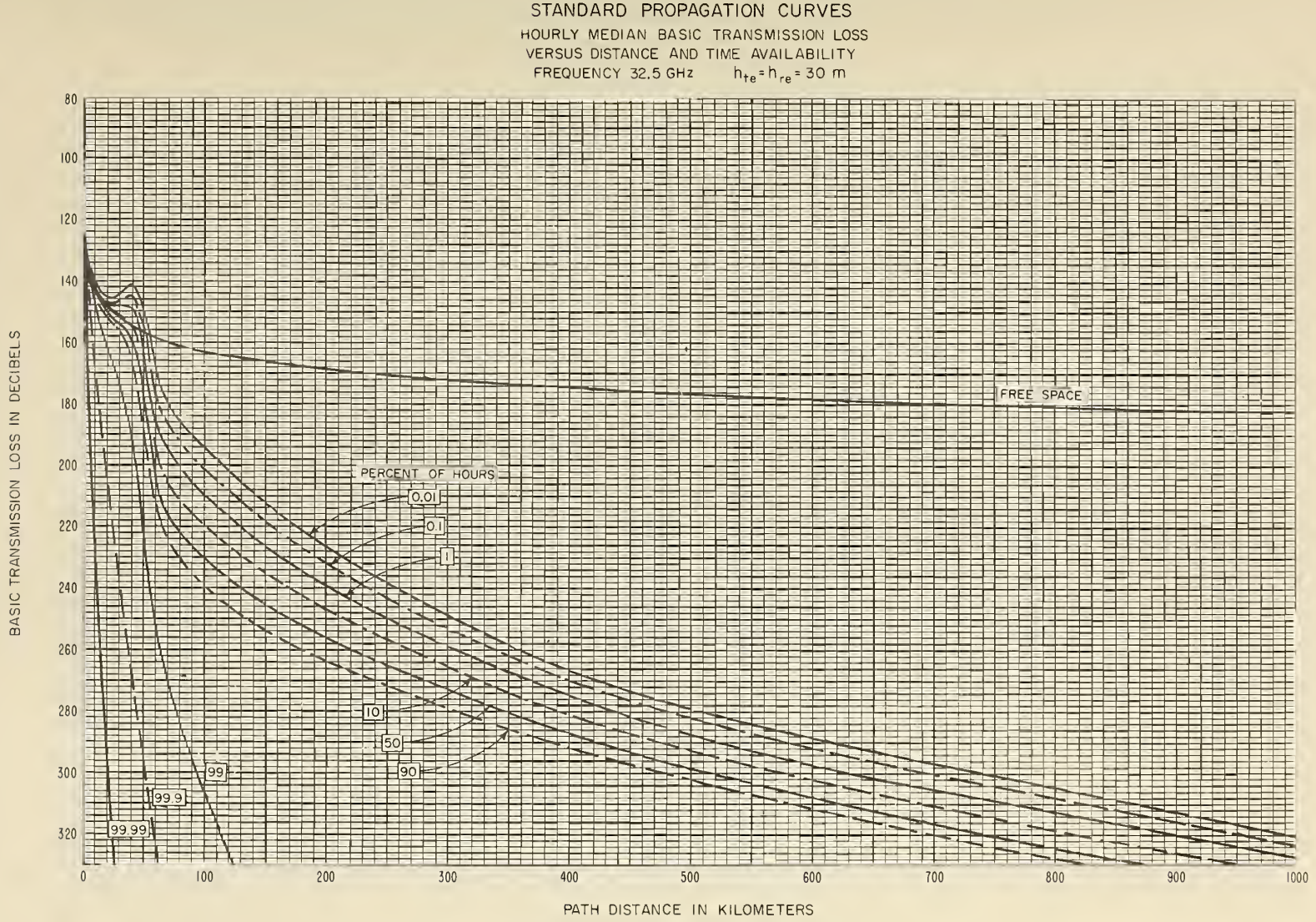
STANDARD PROPAGATION CURVES
HOURLY MEDIAN BASIC TRANSMISSION LOSS
VERSUS DISTANCE AND TIME AVAILABILITY
FREQUENCY 32.5 GHz $h_{te} = h_{re} = 30$ m
BASIC TRANSMISSION LOSS IN DECIBELS
80
100
120
140
160
180
200
220
240
260
280
300
320
FREE SPACE
PERCENT OF HOURS
0.01
0.1
1
10
50
90
99
99.9
99.99
0
100
200
300
400
500
600
700
800
900
1000
PATH DISTANCE IN KILOMETERS

Figure I.15

STANDARD PROPAGATION CURVES

HOURLY MEDIAN BASIC TRANSMISSION LOSS

VERSUS DISTANCE AND TIME AVAILABILITY

$h_{te} = h_{re} = 30$ m

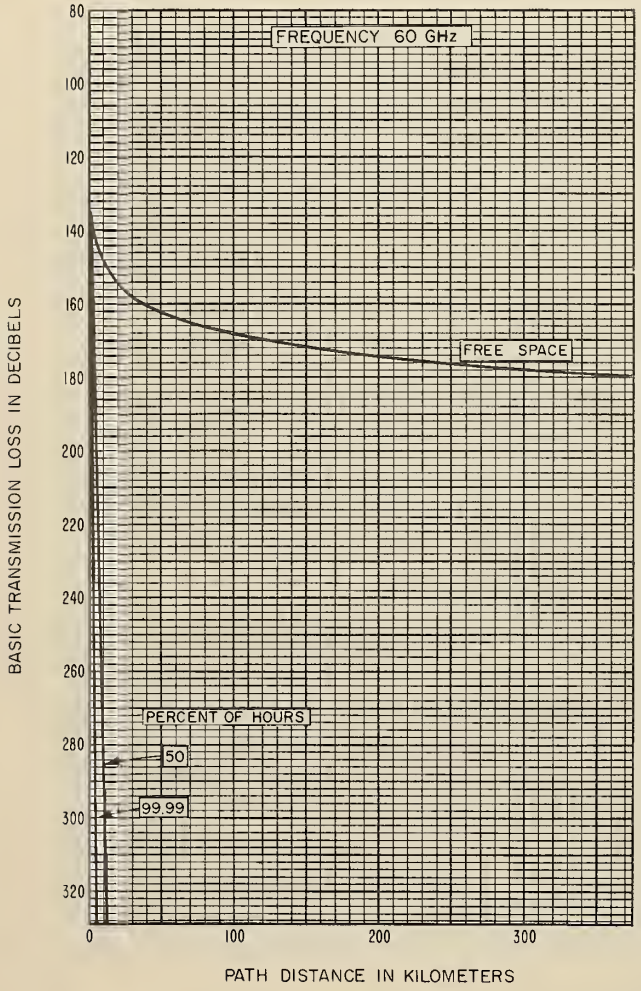

Figure I.16

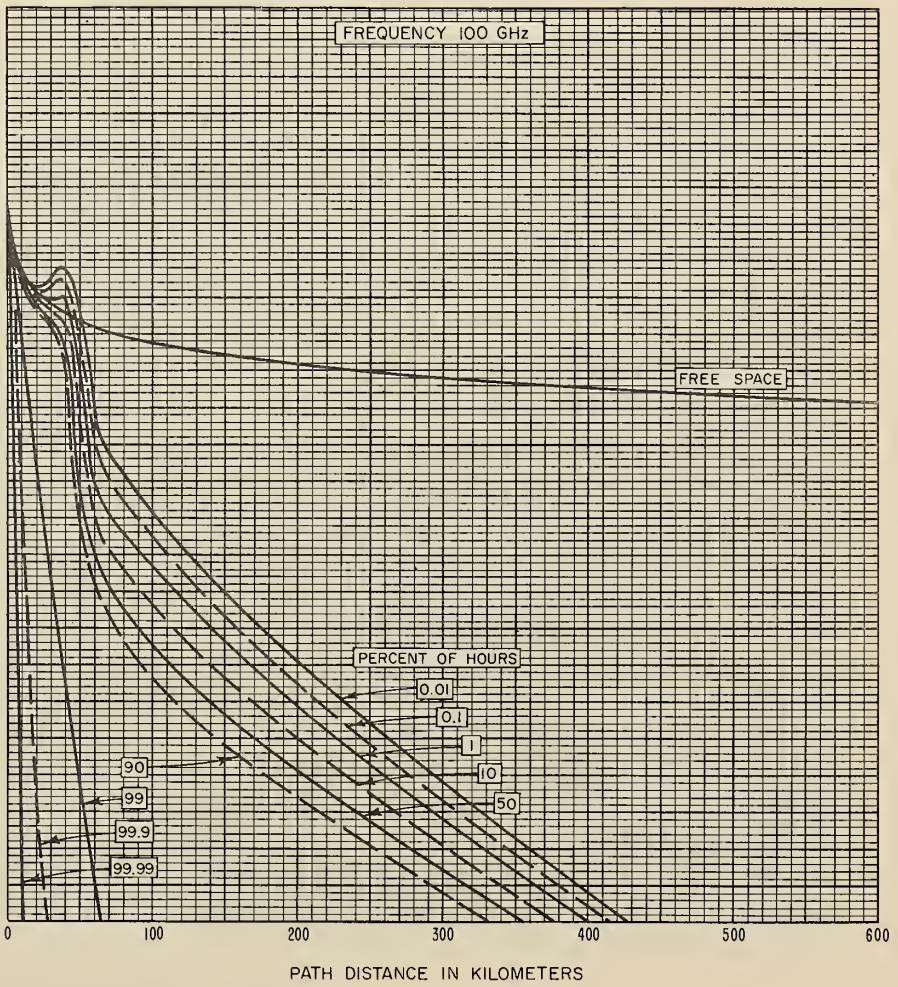

Figure I.17

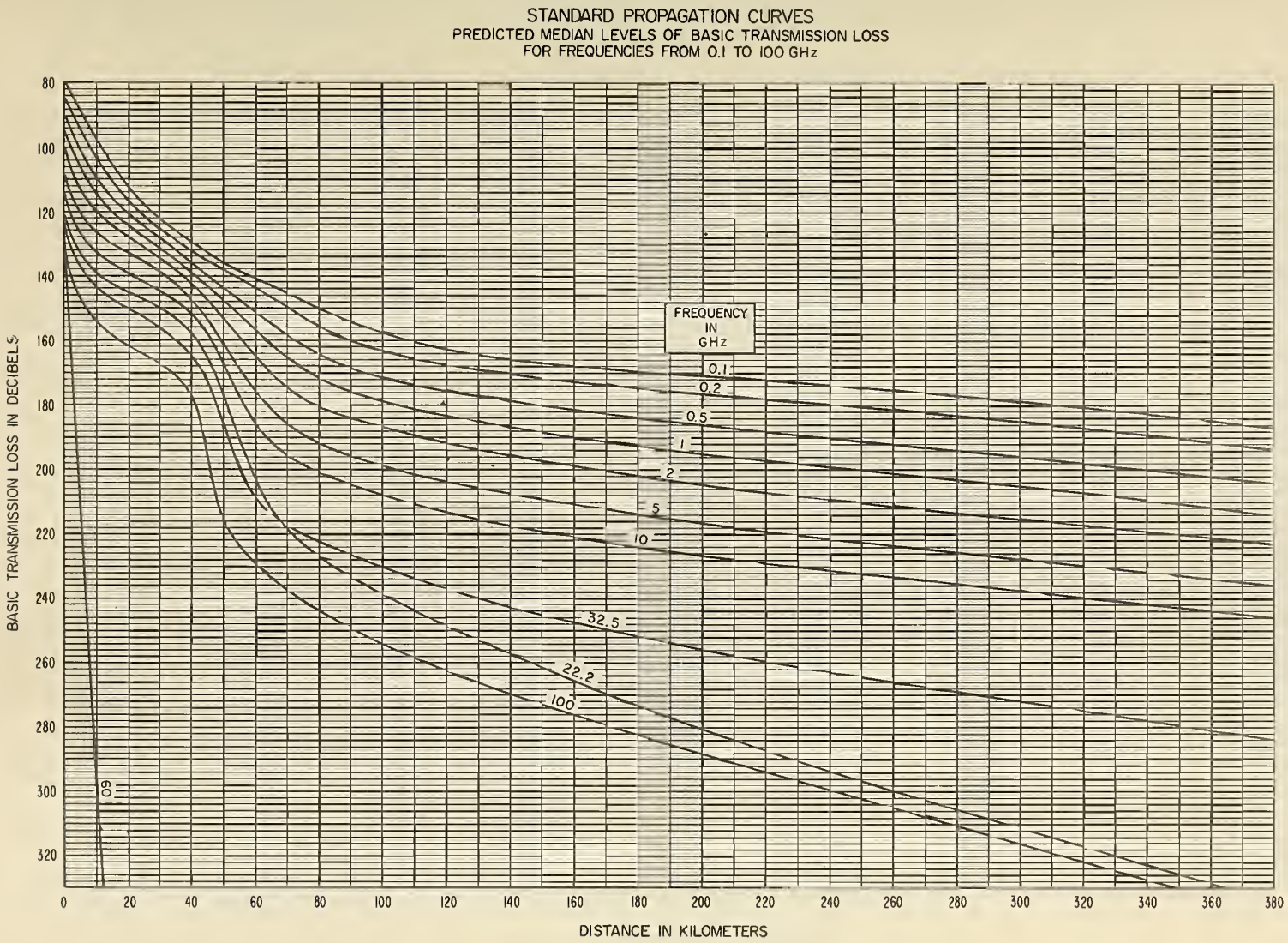
STANDARD PROPAGATION CURVES
PREDICTED MEDIAN LEVELS OF BASIC TRANSMISSION LOSS
FOR FREQUENCIES FROM 0.1 TO 100 GHz
BASIC TRANSMISSION LOSS IN DECIBELS
DISTANCE IN KILOMETERS
FREQUENCY IN GHz
0.1
0.2
0.5
1
2
5
10
32.5
22.2
100
60
80
100
120
140
160
180
200
220
240
260
280
300
320
0
20
40
60
80
100
120
140
160
180
200
220
240
260
280
300
320
340
360
380

Figure 1.18

STANDARD PROPAGATION CURVES

CUMULATIVE DISTRIBUTION OF HOURLY MEDIAN BASIC TRANSMISSION LOSS
RELATIVE TO THE LONG-TERM MEDIAN

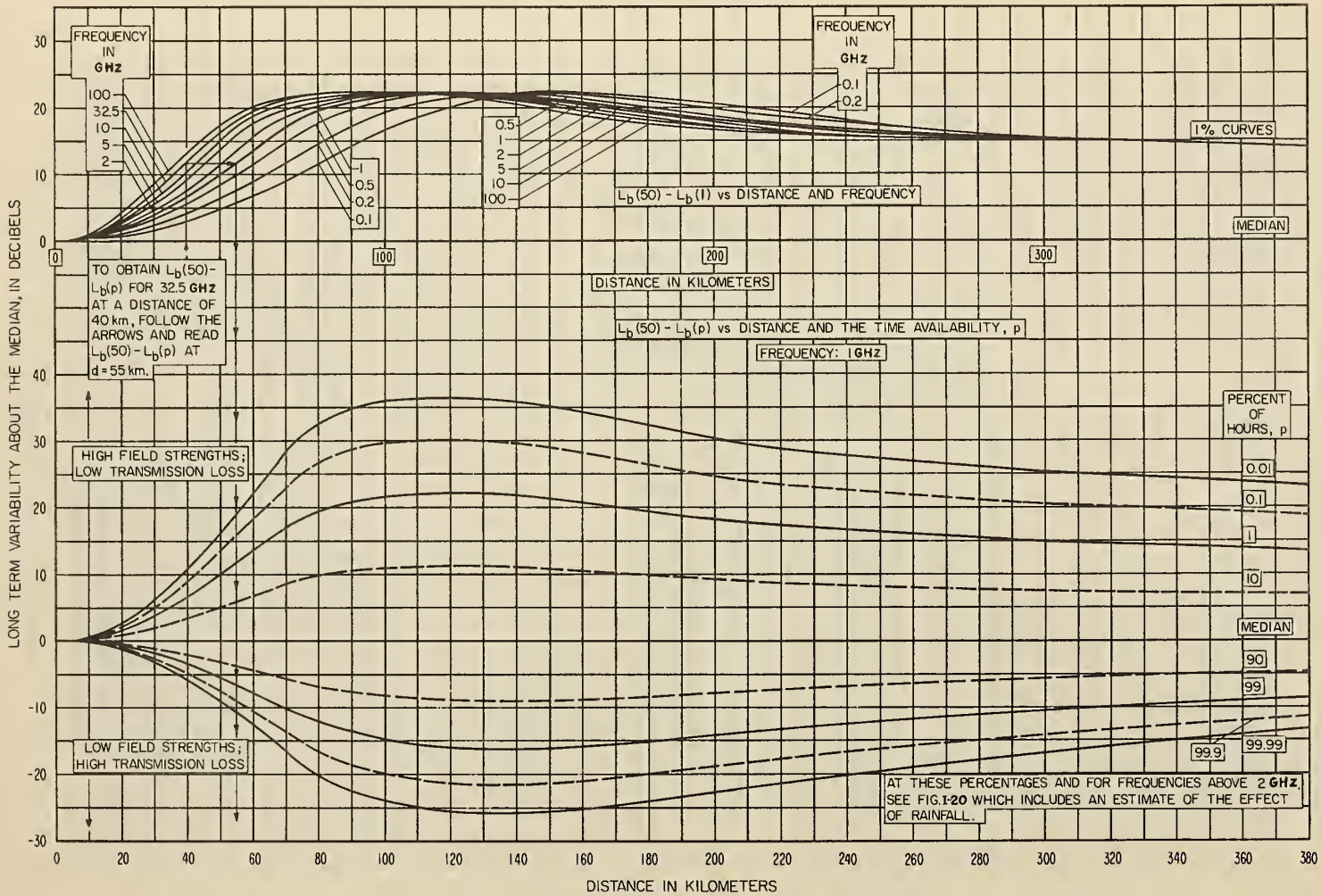

Figure I.19

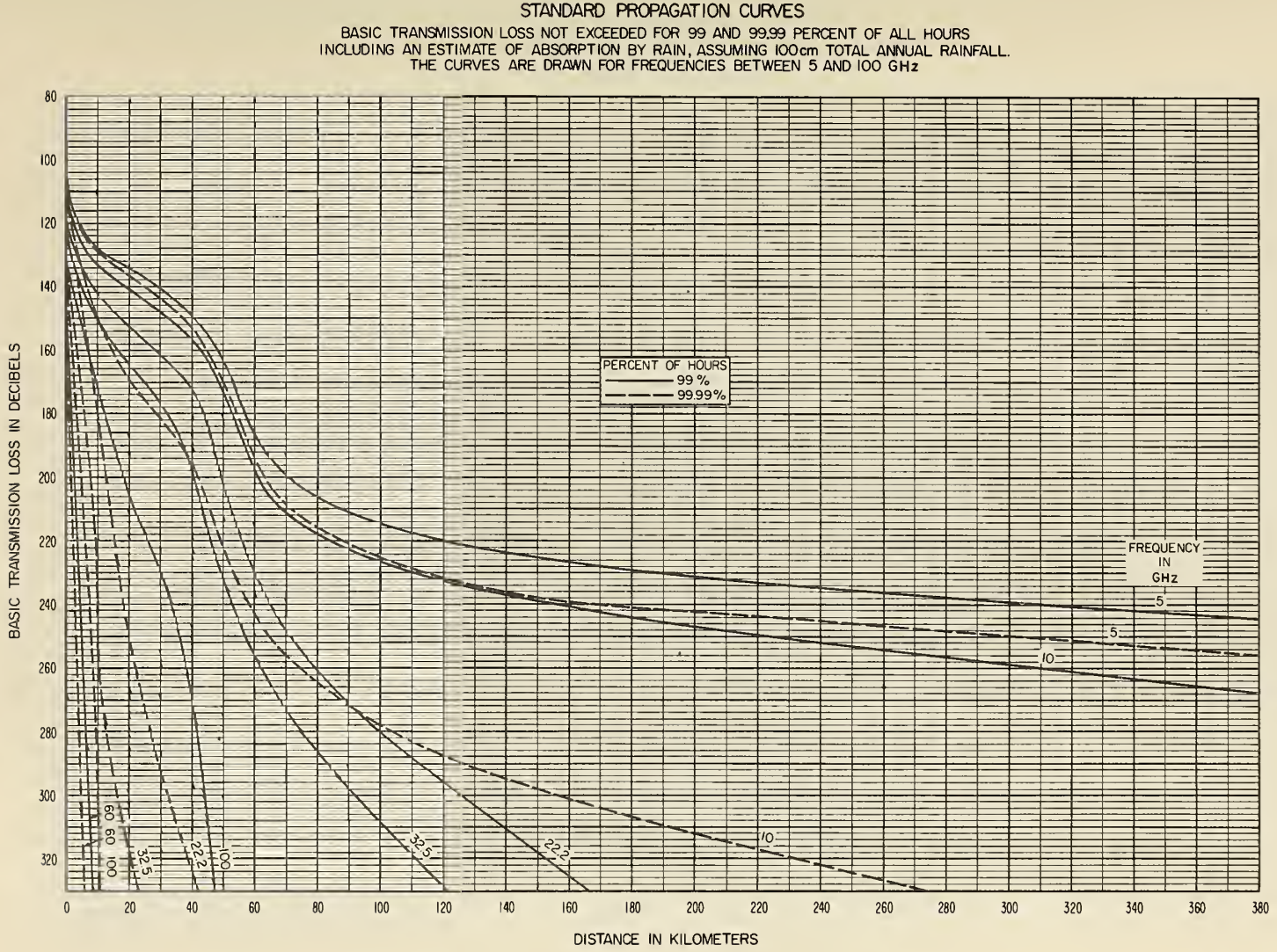
STANDARD PROPAGATION CURVES
BASIC TRANSMISSION LOSS NOT EXCEEDED FOR 99 AND 99.99 PERCENT OF ALL HOURS
INCLUDING AN ESTIMATE OF ABSORPTION BY RAIN, ASSUMING 100cm TOTAL ANNUAL RAINFALL.
THE CURVES ARE DRAWN FOR FREQUENCIES BETWEEN 5 AND 100 GHz
BASIC TRANSMISSION LOSS IN DECIBELS
80
100
120
140
160
180
200
220
240
260
280
300
320
PERCENT OF HOURS
99 %
99.99%
FREQUENCY IN GHz
5
5
10
10
22.2
32.5
100
0 20 40 60 80 100 120 140 160 180 200 220 240 260 280 300 320 340 360 380
DISTANCE IN KILOMETERS

Figure I.20

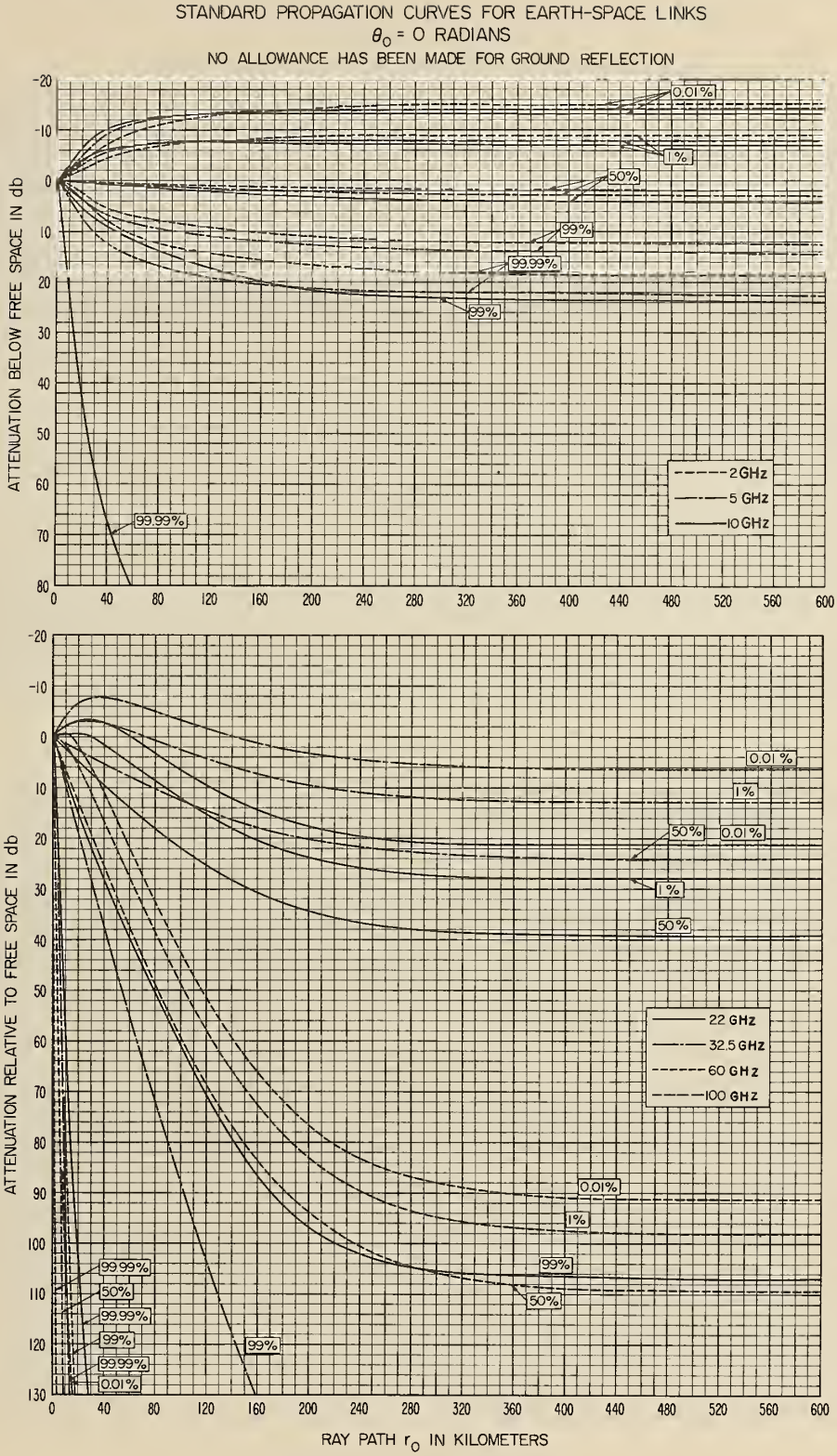
STANDARD PROPAGATION CURVES FOR EARTH-SPACE LINKS
θ_0 = 0 RADIANS
NO ALLOWANCE HAS BEEN MADE FOR GROUND REFLECTION
ATTENUATION BELOW FREE SPACE IN db
0.01%
1%
50%
99%
99.99%
99%
99.99%
2 GHz
5 GHz
10 GHz
ATTENUATION RELATIVE TO FREE SPACE IN db
0.01%
1%
50%
0.01%
1%
50%
22 GHz
32.5 GHz
60 GHz
100 GHz
0.01%
1%
99%
50%
99.99%
50%
99.99%
99%
99%
99.99%
0.01%
RAY PATH r_0 IN KILOMETERS

Figure I.21

STANDARD PROPAGATION CURVES FOR EARTH SPACE LINKS

θ_0 = 0.03 RADIANS

NO ALLOWANCE HAS BEEN MADE FOR GROUND REFLECTION

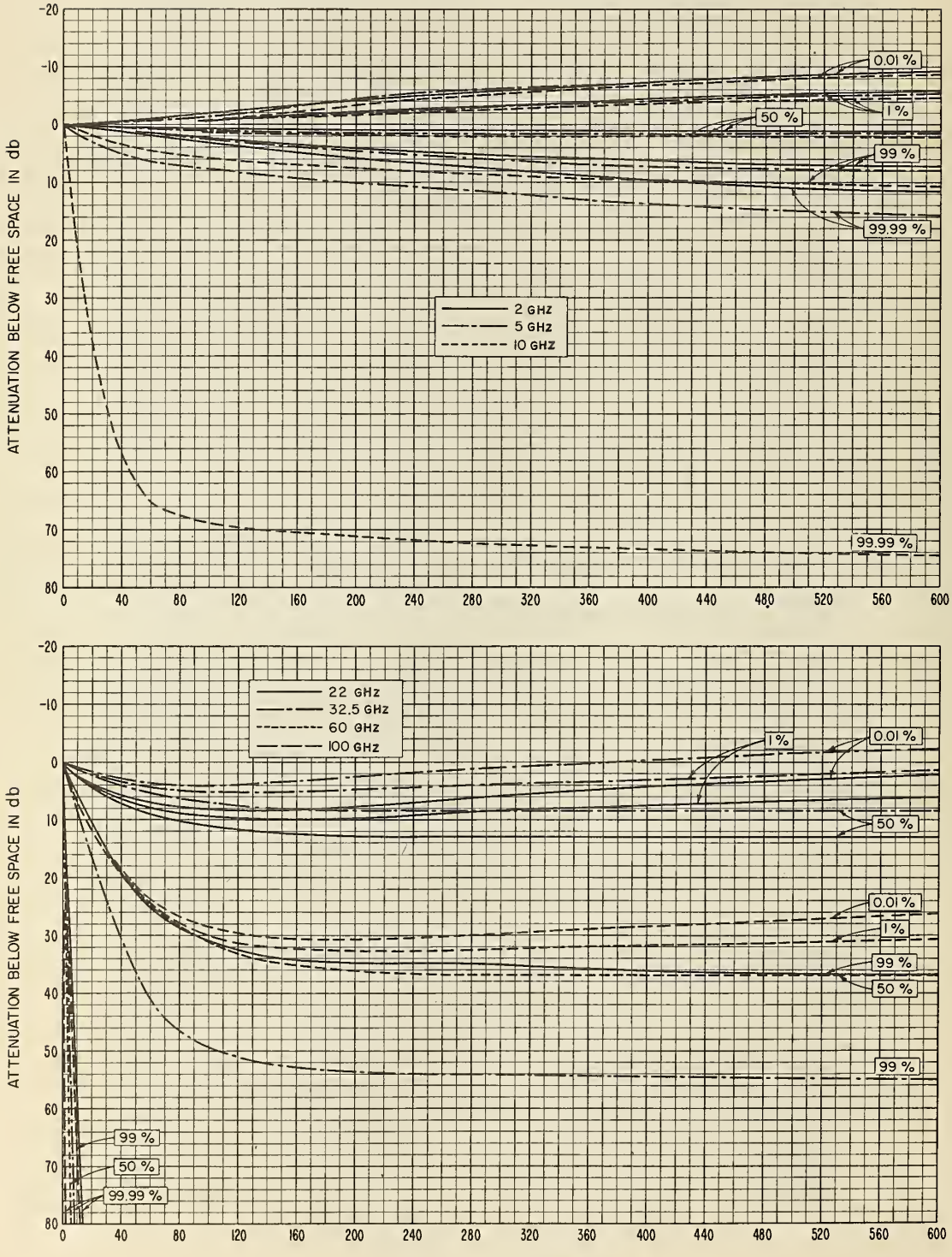

Figure I.22

STANDARD PROPAGATION CURVES FOR EARTH-SPACE LINKS

θ_0=0.1 RADIANS

NO ALLOWANCE HAS BEEN MADE FOR GROUND REFLECTION

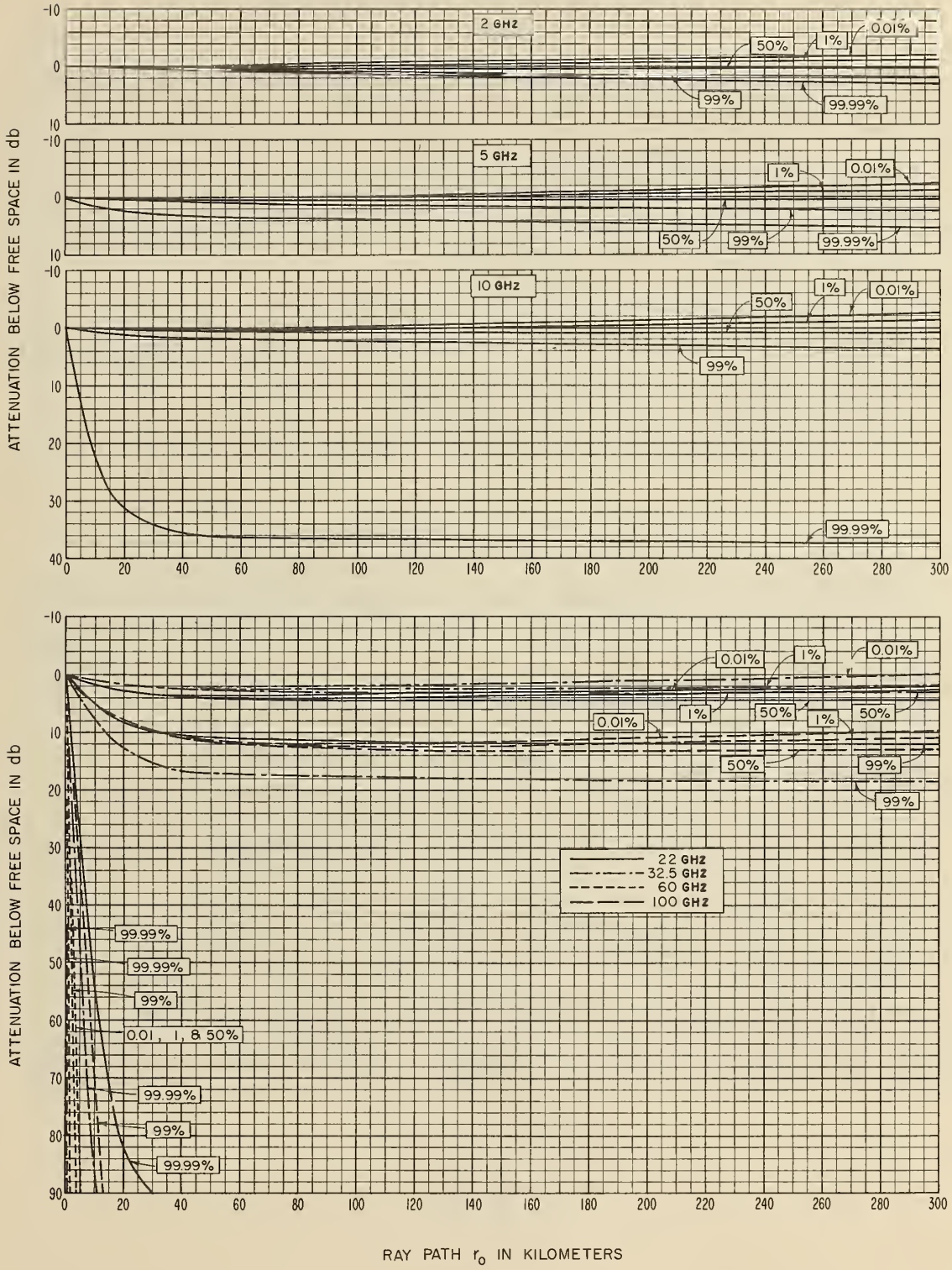

Figure I.23

STANDARD PROPAGATION CURVES FOR EARTH-SPACE LINKS
θ_0 = 0.3 RADIANS
NO ALLOWANCE HAS BEEN MADE FOR GROUND REFLECTION

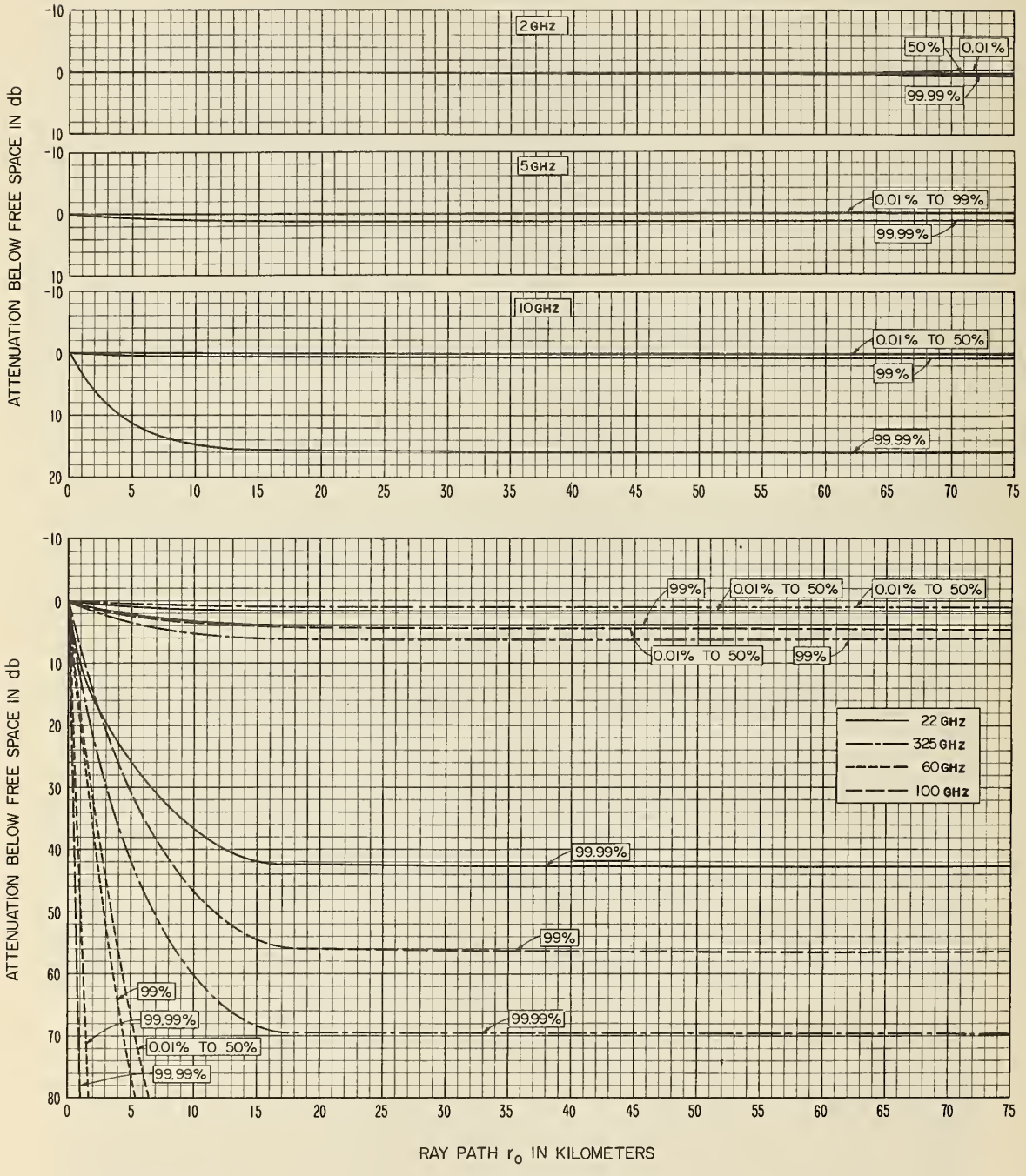

Figure I.24

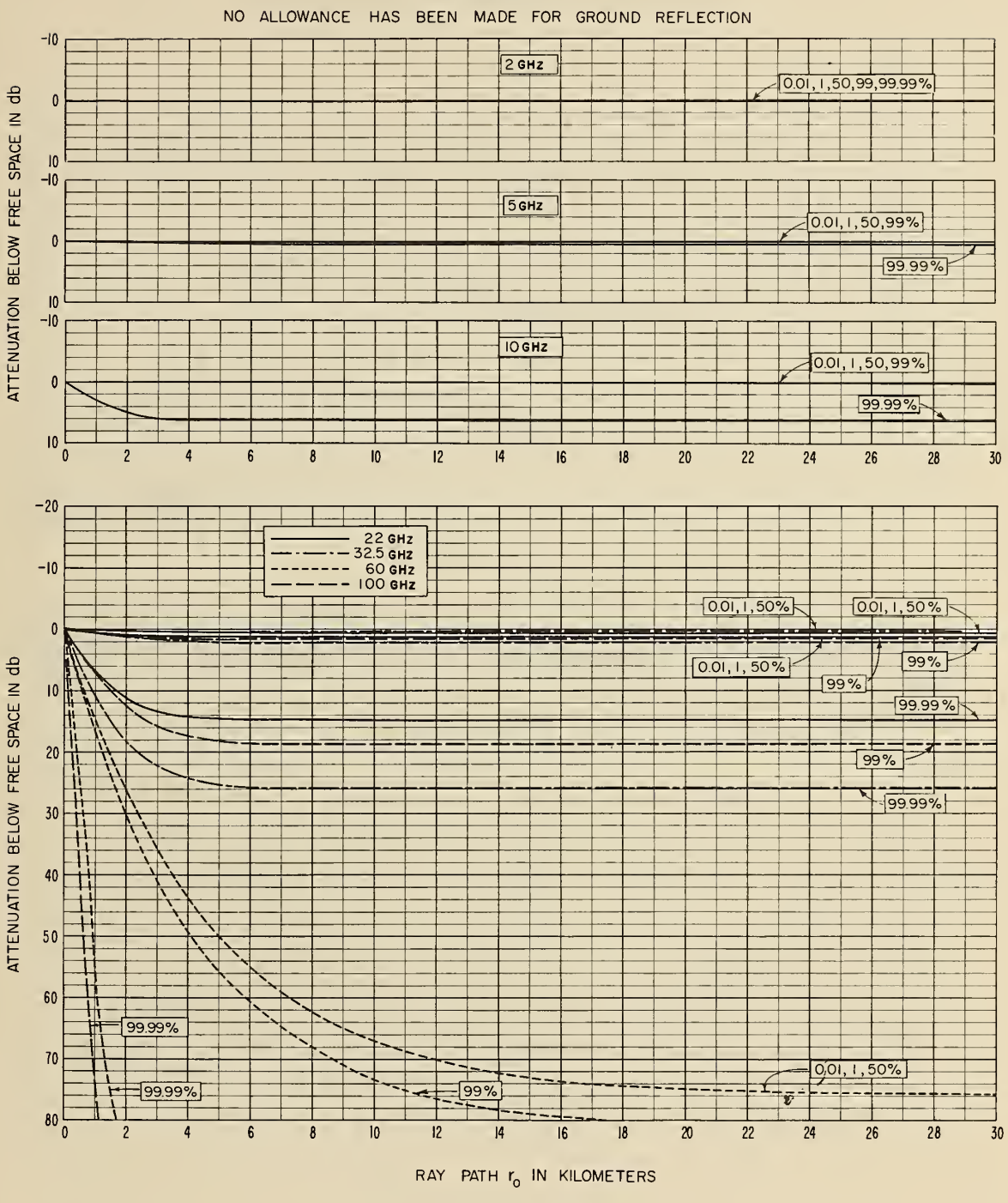
STANDARD PROPAGATION CURVES FOR EARTH-SPACE LINKS
θ_0 = 1.0 RADIAN
NO ALLOWANCE HAS BEEN MADE FOR GROUND REFLECTION
ATTENUATION BELOW FREE SPACE IN db
2 GHz
0.01, 1, 50, 99, 99.99%
5 GHz
0.01, 1, 50, 99%
99.99%
10 GHz
0.01, 1, 50, 99%
99.99%
22 GHz
32.5 GHz
60 GHz
100 GHz
0.01, 1, 50%
0.01, 1, 50%
0.01, 1, 50%
99%
99%
99.99%
99%
99.99%
99.99%
99%
0.01, 1, 50%
RAY PATH r_0 IN KILOMETERS

Figure I.25

STANDARD PROPAGATION CURVES FOR EARTH-SPACE LINKS

$\theta_0 = \pi/2$

NO ALLOWANCE HAS BEEN MADE FOR GROUND REFLECTION

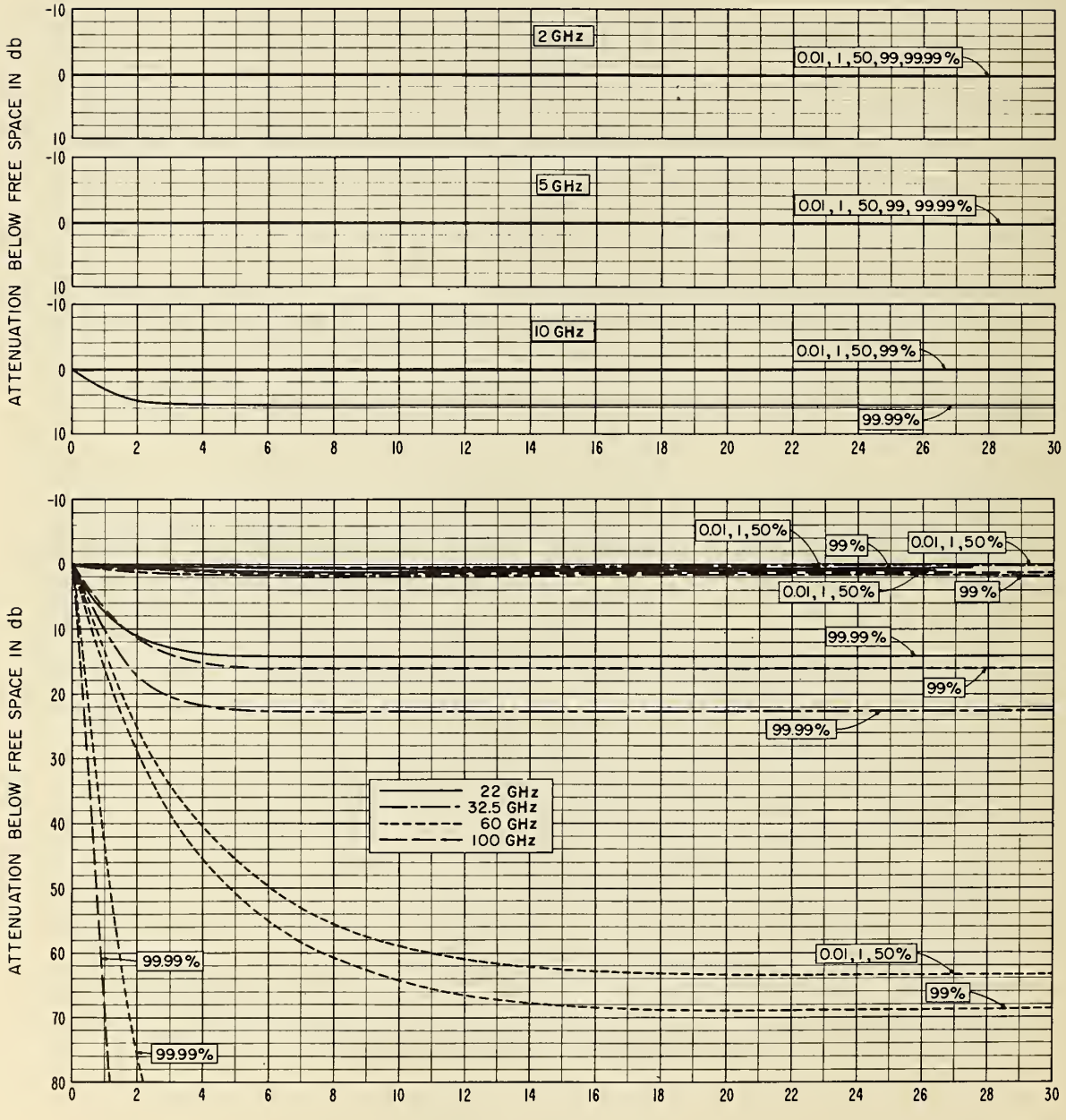

Figure I.26

BEAM ORIENTATION, POLARIZATION, AND MULTIPATH COUPLING LOSS

Ordinarily, to minimize the transmission loss between two antennas, they are oriented to take advantage of maximum directive gains (directivity) and the polarizations are matched. This maximizes the path antenna gain. With a single uniform plane wave incident upon a receiving antenna, there will be a reduction in the power transferred if the antenna beam is not oriented for maximum free space gain. If the polarization of the receiving antenna is matched to that of the incident wave, this loss in path antenna gain is due to "orientation coupling loss", and if there is a polarization mismatch, there will be an additional "polarization coupling loss". In general, more than one plane wave will be incident upon a receiving antenna from a single source because of reflection, diffraction, or scattering by terrain or atmospheric inhomogeneities. Mismatch between the relative phases of these waves and the relative phases of the receiving antenna response in different directions will contribute to a "multipath coupling loss" which will include orientation, polarization, and phase mismatch effects. If multipath propagation involves non-uniform waves whose amplitudes, polarizations, and phases can only be described statistically, the corresponding loss in path antenna gain will include "antenna-to-medium coupling loss", a statistical average of phase incoherence effects.

This annex indicates how multipath coupling loss may be calculated when incident waves are plane and uniform with known phases, and when the directivity, polarization, and phase response of the receiving antenna are known for every direction. It is assumed that the radiation resistance of the receiving antenna is unaffected by its environment, and that the electric and magnetic field vectors of every incident wave are perpendicular to each other and perpendicular to the direction of propagation.

II.1 Representation of Complex Vector Fields

Studying the response of a receiving antenna to coherently phased plane waves with several different directions of arrival, it is convenient to locate the receiving antenna at the center of a coordinate system. A radio ray traveling a distance r from a transmitter to the receiver may be refracted or reflected so that its initial and final directions are different. If $-\hat{f}$ is the direction of propagation at the receiver, $\vec{r} = \hat{f}\, r$ is the vector distance from the receiver to the transmitter if the ray path is a straight line, but not otherwise.

A paper by Kales [1951] shows how the amplitude, phase, and polarization of a uniform, monochromatic, elliptically polarized and locally plane wave may be expressed with the aid of complex vectors. For instance, such a wave may be expressed as the real part of the sum of two linearly polarized complex plane waves $\sqrt{2}\,\vec{e}_r \exp(i\tau)$ and $i\sqrt{2}\,\vec{e}_i \exp(i\tau)$. These components are in time phase quadrature and travel in the same direction $-\hat{f}$, where $i = \sqrt{-1}$ and $\vec{e}_r$ and $\vec{e}_i$ are real vectors perpendicular to $\hat{f}$. The vector $\vec{e}_r + i\vec{e}_i$ is then a complex vector. Field strengths are denoted in volts/km (10^3 microvolts per meter) and field intensities in watts/km^2 (10^{-3} milliwatts per square meter), since all lengths are in kilometers.

The time-varying phase

$$\tau = k(ct - r) \tag{II. 1}$$

is a function of the free-space wavelength λ, the propagation constant $k = 2\pi/\lambda$, the free-space velocity of radio waves $c = 299792.5 \pm 0.3$ km/sec, the time t at the radio source, and the length of a radio ray between the receiver and the source.

Figure II-1 illustrates three sets of coordinates which are useful in studying the phase and polarization characteristics associated with the radiation pattern or response pattern of an antenna. Let $\vec{r} = \hat{r}\, r$ represent the vector distance between the antenna and a distant point, specified either in terms of a right-handed cartesian unit vector coordinate system $\hat{x}_o$, $\hat{x}_1$, $\hat{x}_2$ or in terms of polar coordinates r, θ, ϕ:

$$\vec{r} = \hat{r}\, r = \hat{x}_o x_0 + \hat{x}_1 x_1 + \hat{x}_2 x_2, \qquad r^2 = x_0^2 + x_1^2 + x_2^2 \tag{II. 2a}$$

$$x_0 = r\cos\theta, \qquad x_1 = r\sin\theta\cos\phi, \qquad x_2 = r\sin\theta\sin\phi \tag{II. 2b}$$

$$\hat{r} = \hat{r}(\theta, \phi) = \hat{x}_o\cos\theta + (\hat{x}_1\cos\phi + \hat{x}_2\sin\phi)\sin\theta \tag{II. 2c}$$

As a general rule, either of two antennas separated by a distance r is in the far field or radiation field of the other antenna if $r > 2D^2/\lambda$, where D is the largest linear dimension of either antenna.

The amplitude and polarization of electric field vectors $\vec{e}_\theta$ and $\vec{e}_\phi$, perpendicular to each other and to $\hat{r}$, is often calculated or measured to correspond to the right-handed cartesian unit vector coordinate system $\hat{r}$, $\hat{e}_\theta$, $\hat{e}_\phi$ illustrated in figure II-1. The unit vector $\hat{e}_\phi$ is perpendicular to $\hat{r}$ and $\hat{x}_o$, and $\hat{e}_\theta$ is perpendicular to $\hat{e}_\phi$ and $\hat{r}$. In terms of vector cross-products:

$$\hat{e}_\phi = (\hat{r} \times \hat{x}_o)/\sin\theta = \hat{x}_1\sin\phi - \hat{x}_2\cos\phi \tag{II. 3a}$$

$$\hat{e}_\theta = \hat{e}_\phi \times \hat{r} = (\hat{x}_o - \hat{r}\cos\theta)/\sin\theta \tag{II. 3b}$$

The directive gain g, a scalar, may be expressed as the sum of directive gains g_θ and g_ϕ associated with polarization components $\vec{e}_\theta \equiv \hat{e}_\theta e_\theta$ and $\vec{e}_\phi \equiv \hat{e}_\phi e_\phi$, where the coefficients e_θ and e_ϕ are expressed in volts/km:

$$g = g_\theta + g_\phi \tag{II. 4}$$

Subscripts t and r are used to refer to the gains g_t and g_r of transmitting and receiving antennas, while g is the ratio of the available mean power flux density and e_o^2/η_o, where

e_o as defined by (II.5) is the free space field strength at a distance r in kilometers from an isotropic antenna radiating p_t watts:

$$e_o = [\eta_o p_t/(4\pi r^2)]^{1/2} \text{ volts/km} \tag{II.5}$$

Here, $\eta_o = 4\pi c \cdot 10^{-7} = 376.7304 \pm 0.0004$ ohms is the characteristic impedance of free space. The maximum amplitudes of the θ and ϕ components of a radiated or incident field are $|\vec{e}_\theta|\sqrt{2}$ and $|\vec{e}_\phi|\sqrt{2}$, where

$$|\vec{e}_\theta| = e_\theta = e_o g_\theta^{1/2} \text{ volts/km}, \qquad |\vec{e}_\phi| = e_\phi = e_o g_\phi^{1/2} \text{ volts/km} \tag{II.6}$$

If phases τ_θ and τ_ϕ are associated with the electric field components $\vec{e}_\theta$ and $\vec{e}_\phi$, which are in phase quadrature in space but not necessarily in time, the total complex wave at any point $\vec{r}$ is

$$\sqrt{2}\,(\vec{e}_r + i\vec{e}_i)\exp(i\tau) = \sqrt{2}\,[\vec{e}_\theta \exp(i\tau_\theta) + \vec{e}_\phi \exp(i\tau_\phi)]\exp(i\tau) \tag{II.7}$$

From this expression and a knowledge of $\vec{e}_{\theta,\phi}$, $\tau_{\theta,\phi}$, we may determine the real and imaginary components $\vec{e}_r$ and $\vec{e}_i$, which are in phase quadrature in time but not necessarily in space:

$$\vec{e}_r \equiv \hat{e}_r e_r = \vec{e}_\theta \cos\tau_\theta + \vec{e}_\phi \cos\tau_\phi \tag{II.8a}$$

$$\vec{e}_i \equiv \hat{e}_i e_i = \vec{e}_\theta \sin\tau_\theta + \vec{e}_\phi \sin\tau_\phi \tag{II.8b}$$

The next section of this annex introduces components of this wave which are in phase quadrature in both time and space.

II.2 Principal and Cross-Polarization Components

Principal and cross-polarization components of an incident complex wave $\sqrt{2}\,(\vec{e}_r + i\vec{e}_i)\exp(i\tau)$ may be defined in terms of a time-independent phase τ_i which is a function of $\vec{r}$ [Kales, 1951]. If we write

$$\vec{e}_r + i\vec{e}_i = (\vec{e}_1 + i\vec{e}_2)\exp(i\tau_i) \tag{II.9}$$

and solve for the real and imaginary components of the complex vector $\vec{e}_1 + i\vec{e}_2$, we find that

$$\vec{e}_1 \equiv \hat{e}_1 e_1 = \vec{e}_r \cos\tau_i + \vec{e}_i \sin\tau_i \tag{II.10a}$$

$$\vec{e}_2 \equiv \hat{e}_2 e_2 = \vec{e}_i \cos\tau_i - e_r \sin\tau_i \tag{II.10b}$$

Whichever of these vectors has the greater magnitude is the principal polarization component $\vec{e}_p$, and the other is the orthogonal cross-polarization component $\vec{e}_c$:

$$e_1^2 = e_r^2 \cos^2\tau_i + e_i^2 \sin^2\tau_i + \vec{e}_r \cdot \vec{e}_i \sin(2\tau_i) \tag{II.11a}$$

$$e_2^2 = e_r^2 \sin^2\tau_i + e_i^2 \cos^2\tau_i - \vec{e}_r \cdot \vec{e}_i \sin(2\tau_i) \tag{II.11b}$$

The phase angle τ_i is determined from the condition that $\vec{e}_1 \cdot \vec{e}_2 = 0$:

$$\tan(2\tau_i) = 2\vec{e}_r \cdot \vec{e}_i / (e_r^2 - e_i^2) \tag{II.12}$$

Any incident plane wave, traveling in a direction $-\hat{f}$ is then represented as the real part of the complex wave given by

$$\sqrt{2}\,\vec{e}\exp[i(\tau + \tau_i)] \equiv \sqrt{2}\,(\vec{e}_p + i\vec{e}_c)\exp[i(\tau + \tau_i)] \tag{II.13}$$

The principal and cross-polarization directions $\hat{e}_p$ and $\hat{e}_c$ are chosen so that their vector product is a unit vector in the direction of propagation:

$$\hat{e}_p \times \hat{e}_c = -\hat{f} \tag{II.14}$$

A bar is used under the symbol for the complex vector $\vec{\underline{e}} \equiv \vec{e}_p + i\vec{e}_c$ in (II.13) to distinguish it from real vectors such as $\vec{e}_\theta$, $\vec{e}_\phi$, $\vec{e}_r$, $\vec{e}_i$, $\vec{e}_p$, and $\vec{e}_c$. The absolute values of the vector coefficients e_p and e_c may be found using (II.11).

As the time t at the transmitter or the time τ at the receiver increases, the real vector component of (II.13), or "polarization vector",

$$\sqrt{2}\,[\vec{e}_p \cos(\tau + \tau_i) - \vec{e}_c \sin(\tau + \tau_i)]$$

describes an ellipse in the plane of the orthogonal unit vectors $\hat{e}_p = \vec{e}_p/e_p$ and $\hat{e}_c = \vec{e}_c/e_c$. Looking in the direction of propagation $-r(\theta,\phi)$ with e_p and e_c both positive or both negative, we see a clockwise rotation of the polarization vector as τ increases.

Right-handed polarization is defined by the IRE or IEEE and in CCIR Report 321 [1963m] to correspond to a clockwise rotation of a polarization ellipse, looking in the direction of propagation with r fixed and t or τ increasing. This is opposite to the definition used in classical physics.

The "axial ratio" e_c/e_p of the polarization ellipse of an incident plane wave $\sqrt{2}\,\vec{\underline{e}}\exp[i(\tau + \tau_o)]$ is denoted here as

$$a_x \equiv e_c/e_p \qquad \text{(II. 15)}$$

and may be either positive or negative depending on whether the polarization of the incident wave is right-handed or left-handed. The range of possible values for a_x is -1 to +1.

II.3 Unit Complex Polarization Vectors

If the receiving antenna were a point source of radio waves, it would produce a plane wave $\sqrt{2}\,\vec{\underline{e}}_r \exp[i(\tau + \tau_r)]$ at a point $\vec{r}$ in free space. The receiving pattern of such an antenna as it responds to an incident plane wave $\sqrt{2}\,\vec{\underline{e}} \exp[i(\tau + \tau_r)]$ traveling in the opposite direction $-\hat{f}$ is proportional to the complex conjugate of $\vec{\underline{e}}_r \exp(i\tau_r)$ [S. A. Schelkunoff and H. T. Friis, 1952]:

$$[\vec{\underline{e}}_r \exp(i\tau_r)]^* = (\vec{e}_{pr} - i\vec{e}_{cr}) \exp(-i\tau_r) \tag{II.16}$$

The axial ratio e_{cr}/e_{pr} of the type of wave that would be radiated by a receiving antenna is defined for propagation in the direction $\hat{f}$. An incident plane wave, however, is propagating in the direction $-\hat{f}$, and by definition the sense of polarization of an antenna used for reception is opposite to the sense of polarization when the antenna is used as a radiator. The polarization associated with a receiving pattern is right-handed or left-handed depending on whether a_{xr} is positive or negative, where

$$a_{xr} \equiv -e_{cr}/e_{pr}, \qquad e_{cr} = -e_{pr} a_{xr} \tag{II.17}$$

The amplitudes $|e_{pr}|$ and $|e_{cr}|$ of the principal and cross-polarization field components $\vec{e}_{pr}$ and $\vec{e}_{cr}$ are proportional to the square roots of principal and cross-polarization directive gains g_{pr} and g_{cr}, respectively. It is convenient to define a unit complex polarization vector $\hat{\underline{p}}_r$ which contains all the information about the polarization response associated with a receiving pattern:

$$\hat{\underline{p}}_r = (\hat{e}_{pr} + i\hat{e}_{cr} a_{xr})(1 + a_{xr}^2)^{-1/2} \tag{II.18}$$

$$a_{xr}^2 = g_{cr}/g_{pr} \tag{II.19}$$

The directions $\hat{e}_{pr}$ and $\hat{e}_{cr}$ are chosen so that

$$\hat{e}_{pr} \times \hat{e}_{cr} = \hat{f} \tag{II.20}$$

In a similar fashion, the axial ratio a_x defined by (II.15) and the orientations $\hat{e}_p$ and $\hat{e}_c$ of the principal and cross-polarization axes of the polarization ellipse completely describe the state of polarization of an incident wave $\sqrt{2}\,\vec{\underline{e}} \exp[i(\tau + \tau_i)]$, and its direction of propagation $-\hat{f} = e_p \times e_c$. The unit complex polarization vector for the incident wave is

$$\hat{\underline{p}} = \vec{\underline{e}} / |\vec{\underline{e}}| = (\hat{e}_p + i\hat{e}_c a_x)(1 + a_x^2)^{-1/2} \qquad \text{(II. 21)}$$

The magnitude of a complex vector $\vec{\underline{e}} = \vec{e}_p + i\vec{e}_c$ is the square root of the product of $\vec{\underline{e}}$ and its complex conjugate $\vec{e}_p - i\vec{e}_c$:

$$|\vec{\underline{e}}| = (\vec{\underline{e}} \cdot \vec{\underline{e}}^*)^{1/2} = (e_p^2 + e_c^2)^{1/2} \quad \text{volts/km} \qquad \text{(II. 22)}$$

II.4 Power Flux Densities

The coefficients e_p and e_c of the unit vectors $\hat{e}_p$ and $\hat{e}_c$ are chosen to be r.m.s. values of field strength, expressed in volts/km, and the mean power flux densities s_p and s_c associated with these components are

$$s_p = e_p^2/\eta_o \quad \text{watts/km}^2, \qquad s_c = e_c^2/\eta_o \quad \text{watts/km}^2 \tag{II.23}$$

The corresponding principal and cross-polarization directive gains g_p and g_c are

$$g_p = 4\pi r^2 s_p/p_t, \qquad g_c = 4\pi r^2 s_c/p_t \tag{II.24}$$

where p_t is the total power radiated from the transmitting antenna. This is the same relation as that expressed by (II.6) between the gains g_θ, g_ϕ, and the orthogonal polarization components $\vec{e}_\theta$ and $\vec{e}_\phi$.

The total mean power flux density s at any point where $\vec{e}$ is known to be in the radiation field of the transmitting antenna and any reradiating sources is

$$s = |\vec{e}|^2/\eta_o = g e_o^2/\eta_o = s_p + s_c = (e_p^2 + e_c^2)/\eta_o$$

$$= (e_r^2 + e_i^2)/\eta_o = (e_\theta^2 + e_\phi^2)/\eta_o \quad \text{watts/km}^2 \tag{II.25a}$$

$$g = g_p + g_c = g_\theta + g_\phi = 4\pi r^2 s/p_t = s\,\eta_o/e_o^2 \tag{II.25b}$$

where e_o is given by (II.5). The power flux density s is proportional to the transmitting antenna gain g_t, but in general g is not equal to g_t as there may be a fraction a_p of energy absorbed along a ray path or scattered out of the path. We therefore write

$$g \equiv g_p(1 + a_x^2) = a_p g_{pt}(1 + a_x^2) = a_p g_t \tag{II.26}$$

The path absorption factor a_p can also be useful in approximating propagation mechanisms which are more readily described as a sum of modes than by using geometric optics. For instance, in the case of tropospheric ducting a single dominant TEM mode may correspond theoretically to an infinite number of ray paths, and yet be satisfactorily approximated by a single great-circle ray path if a_p is appropriately defined. In such a case, a_p will occasionally be greater than unity rather than less.

Orienting a receiving dipole for maximum reception to determine s_p and for minimum reception to determine s_c will also determine $\hat{e}_p$ and $\hat{e}_c$, except in the case of circular polarization, where the direction of $\hat{e}_p$ in the plane normal to $\vec{r}$ is arbitrary. In the general case where $|a_x| < 1$, either of two opposite directions along the line of principal polarization is equally suitable for $\hat{e}_p$.

Reception with a dipole will not show the sense of polarization. Right-handed and left-handed circularly polarized receiving antennas will in theory furnish this information, since $\vec{\underline{e}}$ may also be written to correspond to the difference of right-handed and left-handed circularly polarized waves which are in phase quadrature in time and space:

$$\vec{\underline{e}} \equiv (\hat{e}_p + i\hat{e}_c)\left(\frac{e_p + e_c}{2}\right) - i(\hat{e}_c - i\hat{e}_p)\left(\frac{e_p - e_c}{2}\right) \qquad \text{(II. 27)}$$

The mean power flux densities s_r and s_ℓ associated with right-handed and left-handed polarizations are

$$s_r = (e_p + e_c)^2/(2\eta_o) \text{ watts/km}^2 \qquad \text{(II. 28a)}$$

$$s_\ell = (e_p - e_c)^2/(2\eta_o) \text{ watts/km}^2 \qquad \text{(II. 28b)}$$

so the sense of polarization may be determined by whether s_r/s_ℓ is greater than or less than unity. The flux densities s_r and s_ℓ are equal only for linear polarization, where $e_c = 0$.

II. 5 Polarization Efficiency

The polarization efficiency for a transfer of energy from a single plane wave to the terminals of a receiving antenna at a given radio frequency may be expressed as a function of the unit complex polarization vectors defined by (II.18) and (II.21) and the angle ψ_p between principal polarization directions associated with $\vec{\underline{e}}$ and $\vec{\underline{e}}_r$. This polarization efficiency is

$$|\hat{\underline{p}} \cdot \hat{\underline{p}}_r|^2 = \frac{\cos^2\psi_p (a_x a_{xr} + 1)^2 + \sin^2\psi_p (a_x + a_{xr})^2}{(a_x^2 + 1)(a_{xr}^2 + 1)} \qquad \text{(II.29)}$$

where

$$\hat{e}_p \cdot \hat{e}_{pr} = -\hat{e}_c \cdot \hat{e}_{cr} = \cos\psi_p, \qquad \hat{e}_p \cdot \hat{e}_{cr} = \hat{e}_{pr} \cdot \hat{e}_c = \sin\psi_p \qquad \text{(II.30)}$$

As noted in section 2 following (2.27), any receiving antenna is completely "blind" to an incoming plane wave $\sqrt{2}\,\vec{\underline{e}} \exp[i(\tau + \tau_i)]$ which has a sense of polarization opposite to that of the receiving antenna if the eccentricities of the polarization ellipses are the same $\left(|a_x| = |a_{xr}|\right)$ and if the principal polarization direction $\hat{e}_p$ of the incident wave is perpendicular to $\hat{e}_{pr}$. In such a case, $\cos\psi_p = 0$, $a_x = -a_{xr}$, and (II.29) shows that the polarization efficiency $|\hat{\underline{p}} \cdot \hat{\underline{p}}_r|^2$ is zero. As an interesting special case, reflection of a circularly polarized wave incident normally on a perfectly conducting sheet will change the sense of polarization so that the antenna which radiates such a wave cannot receive the reflected wave. In such a case $a_x = -a_{xr} = \pm 1$, so that $|\hat{\underline{p}} \cdot \hat{\underline{p}}_r|^2 = 0$ for any value of ψ_p.

On the other hand, the polarization efficiency given by (II.29) is unity and a maximum transfer of power will occur if $a_x = a_{xr}$ and $\psi_p = 0$, that is, if the sense, eccentricity, and principal polarization direction of the receiving antenna match the sense, eccentricity, and principal polarization direction of the incident wave.

For transmission in free space, antenna radiation efficiencies, their directive gains, and the polarization coupling efficiency are independent quantities, and all five must be maximized for a maximum transfer of power between the antennas. A reduction in either one of the directive gains $g(-\hat{f})$ and $g_r(\hat{f})$ or a reduction in the polarization efficiency $|\hat{\underline{p}} \cdot \hat{\underline{p}}_r|^2$ will reduce the transfer of power between two antennas.

With each plane wave incident on the receiving antenna there is associated a ray of length r from the transmitter, an initial direction of radiation, and the radiated wave $\vec{\underline{e}}_t \exp[i(\tau + \tau_t)]$ which would be found in free space at this distance and in this direction. When it is practical to separate antenna characteristics from environmental and path characteristics, it is assumed that the antenna phase response τ_t, like τ_r, is a characteristic of the antenna and its environment and that

$$\tau_i = \tau_t + \tau_p \qquad \text{(II.31)}$$

where τ_p is a function of the ray path and includes allowances for path length differences and diffraction or reflection phase shifts.

Random phase changes in either antenna, absorption and reradiation by the environment, or random fluctuations of refractive index in the atmosphere will all tend to fill in any sharp nulls in a theoretical free-space radiation pattern $\vec{\underline{e}}$ or $\vec{\underline{e}}_r$. Also, it is not possible to have a complex vector pattern $\vec{\underline{e}}/r$ which is independent of r in the vicinity of antenna nulls unless the radiation field, proportional to $1/r$, dominates over the induction field, which is approximately proportional to $1/r^2$.

II.6 Multipath Coupling Loss

Coherently phased multipath components from a single source may arrive at a receiving antenna from directions sufficiently different so that τ_i and τ_r vary significantly. It is then important to be able to add complex signal voltages at the antenna terminals. Let $n = 1, 2, ---, N$ and assume N discrete plane waves incident on an antenna from a single source. The following expressions represent the complex open-circuit r.m.s. signal voltage v_n corresponding to a radio frequency ν cycles per second, a single incident plane wave $\sqrt{2}\,\vec{\underline{e}}_n \exp[i(\tau + \tau_{in})]$, a loss-free receiving antenna with a directivity gain g_{rn} and an effective absorbing area a_{en}, matched antenna and load impedances, and an input resistance r_ν which is the same for the antenna and its load:

$$v_n = (4 r_\nu s_n a_{en})^{1/2} (\hat{\underline{p}}_n \cdot \hat{\underline{p}}_{rn}) \exp[i(\tau + \tau_{pn} + \tau_{tn} - \tau_{rn})] \text{ volts} \qquad \text{(II.32)}$$

$$s_n = |\vec{\underline{e}}_n|^2 / \eta_o = p_r a_{pn} g_{tn} / (4\pi r_n^2) \text{ watts/km}^2 \qquad \text{(II.33)}$$

$$a_{en} = g_{rn} \lambda^2 / (4\pi) \text{ km}^2 \qquad \text{(II.34)}$$

$$\hat{\underline{p}}_n \cdot \hat{\underline{p}}_{rn} = [(1 + a_{xn}^2)(1 + a_{xrn}^2)]^{-1/2} [(1 + a_{xn} a_{xrn}) \cos\psi_{pn} + i(a_{xn} + a_{xrn}) \sin\psi_{pn}] \qquad \text{(II.35)}$$

If the polarization of the receiving antenna is matched to that of the incident plane wave, then $a_{xn} = a_{xrn}$, $\psi_{pn} = 0$, $\hat{\underline{p}}_n \cdot \hat{\underline{p}}_{rn} = 1$, and

$$v_n = [4 r_\nu p_r a_{pn} g_{tn} g_{rn} \lambda^2 / (4\pi r_n)^2]^{1/2} \exp[i(\tau + \tau_{pn} + \tau_{tn} - \tau_{rn})] \text{ volts} \qquad \text{(II.36)}$$

If the coefficient of the phasor in (II.36) has the same value for two incident plane waves, but the values of $\tau_{in} - \tau_{rn}$ differ by π radians, the sum of the corresponding complex voltages is zero. This shows that the multipath coupling efficiency can theoretically be zero even when the beam orientation and polarization coupling are maximized. Adjacent lobes in a receiving antenna directivity pattern, for instance, may be 180° out of phase and thus cancel two discrete in-phase plane-wave components.

Equation (2.6) in section 2 shows the relation between the total open-circuit r.m.s. voltage

$$v_\nu = \left[\sum_{\substack{n=1 \\ m=1}}^{N} v_n v_m^* \right]^{1/2} \text{ volts} \qquad \text{(II.37)}$$

and the power p_a available at the terminals of a loss-free receiving antenna:

$$p_a = v_\nu^2/(4 r_\nu) \text{ watts} \tag{II.38}$$

In writing p_a for $p_{a\nu}$ in (II.37), the subscript ν has been suppressed, as with almost all of the symbols in this annex. Studying (II.32) - (II.35), (II.37), and (II.38), it is seen that the expression for p_a is symmetrical in the antenna gains g_p, g_{pr}, and $g_c = a_x^2 g_p$, $g_{cr} = a_{xr}^2 g_{pr}$, and that p_a is a linear function of these parameters, though v_ν is not. From this follows a theorem of reciprocity, that the transmission loss $L = -10 \log (p_a/p_t)$ is the same if the roles of the transmitting and receiving antennas are reversed.

The basic transmission loss L_b is the system loss that would be expected if the actual antennas were replaced at the same locations by hypothetical antennas which are:

(a) loss-free, so that $L_{et} = L_{er} = 0$ db. See (2.3).

(b) isotropic, so that $g_t = g_r = 1$ in every direction important to propagation between the actual antennas.

(c) free of polarization coupling loss, so that $|\hat{p} \cdot \hat{p}_r|^2 = 1$ for every locally plane wave incident at the receiving antenna.

(d) isotropic in their phase response, so that $\tau_t = \tau_r = 0$ in every direction.

The available power p_{ab} corresponding to propagation between hypothetical isotropic antennas is then

$$p_{ab} = \frac{p_t \lambda^2}{(4\pi)^2} \sum_{\substack{n=1 \\ m=1}}^{N} \frac{(a_{pn} a_{pm})^{1/2} \cos(\tau_{pn} - \tau_{pm})}{r_n r_m} \tag{II.39}$$

The basic transmission loss L_b corresponding to these assumptions is

$$L_b = -10 \log (p_{ab}/p_t) = P_t - P_{ab} \text{ db} \tag{II.40}$$

The basic transmission loss in free space, L_{bf}, corresponds to $N = 1$, $a_{p1} = 1$, $\tau_{p1} = 0$, $r_1 = r$:

$$L_{bf} = -10 \log [\lambda/(4\pi r)]^2 = 32.45 + 20 \log f + 20 \log r \text{ db} \tag{II.41}$$

where f is in megacycles per second and r is in kilometers. Compare with (2.31).

As may be seen from the above relations, only a fraction s_e of the total flux density s_n per unit radiated power p_t contributes to the available received power p_a from N plane waves. While s_n is expressed in watts/km^2, s_e is expressed in watts/km^2 for each watt

of the power p_t radiated by a single source:

$$s_e = 4\pi p_a/(\lambda^2 p_t) \tag{II.42}$$

For each plane wave from a given source, $\vec{e}_{-n} \exp(i\tau_{in})$ or $\hat{p}_{rn} \exp(-i\tau_{rn})$ may sometimes be regarded as a statistical variable chosen at random from a uniform distribution, with all phases from $-\pi$ to π equally likely. Then real power proportional to $|\vec{e}_{-n} \cdot \vec{e}^{*}_{-rn}|^2$ may be added at the antenna terminals, rather than the complex voltages defined by (II.32) - (II.35). For this case, the statistical "expected value" $\langle s_e \rangle$ of s_e is

$$\langle s_e \rangle = \sum_{n=1}^{N} a_{pn} g_{tn} g_{rn} |\hat{p}_n \cdot \hat{p}_{rn}|^2/(4\pi r_n^2) \tag{II.43}$$

In terms of s_e, the transmission loss L is

$$L = 21.46 + 20 \log f - 10 \log s_e \quad \text{db} \tag{II.44}$$

Substituting $\langle s_e \rangle$ for s_e in (II.44), we would not in general obtain the statistical expected value $\langle L \rangle$ of L, since $\langle L \rangle$ is an ensemble average of logarithms, which may be quite different from the logarithm of the corresponding ensemble average $\langle s_e \rangle$. For this reason, median values are often a more practical measure of central tendency than "expected" values. With p_t and λ fixed, median values of s_e and L always obey the relation (II.44), while average values of s_e and L often do not.

The remainder of this appendix is concerned with a few artificial problems designed to show how these formulas are used and to demonstrate some of the properties of radiation and response patterns. In general, information is needed about antenna patterns only in the few directions which are important in determining the amplitude and fading of a tropospheric signal. Although section II.7 shows how a complex vector radiation or reception pattern may be derived from an integral over all directions, it is proposed that the power radiation efficiencies and the gains $g_r(\hat{r})$ or $g_t(-\hat{r})$ for actual antennas should be determined by measurements in a few critical directions using standard methods and a minimum of calculations.

II.7 Idealized Theoretical Antenna Patterns

Consider a point source of plane waves, represented by complex dipole moments in three mutually perpendicular directions, $\hat{x}_o$, $\hat{x}_1$, and $\hat{x}_2$. These three unit vectors, illustrated in figure II.1, define a right-handed system, and it is assumed that the corresponding elementary dipoles support r.m.s. currents of I_0, I_1, and I_2 amperes, respectively. The corresponding peak scalar current dipole moments are $\sqrt{2}\, I_m \ell$ ampere-kilometers, where $m = 0, 1, 2$, and the sum of the complex vector dipole moments $\hat{x}_m \sqrt{2}\, I_m \ell \exp(i\tau_m)$ may be expressed as follows:

$$\underline{\vec{a}} = \vec{a}_1 + i\vec{a}_2 \tag{II.45a}$$

$$\vec{a}_1 = \sqrt{2}\, I\ell(\hat{x}_o c_0 + \hat{x}_1 c_1 + \hat{x}_2 c_2), \qquad \vec{a}_2 = \sqrt{2}\, I\ell(\hat{x}_o s_0 + \hat{x}_1 s_1 + \hat{x}_2 s_2) \tag{II.45b}$$

$$I^2 = I_0^2 + I_1^2 + I_2^2, \qquad c_m = (I_m/I)\cos\tau_m, \qquad s_m = (I_m/I)\sin\tau_m, \qquad m = 0, 1, 2. \tag{II.46}$$

Here, τ_0, τ_1, and τ_2 represent initial phases of the currents supported by the elementary dipoles. The time phase factor is assumed to be $\exp(ikct)$.

Using the same unit vector coordinate system to represent the vector distance $\vec{r}$ from this idealized point source to a distant point:

$$\vec{r} = \hat{x}_o x_0 + \hat{x}_1 x_1 + \hat{x}_2 x_2 = \hat{r}\, r \tag{II.47}$$

where x_0, x_1, and x_2 are given by (II.2b) as functions of r, θ, ϕ. The complex wave at $\vec{r}$ due to any one of the elementary dipoles is polarized in a direction

$$\hat{r} \times (\hat{x}_m \times \hat{r}) = \hat{x}_m - \hat{r}\, x_m/r \tag{II.48}$$

which is perpendicular to the propagation direction $\hat{r}$ and in the plane of $\hat{x}_m$ and $\hat{r}$. The total complex wave at $\vec{r}$ may be represented in the form given by (II.8):

$$\sqrt{2}\,\vec{e}(\vec{r})\exp(i\tau) = \sqrt{2}\,(\vec{e}_r + i\vec{e}_i)\exp(i\tau) = \sqrt{2}\,(\vec{e}_p + i\vec{e}_c)\exp[i(\tau + \tau_t)]$$

$$= [\hat{r} \times (\underline{\vec{a}} \times \hat{r})]\,[\eta_o/(2\lambda r)]\exp(i\tau) \tag{II.49}$$

$$\tau = k(ct - r) + \pi/4 \tag{II.50}$$

$$\sqrt{2}\,\vec{e}_r = [\vec{a}_1 - \hat{r}(\vec{a}_1 \cdot \hat{r})]\,\eta_o/(2\lambda r) \text{ volts/km} \tag{II.51a}$$

$$\sqrt{2}\,\vec{e}_i = [\vec{a}_2 - \hat{f}(\vec{a}_2 \cdot \hat{f})]\,\eta_o/(2\lambda r) \text{ volts/km} \qquad \text{(II. 51b)}$$

The total mean power flux density $s(\vec{r})$ at $\vec{r}$ is given by (II.13):

$$s(\vec{r}) = (e_r^2 + e_i^2)/\eta_o = [a_1^2 - (\vec{a}_1 \cdot \hat{r})^2 + a_2^2 - (\vec{a}_2 \cdot \hat{r})^2]/\eta_o$$

$$= \frac{\eta_o (I\ell)^2}{4\lambda^2 r^2}\left[1 - (I_0^2 x_0^2 + I_1^2 x_1^2 + I_2^2 x_2^2)/(Ir)^2 - 2(c_{01} x_0 x_1 + c_{02} x_0 x_2 + c_{12} x_1 x_2)/r^2\right] \qquad \text{(II. 52)}$$

$$c_{mn} = (I_m I_n / I^2)\cos(\tau_m - \tau_n)\,. \qquad \text{(II. 53)}$$

The total radiated power p_t is obtained by integrating $s(r)$ over the surface of a sphere of radius r, using the spherical coordinates r, θ, ϕ illustrated in figure II. 1:

$$p_t = \int_o^{2\pi} d\phi \int_o^{\pi} d\theta\, r^2\, s(\vec{r}) \sin\theta = \frac{2\pi\,\eta_o (I\ell)^2}{3\lambda^2} \text{ watts} \qquad \text{(II. 54)}$$

From (II.54) it is seen that the peak scalar dipole moment $\sqrt{2}I\ell$ used to define $\vec{a}_1$ and $\vec{a}_2$ in (II.45) may be expressed in terms of the total radiated power:

$$\sqrt{2}I\ell = \lambda\sqrt{3p_t/(\pi\eta_o)} \text{ ampere-kilometers} \qquad \text{(II. 55)}$$

The directive gain $g(\hat{r})$ is

$$g(\hat{r}) = 4\pi r^2\, s(\vec{r})/p_t = \frac{3}{2}\left[1 - \left(\frac{I_0}{I}\right)^2 \cos^2\theta - \left(\frac{I_1}{I}\right)^2 \sin^2\theta \cos^2\phi\right.$$

$$\left. - \left(\frac{I_2}{I}\right)^2 \sin^2\theta \sin^2\phi - \left(c_{01}\cos\phi + c_{02}\sin\phi\right)\sin(2\theta) - c_{12}\sin^2\theta\,\sin(2\phi)\right] \qquad \text{(II. 56)}$$

This is the most general expression possible for the directive gain of any combination of elementary electric dipoles centered at a point. Studying (II.56), it may be shown that no combination of values for I_0, I_1, I_2, τ_0, τ_1, τ_2 will provide an isotropic radiator. As defined in this appendix, an isotropic antenna radiates or receives waves of any phase and polarization equally in every direction.

For the special case where $I_0 = I_1 = I_2 = I/\sqrt{3}$, $\tau_0 = \pi/2$, $\tau_1 = 0$, and $\tau_2 = \pi$, (II.57) shows that

$$g(\hat{r}) = 1 + \sin^2\theta \sin\phi \cos\phi \qquad \text{(II.57)}$$

With these specifications, (II.46) shows that $c_0 = 0$, $c_1 = -c_2 = 1/\sqrt{3}$, $s_0 = 1/\sqrt{3}$, $s_1 = s_2 = 0$, and (II.45) with (II.55) shows that

$$\vec{a}_1 = (\hat{x}_1 - \hat{x}_2)b\,, \qquad \vec{a}_2 = \hat{x}_o b \qquad \text{(II.58a)}$$

$$b = \lambda\left[p_r/(\pi\eta_o)\right]^{1/2} \qquad \text{(II.58b)}$$

Substituting next in (II.51) with the aid of (II.2):

$$\sqrt{2}\,\vec{e}_r = e_o(\hat{x}_1 - \hat{x}_2 - \hat{r}\,b_2)\,, \qquad \sqrt{2}\,\vec{e}_i = e_o(\hat{x}_o - \hat{r}\cos\theta) \qquad \text{(II.59)}$$

$$e_o = \left[\eta_o\, p_t/(4\pi r^2)\right]^{1/2}\,, \qquad b_2 = \sin\theta(\cos\phi - \sin\phi) \qquad \text{(II.60)}$$

The principal and cross-polarization gains determined using (II.24) and (II.25) are

$$g_p(\hat{r}) = 1 + \sin^2\theta(\sin\phi\cos\phi - \tfrac{1}{2})\,, \qquad g_c(\hat{r}) = \tfrac{1}{2}\sin^2\theta \qquad \text{(II.61)}$$

The subscripts p and c in (II.61) should be reversed whenever $g(\theta, \phi)$ is less than $\sin^2\theta$. Minimum and maximum values of g are 1/2 and 3/2 while g_p ranges from 1/3 to 1 and g_c from 0 to 1/2.

The importance of phases to multipath coupling is more readily demonstrated using a somewhat more complicated antenna. The following paragraphs derive an expression for a wave which is approximately plane at a distance r exceeding 200 wavelengths, radiated by an antenna composed of two three-dimensional complex dipoles located at $-5\lambda\hat{x}_o$ and $+5\lambda\hat{x}_o$ and thus spaced 10 wavelengths apart. When the radiation pattern has been determined, it will be assumed that this is the receiving antenna. Its response to known plane waves from two given directions will then be calculated.

With the radiated power p_t divided equally between two three-dimensional complex dipoles, $\vec{\underline{a}}$ is redefined as

$$\vec{\underline{a}} = (b/\sqrt{2})\,\vec{\underline{a}}_o\,, \qquad \vec{\underline{a}}_o = \hat{x}_1 - \hat{x}_2 + i\hat{x}_o \qquad \text{(II.62)}$$

Since 5λ is negligible compared to r except in phase factors critically depending on $r_1 - r_2$, the exact expressions

$$\vec{r}_1 = \vec{r} - 5\lambda\,\hat{x}_o\,, \qquad \vec{r}_2 = \vec{r} + 5\lambda\,\hat{x}_o \tag{II.63}$$

lead to the following approximations and definitions:

$$r_1 = r(1-\epsilon)\,, \quad r_2 = r(1+\epsilon)\,, \quad \epsilon = 5(\lambda/r)\cos\theta \tag{II.64}$$

$$\hat{r}_1 = \hat{r}(1+\epsilon) - \hat{x}_o\epsilon\,\sec\theta\,, \quad \hat{r}_2 = \hat{r}(1-\epsilon) + \hat{x}_o\epsilon\,\sec\theta \tag{II.65}$$

$$\hat{r} = \hat{x}_o\cos\theta + (\hat{x}_1\cos\phi + \hat{x}_2\sin\phi)\sin\theta \tag{II.66}$$

For distances r exceeding 200 wavelengths, $|\epsilon| < 0.025$ and ϵ^2 is neglected entirely, so that

$$\hat{r}_1\,r_1 = \vec{r} - 5\lambda\,\hat{x}_o\,, \qquad \hat{r}_2\,r_2 = \vec{r} + 5\lambda\,\hat{x}_o \tag{II.67}$$

At a point $\vec{r}$, the complex wave radiated by this antenna is approximately plane and may be represented as

$$\sqrt{2}\left(\vec{e}_r + i\,\vec{e}_i\right)\exp(i\tau) = \sqrt{2}\left[\vec{\underline{e}}_1\exp(i\tau_1) + \vec{\underline{e}}_2\exp(i\tau_2)\right] \tag{II.68}$$

where

$$\tau = k(ct - r) + \pi/4 \tag{II.69}$$

$$\tau_1 = \tau + \tau_a\,, \qquad \tau_2 = \tau - \tau_a\,, \qquad \tau_a = 10\pi\cos\theta \tag{II.70}$$

As in (II.49), the waves radiated by the two main elements of this antenna are represented in (II.68) as the product of phasors $\exp(i\tau_1)$ and $\exp(i\tau_2)$ multiplied by the complex vectors $\sqrt{2}\,\vec{\underline{e}}_1$ and $\sqrt{2}\,\vec{\underline{e}}_2$, respectively:

$$\sqrt{2}\,\vec{\underline{e}}_1 = \left[\hat{r}_1 \times \left(\vec{\underline{a}} \times \hat{r}_1\right)\right]\eta_o/(2\lambda r) = (e_o/2)\left[\vec{\underline{a}}_o - \hat{r}_1\left(\vec{\underline{a}}_o \cdot \hat{r}_1\right)\right] \tag{II.71a}$$

$$\sqrt{2}\,\vec{\underline{e}}_2 = \left[\hat{r}_2 \times \left(\vec{\underline{a}} \times \hat{r}_2\right)\right]\eta_o/(2\lambda r) = (e_o/2)\left[\vec{\underline{a}}_o - \hat{r}_2\left(\vec{\underline{a}}_o \cdot \hat{r}_2\right)\right] \tag{II.71b}$$

Evaluating $\vec{a}_o \cdot \hat{r}_1$, $\vec{a}_o \cdot \hat{r}_2$, $\vec{e}_1$, and $\vec{e}_2$ with the aid of (II.62), (II.65), (II.66) and (II.71):

$$\vec{a}_o \cdot \hat{r}_1 = b_2(1+\epsilon) + i\left[\cos\theta - \epsilon(\sec\theta - \cos\theta)\right] \tag{II.72a}$$

$$\vec{a}_o \cdot \hat{r}_2 = b_2(1-\epsilon) + i\left[\cos\theta + \epsilon(\sec\theta - \cos\theta)\right] \tag{II.72b}$$

$$\vec{e}_1 = (e_o/2)\left\{\left[\hat{x}_1 - \hat{x}_2 - \hat{r}\, b_2(1+2\epsilon) + \hat{x}_o b_2\, \epsilon \sec\theta\right]\right.$$

$$\left. + i\left[\hat{x}_o(1+\epsilon) - \hat{r}\cos\theta + \hat{r}\,\epsilon(\sec\theta - 2\cos\theta)\right]\right\} \tag{II.73a}$$

$$\vec{e}_2 = (e_o/2)\left\{\left[\hat{x}_1 - \hat{x}_2 - \hat{r}\, b_2(1-2\epsilon) - \hat{x}_o b_2\, \epsilon \sec\theta\right]\right.$$

$$\left. + i\left[\hat{x}_o(1-\epsilon) - \hat{r}\cos\theta - \hat{r}\,\epsilon(\sec\theta - 2\cos\theta)\right]\right\} \tag{II.73b}$$

Since the sum and difference of $\exp(i\tau_1)$ and $\exp(i\tau_2)$ are $2\cos\tau_a \exp(i\tau)$ and $2i\sin\tau_a \exp(i\tau)$, respectively, $\vec{e}_r$ and $\vec{e}_i$ as defined by (II.68) are

$$\vec{e}_r = e_o\left\{\left[\hat{x}_1 - \hat{x}_2 - \hat{r}\, b_2\right]\cos\tau_a - \epsilon\left[\hat{x}_o + \hat{r}(\sec\theta - 2\cos\theta)\right]\sin\tau_a\right\} \tag{II.74a}$$

$$\vec{e}_i = e_o\left\{\left[\hat{x}_o - \hat{r}\cos\theta\right]\cos\tau_a - b_2\left[2\hat{r} - \hat{x}_o \sec\theta\right]\sin\tau_a\right\} \tag{II.74b}$$

The complex wave $\sqrt{2}\left(\vec{e}_r + i\vec{e}_i\right)$ is a plane wave only when $\vec{e}_r$ and $\vec{e}_i$ are both perpendicular to the direction of propagation, $\hat{r}$, or when

$$\hat{r} \cdot \left(\vec{e}_r + i\vec{e}_i\right) = \epsilon \sin\tau_a\left[(\cos\theta - \sec\theta) + i\sin\theta(\cos\phi - \sin\phi)\right] = 0 \tag{II.75}$$

which requires that $\epsilon = 0$, $\sin\tau_a = 0$, or $\theta = 0$. If ϵ is negligible, the total mean power flux density in terms of the directive gain $g(\hat{r})$ is given by

$$s(\vec{r}) = \left(e_r^2 + e_i^2\right)/\eta_o = g(\hat{r})\, e_o^2/\eta_o \tag{II.76}$$

$$g(\hat{r}) = 2(1 + \sin^2\theta \sin\phi \cos\phi)\cos^2\tau_a \qquad \text{(II. 77)}$$

That p_t is the corresponding total radiated power may be verified by substituting (II.76) and (II.77) in (II.54), with the aid of (II.60) and (II.70).

Now let this antenna be a receiving antenna, and suppose that direct and ground-reflected waves arrive from directions $\hat{r}(\theta, \phi)$ equal to

$$\hat{r}_1(0.32, \pi/4) = 0.9492\,\hat{x}_o + 0.2224(\hat{x}_1 + \hat{x}_2) \qquad \text{(II.78a)}$$

$$\hat{r}_2(0.28, 0.75) = 0.9611\,\hat{x}_o + 0.1430\,\hat{x}_1 + 0.1332\,\hat{x}_2 \qquad \text{(II.78b)}$$

Note that $\hat{r}_1$ and $\hat{r}_2$ in (II.78) are not related to $\hat{r}_1$ and $\hat{r}_2$ in (II.65), but are two particular values of $\hat{r}$. Corresponding values of τ_a, $\cos\tau_a$, and $\sin\tau_a$ are

$$\tau_{a1} = 29.82111\,, \quad \cos\tau_{a1} = -0.0240\,, \quad \sin\tau_{a1} = -0.9997 \qquad \text{(II. 79a)}$$

$$\tau_{a2} = 30.19245\,, \quad \cos\tau_{a2} = 0.3404\,, \quad \sin\tau_{a2} = -0.9403 \qquad \text{(II. 79b)}$$

The incoming waves in the two directions $\hat{r}_1$ and $\hat{r}_2$ are assumed to be plane, and the distances r_1 and r_2 to their source are assumed large enough so that $\epsilon_1 \sin\tau_{a1}$ and $\epsilon_2 \sin\tau_{a2}$ are negligible compared to $\cos\tau_{a1}$ and $\cos\tau_{a2}$, respectively. The plane wave response of the receiving antenna in these directions may be expressed in terms of the complex vectors associated with $\hat{r}_1$ and $\hat{r}_2$:

$$\vec{e}_{r1} + i\vec{e}_{i1} = -0.024\,e_o\left[(\hat{x}_1 - \hat{x}_2) + i(0.099\,\hat{x}_o - 0.211\,\hat{x}_1 - 0.211\,\hat{x}_2)\right] \qquad \text{(II. 80a)}$$

$$\vec{e}_{r2} + i\vec{e}_{i2} = 0.340\,e_o\left[(-0.013\,\hat{x}_o + 0.998\,\hat{x}_1 - 1.002\,\hat{x}_2) + i(0.076\,\hat{x}_o - 0.137\,\hat{x}_1 - 0.128\,\hat{x}_2)\right] \qquad \text{(II. 80b)}$$

Since $\vec{e}_{r1} \cdot \vec{e}_{r2} = 0$, (II.11) with (II.9) and (II.10) shows that $\tau_{r1} = 0$, so that $\vec{e}_{r1}$ and $\vec{e}_{i1}$ are principal and cross-polarization components of the complex vector receiving pattern:

$$\vec{e}_{pr1} + i\vec{e}_{cr1} = \vec{e}_{r1} + i\vec{e}_{i1} \qquad \text{(II. 81a)}$$

These same equations show that $\tau_{r2} = -0.005$ and that

$$\vec{e}_{pr2} + i\vec{e}_{cr2} = 0.340\, e_o\left[(-0.013\,\hat{x}_o + 0.999\,\hat{x}_1 - 1.001\,\hat{x}_2) + i(0.076\,\hat{x}_o - 0.132\,\hat{x}_1 - 0.113\,\hat{x}_2)\right] \tag{II.81b}$$

differing only slightly from (II.80b), since τ_{r2} is almost zero.

The axial ratios of the two polarization ellipses, defined by (II.17), are

$$a_{xr1} = -0.222\,, \qquad a_{xr2} = -0.143 \tag{II.82}$$

and the unit complex polarization vectors $\hat{\underline{p}}_{r1}$ and $\hat{\underline{p}}_{r2}$ defined by (II.18) are therefore

$$\hat{\underline{p}}_{r1} = 0.674(\hat{x}_1 - \hat{x}_2) + i(0.067\,\hat{x}_o - 0.142\,\hat{x}_1 - 0.142\,\hat{x}_2) \tag{II.83a}$$

$$\hat{\underline{p}}_{r2} = (-0.009\,\hat{x}_o + 0.692\,\hat{x}_1 - 0.694\,\hat{x}_2) + i(0.053\,\hat{x}_o - 0.095\,\hat{x}_1 - 0.089\,\hat{x}_2) \tag{II.83b}$$

The antenna gains $g_r(\hat{r}_1)$ and $g_r(\hat{r}_2)$ are given by (II.77):

$$g_r(\hat{r}_1) = 0.0021, \quad g_r(\hat{r}_2) = 0.241 \tag{II.84}$$

which shows that the gain $G_r(\hat{r}_1) = 10 \log g_r(\hat{r}_1)$ associated with the direct ray is 29.2 db below that of an isotropic antenna, while the gain $G_r(\hat{r}_2)$ associated with the ground-reflected ray is -6.2 db. It might be expected that only the incident wave propagating in the direction $-\hat{r}_2$ would need to be considered in determining the complex voltage at the receiving antenna terminals. Suppose, however, that the ground-reflected ray has been attenuated considerably more than the direct ray, so that the path attenuation factor a_{p2} is 0.01, while $a_{p1} = 1$. Suppose further that the transmitting antenna gain associated with the ground-reflected ray is 6 db less than that associated with the direct ray. Then the mean incident flux density s_2 associated with the ground-reflected ray will be 26 db less than the flux density s_1 associated with the direct ray.

In order to calculate the complex received voltage v given by (II.37), then, the following is assumed:

$$r_v = 52 \text{ ohms}\,, \qquad s_1 = 1 \text{ watt/km}^2 \; (= -30 \text{ dbm/m}^2)$$

$$s_2 = 0.0025 \text{ watts/km}^2 , \quad \lambda = 0.0003 \text{ km} (f = 1000 \text{ MHz})$$

$$a_{x1} = 0.2 , \quad a_{x2} = 0.4 , \quad \psi_{p1} = \pi/2 , \quad \psi_{p2} = 1.5$$

$$\tau_{i1} = \tau_{p1} + \tau_{t1} = 0 , \quad \tau_{i2} = \tau_{p2} + \tau_{t2} = \pi \qquad \text{(II. 85)}$$

It will be seen that these assumptions imply a more nearly complete polarization coupling loss between the direct wave and the receiving antenna than between the ground-reflected wave and the receiving antenna. The effective absorbing area of the receiving antenna for each wave, as given by (II.34) is

$$a_{e1} = 1.504 \times 10^{-11} \text{ km}^2 , \quad a_{e2} = 1.726 \times 10^{-9} \text{ km}^2 \qquad \text{(II. 86)}$$

The polarization factors are

$$(\hat{\underline{p}}_1 \cdot \hat{\underline{p}}_{r1}) = - 0.021 \, i , \quad (\hat{\underline{p}}_2 \cdot \hat{\underline{p}}_{r2}) = 0.062 + 0.236 \, i \qquad \text{(II. 87)}$$

and the phase factors are $\exp(i\tau)$ and $\exp[i(\tau + 3.137)]$, respectively. Substituting these values in (II.32), the complex voltages are

$$v_1 = - 1.175(10^{-6}) i \exp(i\tau) , \quad v_2 = -(1.887 + 7.071 i)(10^{-6}) \exp(i\tau) \qquad \text{(II. 88)}$$

The real voltage at the antenna terminals, as given by (II.37) is

$$v_\nu = (v_1 + v_2)(v_1 + v_2)^* = 8.33 \times 10^{-6} \text{ volts} = 8.33 \text{ microvolts} \qquad \text{(II. 89)}$$

and the corresponding power p_a available at the terminals of the loss-free receiving antenna is

$$p_a = 0.334 \times 10^{-12} \text{ watts} , \quad P_a = - 125 \text{ dbw} = - 95 \text{ dbm} \qquad \text{(II. 90)}$$

as given by (II.38).

II. 8 Conclusions

The foregoing exercise demonstrates that:

(1) Even small changes in antenna beam orientation, transmission loss, polarization coupling, and multipath phasing may have a visible effect on the available power at the terminals of a receiving antenna.

(2) If the formulation of the general relationships for a completely polarized wave is programmed for a digital computer, it may be feasible to estimate the complete statistics of a received signal whenever reasonable assumptions can be made about the statistics of the parameters described in this annex.

(3) The measurement of antenna characteristics in a few critical directions will often be sufficient to provide valuable information to be used with the relationships given here. The measurement of Stokes' parameters, for instance, will provide information about a_{xr}, g_r, ψ_p, and both the polarized field intensity s_r and the unpolarized field intensity s_o. These parameters [Stokes, 1922] are

$$s_r + s_o = \text{total mean field intensity} \tag{II.91}$$

$$Q = s_r \cos(2\beta) \cos(2\psi_p) \tag{II.92}$$

$$U = s_r \cos(2\beta) \sin(2\psi_p) \tag{II.93}$$

$$V = s_r \sin(2\beta) \tag{II.94}$$

where

$$\beta = \tan^{-1} a_{xr} \tag{II.95}$$

The unpolarized or randomly polarized field intensity s_o is determined from (II.91) and the identity

$$s_r = (Q^2 + U^2 + V^2)^{1/2} \tag{II.96}$$

Using standard sources and antenna model ranges, the gain g_r may be determined from

$$g_r = s_r/(e_o^2/\eta_o), \quad e_o^2 = \eta_o p_t/(4\pi r^2) \tag{II.97}$$

assuming, if e_o is measured, that any power reception efficiency $1/\ell_{er}$ less than unity will affect s_r and e_o^2 alike.

Finally, a method for measuring relative phase responses τ_r is also needed. In individual cases, multipath coupling loss may be insufficient to provide adequate unwanted signal rejection. Variations of τ_r may lead to phase interference fading of wanted signals, just as variations of a_p are associated with long-term power fading. Because of the complexity of these phenomena, they are usually described in terms of cumulative distributions of signal amplitudes or fade durations. Fortunately, even crude measurements or simple theories may then suffice to provide statistical information about τ_r.

COORDINATE SYSTEMS FOR STUDYING ANTENNA PATTERNS

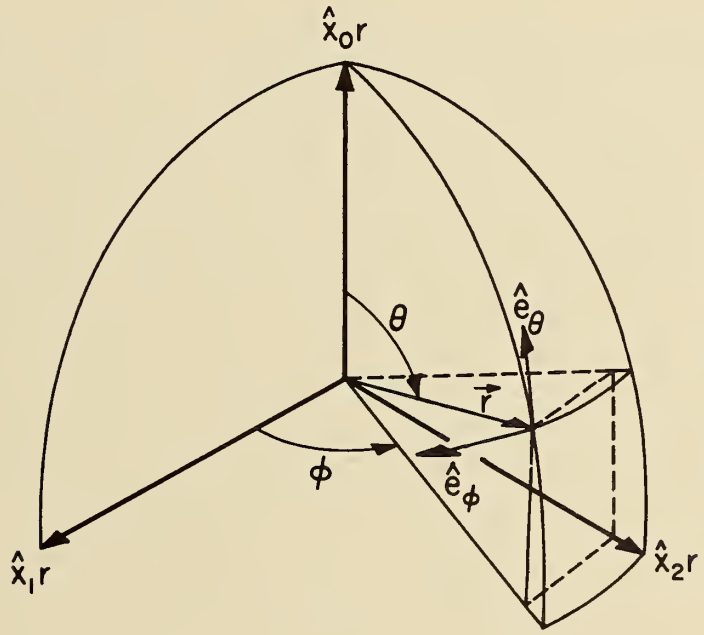

Figure II.1

Annex III

FORMULAS, COMPUTER METHODS, AND SAMPLE CALCULATIONS

The material of this annex is organized into the following sections:

1. Line-of-sight
2. Diffraction over a single isolated obstacle
3. Diffraction over a single isolated obstacle with ground reflections
4. Diffraction over irregular terrain
5. Forward scatter
6. Forward scatter with antennas elevated
7. Long-term variability
8. Sample calculations

Section 1 lists geometric optics formulas for computing transmission loss over a smooth earth, for determining the magnitude and phase of the reflection coefficient, and for computing a first Fresnel zone along a great circle path. Graphs of the magnitude R and phase c of the reflection coefficient are included. Section 2 gives mathematical expressions that approximate the curves $A(v, 0)$, $A(0, \rho)$ and $U(v\rho)$ for convenience in using a digital computer. Section 3 lists geometric optics formulas used to compute diffraction attenuation when several components of the received field are affected by reflection from the earth's surface. Section 4 defines the parameters K and b for both horizontally and vertically polarized radio waves. Section 5 shows the function $F(\theta d)$ for N_s = 250, 301, 350, and 400, and for values of s from 0.01 to 1. Curve fits to the function $F(\theta d)$ and equations for computing $H_o(\eta_s = 0)$ are included. Section 6 suggests modifications of the prediction methods for use when antenna beams are elevated or directed out of the great circle plane. Section 7 shows diurnal and seasonal changes in long-term variability. Mathematical expressions used to compute predicted distributions are shown and a method of mixing distributions is described. Section 8 illustrates the application of prediction methods to specific problems:

Example 1. Line-of-sight communication,

Example 2. Diffraction over an isolated rounded obstacle,

Example 3. A transhorizon path: diffraction and scatter losses are computed to obtain a reference median transmission loss. The predicted distribution of hourly median values of transmission loss is compared with observed values.

III. 1 Line-of-Sight

Simple formulas for line-of-sight propagation which suffice for most applications, are given in section 5 of the report. Formulas for geometry over a smooth earth and for determining the magnitude and phase of the reflection coefficient are given here. These formulas may be used when the great circle path terrain visible to both antennas will support a substantial amount of reflection, and it is reasonable to fit a smooth convex curve of radius a to this portion of the terrain.

Figure 5.1b illustrates the geometry appropriate for reflection of a single ray by a smooth earth of effective radius a. In the figure, ψ is the grazing angle at the geometrical reflection point located at a distance d_1 from an antenna of height h_1 and at a distance d_2 from an antenna of height h_2. The total path distance $d = d_1 + d_2$ is measured along an arc of radius a. The difference, Δr, between the reflected ray path length $r_1 + r_2$ and the length of the direct ray, r_o, is calculated to find the phase of a radio field which is the sum of ground-reflected and free space fields. If Δr is less than 0.06λ, these ray optics formulas are not applicable. For almost all cases of interest the angle ψ is small and the straight line distances r_1, r_2 and r_o are very nearly equal to the mean sea level arc distances d_1, d_2 and d. The geometric optics formulas given below usually require double-precision arithmetic.

$$\tan\psi = \cot(d_1/a) - (1 + h_1/a)^{-1} \csc(d_1/a) \cong \frac{h_1}{d_1} - \frac{d_1}{2a} \qquad \text{(III. 1)}$$

$$\tan\psi = \cot(d_2/a) - (1 + h_2/a)^{-1} \csc(d_2/a) \cong \frac{h_2}{d_2} - \frac{d_2}{2a} \qquad \text{(III. 2)}$$

$$r_o = a\left\{(h_1/a)^2 + (h_2/a)^2 - 2(h_1/a)(h_2/a) + 2[1 + h_1/a + h_2/a + (h_1/a)(h_2/a)][1 - \cos(d/a)]\right\}^{1/2} \qquad \text{(III. 3)}$$

$$r_1 = \left[(a \sin\psi)^2 + h_1(2a + h_1)\right]^{1/2} - a \sin\psi \qquad \text{(III. 4)}$$

$$r_2 = \left[(a \sin\psi)^2 + h_2(2a + h_2)\right]^{1/2} - a \sin\psi \qquad \text{(III. 5)}$$

$$\Delta r = r_1 + r_2 - r_o = 4 r_1 r_2 \sin^2\psi / (r_1 + r_2 + r_o) \qquad \text{(III. 6)}$$

Equating (III. 1) and (III. 2) and substituting $d - d_1$ for d_2 in (III. 2), the distance d_1 may be determined graphically or by trial and error, and $\tan\psi$ is then calculated using (III. 1).

Using double precision arithmetic, (III.1) through (III.6) give an accurate estimate of the path difference Δr for reflection of a single ray from a smooth earth. This value is then used in (5.1) of section 5 to obtain the long-term median reference value of transmission loss L_{cr}.

If either h_1 or h_2 greatly exceeds one kilometer, and if it is considered worthwhile to trace rays through the atmosphere in order to determine ψ more accurately, values of d_1 or d_2, tabulated by Bean and Thayer [1959], may be used. Given h_1, h_2, and the surface refractivity, N_s, select trial values for ψ, calculate d_1 and d_2, and continue until $d_1 + d_2 = d$. Then (III.1) and (III.2) must be solved for new values of h_1 and h_2 if (III.3), (III.4), and (III.5) are used to obtain the path difference, $\Delta r = r_1 + r_2 - r_o$.

The symbols R in (5.1) and c in (5.4) represent the magnitude and the phase angle relative to π, respectively, of the theoretical coefficient $R \exp[-i(\pi - c)]$ for reflection of a plane wave from a smooth plane surface of a given conductivity σ and relative dielectric constant ϵ. Values of R and c as a function of the grazing angle ψ are shown in figures III.1 to III.8 for vertical and horizontal polarization over good, average, and poor ground, and over sea water. The magnitude R of the smooth plane earth reflection coefficient is designated R_v or R_h for vertical or horizontal polarization respectively, and is read on the left-hand ordinate scale using the solid curves. The phase angle relative to π, is designated c_v or c_h for vertical or horizontal polarization respectively, and is read in radians on the right-hand scale using the dashed curves. As seen from these figures in most cases when the angle ψ is small, R is very nearly unity and c may be set equal to zero. A notable exception occurs in the case of propagation over sea water using vertical polarization.

In preparing figures III.1 to III.8, the following general expressions for the magnitudes R_v and R_h and lags $(\pi - c_v)$ and $(\pi - c_h)$ were used. In these equations, ϵ is the ratio of the surface dielectric constant to that of air, σ is the surface conductivity in mhos per meter, f is the radio frequency in megacycles per second, and ψ is the grazing angle in radians.

$$x = 1.80 \times 10^4 \, \sigma / f, \quad q = x/(2p) \tag{III.7}$$

$$2p^2 = \left[(\epsilon - \cos^2 \psi)^2 + x^2 \right]^{1/2} + (\epsilon - \cos^2 \psi) \tag{III.8}$$

$$b_v = \frac{\epsilon^2 + x^2}{p^2 + q^2}, \quad b_h = \frac{1}{p^2 + q^2} \tag{III.9}$$

$$m_v = \frac{2(p\epsilon + qx)}{p^2 + q^2}, \quad m_h = \frac{2p}{p^2 + q^2} \tag{III.10}$$

$$R_v^2 = \left[1 + b_v \sin^2 \psi - m_v \sin \psi \right] \left[1 + b_v \sin^2 \psi + m_v \sin \psi \right]^{-1} \qquad \text{(III. 11)}$$

$$R_h^2 = \left[1 + b_h \sin^2 \psi - m_h \sin \psi \right] \left[1 + b_h \sin^2 \psi + m_h \sin \psi \right]^{-1} \qquad \text{(III. 12)}$$

$$\pi - c_v = \tan^{-1}\left(\frac{x \sin \psi - q}{\epsilon \sin \psi - p} \right) - \tan^{-1}\left(\frac{x \sin \psi + q}{\epsilon \sin \psi + p} \right) \qquad \text{(III. 13)}$$

$$\pi - c_h = \tan^{-1}\left(\frac{-q}{\sin \psi - p} \right) - \tan^{-1}\left(\frac{q}{\sin \psi + p} \right) \qquad \text{(III. 14)}$$

The angle c_v is always positive and less than π, and c_h is always negative with an absolute magnitude less than π. The pseudo Brewster angle, where c_v suddenly changes from near zero to $\pi/2$, and where R_v is a minimum, is $\sin^{-1}\sqrt{1/b_v}$.

For grazing angles less than 0.1 radian, for overland propagation, and for frequencies above 30 Mc/s, excellent approximations to (III.11) and (III.12) are provided by the following formulas:

$$R_v = \exp(-m_v \psi) \qquad \text{(III. 15)}$$

$$R_h = \exp(-m_h \psi) \qquad \text{(III. 16)}$$

The assumption of a discrete reflection point with equal angles of incidence and reflection as shown in figure 5.1 is an oversimplification. Actually, reflection occurs from all points of the surface. For irregular terrain, this is taken into account by a terrain roughness factor σ_h, (subsection 5.1), which is the r.m.s. deviation of terrain relative to a smooth curve computed within the limits of a first Fresnel zone in a horizontal plane. The outline of such a Fresnel ellipse is determined by the condition that the length of a ray path, $r_{11} + r_{21}$, corresponding to scattering from a point on the edge of the ellipse is half a wave length longer than the geometrical ray path, $r_1 + r_2$, where the angles of incidence and reflection are equal.

The first Fresnel ellipse cuts the great circle plane at two points, x_a and x_b kilometers from the transmitter. The distances x_a and x_b are defined by the relation

$$\sqrt{r_1^2 \sin^2 \psi + x^2} + \sqrt{r_2^2 \sin^2 \psi + \left[(r_1 + r_2) \cos \psi - x \right]^2} = r_1 + r_2 + \lambda/2 \qquad \text{(III. 17)}$$

The exact solution for x is

$$2x_{a,b}(1+\delta) = [(r_1+r_2)(1+\delta) + (r_1-r_2)]\cos\psi \pm (r_1+r_2+\lambda/2)\,\delta\sqrt{1+4r_1r_2/[(r_1+r_2)^2\,\delta]} \tag{III. 18}$$

where

$$r_1^2 = h_1'^2 + d_1^2\ , \quad r_2^2 = h_2'^2 + d_2^2\ , \quad (r_1+r_2)^2 = (h_1'+h_2')^2 + d^2$$

$$\cos\psi = d_1/r_1 = d_2/r_2\ , \quad \sin\psi = h_1'/r_1 = h_2'/r_2$$

$$\delta = \left[\frac{\lambda^2}{4(r_1+r_2)^2} + \frac{\lambda}{r_1+r_2}\right]/\sin^2\psi$$

d_1, d_2 are defined by (5.7), and λ is the radio wavelength in kilometers.

As an alternative method, the points x_a and x_b may be computed in terms of path distance, the heights h_1' and h_2', and the radio frequency. In this method, the distance x_0 to the center of the first Fresnel zone is first computed, then the distance x_1 from the center to the margin of the zone is subtracted from x_0 to give x_a, and added to give x_b.

$$x_0 = d/2\left[1 + B\,f(h_1'^2 - h_2'^2)\right] \quad \text{km} \tag{III. 19}$$

where

$$B = \left[0.3d(1+2h_1'h_2'/d^2) + f(h_1'+h_2')^2\right]^{-1} \tag{III. 20}$$

$$x_1 = 0.548\,B\,d^2\left\{\left[f\,h_1'h_2'/d + 0.075(1+2h_1'h_2'/d^2)\right]\left[\frac{1+(h_1'+h_2')^2/d^2}{1+2h_1'h_2'/d^2}\right]\right\}^{1/2} \tag{III. 21}$$

$$x_a = x_0 - x_1 \quad \text{km}\ , \quad x_b = x_0 + x_1 \quad \text{km}$$

The method given in (III.19) to (III.21) is applicable whenever $d >> \lambda$. If in addition, $h_1' h_2' << d^2$, the computation of B, and x_1 may be simplified as follows:

$$B = \left[0.3d + f(h_1' + h_2')^2 \right]^{-1} \tag{III. 22}$$

$$x_1 = 0.548\ B\ d^2 \left\{ \left[f\, h_1' h_2'/d + 0.075 \right] \left[1 + (h_1' + h_2')^2/d^2 \right] \right\}^{1/2} \tag{III. 23}$$

THE COMPLEX REFLECTION COEFFICIENT $Re^{i(\pi - c)}$

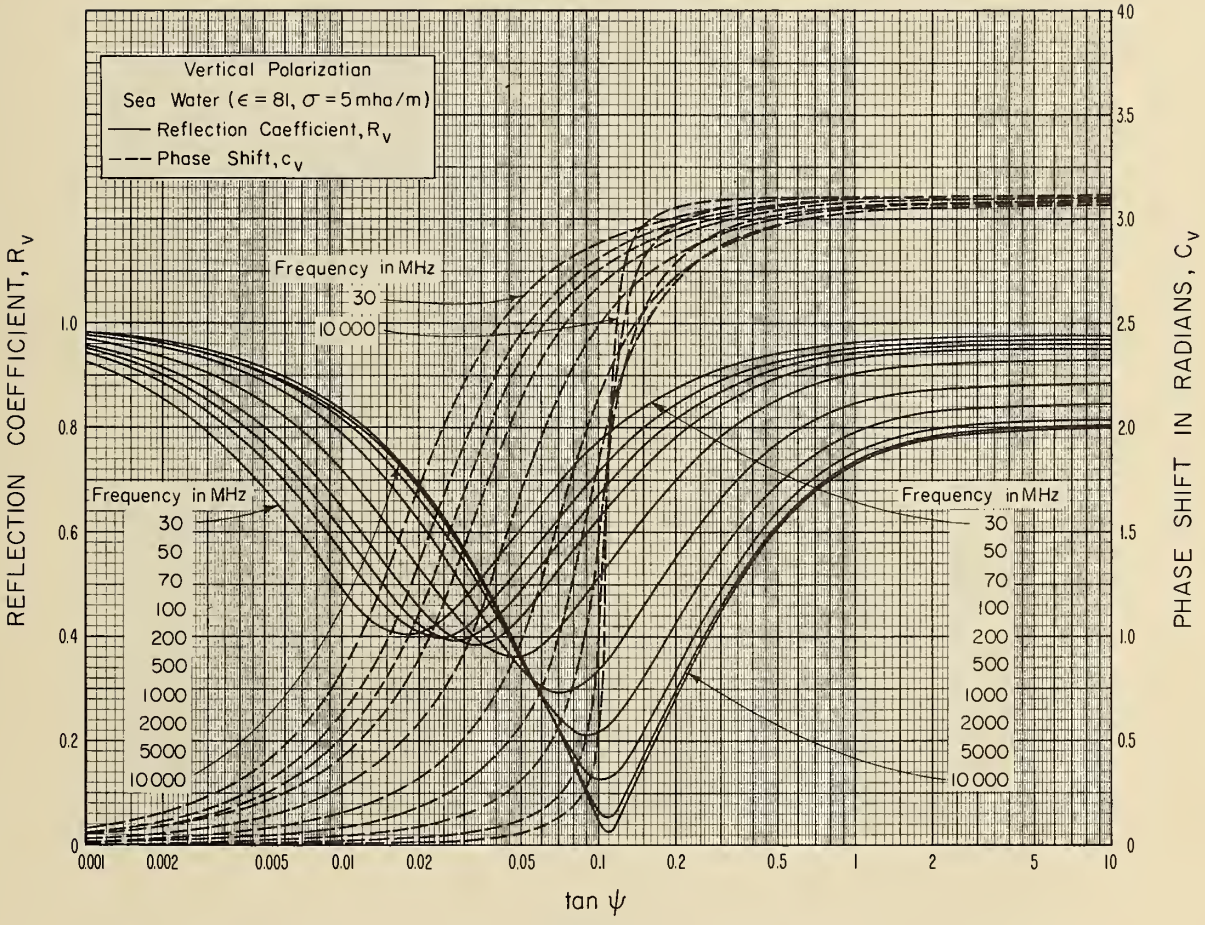

Figure III.1

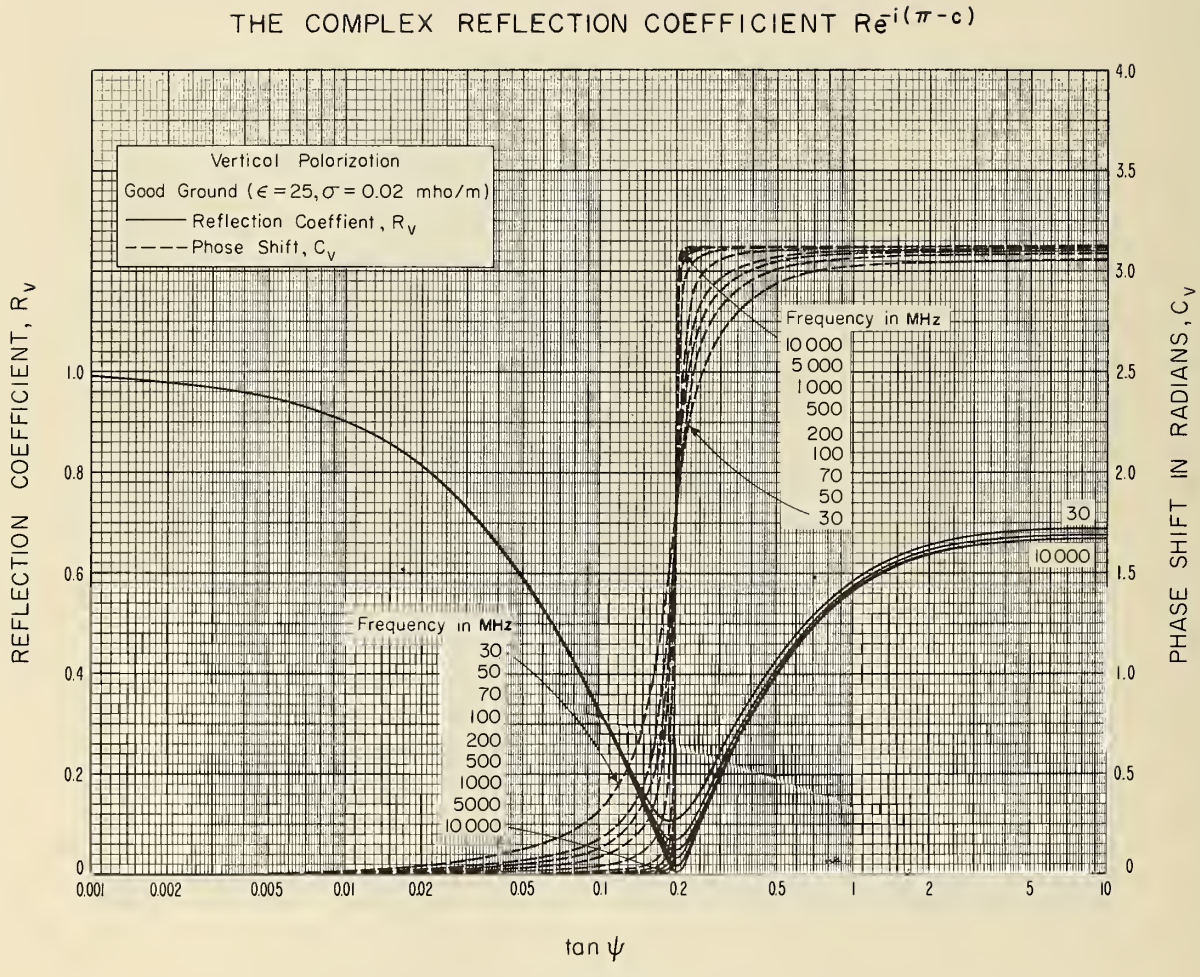
THE COMPLEX REFLECTION COEFFICIENT $Re^{i(\pi-c)}$
Verticol Polorizotion
Good Ground ($\epsilon = 25, \sigma = 0.02$ mho/m)
Reflection Coeffient, R_v
Phose Shift, C_v
Frequency in MHz
10 000
5 000
1 000
500
200
100
70
50
30
Frequency in MHz
30
50
70
100
200
500
1000
5000
10 000
30
10 000
REFLECTION COEFFICIENT, R_v
PHASE SHIFT IN RADIANS, C_v
0
0.2
0.4
0.6
0.8
1.0
0.5
1.0
1.5
2.0
2.5
3.0
3.5
4.0
0.001
0.002
0.005
0.01
0.02
0.05
0.1
0.2
0.5
1
2
5
10
tan ψ

Figure III.2

THE COMPLEX REFLECTION COEFFICIENT $Re^{i(\pi - c)}$

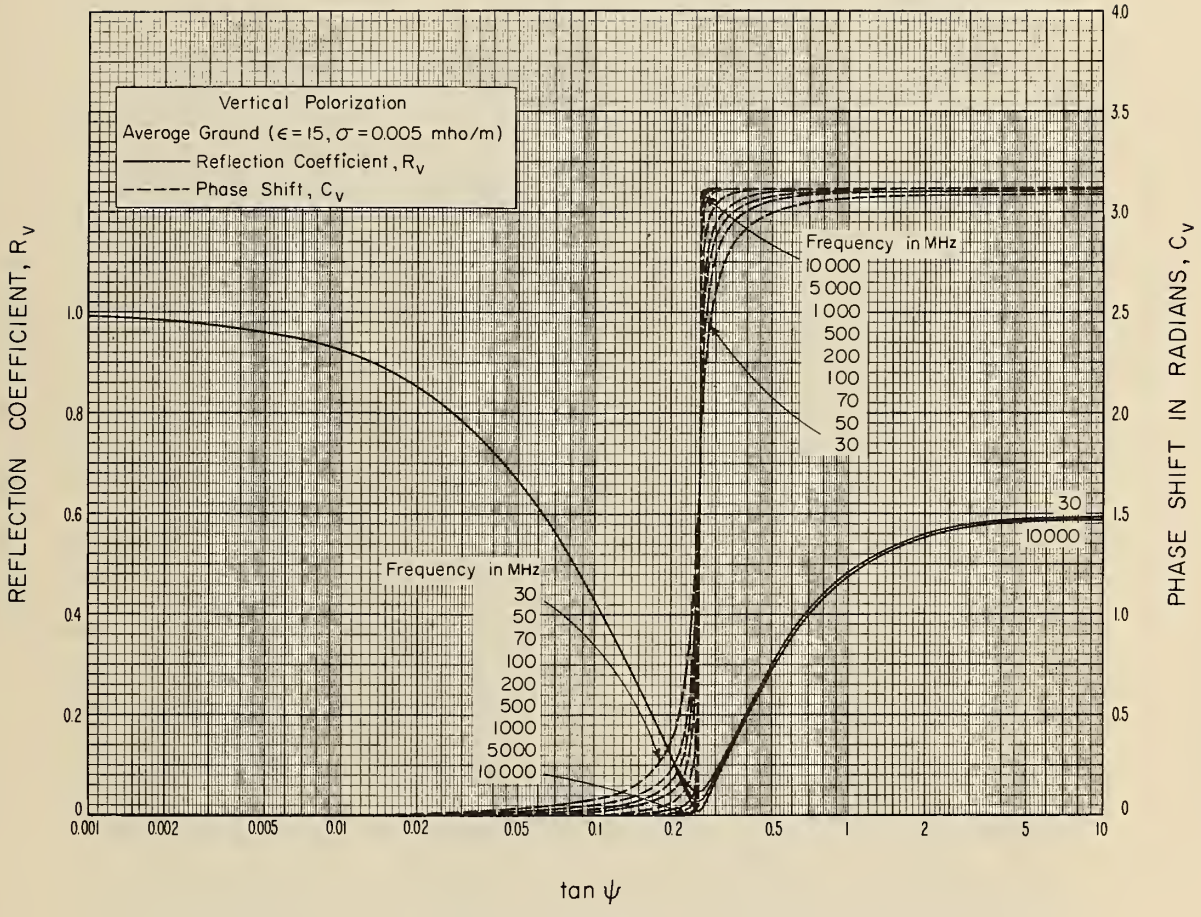

Figure III.3

THE COMPLEX REFLECTION COEFFICIENT $Re^{-i(\pi - c)}$

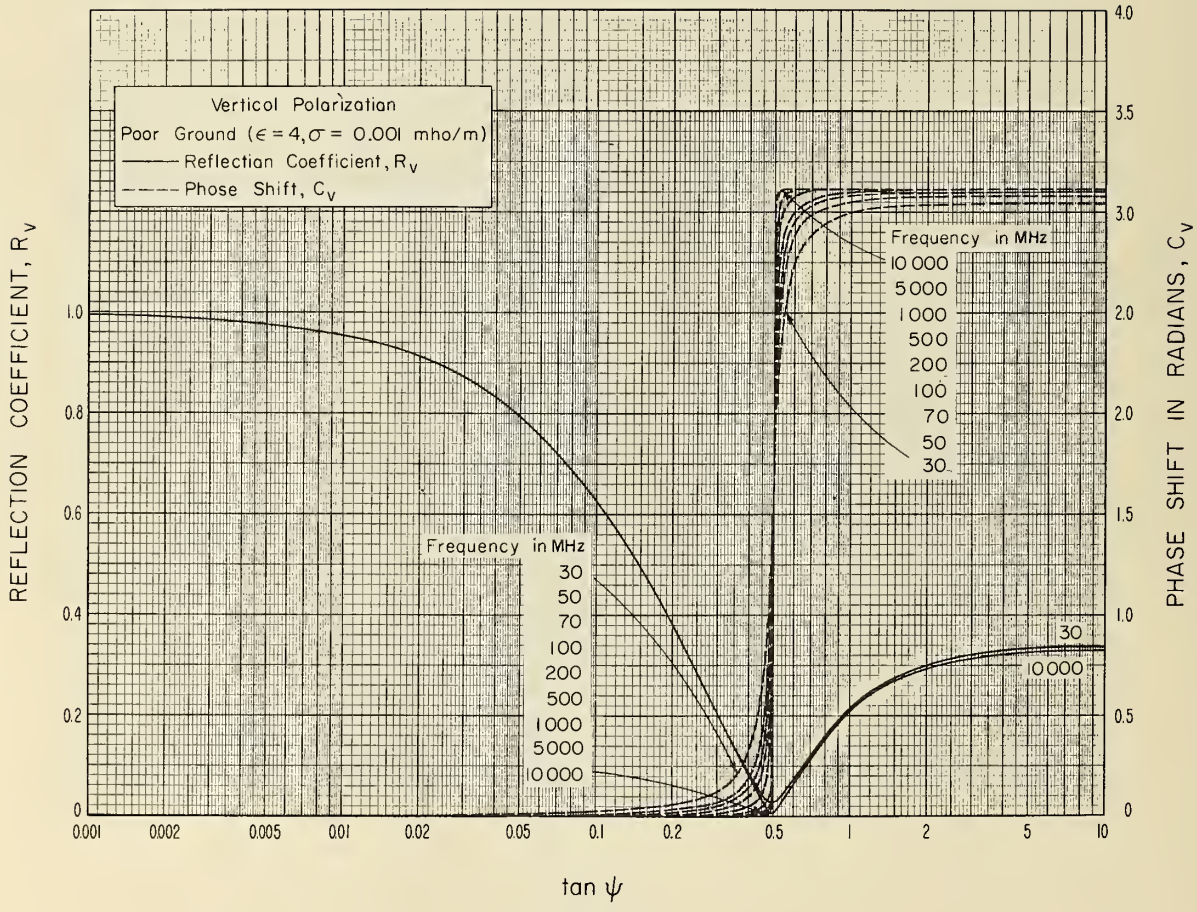

Figure III.4

THE COMPLEX REFLECTION COEFFICIENT $Re^{-i(\pi - c)}$

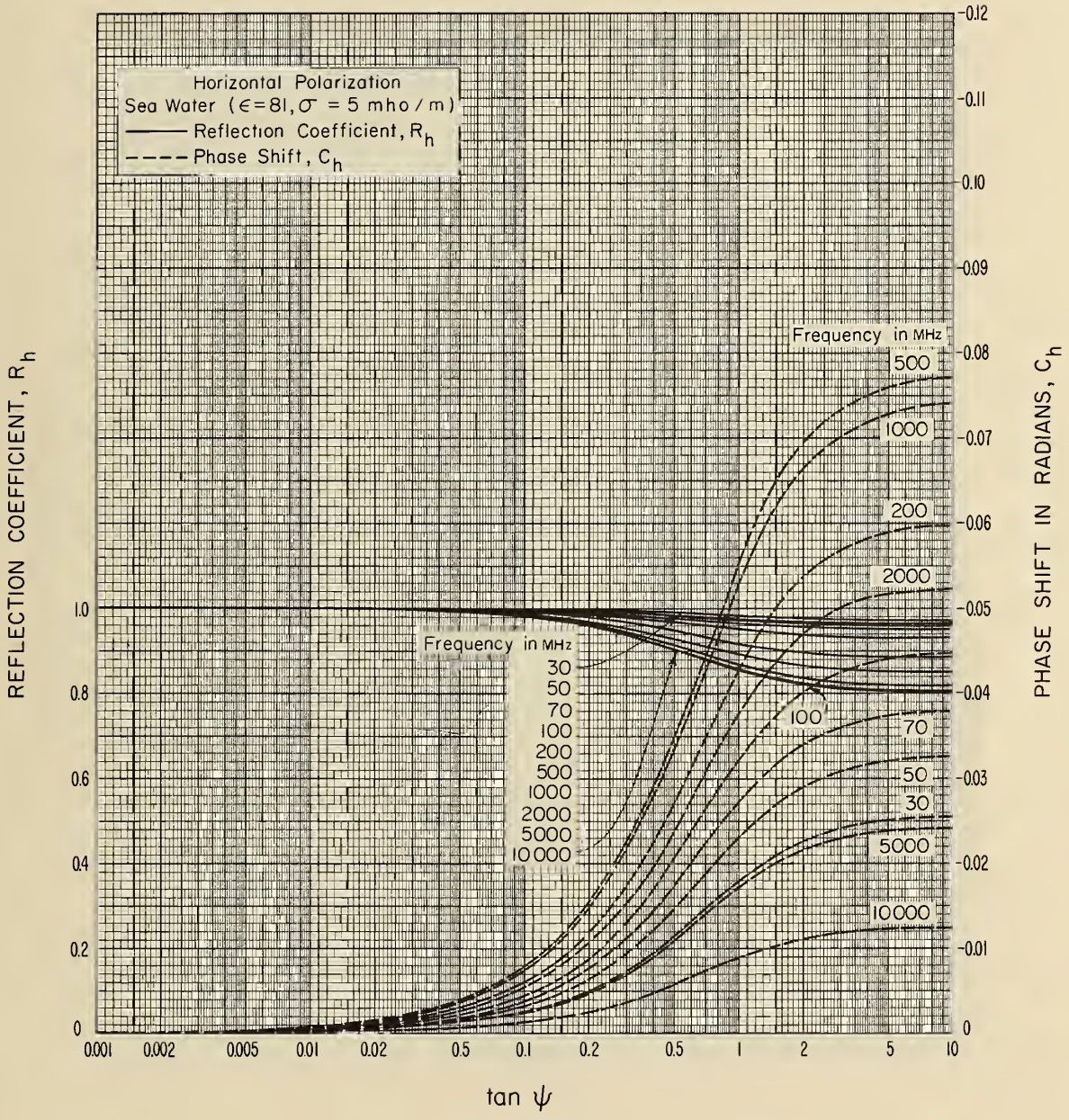

Figure III.5

THE COMPLEX REFLECTION COEFFICIENT $Re^{-i(\pi - c)}$

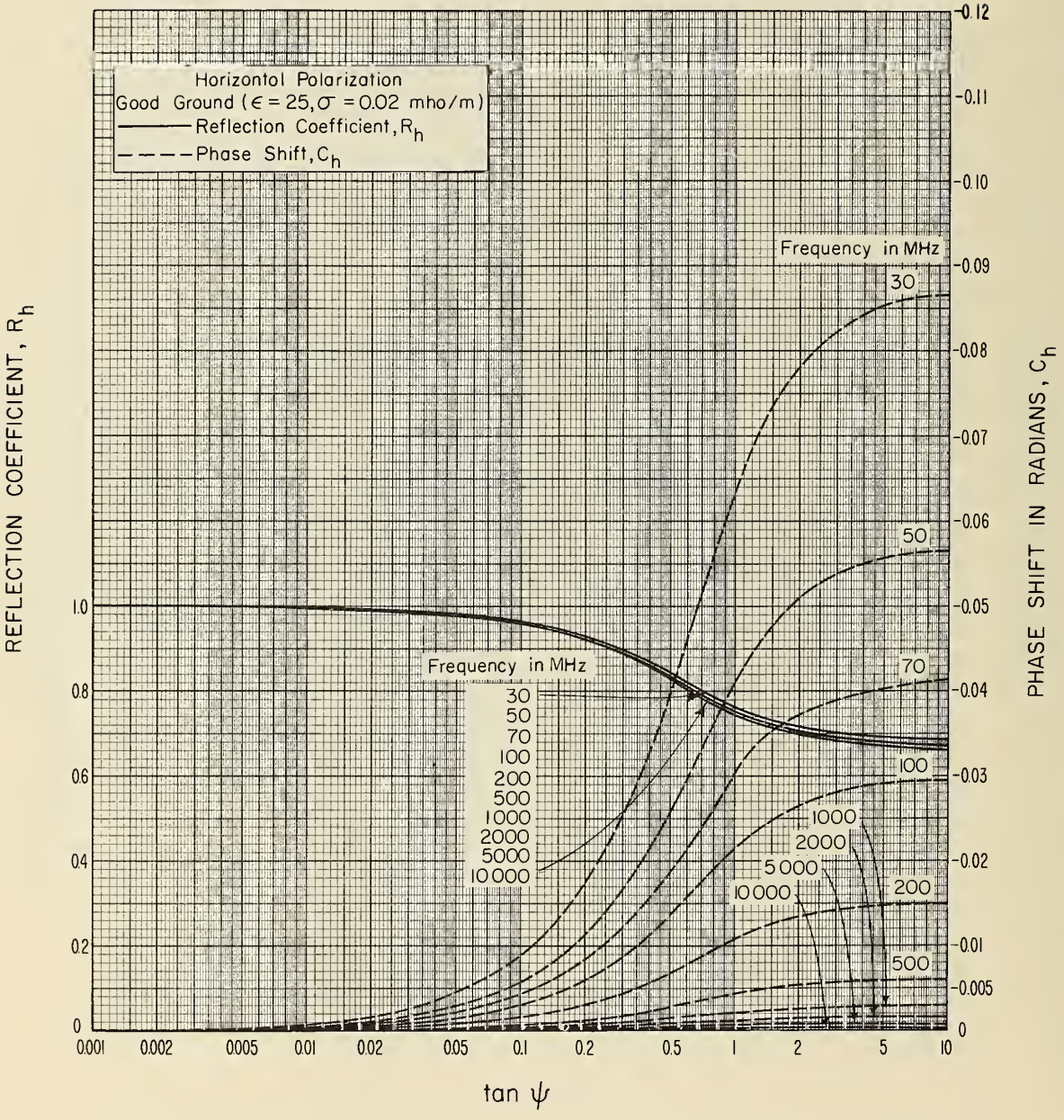

Figure III.6

THE COMPLEX REFLECTION COEFFICIENT $Re^{-i(\pi - c)}$

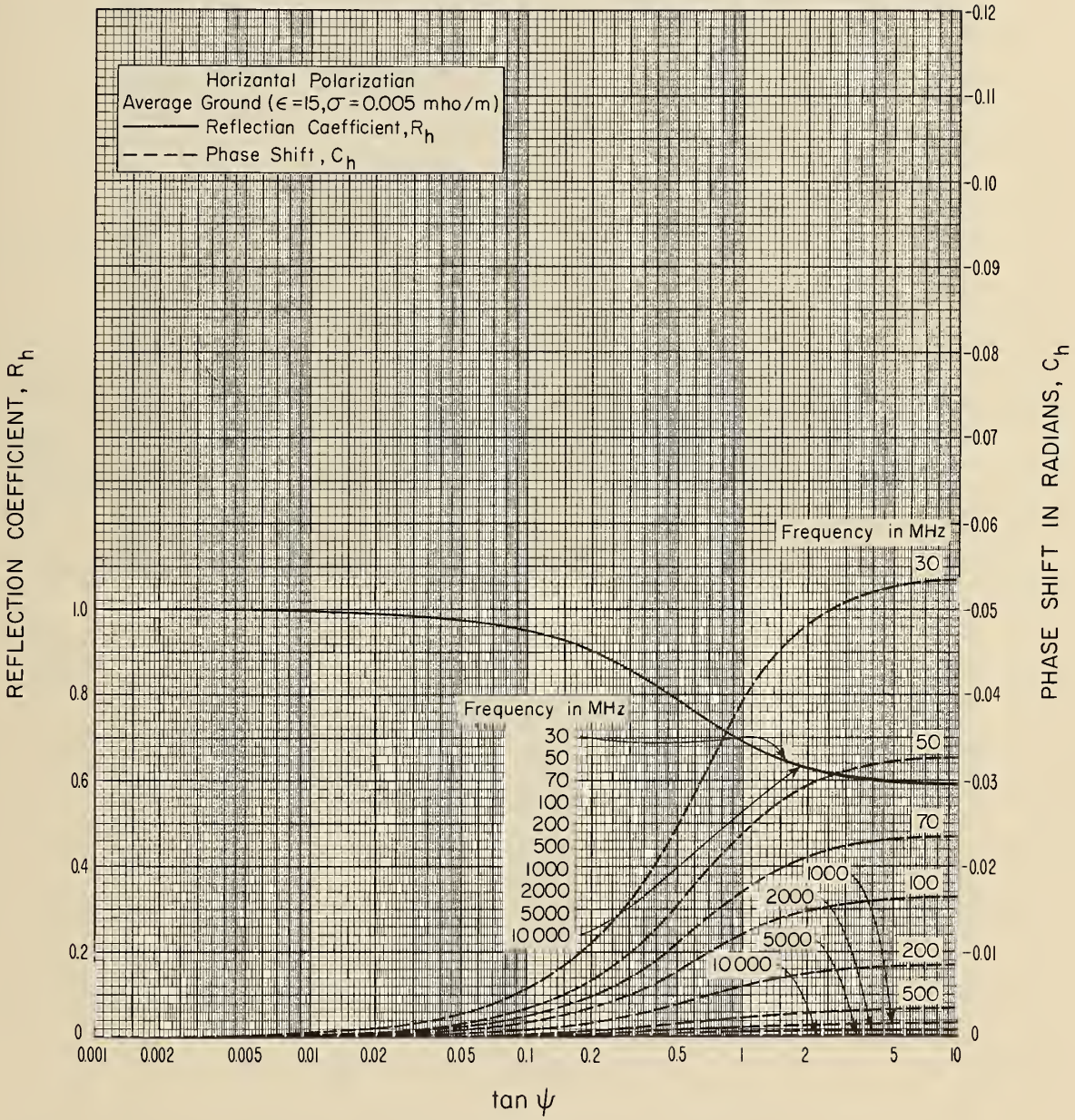

Figure III.7

THE COMPLEX REFLECTION COEFFICIENT $Re^{-i(\pi - c)}$

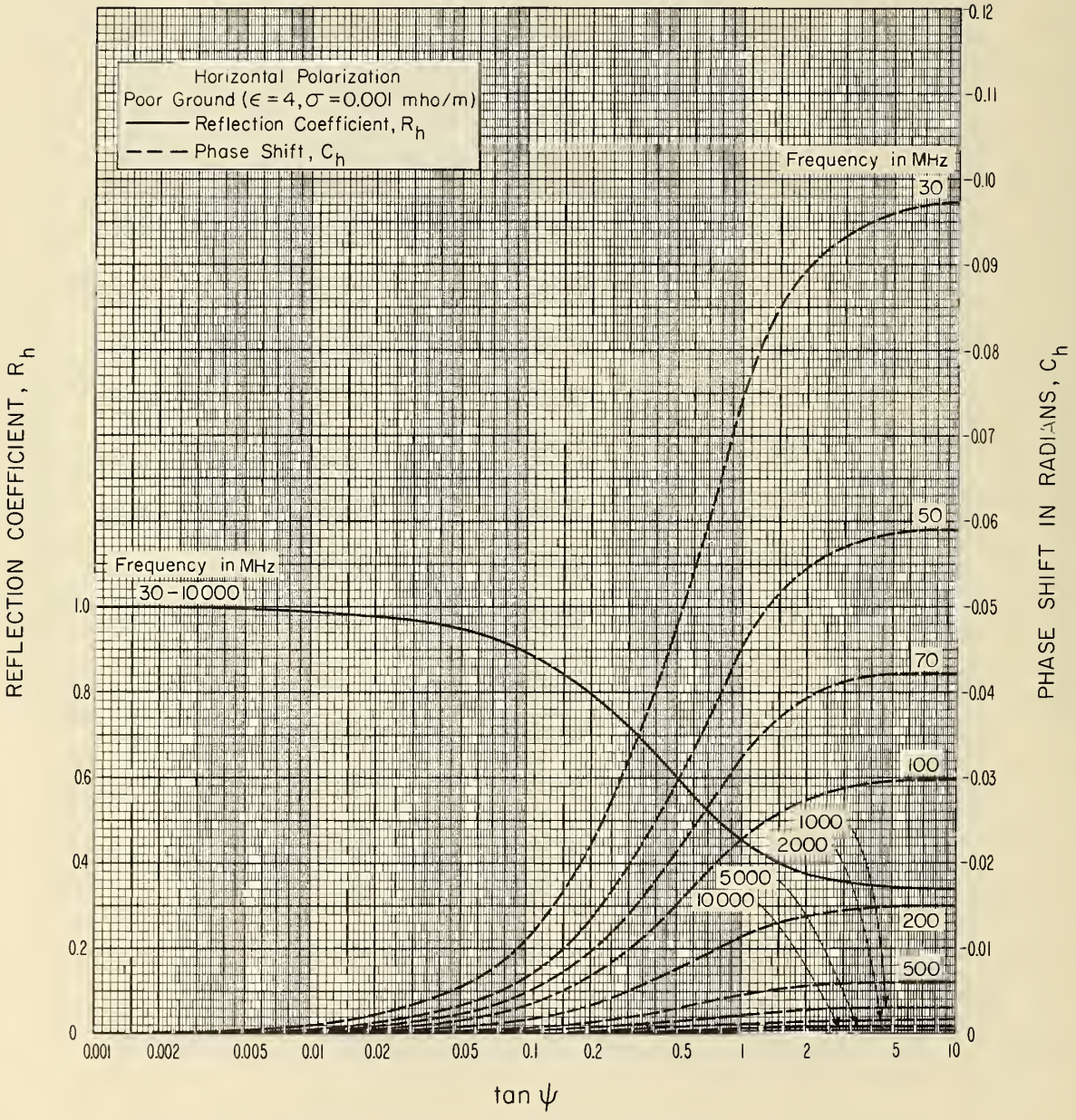

Figure III.8

III. 2 Diffraction over a Single Isolated Obstacle.

The theoretical diffraction loss curves on figures 7.1 to 7.4 have been fitted by arbitrary mathematical expressions for convenience in using a digital computer.

The diffraction loss for an isolated rounded obstacle and irregular terrain is given in section 7 as:

$$A(v, \rho) = A(v, 0) + A(0, \rho) + U(v\rho) \quad db \qquad (7.7)$$

where the parameter v is defined as

$$v = \pm 2\sqrt{\Delta r/\lambda} \cong \pm \sqrt{2d\,\alpha_o\beta_o/\lambda} \qquad (7.1a)$$

or

$$v = \pm 2.583\,\theta\sqrt{f\,d_1d_2/d} \qquad (7.1b)$$

and ρ an index of curvature of the rounded obstacles is defined as:

$$\rho = 0.676\, r^{1/3} f^{-1/6} [d/r_1r_2)]^{1/2} \qquad (7.8)$$

For an ideal knife edge, ($\rho = 0$), the diffraction loss is $A(v, 0)$ and is shown on figure 7.1. For values of v from minus one to large positive values, this curve may be approximated using the following mathematical expressions:

For $-1 \leq v \leq 0$,

$$A(v, 0) = 2.78\, v^2 + 9.95\, v + 6.17 \quad db\,. \qquad (III.24a)$$

For $0 \leq v \leq 3$,

$$A(v, 0) = 6.08 - 0.005\, v^4 + 0.159\, v^3 - 1.7\, v^2 + 9.3\, v \quad db\,. \qquad (III.24b)$$

For $v > 3$,

$$A(v, 0) = 12.953 + 20 \log v \quad db\,. \qquad (III.24c)$$

The theoretical curve for $A(0, \rho)$. is approximated by:

$$A(0, \rho) = 5.86 + 1.49\, \rho^3 + 1.46\, \rho^2 + 6.49\, \rho \quad db\,, \qquad (III.25)$$

and the curve $U(v\rho)$ is approximated as follows:

For $v\rho < 2$, $U(v\rho) = (43.6 + 23.5\, v\rho) \log (1 + v\rho) - 6 - 6.7\, v\rho$ db . (III. 26a)

For $v\rho \geq 2$, $U(v\rho) = 22\, v\rho - 20 \log (v\rho) - 14.13$ db . (III. 26b)

An average allowance for terrain foreground effects may be made by adding a term $10 \exp(-2.3\rho)$ to $A(0, \rho)$. This term gives a correction which ranges from 10 db for $\rho = 0$ to 1 db for $\rho = 1$.

When reflections from terrain on either or both sides of the obstacle should be considered, the method given in the following section may be used. This method considers the diffraction loss and phase lag over the diffracting obstacle, and the path length differences and reflection coefficients of the reflected waves.

III. 3 Diffraction over a Single Isolated Obstacle with Ground Reflections

Diffraction over an isolated obstacle is discussed in section 7, where ways of approximating the effects of reflection and diffraction from foreground terrain are indicated. Where the effects of reflection are expected to be of great importance, such as in the case of propagation over a large body of water, the following geometric optics method may be used.

Figure III.9 illustrates four distinct ray paths over a knife edge; the first ray is not reflected from the ground, the second and third are each reflected once, and the fourth ray is reflected once on each side of the knife edge. Each ray is subject to a diffraction loss f_j and a phase lag Φ_j at the knife edge, where $j = 1, 2, 3, 4$. Both f_j and Φ_j depend on the knife-edge parameter v given in section III.2. When the isolated obstacle is rounded, rather than an ideal knife edge, the diffraction loss depends on v and ρ, where ρ is the index of curvature of the crest radius, defined in section III.2. The parameter v may be written:

$$v_j = \pm 2\sqrt{\Delta_j/\lambda} \cong \pm \sqrt{2d\,\alpha_{oj}\beta_{oj}/\lambda} \qquad \text{(III. 27)}$$

where Δ_j is

$$\Delta_1 = r_1 + r_2 - r_0, \quad \Delta_2 = r_{11} + r_{12} + r_2 - r_{02}$$

$$\Delta_3 = r_1 + r_{21} + r_{22} - r_{03}, \quad \Delta_4 = r_{11} + r_{12} + r_{21} + r_{22} - r_{04} \qquad \text{(III. 28)}$$

Path differences Δ_j used to calculate v_j in (III. 27) are closely approximated by the following formulas:

$$\Delta_j = d_r\,\theta_j^2, \quad d_r = d_1 d_2/(2d), \quad \theta_j = \theta + \theta_{jr}$$

$$\theta_{1r} = 0, \quad \theta_{2r} = 2d_{11}\psi_1/d_1, \quad \theta_{3r} = 2d_{22}\psi_2/d_2, \quad \theta_{4r} = \theta_{2r} + \theta_{3r} \qquad \text{(III. 29)}$$

The total phase change $\Phi(v, \rho)$ at an isolated rounded obstacle is

$$\Phi_j = \Phi_j(v, \rho) = 90\,v^2 + \phi(v, 0) + \phi(0, \rho) + \phi(v\rho) \qquad \text{(III. 30a)}$$

where the functions $\phi(v, 0)$, $\phi(0, \rho)$, and $\phi(v\rho)$ are plotted as dashed curves on figures 7.1, 7.3, and 7.4. For an ideal knife edge, where the radius of curvature of the crest is zero, $\rho = 0$, and (III. 30a) reduces to

for $v > 0$ $$\Phi_j(v, 0) = 90\,v^2 + \phi(v, 0) \qquad \text{(III. 30b)}$$

for $v \leq 0$ $$\Phi_j(v, 0) = \phi(v, 0) \qquad \text{(III. 30c)}$$

The three components of the received field which are affected by reflection from the earth's surface depend also upon effective ground reflection coefficients $R_{e2} \exp[-i(\pi - c_2)]$ and $R_{e3} \exp[-i(\pi - c_3)]$, defined in section 5, and upon ray path differences Δ_{2r} and Δ_{3r}:

$$\Delta_{2r} = r_{11} + r_{12} - r_1 \cong 2\psi_1^2 d_{11} d_{12}/d_1$$

$$\Delta_{3r} = r_{21} + r_{22} - r_2 \cong 2\psi_2^2 d_{21} d_{22}/d_2 \qquad \text{(III. 31)}$$

Usually, it may be assumed that $c_2 = c_3 = 0$ so that the reflection coefficients are $-R_{e2}$ and $-R_{e3}$.

Introducing the propagation constant $k = 2\pi/\lambda$, the attenuation relative to free space is then

$$A = -20 \log \left\{ \left| f_1 \exp(-i\Phi_1) - R_{e2} f_2 \exp\left[-i(\Phi_2 + k\Delta_2)\right] \right.\right.$$

$$\left.\left. - R_{e3} f_3 \exp\left[-i(\Phi_3 + k\Delta_3)\right] + R_{e2} R_{e3} f_4 \exp\left[-i(\Phi_4 + k\Delta_2 + k\Delta_3)\right] \right| \right\} \text{ db} \qquad \text{(III. 32)}$$

where

$$f_j = +\tfrac{1}{2}\sqrt{(1 - C_j - S_j)^2 + (C_j - S_j)^2}, \quad \tan \Phi_j = \frac{C_j - S_j}{1 - C_j - S_j}$$

$$C_j = \int_o^{v_j} \cos\left(\frac{\pi t^2}{2}\right) dt, \quad S_j = \int_o^{v_j} \sin\left(\frac{\pi t^2}{2}\right) dt \qquad \text{(III. 33)}$$

Pearcey [1956], and the NBS AMS 55 Handbook of Mathematical Functions [1964] give complete tables, series expansions, and asymptotic expressions for the Fresnel integrals C_j and S_j. The magnitude $f_j \equiv f(v_j)$ for $v = v_j$ may also be determined from figure 7.1 and the expression

$$\log f(v_j) = -A(v_j)/20 \qquad \text{(III. 34)}$$

and where v is larger than 3:

$$f_j = 0.22508/v_j, \quad \Phi_j = \frac{\pi}{4}\left(1 + 2v_j^2\right) \text{ radians} \qquad \text{(III. 35)}$$

Figure III. 10 is a nomogram which may be used in the determination of $f(v_j)$ and $\Phi(v_j)$ for both positive and negative values of v. This nomogram is based on the representation

of Fresnel integrals by the Cornu spiral.

The general problem requires calculating θ, d, d_1, d_2, d_{11}, d_{12}, d_{21}, d_{22}, ψ_1, and ψ_2, as shown in figure III.9.

1. Calculate θ_j and Δ_j for $j = 1, 2, 3, 4$, using (III.29).
2. Calculate v_j, C_j, S_j, f_j, and Φ_j, using (III.27), (III.33), and figure 7.1.
3. Calculate Δ_{2r} and Δ_{3r} from (III.31).
4. Calculate R_{e2} and R_{e3} from (5.1), or assume that $R_{e2} = R_{e3} = 1$.
5. Substitute these values in (III.32).

To check the calculation of each v_j, the approximation given in (III.27) may be used, with the following formulas for $\alpha_{oj} = d_2\,\theta_j/d$ and $\beta_{oj} = d_1\,\theta_j/d$:

$$\alpha_{01} = d_2\,\theta/d \qquad \beta_{01} = d_1\,\theta/d$$

$$\alpha_{02} = \alpha_{01} + 2\,d_{11}\,\psi_1\,d_2/(d_1\,d) \qquad \beta_{02} = \beta_{01} + 2\,d_{11}\,\psi_1/d$$

$$\alpha_{03} = \alpha_{01} + 2\,d_{22}\,\psi_2/d \qquad \beta_{03} = \beta_{01} + 2\,d_{22}\,\psi_2\,d_1/(d_2\,d)$$

$$\alpha_{04} = \alpha_{02} + \alpha_{03} - \alpha_{01} \qquad \beta_{04} = \beta_{02} + \beta_{03} - \beta_{01} \qquad \text{(III.36)}$$

Two special cases will be described for which (III.29) and (III.31) may be simplified. First, assume that each reflecting surface may be considered a plane. Let h_t and h_{tm} be the heights of the transmitting antenna and the knife edge above the first plane, and let h_{rm} and h_r be the heights of the knife edge and the receiving antenna above the second reflecting plane. Assume that Δr is very small for every Δ. In terms of the heights h_t, h_{tm}, h_{rm}, h_r, the parameters θ, d_1, and d_2 and the parameter $d_r \equiv d_1\,d_2/(2d)$:

$$\Delta_{2r} = 2\,h_t\,h_{tm}/d_1, \quad \Delta_{3r} = 2\,h_r\,h_{rm}/d_2$$

$$\Delta_1 = d_r\,\theta^2, \quad \Delta_2 = d_r\,(\theta + h_{tm}\,\Delta_{2r})^2$$

$$\Delta_3 = d_r\,(\theta + h_{rm}\,\Delta_{3r})^2, \quad \Delta_4 = d_r\,(\theta + h_{tm}\,\Delta_{2r} + h_{rm}\,\Delta_{3r})^2 \qquad \text{(III.37)}$$

The second special case assumes a knife edge over an otherwise smooth earth of effective radius a, with antenna heights h_t and h_r small compared to the height of the knife edge. In this case, h_t and h_r are heights above the smooth curved earth. The angle of elevation of the knife edge relative to the horizontal at one antenna is θ_{ht} and relative to the horizontal at the other antenna is θ_{hr}. Referring to (5.12):

$$\Delta_{2r} = h_t\left[\sqrt{\theta_{ht}^2 + 4h_t/(3a)} + \theta_{ht}\right], \quad \Delta_{3r} = h_r\left[\sqrt{\theta_{hr}^2 + 4h_r/(3a)} + \theta_{hr}\right] \qquad \text{(III. 38)}$$

For this special case, the formulas (III.29) for Δ_j may be simplified by writing

$$\theta_{2r} = \Delta_{2r}^2\, d_1/(2h_t), \quad \theta_{3r} = \Delta_{3r}^2\, d_2/(2h_r) \qquad \text{(III. 39)}$$

BEYOND-HORIZON KNIFE-EDGE DIFFRACTION WITH GROUND REFLECTIONS

(KNIFE-EDGE NORMAL TO RAY PATH)

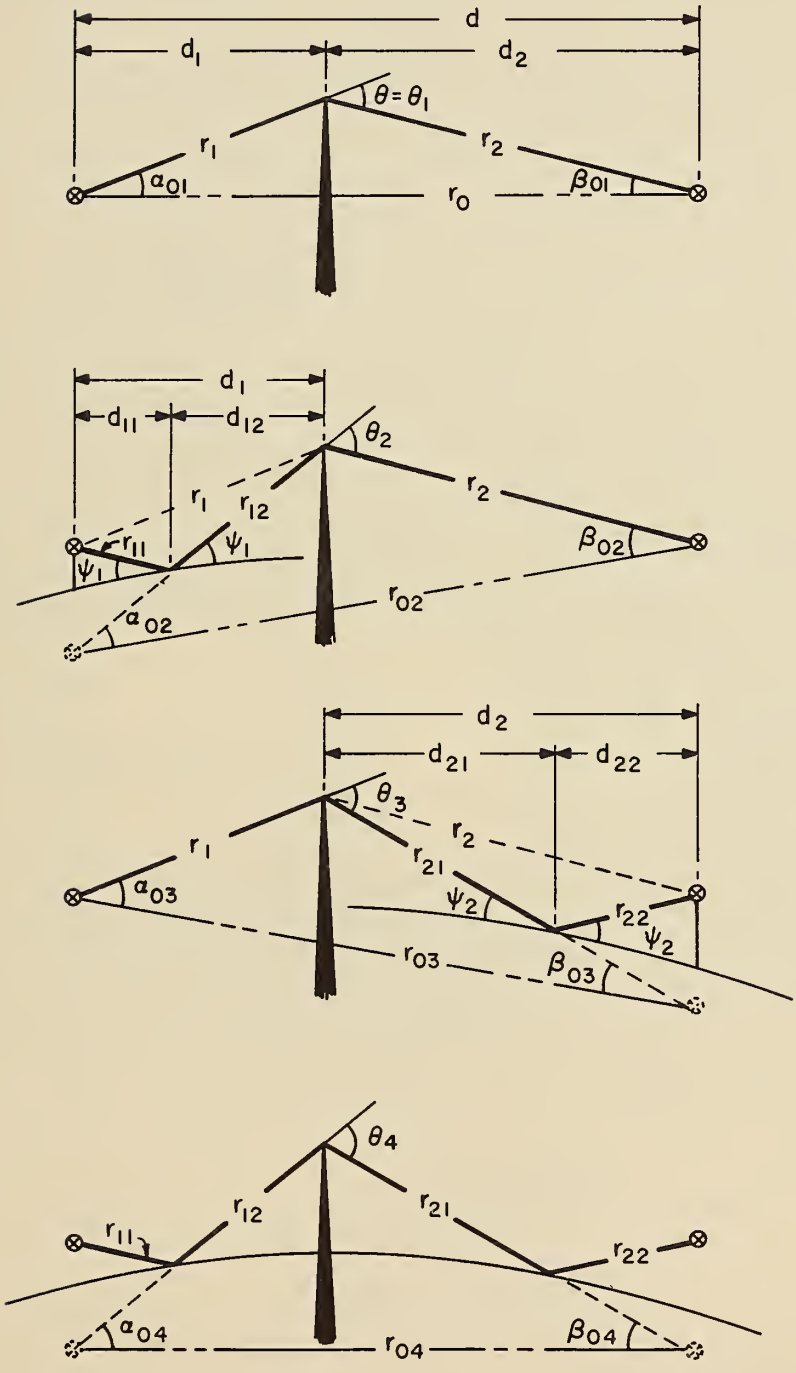

Figure III.9

CORNU'S SPIRAL

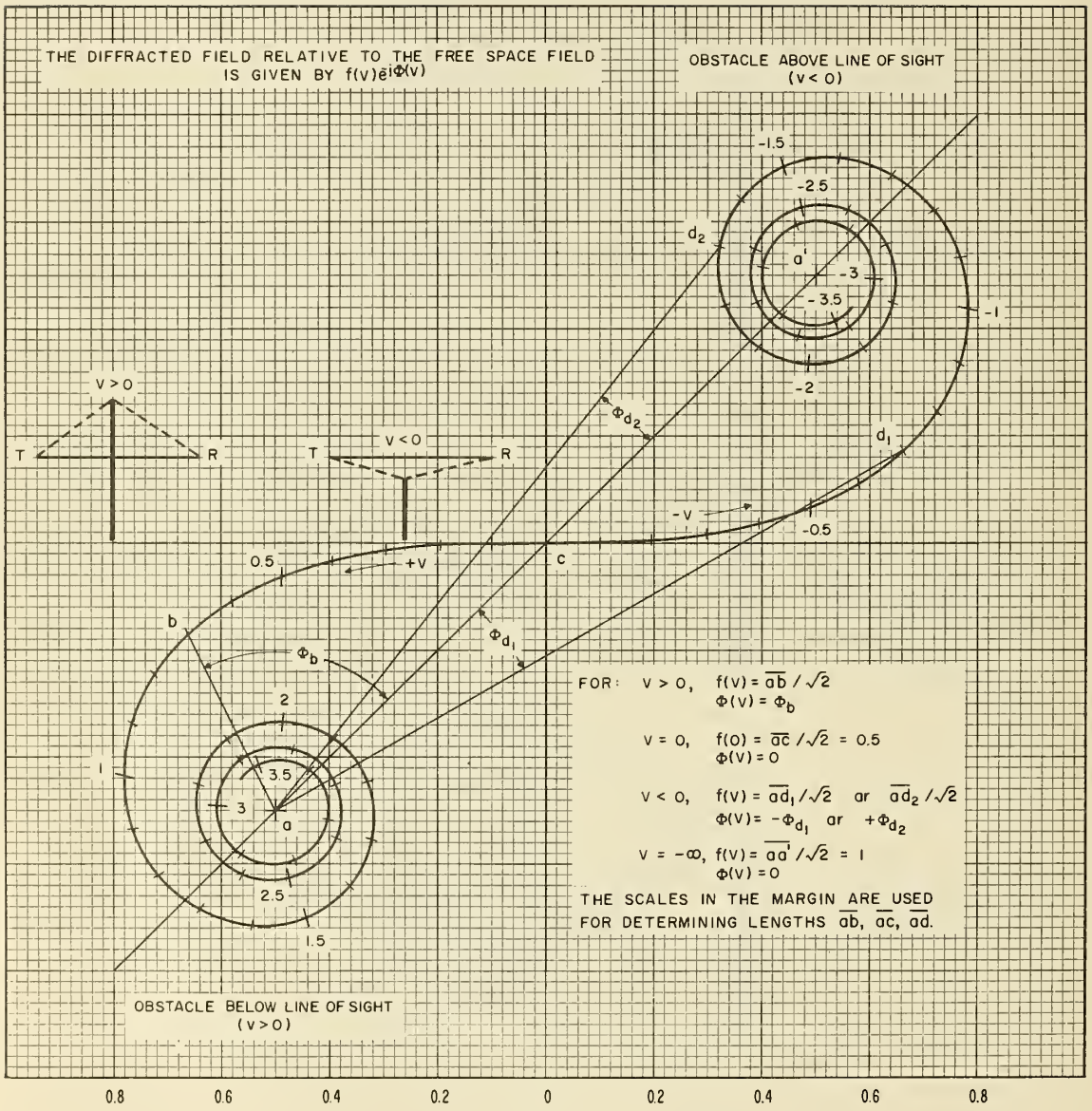

Figure III.10

III. 4 Parameters K and b° for Smooth Earth Diffraction

In section 8, the parameters K and b° are shown on figures 8.1 and 8.2 for horizontally and vertically polarized waves for poor, average, and good ground, and for sea water.

Assuming a homogeneous ground in which the relative dielectric constant ϵ and conductivity σ of the ground are everywhere constant, K and b° are defined as follows:

For horizontal polarization,

$$K_h = 1.7778 \times 10^{-2} C_o f^{-\frac{1}{3}} [(\epsilon - 1)^2 + x^2]^{-\frac{1}{4}} \qquad \text{(III. 40a)}$$

$$b_h = 180^\circ - \tan^{-1}\left(\frac{\epsilon - 1}{x}\right) \quad \text{degrees} . \qquad \text{(III. 40b)}$$

For vertical polarization,

$$K_v = (\epsilon^2 + x^2)^{\frac{1}{2}} K_h \qquad \text{(III. 41a)}$$

$$b_v = 2 \tan^{-1}(\epsilon/x) - \tan^{-1}\left(\frac{\epsilon - 1}{x}\right) \quad \text{degrees} . \qquad \text{(III. 41b)}$$

where x depends on the ground conductivity σ in mhos per meter and the radio frequency f in megacycles per second, and has been defined by (III. 7) as

$$x = 1.8 \times 10^4 \sigma/f$$

C_o is defined in section 8 as

$$C_o = (8497/a)^{\frac{1}{3}}$$

where a is the effective earth's radius in kilometers.

When $\sigma/f >> (\epsilon/2) \times 10^{-4}$, the parameters K and b° may be written as

$$K_h \simeq 1.325 \times 10^{-4} C_o f^{1/6} \sigma^{-1/2} , \quad b_h \simeq 180^\circ \qquad \text{(III. 42)}$$

$$K_v \simeq 2.385 C_o \sigma^{1/2} f^{-5/6} , \quad b_v \simeq 0^\circ \qquad \text{(III. 43)}$$

and when $\sigma/f << (\epsilon/2) \times 10^{-4}$, the parameters K and b° may be written as

$$K_h \simeq 1.7778 \times 10^{-2} C_o f^{-\frac{1}{3}} (\epsilon - 1)^{-\frac{1}{2}} , \quad b_h \simeq 90^\circ \qquad \text{(III. 44)}$$

$$K_v \simeq \epsilon K_h , \quad b_v \simeq 90^\circ \qquad \text{(III. 45)}$$

III. 5 Forward Scatter

The attenuation function $F(\theta d)$ for $N_s = 250$, 301, 350, and 400, shown in figure 9.1, may be used for most land-based scatter links. When a path is highly asymmetrical, the attenuation for a given value of θd is less than it would be for a symmetrical path. Figures III.11 to III.14 show the function $F(\theta d)$ for values of s from 0.01 to 1, for each of four values of N_s. For values of $\theta d \leq 10$, the effect of asymmetry is negligible, but increases with increasing θd, particularly when $s < 0.5$.

For values of s between 0.7 and 1, the function $F(\theta d)$ may be computed as follows:

$$0.01 \leq \theta d < 10 , \qquad F(\theta d) = K(N_s) + 0.34\theta d + 30 \log(\theta d) \tag{III. 46}$$

where

$$K(N_s) = 139.5 + 0.06\, N_s - 2.4 \times 10^{-4}\, N_s^{\,2}$$

$$10 \leq \theta d < 70 , \qquad F(\theta d) = K_o(N_s) + K_1(N_s)\theta d + K_2(N_s) \log(\theta d) \tag{III. 47}$$

where

$$K_0(N_s) = 140.7 + 0.06\, N_s - 3.2 \times 10^{-4}\, N_s^{\,2}$$

$$K_1(N_s) = 3.925 + 3.3 \times 10^{-3}\, N_s - 1.9 \log N_s$$

$$K_2(N_s) = 22.5 + 0.05\, N_s$$

$$\theta d \geq 70 , \qquad F(\theta d) = K(N_s) + 0.158\, \theta d + 44 \log(\theta d) \tag{III. 48}$$

where

$$K(N_s) = 123.6 - 0.008\, N_s$$

Using equations (III.46) to (III.48), the function $F(\theta d)$ may be computed for any value of N_s. For the values of N_s shown in figures III.11 to III.14, $K(N_s)$ has the following values:

	N_s	250	301	350	400
$0.01 \leq \theta d < 10$	$K(N_s)$	139.5	135.82	131.10	125.10
$10 \leq \theta d < 70$	$K_o(N_s)$	135.70	129.77	122.50	113.50
	$K_1(N_s)$	0.194	0.212	0.246	0.301
	$K_2(N_s)$	35	37.5	40	42.5
$\theta d \geq 70$	$K(N_s)$	121.6	121.2	120.8	120.4

The frequency gain function, H_o, for the special case $h_{te} = h_{re}$ frequently used in systems design, is shown as a function of r on figures III.15 to III.19 for $\eta_s = 1$, 2, 3, 4, 5, and for $s = 0.75$ to 1, 0.5, 0.25 and 0.1. In this case, no correction factor ΔH_o is required.

The function H_o for $\eta_s = 0$, shown on figure 9.5 corresponds to the assumption of a constant atmospheric refractive index. This function may be computed as follows:

$$H_o(\eta_s = 0) = 10 \log \left\{ \frac{2(1 - h_{re}^2/h_{te}^2)}{r_2^2 [h(r_1) - h(r_2)]} \right\} \qquad \text{(III. 49)}$$

where $r_1 = 4\pi\theta h_{te}/\lambda$, $r_2 = 4\pi\theta h_{re}/\lambda$,

$$h(r_1) = r_1 f(r_1) , \quad f(r_1) = Ci(r_1) \sin r_1 + [\pi/2 - Si(r_1)] \cos r_1 \qquad \text{(III. 50)}$$

and

$$h(r_2) = r_2 f(r_2) , \quad f(r_2) = Ci(r_2) \sin r_2 + [\pi/2 - Si(r_2)] \cos r_2$$

$$Ci(r) = \int_{\infty}^{r} \frac{\cos t}{t} dt , \quad Si(r) = \int_{0}^{r} \frac{\sin t}{t} dt \qquad \text{(III. 51)}$$

Values of the sine integral $Si(r)$ and the cosine integral $Ci(r)$ for arguments from 10 to 100 are tabulated in volume 32 of the U. S. NBS Applied Math Series [1954]. See also [NBS AMS 1964]. The function $h(r)$ is shown graphically in figures III.20 and III.21.

For the special case of equal effective antenna heights, $h_{te} = h_{re}$, equation (III.49) is not applicable. In this case $H_o(\eta_s = 0)$ is computed as:

$$H_o(\eta_s = 0) = 10 \log \left\{ \frac{4}{r^2 [h(r) - r\, g(r)]} \right\} \qquad \text{(III. 52)}$$

where

$$g(r) = Ci(r) \cos r - [\pi/2 - Si(r)] \sin r \qquad \text{(III. 53)}$$

When the effective height of one antenna is very much greater than that of the other, the computation may be simplified as follows:

For $r_2 << r_1$, $$H_o(\eta_s = 0) = 10 \log \left\{ \frac{2}{r_2^2 [1 - h(r_2)]} \right\} \qquad \text{(III. 54a)}$$

For $r_2 >> r_1$, $$H_o(\eta_s = 0) = 10 \log \left\{ \frac{2}{r_1^2 [1 - h(r_1)]} \right\} \qquad \text{(III. 54b)}$$

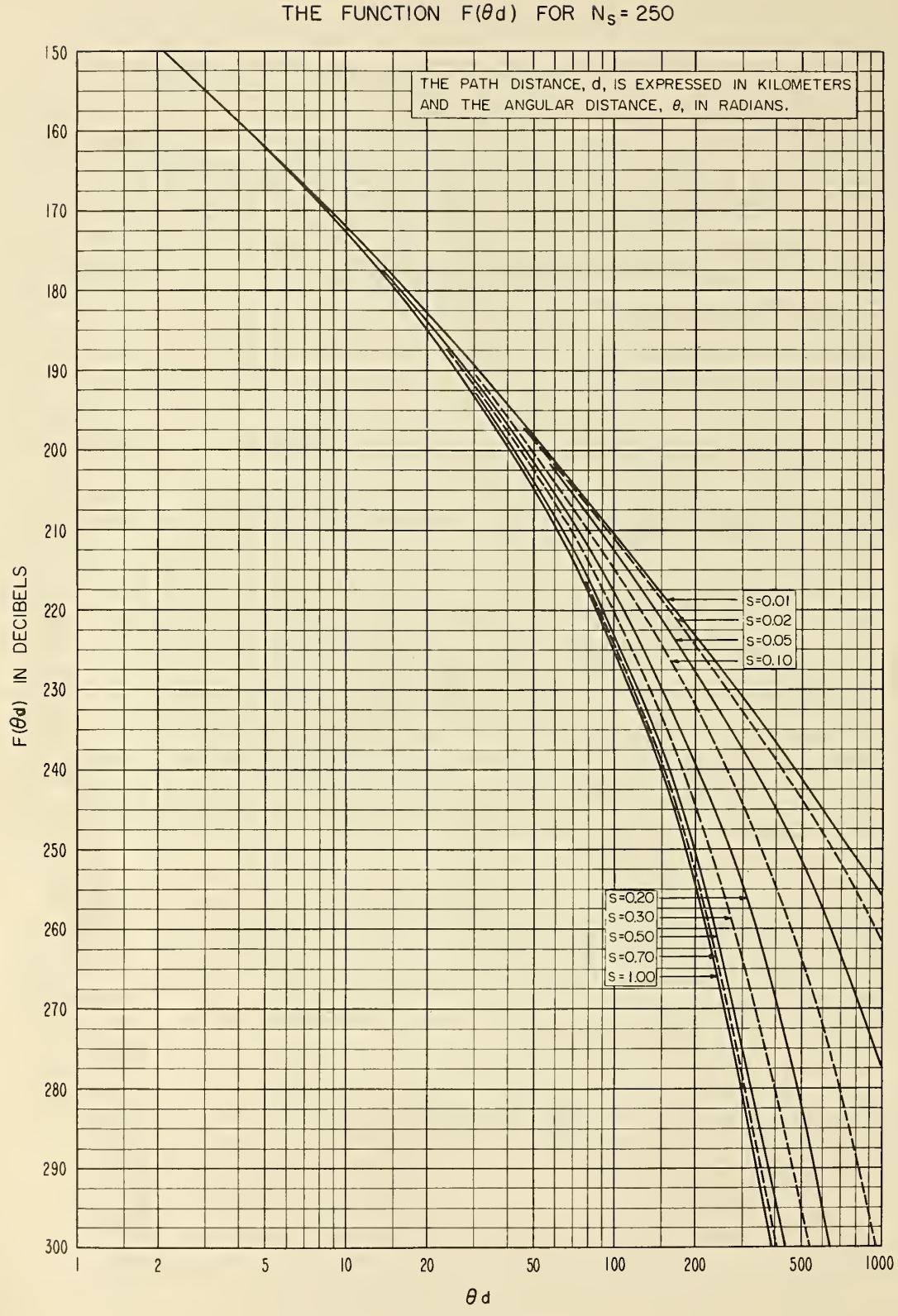

Figure III.11

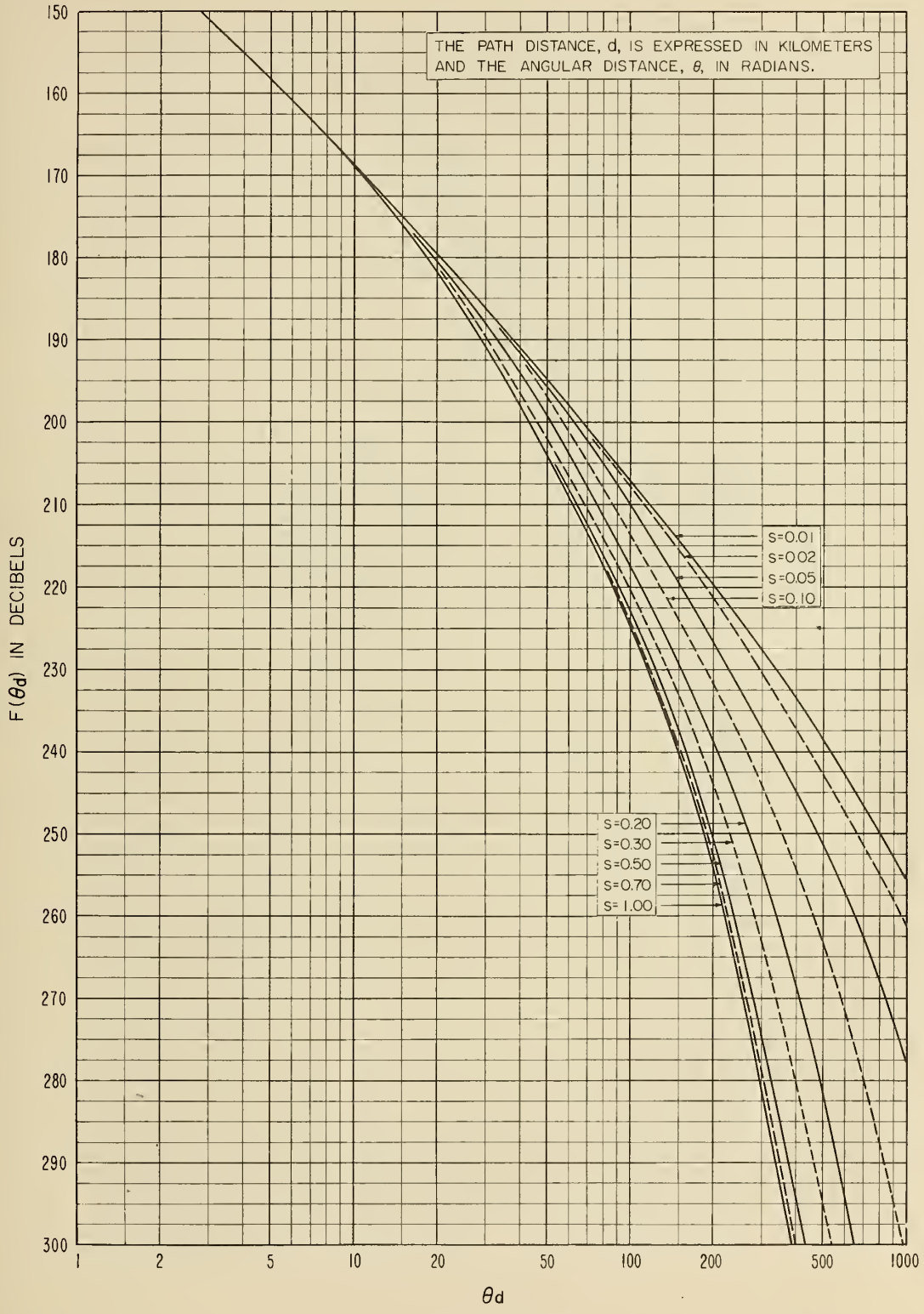

Figure III.12

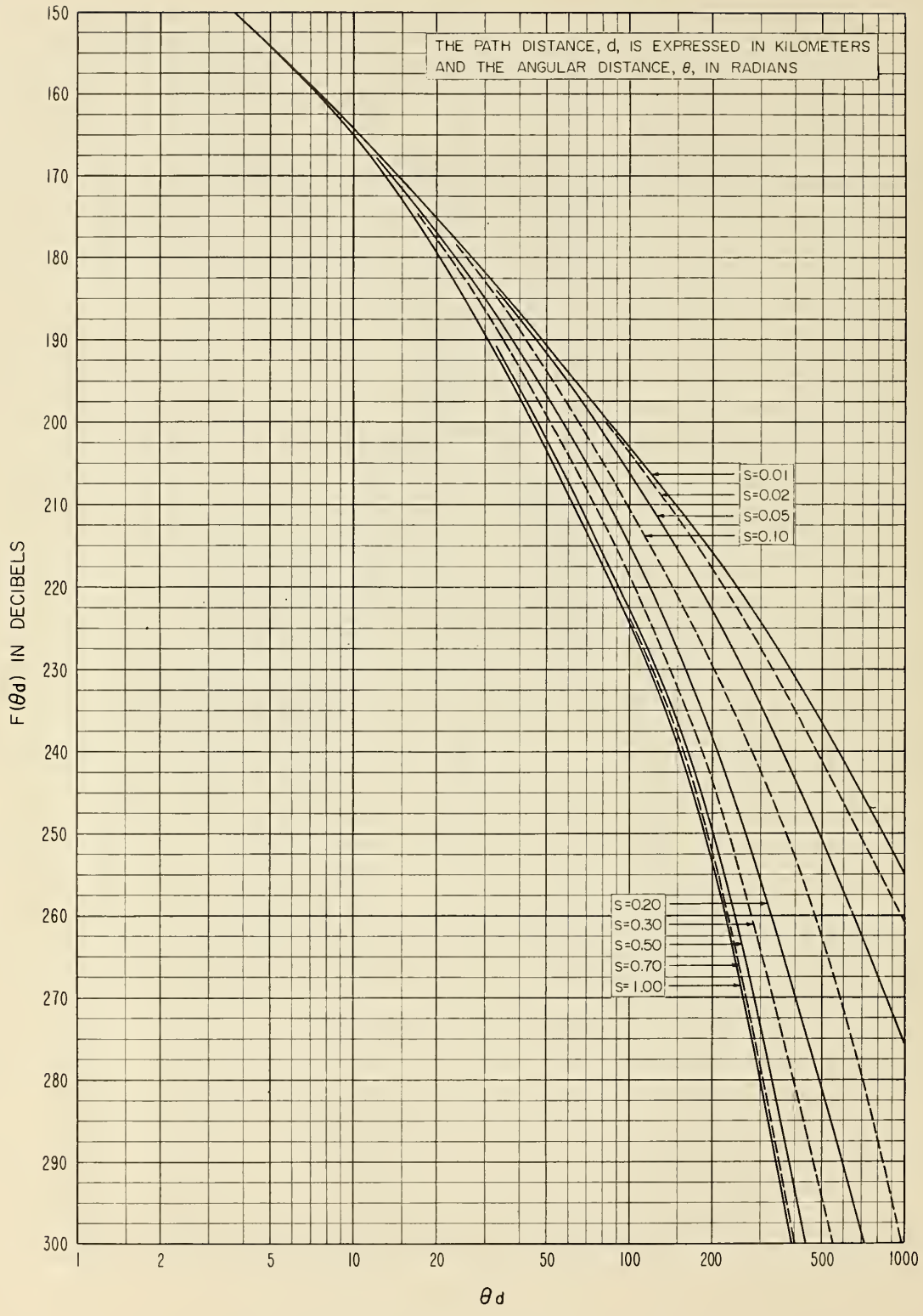

Figure III.13

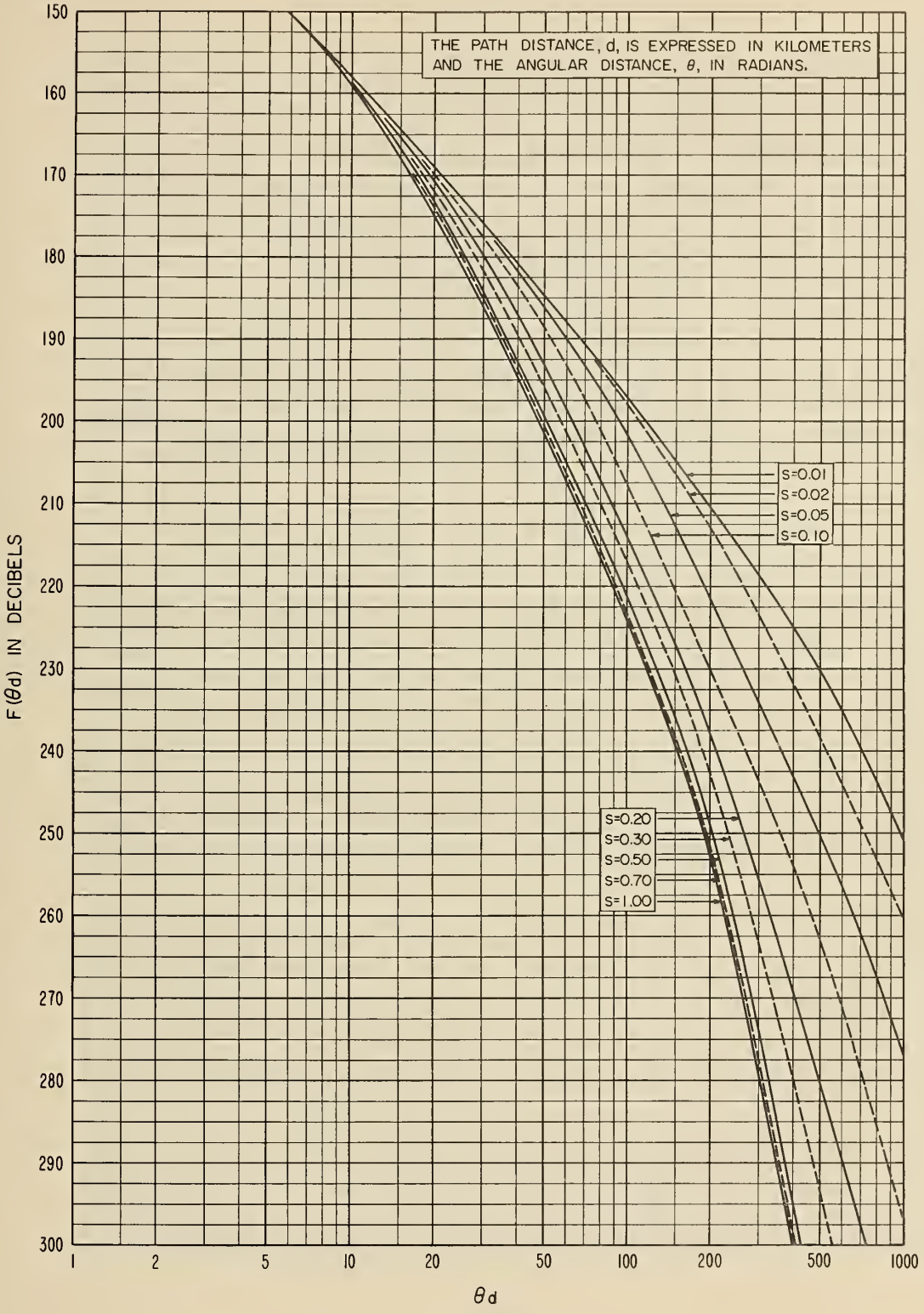

Figure III.14

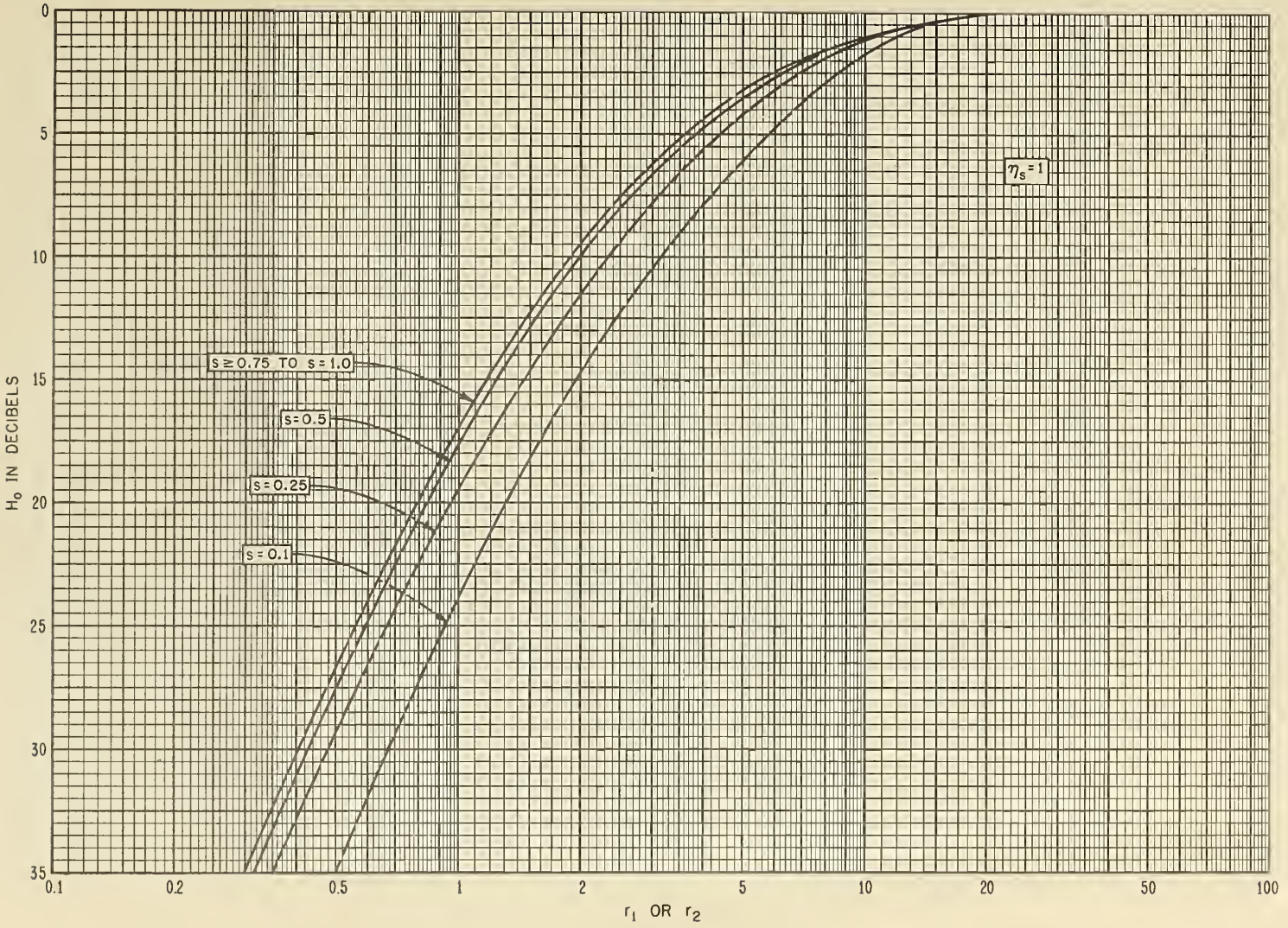

Figure III.15

THE FREQUENCY GAIN FUNCTION, H_o

$h_{te} = h_{re}$

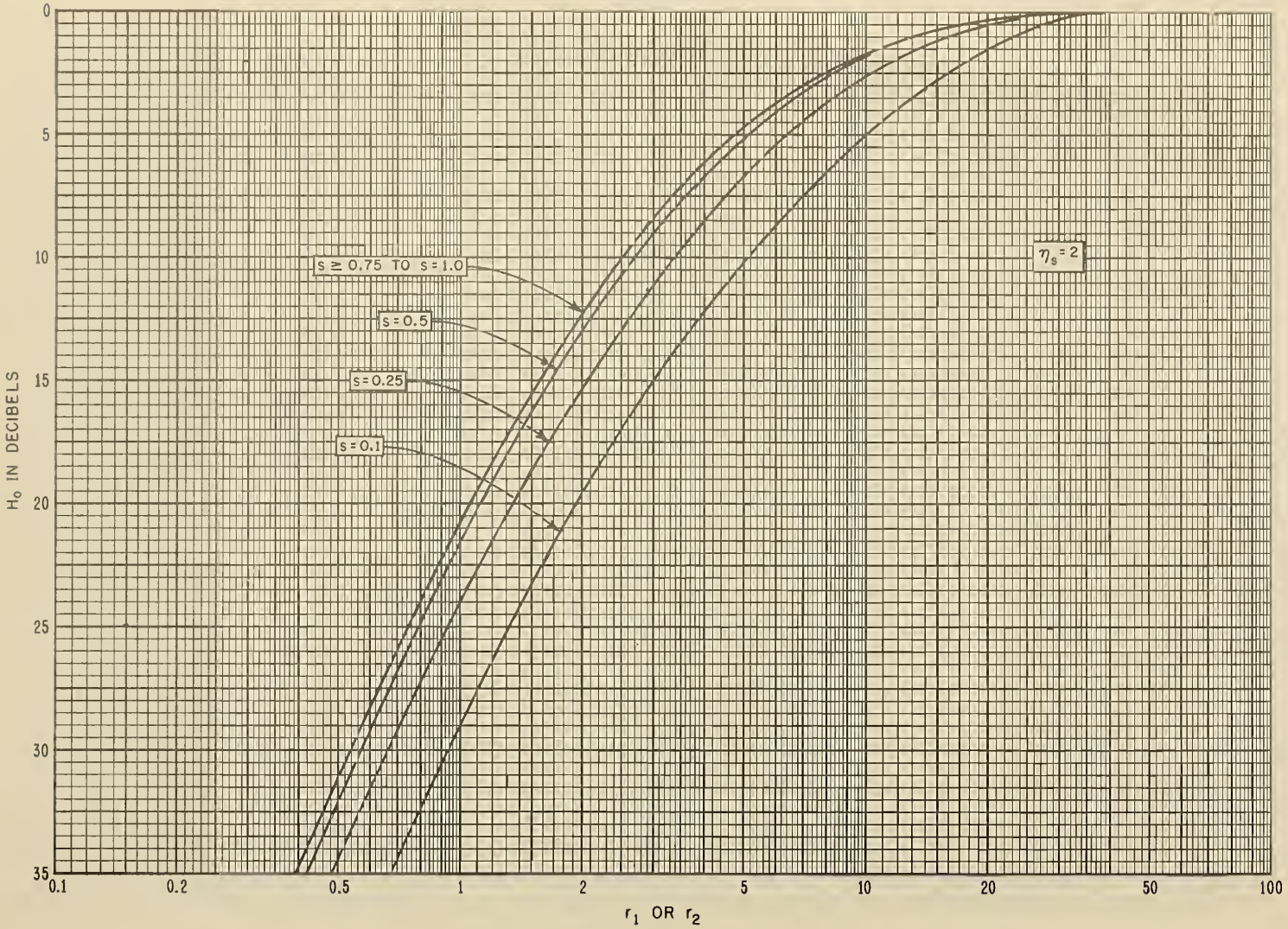

Figure III.16

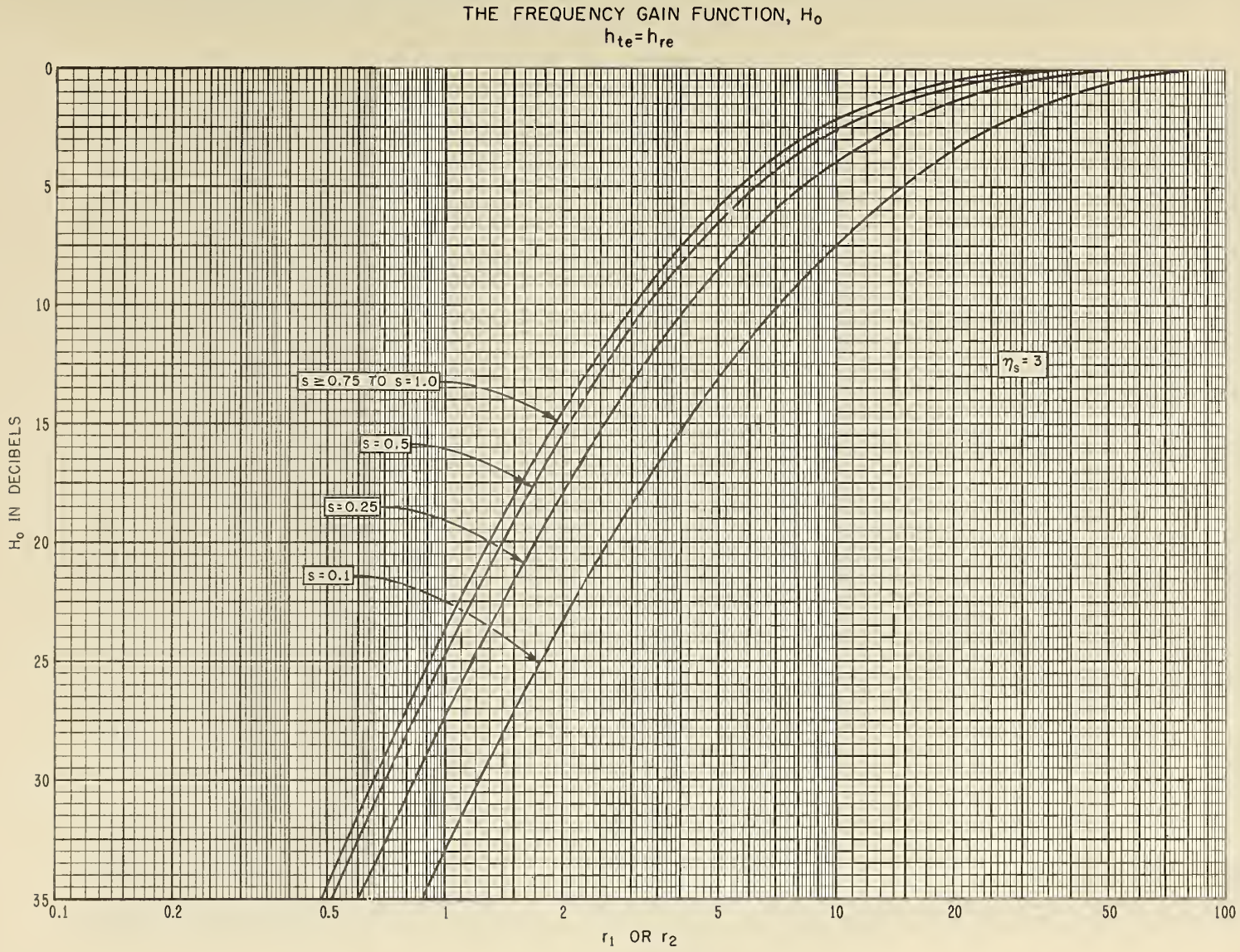

Figure III.17

THE FREQUENCY GAIN FUNCTION, H_o
$h_{te} = h_{re}$

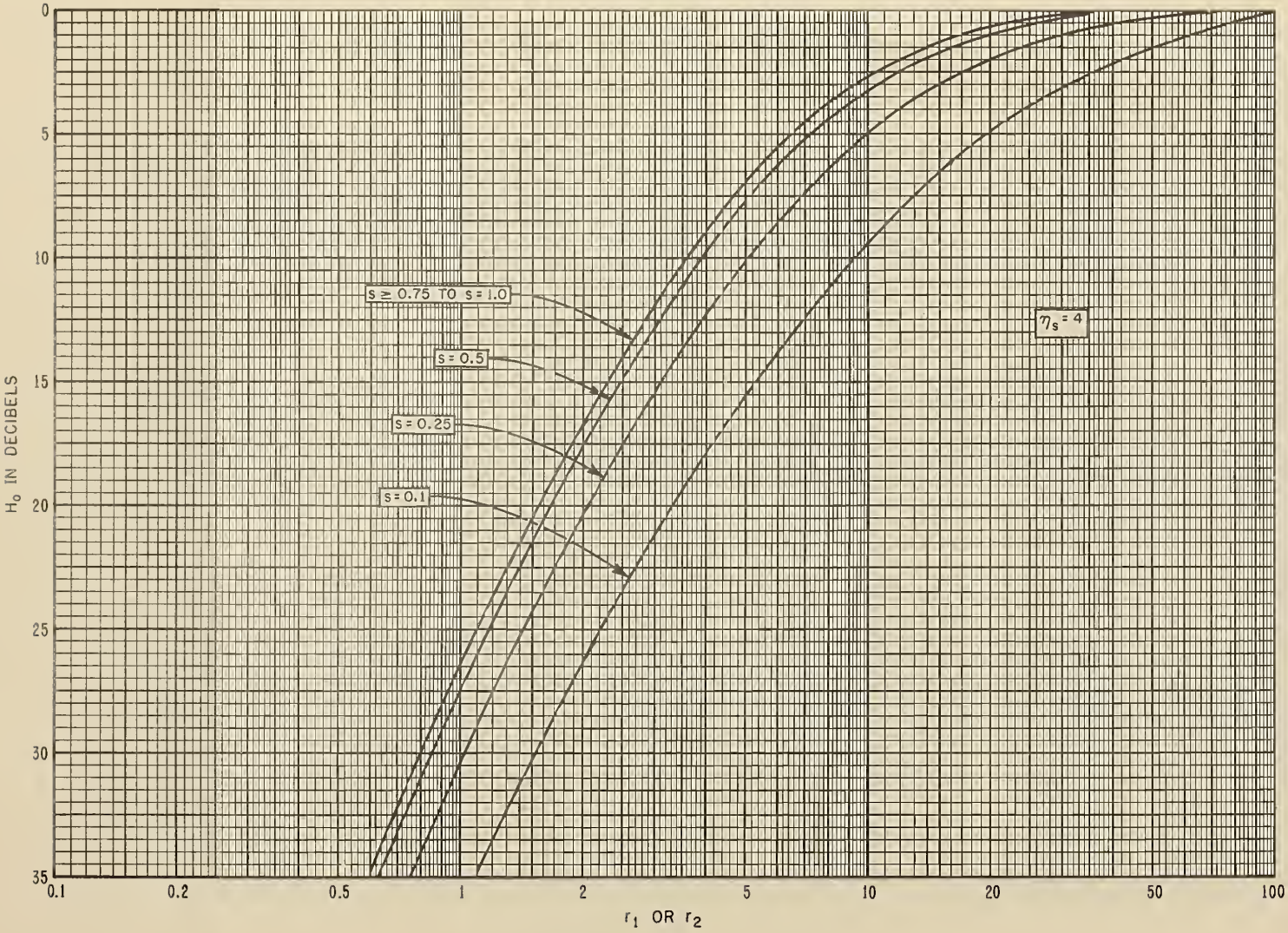

Figure III.18

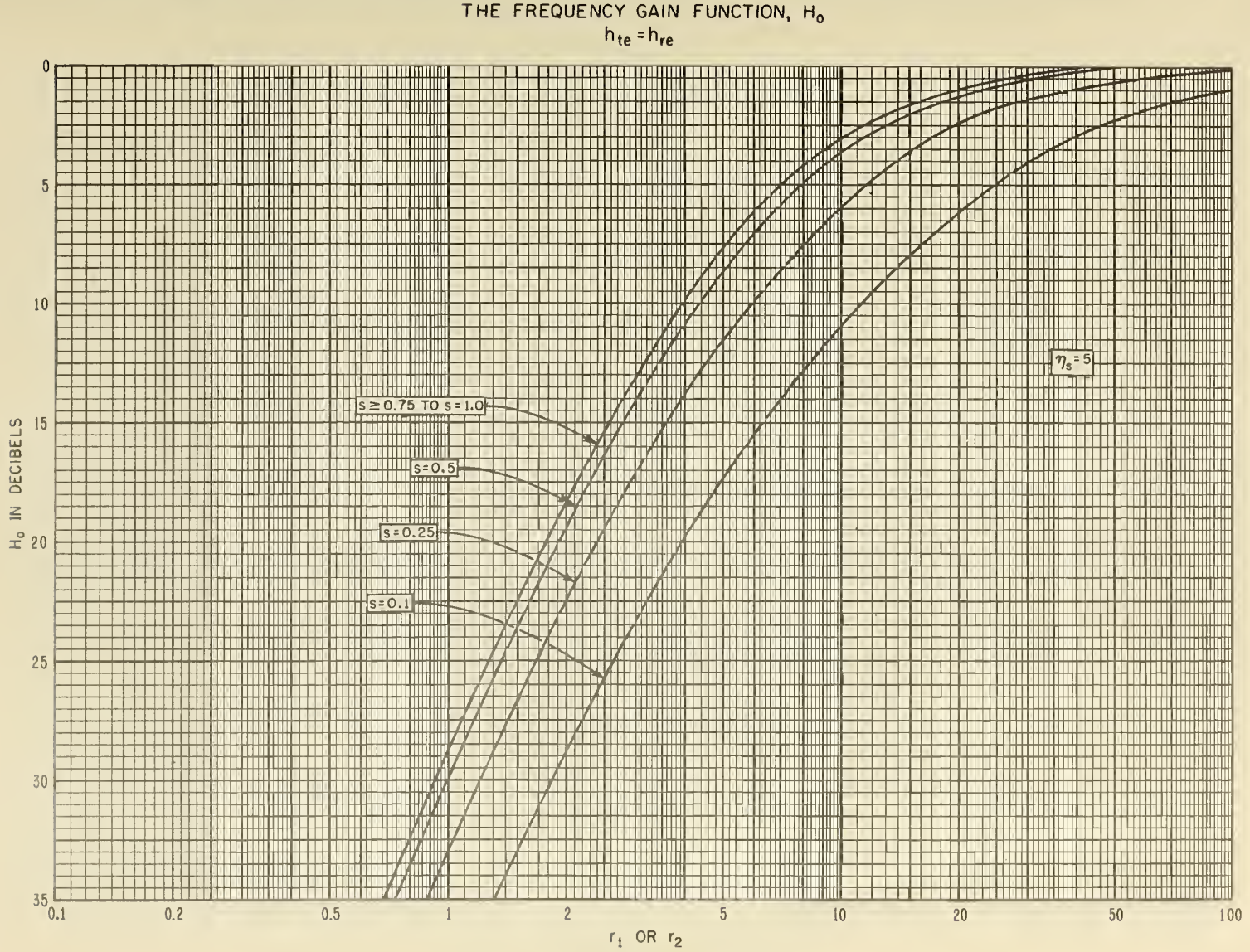

Figure III.19

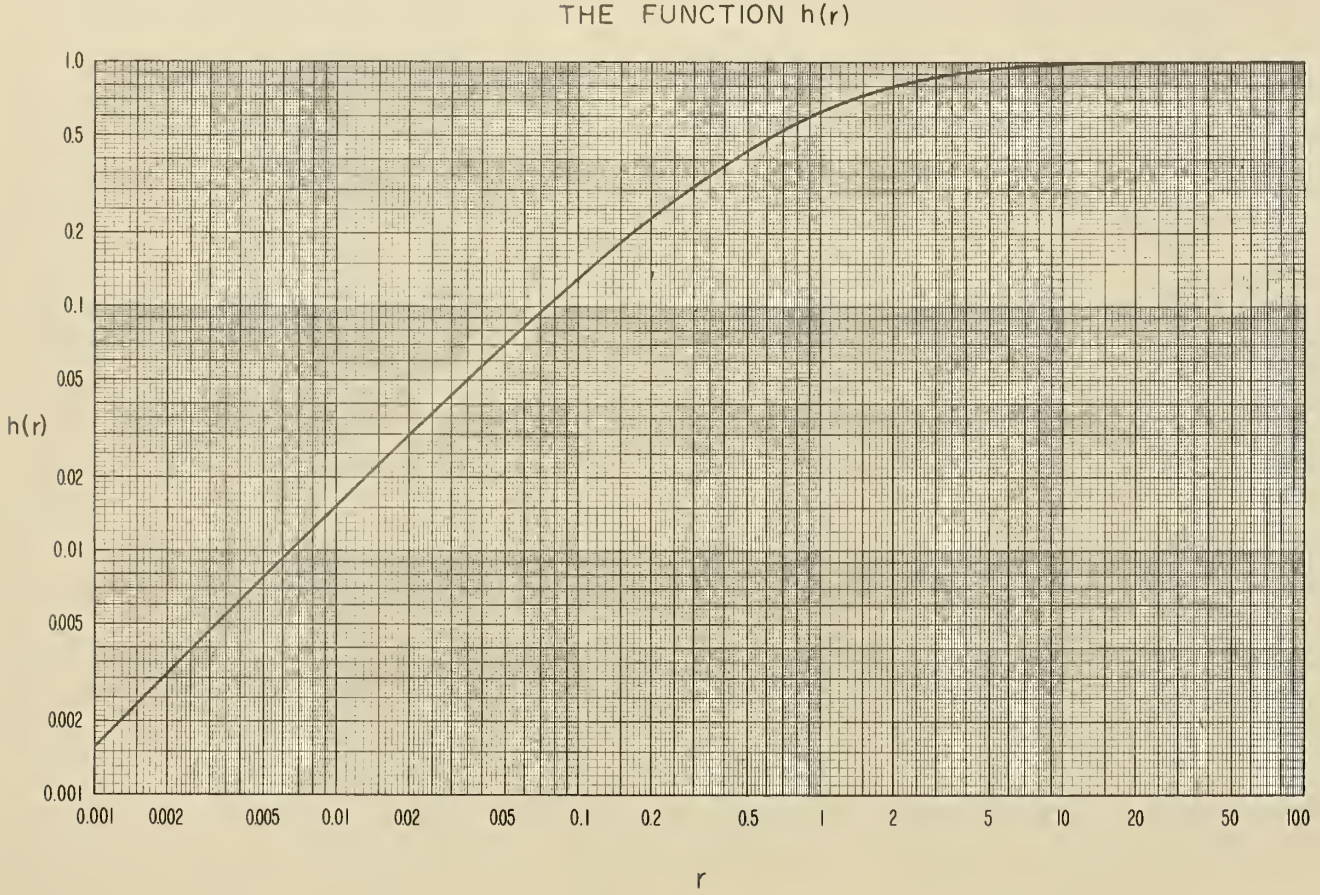

Figure III.20

THE FUNCTION h(r)

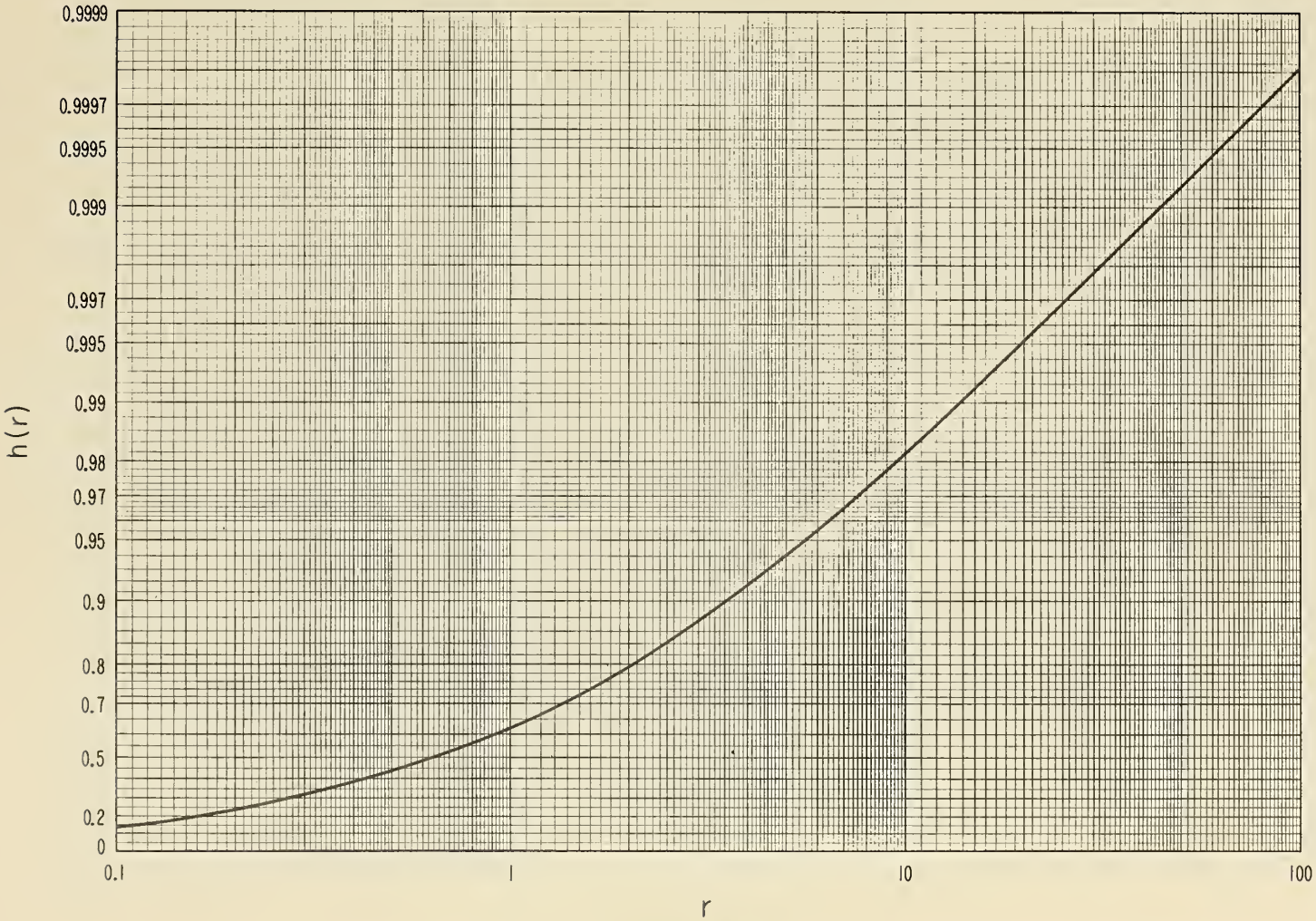

Figure III.21

III. 6 Transmission Loss with Antenna Beams Elevated or Directed Out of the Great Circle Plane

The methods of section 9 may be modified to calculate a reference value of long-term median transmission loss when antenna beams are either elevated or directed away from the great circle path between antennas. For many applications, the average transmission loss between antennas with random relative orientation is about 10 db more than the basic transmission loss, which assumes zero db antenna gains.

Figure III.22 shows scattering subvolumes at intersections of antenna main beams and side lobes. A "scatter" theory assumes that the total power available at a receiver is the sum of the powers available from many scattering subvolumes. For high gain antennas, the intersection of main beams defines the only important scattering volume. In general, all power contributions that are within 10 db of the largest one should be added.

For a total radiated power p_t :

$$p_a/p_t = 10^{-0.1\, L_{sr}}, \qquad p_{ai}/p_t = 10^{-0.1\, L_i} \tag{III.55}$$

where L_{sr} is the transmission loss and L_i is the loss associated with the ith power contribution, p_{ai}:

$$L_{sr} = -10 \log (p_a/p_t) = -10 \log \sum_i 10^{-0.1\, L_i} \tag{III.56}$$

$$L_i = 30 \log f - 20 \log (d^2/r_o) + F(\theta_{ei} d) - F_{oi} + H_{oi} + A_a - G_{ti} - G_{ri} + L_{gi} \tag{III.57}$$

In (III.57) f, d, and A_a are defined as in (9.1) and the other terms are related to similar terms in (9.1). If the effective scattering angle θ_{ei} for the ith intersection is equal to the minimum scattering angle θ, then $F(\theta_{ei} d)$, F_{oi}, H_{oi} are equal to $F(\theta d)$, F_o, and H_o, and $G_{ti} + G_{ri} - L_{gi} = G_p$. Note that a term $20 \log (r_o/d)$ has been added in (III.57) to provide for situations where the straight line distance r_o between antennas is much greater than the sea-level arc distance d. Such differences occur in satellite communication.

Scattering planes, defined by the directions of incident and scattered energy, may or may not coincide with the plane of the great circle path. Each "scattering plane" is determined by the line between antenna locations and the axis of the stronger of the two intersecting beams, making an angle ζ with the great circle plane.

The free space directive gain patterns of the antennas are replaced by equivalent values for ease in computation. For an idealized pencil-beam antenna with a half-power beamwidth 2δ and a circular beam cross-section, the directive gain g is $4/\delta^2$, assuming that all of the power is radiated through the main beam and between the half-power points. An equivalent beam pattern with a square cross-section and a semi-beamwidth δ_o has a gain of π/δ_o^2, thus $\delta_o = \delta\sqrt{\pi/4}$, and the maximum free space gains are

$$G_t = 10 \log g_{to} = 4.97 - 10 \log \delta_{two}\, \delta_{tzo} \quad \text{db} \qquad \text{(III. 58a)}$$

$$G_r = 10 \log g_{ro} = 4.97 - 10 \log \delta_{rwo}\, \delta_{rzo} \quad \text{db} \qquad \text{(III. 58b)}$$

where the subscripts w and z refer to azimuthal and vertical angles. In most cases, δ_{wo} and δ_{zo} may be replaced by their geometric mean, $\delta_o = (\delta_{wo}\delta_{zo})^{1/2}$. The free space directive gain of a main beam may be measured or approximated as $g_o \simeq \pi/(2\,\delta_{wo}\delta_{zo})$. Gains for side lobes are determined from g_o and the ratios g_1/g_o, g_2/g_o, ..., which may be measured or calculated. The average gain g_b for other directions depends on the fraction of power radiated in those directions. For instance, if half the total power of a transmitter is radiated in these directions, and if the polarization coupling loss, L_{cp}, is 3 db, then

$$G_{bt} - L_{cp} = -6 \text{ db}$$

since the definition of the directive gain, G_{bt}, assumes for every direction the receiving antenna polarization appropriate for maximum power transfer.

Figure III.23 shows an antenna power pattern in several different ways, including a Mercator projection of the surface of a unit sphere.

The plane that determines the "bottom" of a beam is perpendicular to the great circle plane and forms an angle ψ_i with a horizon plane:

$$\psi_{ti} = \theta_{bti} - \theta_{et}\,, \qquad \psi_{ri} = \theta_{bri} - \theta_{er} \qquad \text{(III. 59)}$$

where θ_b is the angle of elevation of the lower half-power point of a beam above the horizontal, and θ_{et} is defined in section 6. If an antenna beam is elevated sufficiently so that ray bending may be neglected, the angles α_e and β_e are denoted α_{eo} and β_{eo}:

$$\alpha_{eo} = (\alpha_{oo} + \psi_t) \sec \zeta\,, \qquad \beta_{eo} = (\beta_{oo} + \psi_r) \sec \zeta \qquad \text{(III. 60)}$$

where ζ is the angle away from the great circle plane. The angles α_{oo} and β_{oo} are defined as in section 6 using the actual radius, $a_o \simeq 6370$ km, instead of an effective radius a.

When ray bending must be considered, the equations for α_e and β_e are

$$\alpha_e = \alpha_{eo} + \tau\left(\theta_{bt}, \frac{d_{Lt}\sec\zeta}{2}, N_s\right) - \tau\left(\theta_{bt}, \frac{d\sec\zeta}{2}, N_s\right) \qquad \text{(III.61a)}$$

$$\beta_e = \beta_{eo} + \tau\left(\theta_{br}, \frac{d_{Lr}\sec\zeta}{2}, N_s\right) - \tau\left(\theta_{br}, \frac{d\sec\zeta}{2}, N_s\right) \qquad \text{(III.61b)}$$

where $\tau(\theta_b, d, N_s)$ is the bending of a radio ray which takes off at an angle θ_b above the horizontal and travels d kilometers through an atmosphere characterized by a surface refractivity N_s. The ray bending τ may be determined using methods and tables furnished by Bean and Thayer [1959]. For short distances, d, or large angles, θ_b, τ is negligible. If θ_b is less than 0.1 radians, the effective earth's radius approximation is adequate for determining τ,

$$\tau\left(\theta_b, \frac{d\sec\zeta}{2}, N_s\right) = \frac{d}{a_o}\left[1 - a_o/a(N_s)\right] \qquad \text{(III.62)}$$

The reference value of long-term median transmission loss L_{sr} is computed using (III.56) where the losses associated with several scattering subvolumes are computed using (III.57). The attenuation function $F(d\theta_{ei})$ is read from figure 9.1 or figures III.11 - III.14 as a function of θ_{ei}.

The generalized scattering efficiency term F_{oi} is

$$F_{oi} = 1.086(\eta_{se}/h_e)(2h_o - h_1 - h_e - h_{Lt} - h_{Lr}) \quad \text{db} \qquad \text{(III.63)}$$

where

$$\theta_e = \alpha_e + \beta_e, \quad s_e = \alpha_e/\beta_e, \quad h_e = s_e\, d\theta_e/(1+s_e)^2, \quad \eta_{se} = \eta_s(h_e, N_s) \qquad \text{(III.64)}$$

and the other terms are defined in section 9. In computing the frequency gain function H_{oi}, if $\alpha_e > \alpha_o$ use $r_1 = \infty$, if $\beta_e > \beta_o$ use $r_2 = \infty$; then $H_{oi} = H_o + 3$ db. If both antennas are elevated above the horizon rays, $H_{oi} = 6$ db. Atmospheric absorption A_a is discussed in section 3. The gains G_{ti} and G_{ri} are the free space directive gains defined by (III.58), and the loss in gain L_{gi} is computed as shown in section 9 replacing η_s, s, δ, and θ by η_{se}, s_e, δ_e, and θ_e.

In computing long-term variability of transmission loss for beams elevated above the horizon plane, the estimates of V and Y given in section 10 should be reduced by the factor $f(\theta_h)$ shown in figure III.24, with $\theta_h = \theta_b$:

$$V_e(50, d_e) = V(50, d_e)\, f(\theta_h) \qquad \text{(III.65a)}$$

$$Y_e(p, d_e) = Y(p, d_e)\, f(\theta_h) \qquad \text{(III.65b)}$$

The angle θ_h used in (III.65) should be the elevation above the horizontal of the scattering subvolume corresponding to the minimum value of L_i.

SCATTERING SUBVOLUMES IN A SCATTERING PLANE

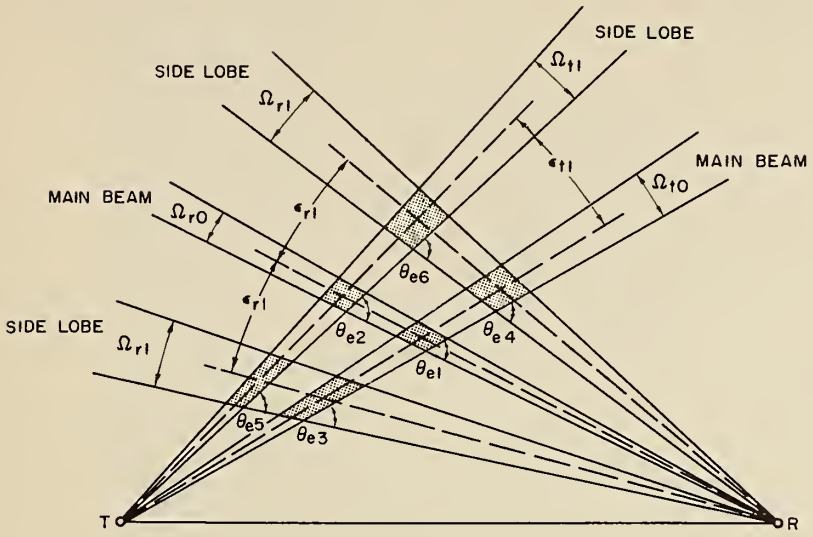

$\Omega = 2\delta$

ILLUSTRATION OF A SCATTERING PLANE CONTAINING
THE MAIN BEAM OF THE RECEIVING ANTENNA

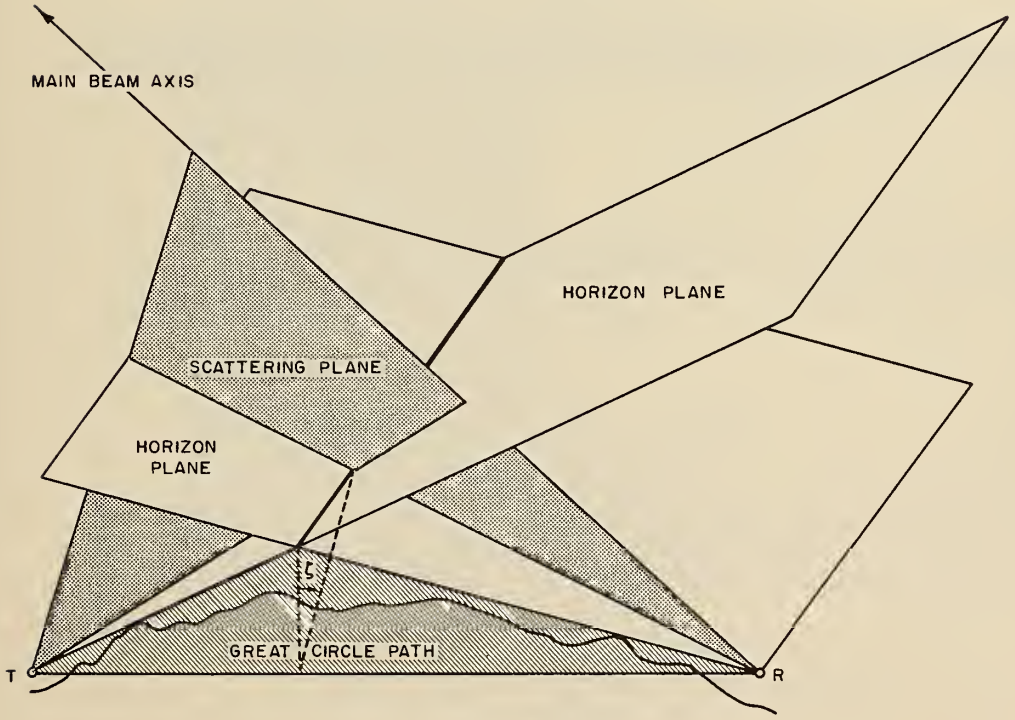

Figure III.22

FREE SPACE ANTENNA PATTERN

INTERSECTION OF AN EQUIVALENT ANTENNA POWER PATTERN WITH THE SURFACE OF A UNIT SPHERE

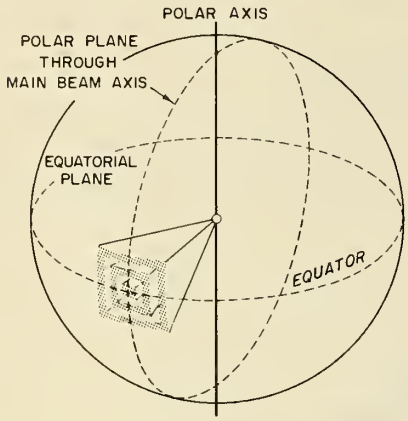

PATTERN PARAMETERS	
$\delta_{t0} = 0.04$	$\delta_{tw0} = 0.06$
$\delta_{tz1} = 0.02$	$\delta_{tw1} = 0.02$
$\delta_{tz2} = 0.02$	$\delta_{tw2} = 0.02$
$\epsilon_{tz1} = 0.12$	$\epsilon_{tw1} = 0.20$
$\epsilon_{tz2} = 0.22$	$\epsilon_{tw2} = 0.30$
$g_{t0} = 654.5$	$G_{t0} = 28.16$ db
$g_{t1} = 20.7$	$G_{t1} = 13.16$ db
$g_{t2} = 3.28$	$G_{t2} = 5.16$ db
$g_{bt} = 0.395$	$G_{bt} = -4.04$ db

ANTENNA VOLTAGE PATTERN. POLAR DIAGRAM IN THE EQUATORIAL PLANE

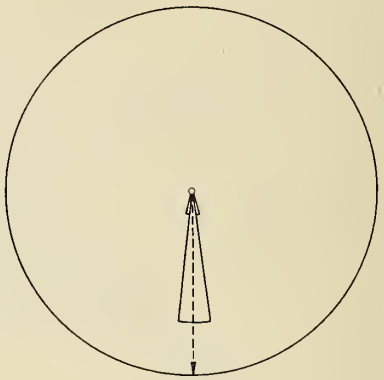

CARTESIAN DIAGRAM OF TRANSMITTING ANTENNA POWER PATTERN IN THE EQUATORIAL PLANE

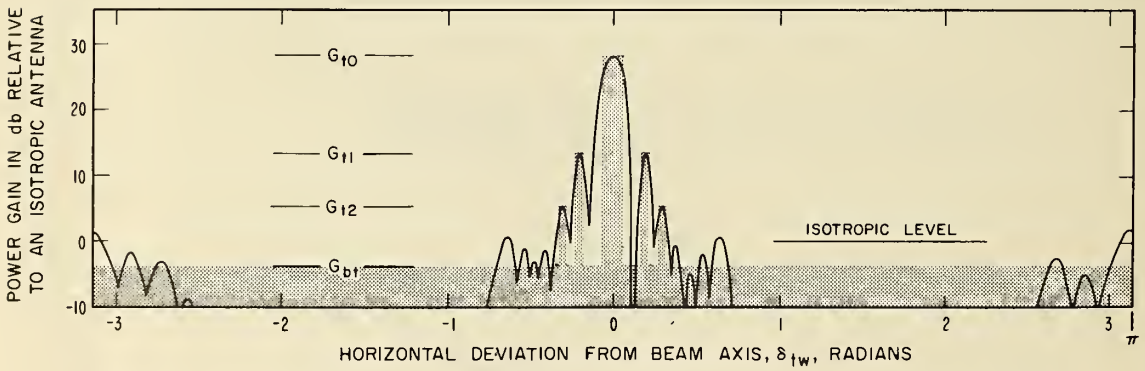

MERCATOR PROJECTION OF THE INTERSECTION OF THE EQUIVALENT TRANSMITTING ANTENNA POWER PATTERN WITH THE SURFACE OF A UNIT SPHERE

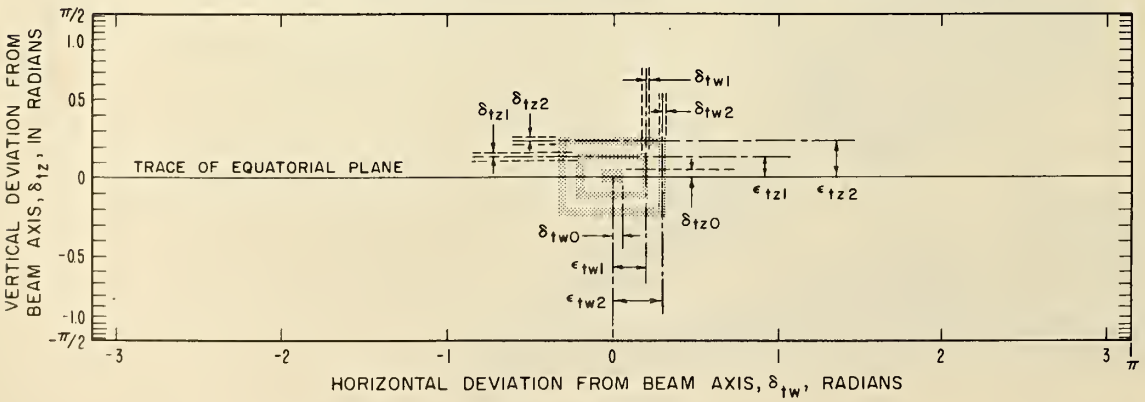

Figure III.23

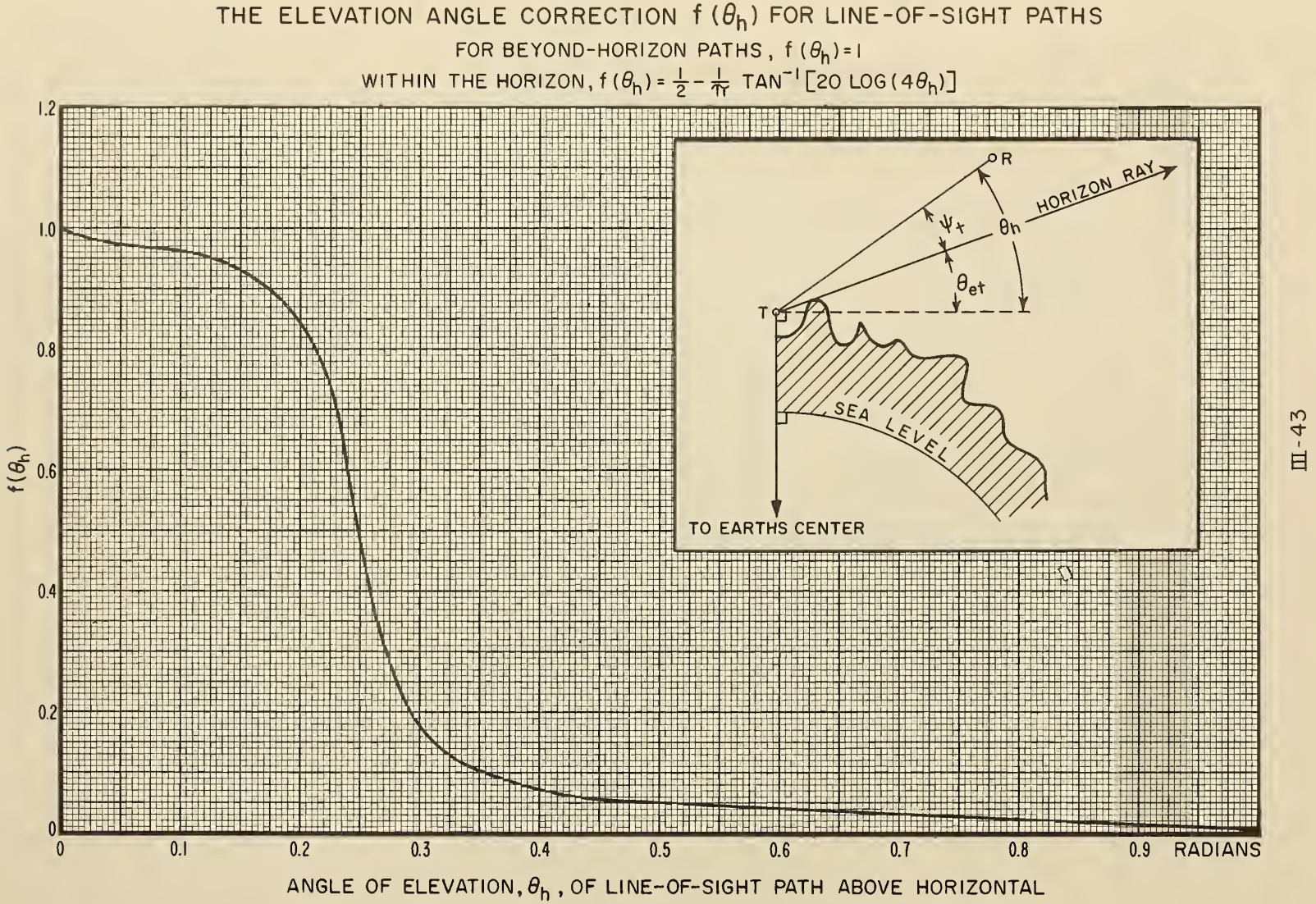

Figure III.24

III.7 Long-Term Power Fading

Long-term power fading is discussed in section 10. Figures 10.5 to 10.16 show empirical estimates of all-year variability for (1) continental temperate (2) maritime temperate overland and (3) maritime temperate oversea climates. The curves shown on these figures are based on a large amount of data. Estimates of variability in other climates are based on what is known about meteorological conditions and their effects on radio propagation, but have relatively few measurements to support them.

Figures III.25 to III.29 show curves of variability relative to the long-term median, prepared by the CCIR [1963 f] for the following climatic regions:

(4) Maritime Subtropical, Overland.

(5) Maritime Subtropical, Oversea.

(6) Desert.

(7) Equatorial.

(8) Continental Subtropical.

In some cases, random path differences have undoubtedly been attributed to climatic differences. Available data were normalized to a frequency of 1000 MHz, and the curves correspond to this frequency. They show all-year variability $Y_o(p, d_e)$ about the long-term median as a function of the effective distance d_e defined by (10.3). Variability estimates for other frequencies are obtained by using the appropriate correction factor $g(f)$ shown in figure III.30:

$$Y(p) = Y_o(p, d_e)\, g(f) \qquad \text{(III.66)}$$

The empirical curves $g(f)$ are not intended as an estimate of the dependence of long-term variability on frequency, but represent an average of many effects that are frequency-sensitive, as discussed in section 10.

Variability about the long-term median transmission loss $L(50)$ is related to the long-term reference median L_{cr} by means of the function $V(50, d_e)$ shown on figure 10.1. The predicted long-term median transmission loss is then:

$$L(50) = L_{cr} - V(50, d_e) \qquad \text{(III.67)}$$

and the predicted value for any percentage of time is

$$L(p) = L(50) - Y(p) \qquad \text{(III.68)}$$

as described in section 10.

III. 7. 1 Diurnal and Seasonal Variability in a Continental Temperate Climate

The curves shown in figures 10.5 to 10.16 and III.25 to III.29 represent variability about the long-term median for all hours of the day throughout the entire year. For certain applications, it is important to know something about the diurnal and seasonal changes that may be expected. Such changes have been studied in the continental United States, where a large amount of data is available. Measurement programs recorded VHF and UHF transmission loss over particular paths for at least a year to determine seasonal variations. Data were recorded over a number of paths for longer periods of time to study year-to-year variability.

As a general rule, transmission loss is less during the warm summer months than in winter, and diurnal trends are usually most pronounced in summer, with maximum transmission loss occurring in the afternoon. The diurnal range in signal level may be about 10 db for paths that extend just beyond the radio horizon, but is much less for very short or very long paths. Variation with season usually shows maximum losses in mid-winter, especially on winter afternoons, and high fields in summer, particularly during morning hours. Transmission loss is often much more variable over a particular path in summer than it is during the winter, especially when ducts and elevated layers are relatively common.

The data were divided into eight "time blocks" defined in table III. 1. The data were assumed to be statistically homogeneous within each of the time blocks. With more and shorter time blocks, diurnal and seasonal trends would be more precisely defined, except that no data would be available in some of the time blocks over many propagation paths. Even with the division of the year into winter and summer and the day into four periods as in table III. 1, it is difficult to find sufficient data to describe the statistical characteristics expected of transmission loss in Time Blocks 7 and 8.

Table III. 1

Time Blocks

No.	Months	Hours
1	Nov. - Apr.	0600 - 1300
2	Nov. - Apr.	1300 - 1800
3	Nov. - Apr.	1800 - 2400
4	May - Oct.	0600 - 1300
5	May - Oct.	1300 - 1800
6	May - Oct.	1800 - 2400
7	May - Oct.	0000 - 0600
8	Nov. - Apr.	0000 - 0600

In some applications, it is convenient to combine certain time blocks into groups, for instance, some characteristics of long-term variability are significantly different for the winter group (Time Blocks 1, 2, 3, 8) than for the summer group (Time Blocks 4, 5, 6, 7).

In other climatic regions, if the annual range of monthly average values of N_s is less than 20 N units (figure III.31), seasonal variations are expected to be negligible. One would also expect less diurnal change, for example, in a maritime temperate climate where changes in temperature during the day are less extreme. In climates where N_s changes considerably throughout the year, the consecutive 4 - 6 month period when N_s is lowest may be assumed to correspond to "winter", whatever months may be involved.

The parameter $V(50, d_e)$ for each of the eight time blocks and for "summer" and "winter" is shown in figure III.32. Curves of the variability $Y_o(p, d_e)$ about the long-term median for each of these times of day and seasons are shown in figures III.33 to III.42. These curves are drawn for a frequency of 100 MHz. Figures III.33 and III.34 show the 1 to 99 percent range of $Y_o(p, d_e)$ for the winter time blocks, 1, 2, 3, 8 and the summer time blocks 4, 5, 6, 7. Each group of data was analyzed separately. Some of the differences shown between time blocks 1, 2, 3 and 8 are probably not statistically significant. Marked differences from one time block to another are observed during the summer months.

The curves for summer, winter, and all hours shown in figures 10.1 through 10.10 represent a much larger data sample. For a number of the paths time block information was not available.

The smooth curves of $V(50, d_e)$ and $Y_o(p, d_e)$ versus d_e shown in figures 10.1, 10.2, and III.32 to III.42 may be represented by an analytic function of the general form:

$$\left.\begin{matrix} V(50) \\ Y_o(10) \\ -Y_o(90) \end{matrix}\right\} = \left[c_1 d_e^{n_1} - f_2(d_e) \right] \exp\left(- c_3 d_e^{n_3}\right) + f_2(d_e) \qquad \text{(III.69)}$$

where

$$f_2(d_e) = f_\infty \left[1 - (1 - f_m/f_\infty) \exp\left(- c_2 d_e^{n_2} \right) \right] \qquad \text{(III.70)}$$

The terms c_1, c_2, c_3, n_1, n_2, n_3, f_m, and f_∞ in (III.69) and (III.70) are constants for any given time block and value of p. The parameters f_m and f_∞ are maximum and asymptotic values, respectively. Tables III.2 to III.4 list values of the eight parameters required in (III.69) to obtain $V(50, d_e)$, $Y_o(10, d_e)$, and $-Y_o(90, d_e)$ for the eight time blocks in table III.1, and for summer, winter, and all hours. The constants given in Tables III.2 to III.4 for summer, winter and all hours were determined using only radio paths for which time block information is available. They do not yield the curves shown in figures 10.1 and 10.2 of section 10, which represents a much larger data sample.

TABLE III.2

Constants for Calculating $V(50, d_e)$

Time Block	d_e in miles c_1	c_2	c_3	d_e in km. c_1	c_2	c_3	n_1	n_2	n_3	f_m	f_∞
4	5.10^{-6}	1.24^{-16}	5.70^{-7}	1.35^{-6}	5.02^{-18}	1.32^{-7}	2.80	6.74	3.08	5.2	4.0
5	3.80^{-6}	1.24^{-16}	2.41^{-8}	1.05^{-6}	5.02^{-18}	4.14^{-9}	2.70	6.74	3.70	2.4	1.8
6	4.96^{-4}	1.58^{-16}	1.69^{-8}	2.04^{-4}	6.61^{-18}	2.82^{-9}	1.87	6.67	3.76	5.2	4.2
7	1.78^{-3}	6.61^{-15}	3.50^{-5}	8.00^{-4}	3.91^{-16}	1.20^{-5}	1.68	5.94	2.25	7.1	5.6
S*	3.69^{-5}	1.36^{-15}	5.72^{-6}	1.18^{-5}	6.72^{-17}	1.65^{-6}	2.40	6.32	2.61	5.1	4.0
1	4.68^{-4}	7.65^{-16}	4.12^{-4}	2.11^{-4}	3.44^{-17}	1.73^{-4}	1.67	6.52	1.82	1.2	0.5
3	7.43^{-4}	4.68^{-13}	1.15^{-3}	3.47^{-4}	3.76^{-14}	5.42^{-4}	1.60	5.30	1.58	1.3	0.6
8	7.97^{-4}	1.25^{-21}	4.77^{-5}	3.63^{-4}	1.80^{-23}	1.55^{-5}	1.65	8.91	2.36	1.95	0.8
W*	2.56^{-3}	9.71^{-32}	3.46^{-5}	1.40^{-3}	1.79^{-34}	1.05^{-5}	1.27	13.23	2.51	1.05	0.5
A*	3.83^{-4}	1.74^{-23}	2.45^{-5}	1.63^{-4}	1.81^{-25}	8.12^{-6}	1.80	9.59	2.32	3.0	1.9

* Time Blocks "S", "W", and "A" are all hours summer, all hours winter, and all hours all year, respectively. See Table III.1 for definitions of the other time blocks.
Small digits represent the exponent of the number, for example $5.10^{-6} = 5.10 \times 10^{-6}$.

TABLE III. 3

Constants for Calculating $Y_o(10, d_e)$

Time Block	d_e in miles c_1	c_2	c_3	d_e in km. c_1	c_2	c_3	n_1	n_2	n_3	f_m	f_∞
4	2.33^{-2}	2.54^{-5}	6.01^{-8}	1.22^{-2}	9.81^{-6}	1.09^{-8}	1.36	2.00	3.58	10.8	5.5
5	6.83^{-4}	9.94^{-6}	1.95^{-10}	2.58^{-4}	3.41^{-6}	2.01^{-11}	2.05	2.25	4.78	8.0	4.0
6	8.10^{-3}	9.76^{-5}	4.43^{-8}	3.84^{-3}	4.22^{-5}	7.76^{-9}	1.57	1.76	3.66	9.6	5.2
7	1.60^{-2}	8.68^{-5}	1.61^{-7}	7.95^{-3}	3.76^{-5}	3.19^{-8}	1.47	1.76	3.40	11.2	5.5
S *	9.34^{-3}	4.09^{-5}	1.08^{-7}	4.47^{-3}	1.66^{-5}	2.06^{-8}	1.55	1.90	3.48	9.98	5.1
1	3.23^{-4}	3.60^{-6}	3.91^{-7}	1.09^{-4}	1.21^{-6}	8.29^{-8}	2.28	2.29	3.26	9.6	2.8
2	3.78^{-5}	1.71^{-7}	1.78^{-7}	1.04^{-5}	4.28^{-8}	3.51^{-8}	2.71	2.91	3.41	9.15	2.8
3	5.61^{-4}	4.29^{-6}	2.12^{-7}	2.02^{-4}	1.45^{-6}	4.27^{-8}	2.15	2.28	3.37	9.4	2.8
8	4.82^{-4}	2.45^{-6}	5.87^{-7}	1.70^{-4}	7.93^{-7}	1.29^{-7}	2.19	2.37	3.18	9.5	3.0
W *	6.72^{-4}	6.12^{-7}	7.10^{-8}	2.46^{-4}	1.74^{-7}	1.27^{-8}	2.11	2.64	3.62	9.37	2.8
A *	1.34^{-3}	4.72^{-6}	1.87^{-6}	5.25^{-4}	1.57^{-6}	4.70^{-7}	1.97	2.31	2.90	10.0	5.4

* Time Blocks "S", "W", and "A" are all hours summer, all hours winter, and all hours all year, respectively. See Table III.1 for definitions of the other time blocks.
Small digits represent the exponent of the number, for example $2.33^{-2} = 2.33 \times 10^{-2}$.

TABLE III. 4

Constants for Calculating $-Y_o(90, d_e)$

Time Block	d_e in miles c_1	c_2	c_3	d_e in km. c_1	c_2	c_3	n_1	n_2	n_3	f_m	f_∞
4	4.97^{-4}	6.61^{-6}	9.36^{-15}	1.84^{-4}	2.22^{-6}	3.65^{-16}	2.09	2.29	6.82	8.0	4.0
5	9.47^{-4}	1.35^{-5}	2.46^{-15}	3.80^{-4}	4.76^{-6}	8.39^{-17}	1.92	2.19	7.10	6.6	3.3
6	4.03^{-3}	1.62^{-5}	8.24^{-12}	1.81^{-3}	5.82^{-6}	6.37^{-13}	1.67	2.15	5.38	8.4	4.1
7	6.83^{-3}	7.40^{-6}	2.91^{-8}	3.19^{-3}	2.51^{-6}	5.03^{-9}	1.60	2.27	3.69	10.0	4.4
S *	1.78^{-3}	1.24^{-4}	2.08^{-7}	7.42^{-4}	5.55^{-5}	4.37^{-8}	1.84	1.69	3.28	8.25	4.0
1	4.68^{-4}	2.41^{-7}	2.20^{-9}	1.72^{-4}	6.39^{-8}	2.93^{-10}	2.10	2.79	4.24	8.2	2.4
2	3.61^{-5}	6.87^{-12}	4.40^{-8}	1.05^{-5}	7.00^{-13}	7.64^{-9}	2.59	4.80	3.68	7.05	2.8
3	1.14^{-4}	1.78^{-8}	1.43^{-6}	3.64^{-5}	3.74^{-9}	3.53^{-7}	2.40	3.28	2.94	7.8	2.2
8	7.12^{-6}	5.07^{-7}	1.33^{-6}	1.64^{-6}	1.43^{-7}	3.14^{-7}	3.08	2.66	3.03	8.6	2.6
W *	1.35^{-5}	5.38^{-8}	2.87^{-6}	3.45^{-6}	1.25^{-8}	7.50^{-7}	2.87	3.07	2.82	7.92	2.45
A *	7.60^{-4}	1.49^{-7}	4.56^{-7}	2.93^{-4}	3.78^{-8}	1.02^{-7}	2.00	2.88	3.15	8.2	3.2

* Time Blocks "S", "W", and "A" are all hours summer, all hours winter, and all hours all year, respectively. See Table III.1 for definitions of other time blocks.
Small digits represent the exponent of the number, for example, $4.97^{-4} = 4.97 \times 10^{-4}$.

III. 7. 2 To Mix Distributions

When a prediction is required for a period of time not shown on the figures or listed in the tables, it may sometimes be obtained by mixing the known distributions. For example, the distributions for time blocks 5 and 6 would be mixed if one wished to predict a cumulative distribution of transmission loss for summer afternoon and evening hours. In mixing distributions, it is important to average percentages rather than levels of transmission loss. Distributions of data for time blocks may also be mixed to provide distributions for other periods of time. For example, data distributions for time blocks 1, 2, 3, and 8 were mixed to provide distributions of data for "winter". When averages are properly weighted, such mixed distributions are practically identical to direct cumulative distributions of the total amount of data available for the longer period.

The cumulative distribution of N observed hourly median values is obtained as follows: (1) the values are arranged in order from smallest to largest, L_1, L_2, L_3, ---, L_n, ---, L_N, (2) the percentage p of hourly median values less than L_n is computed:

$$p(n) = \frac{n}{N} - \frac{1}{2N};$$

(3) a plot of L_n versus $100\ p(n)$ for values of p from $1/(2N)$ to $1 - 1/(2N)$ is the observed cumulative distribution.

To mix two distributions, the following procedure is used: (1) choose ten to fifteen levels of transmission loss L_1, ---, L_n, covering the entire range of $L(p)$ for both distributions, (2) at each of these levels, read the value p for each distribution and average these values, (3) plot each selected level of transmission loss at the corresponding average percentage to obtain the "mixed" distribution. In this way, any number of distributions may be combined, if each of them represents the same number of hours. In general, a weighted average percentage p should be computed, using as weights the number of hours represented by each distribution.

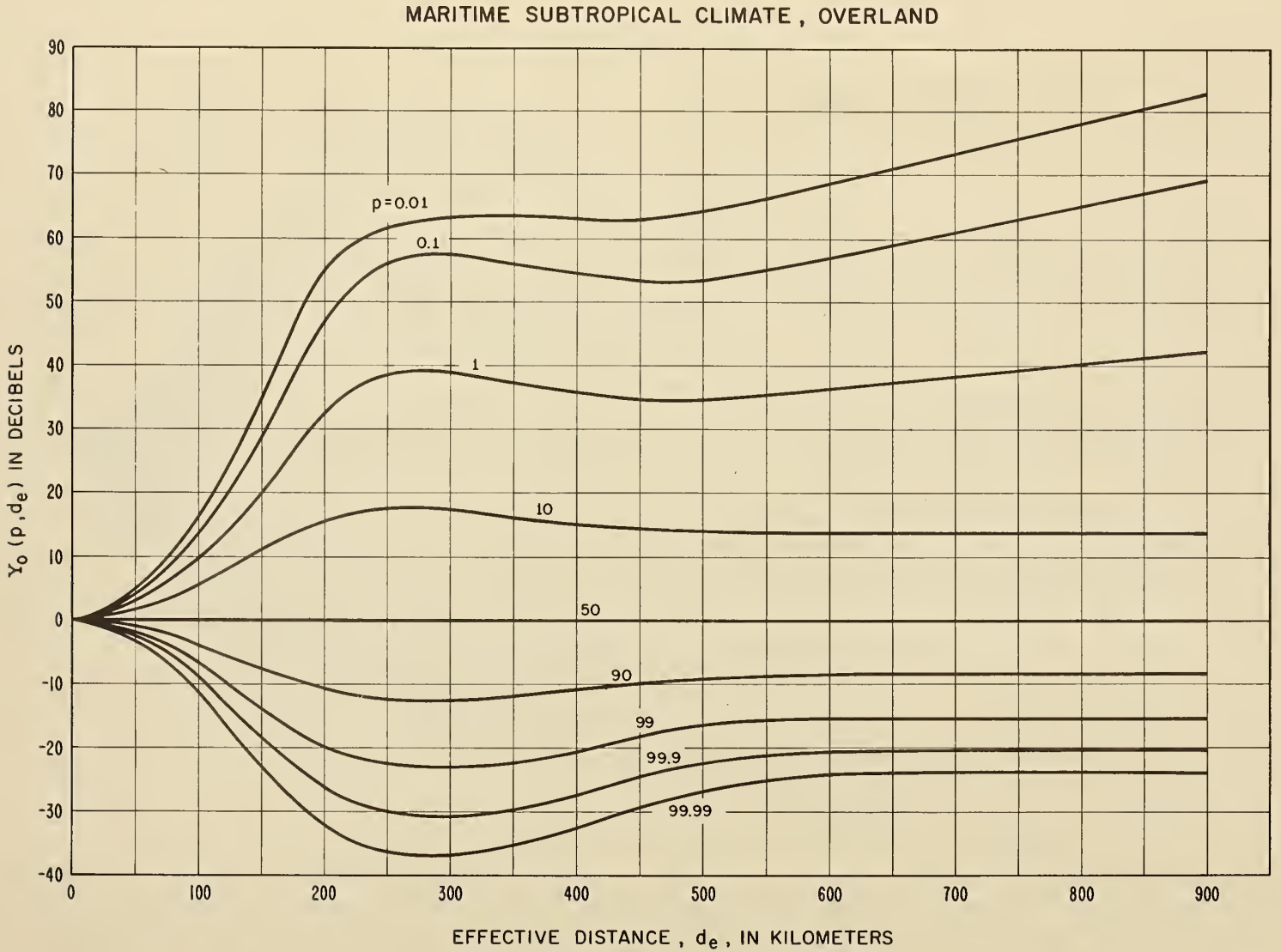

Figure III.25

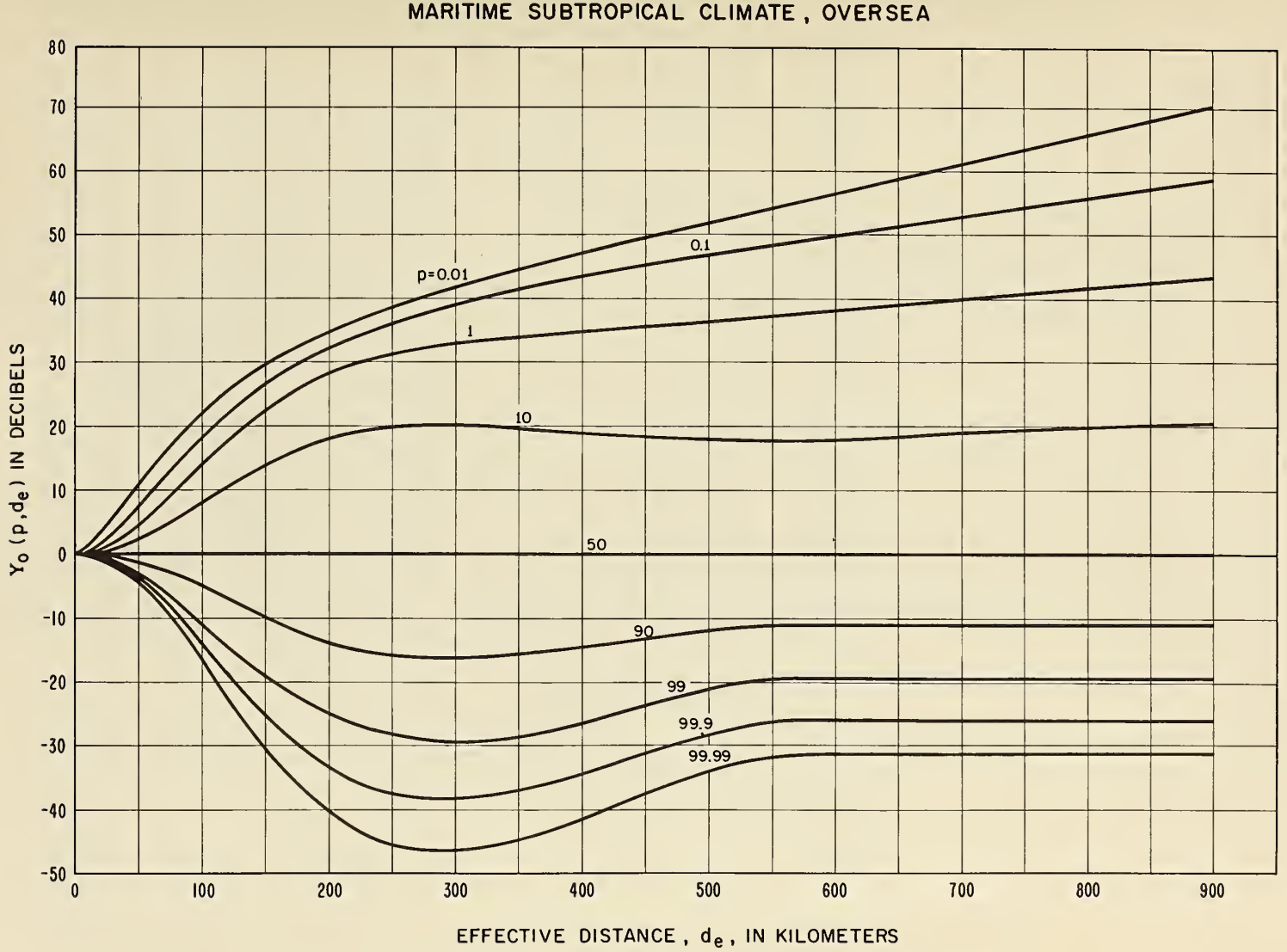

Figure III.26

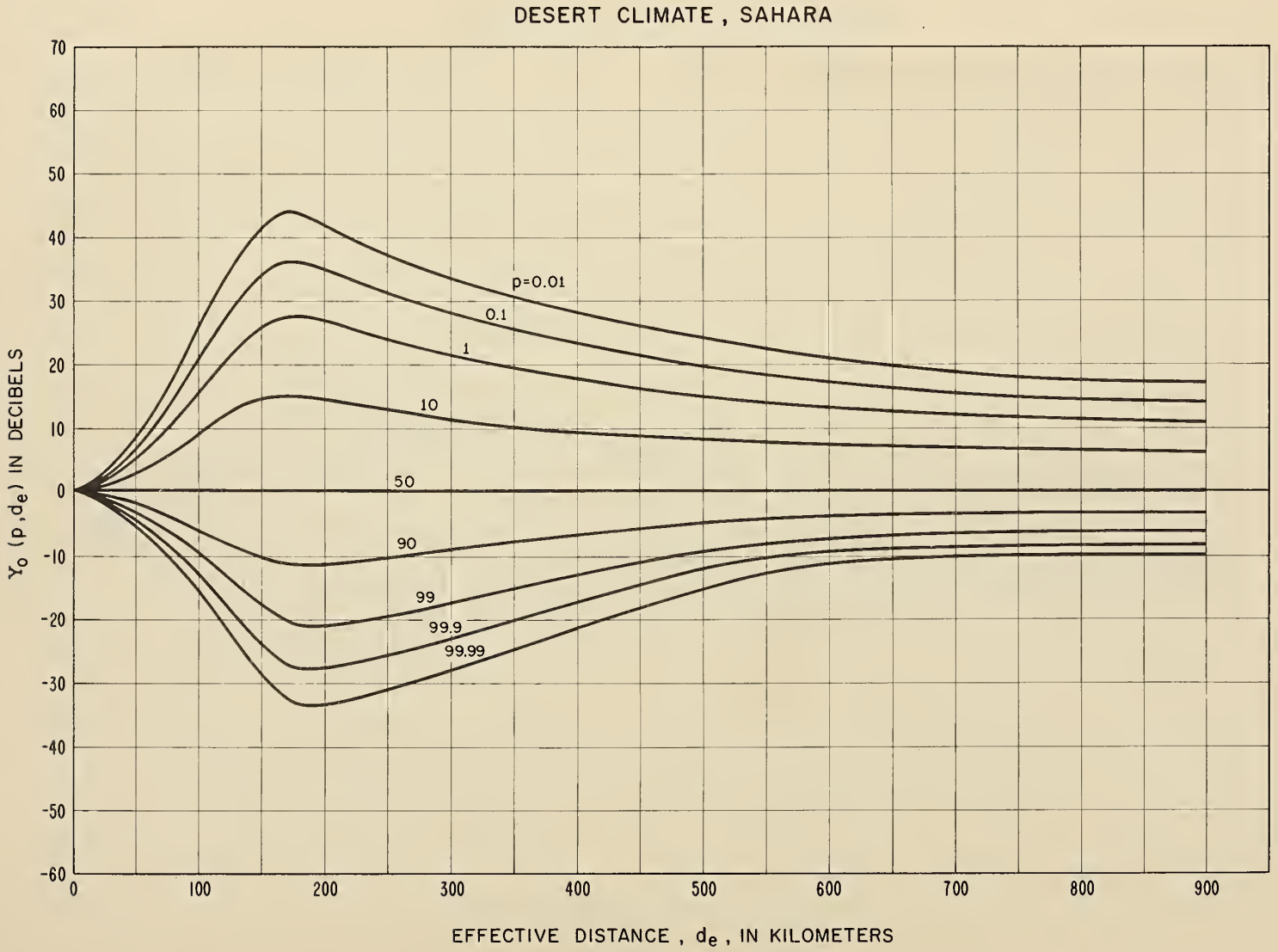

Figure III.27

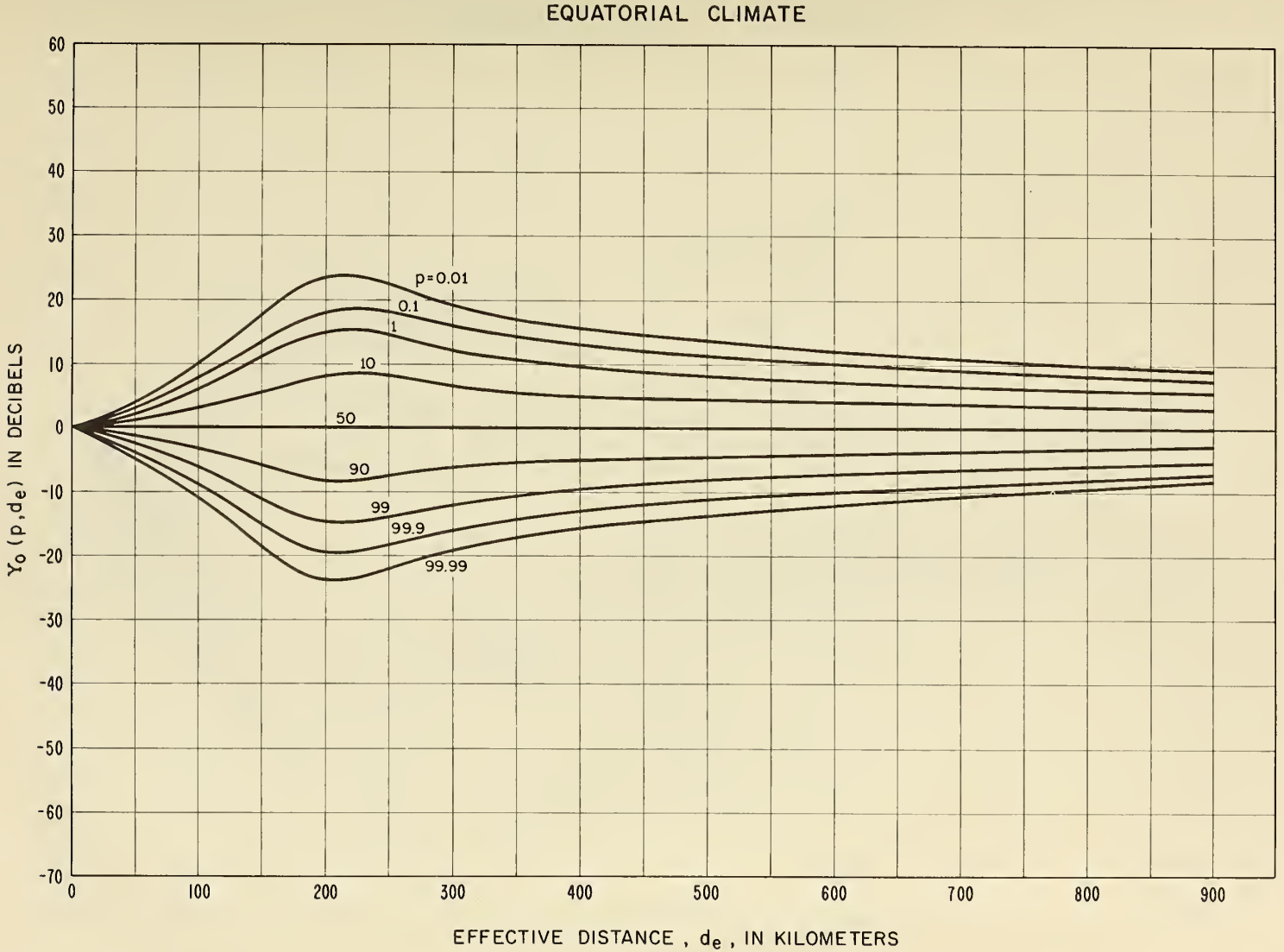

Figure III.28

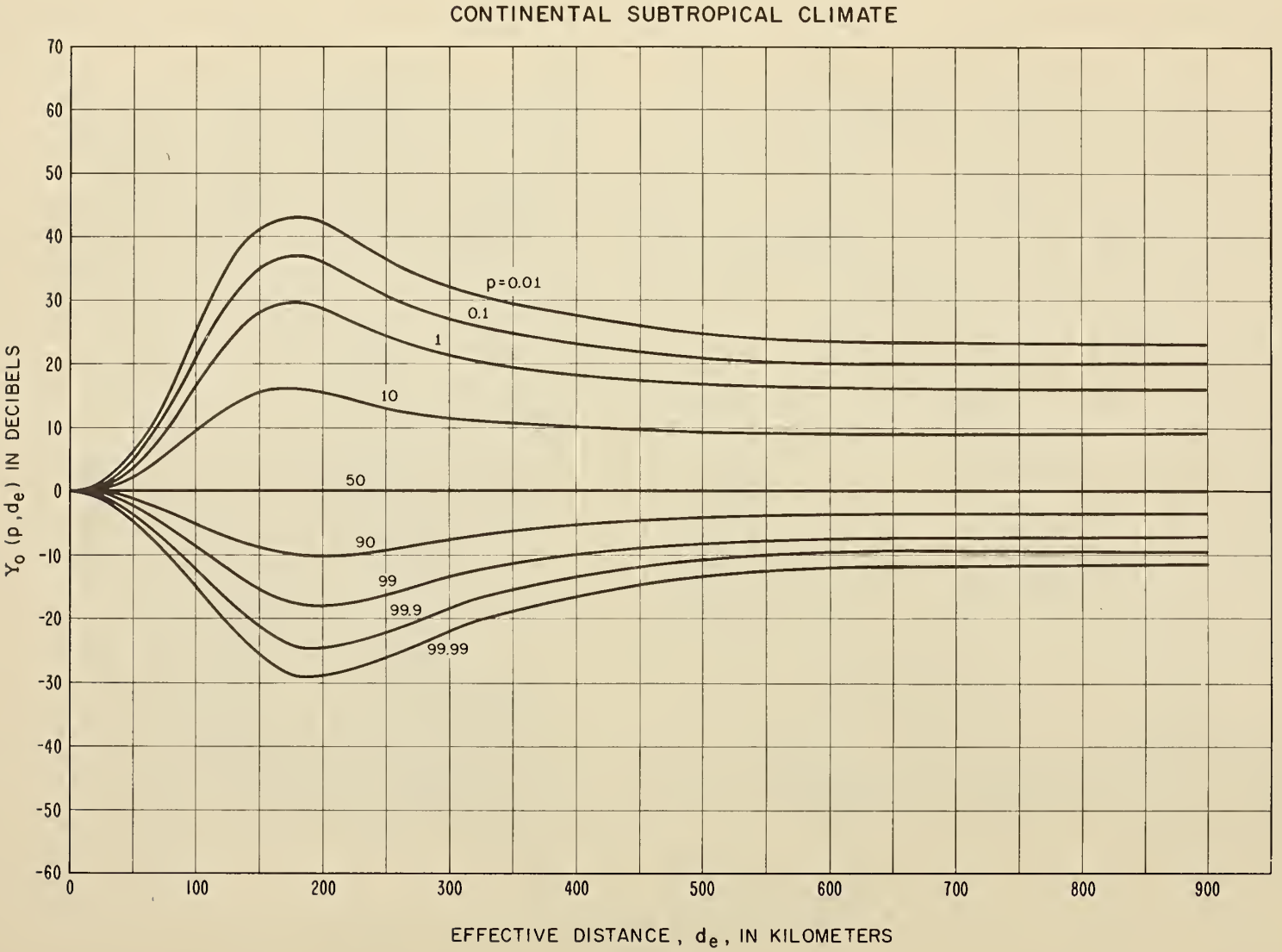

Figure III.29

THE FACTOR g(f)

g(f) = 1 FOR CLIMATES 4, 5, AND 7.

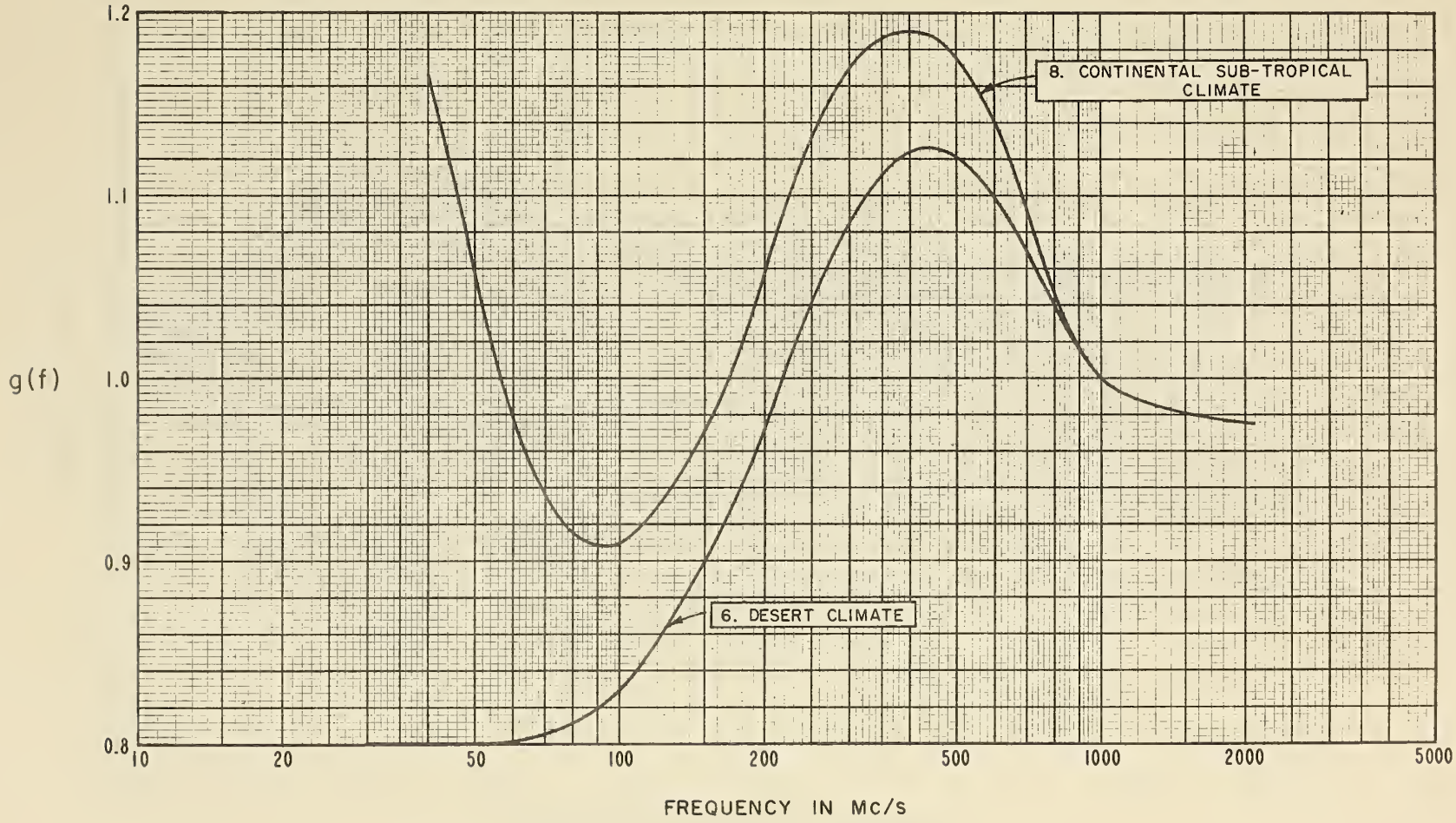

Figure III.30

ANNUAL RANGE OF MONTHLY MEAN N_s

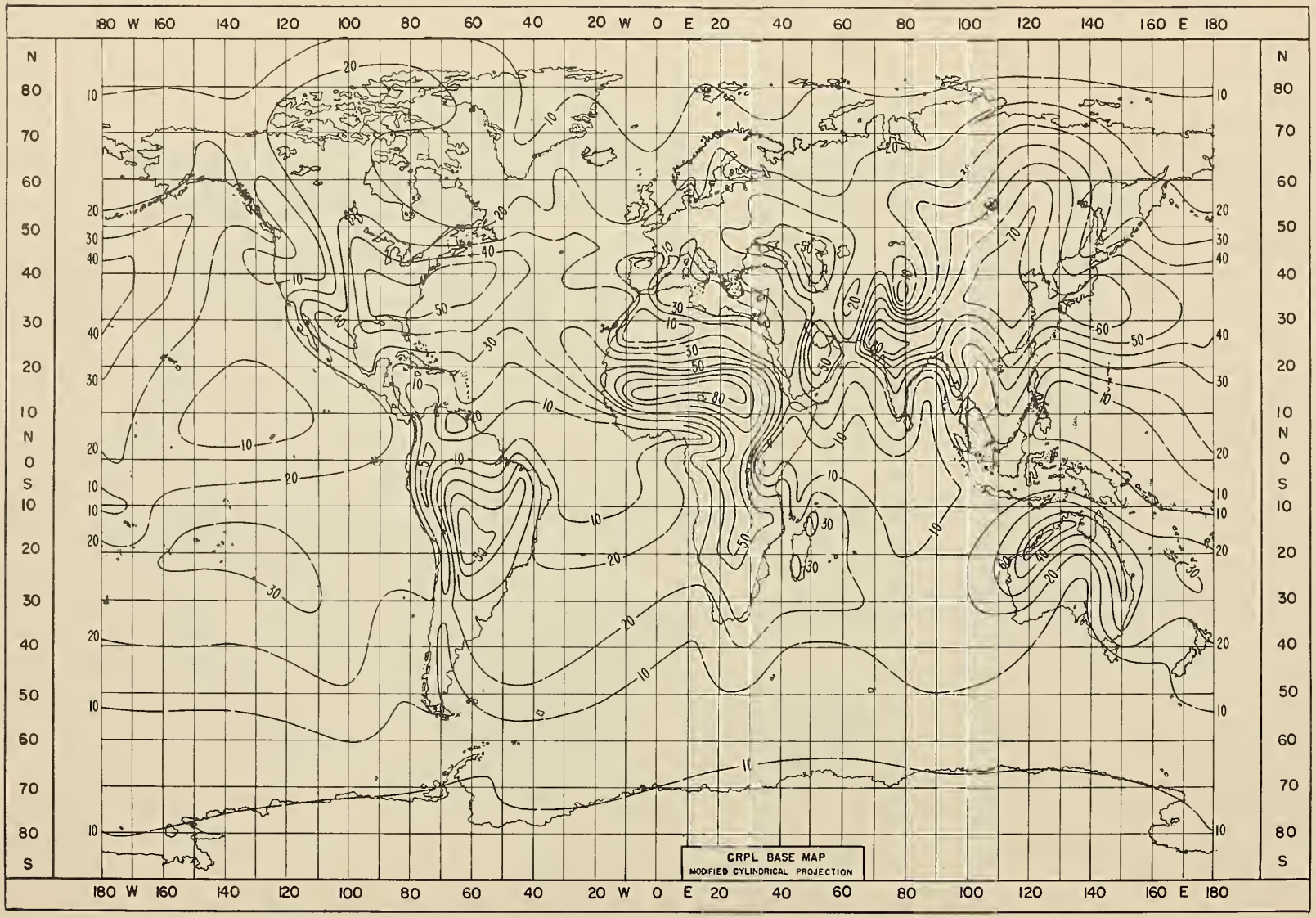

Figure III.31

THE FUNCTION $V(50, d_e)$ FOR VARIOUS PERIODS OF TIME IN THE U.S.A.

$L(50) = L_{cr} - V(50, d_e)$ db

TIME BLOCK	
WINTER	SUMMER
1. NOV.-APR. 0600-1300	4. MAY-OCT. 0600-1300
2. NOV.-APR. 1300-1800	5. MAY-OCT. 1300-1800
3. NOV.-APR. 1800-2400	6. MAY-OCT. 1800-2400
8. NOV.-APR. 0000-0600	7. MAY-OCT. 0000-0600

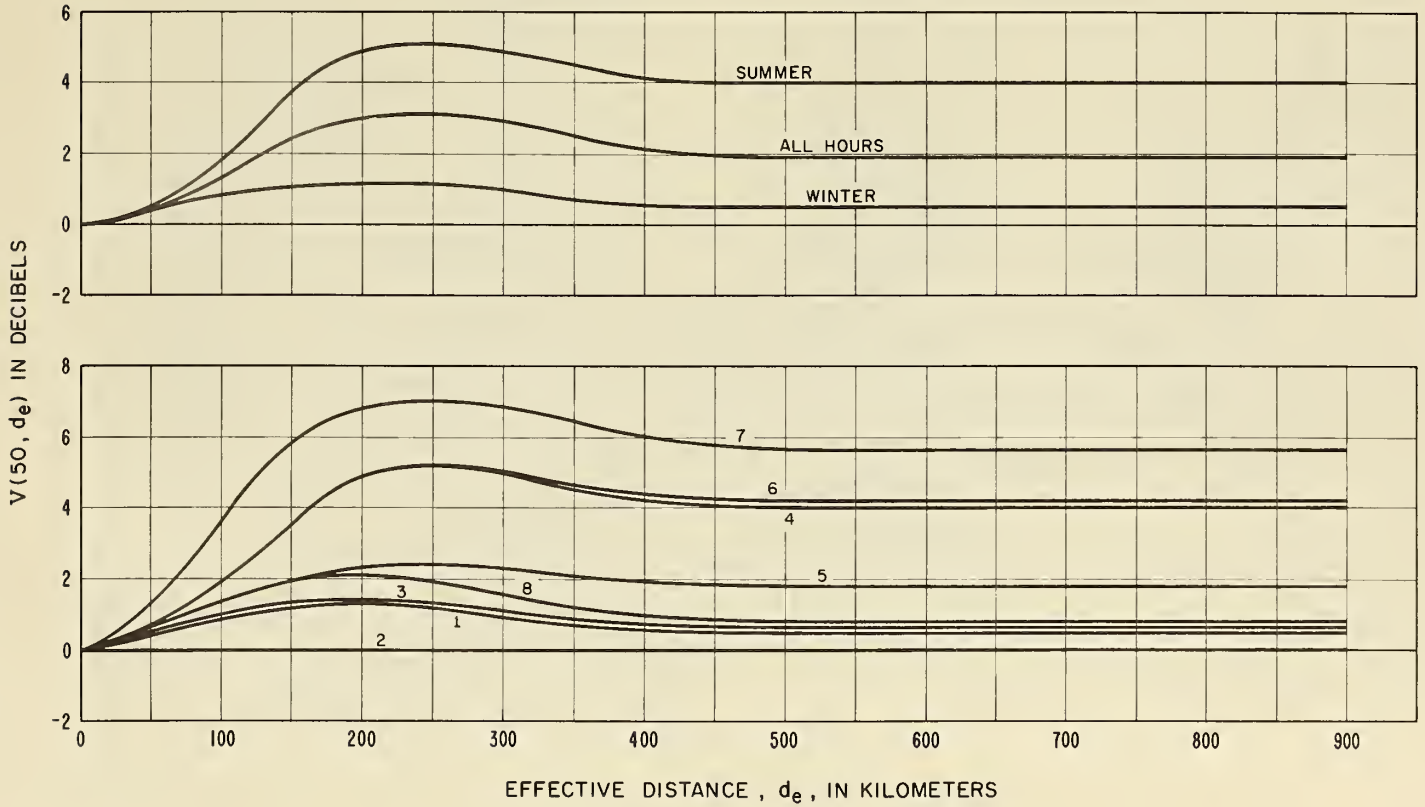

Figure III.32

WINTER TIME BLOCKS, NOV. - APRIL, U. S. A.
CURVES FOR 88 - 108 MHz

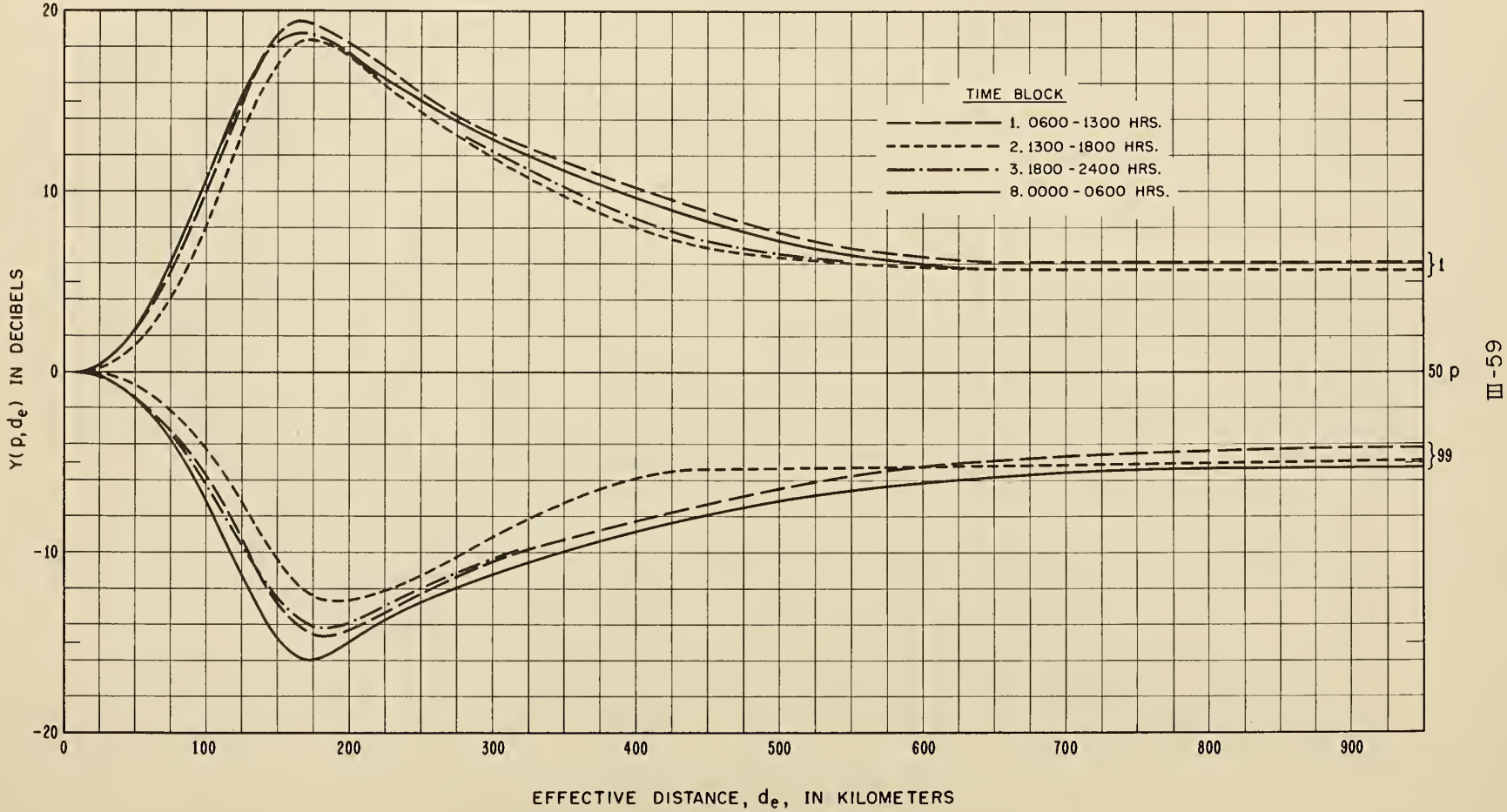

Figure III.33

SUMMER TIME BLOCKS, MAY - OCT., U. S. A.
CURVES FOR 88 - 108 MHz

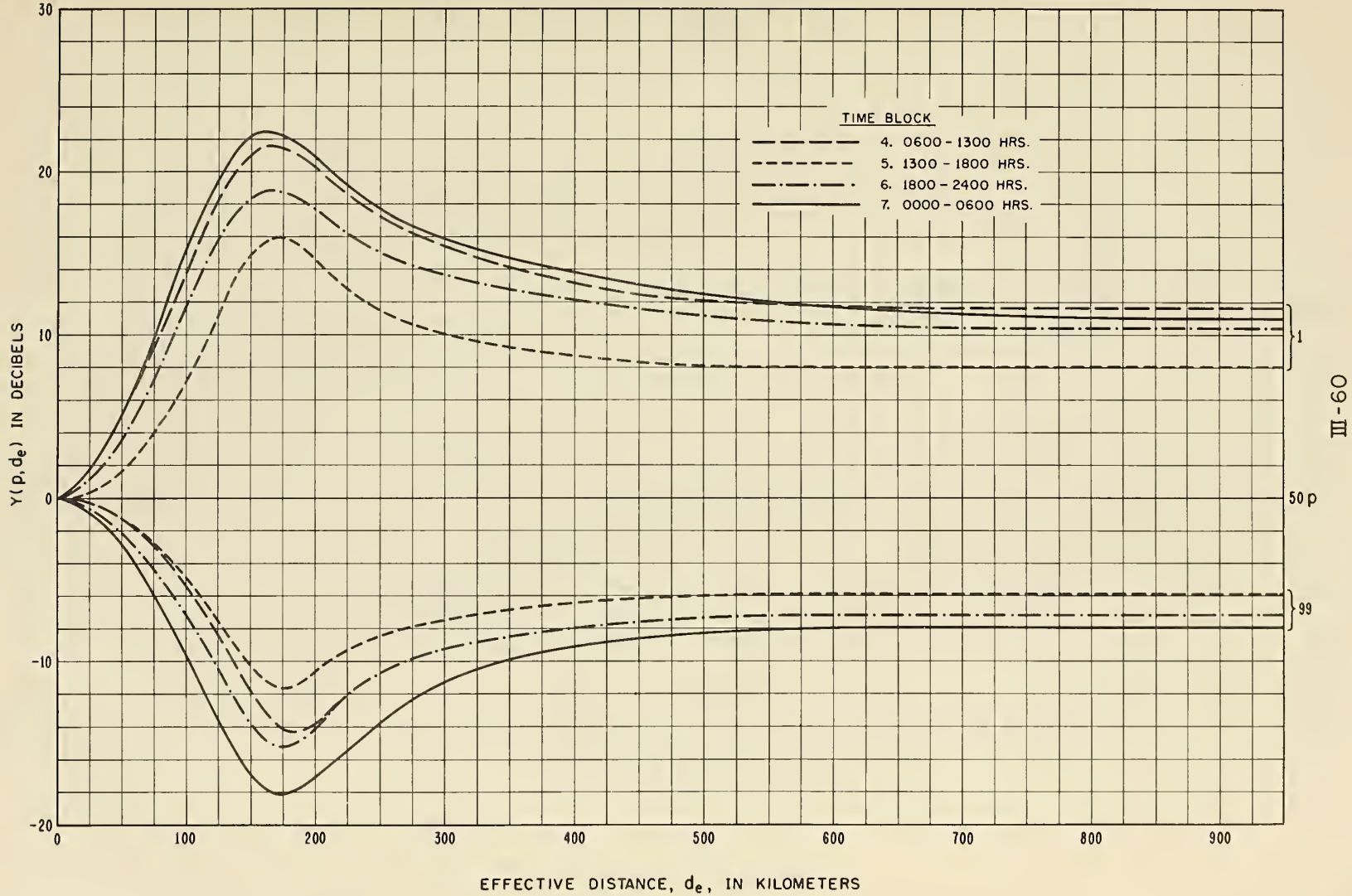

III-60

Figure III.34

TIME BLOCK 1, NOV. - APRIL, 0600 - 1300 HRS., U. S. A.
CURVES SHOW Y(p, d_e) FOR THE FREQUENCY RANGE 88 - 108 MHz

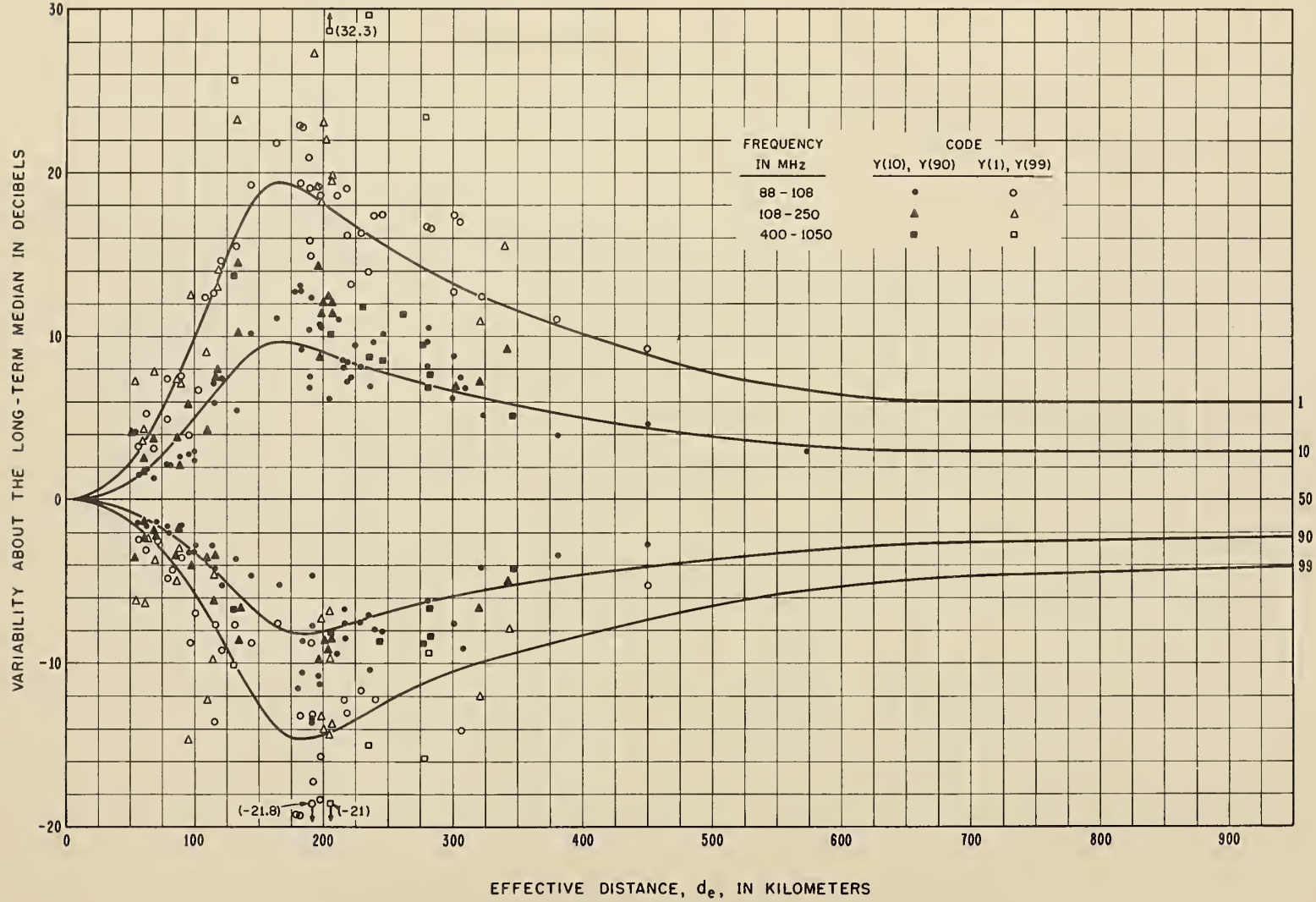

Figure III.35

TIME BLOCK 2, NOV. - APRIL, 1300 - 1800 HRS., U. S. A.
CURVES SHOW Y(p, d_e) FOR THE FREQUENCY RANGE 88 - 108 MHz

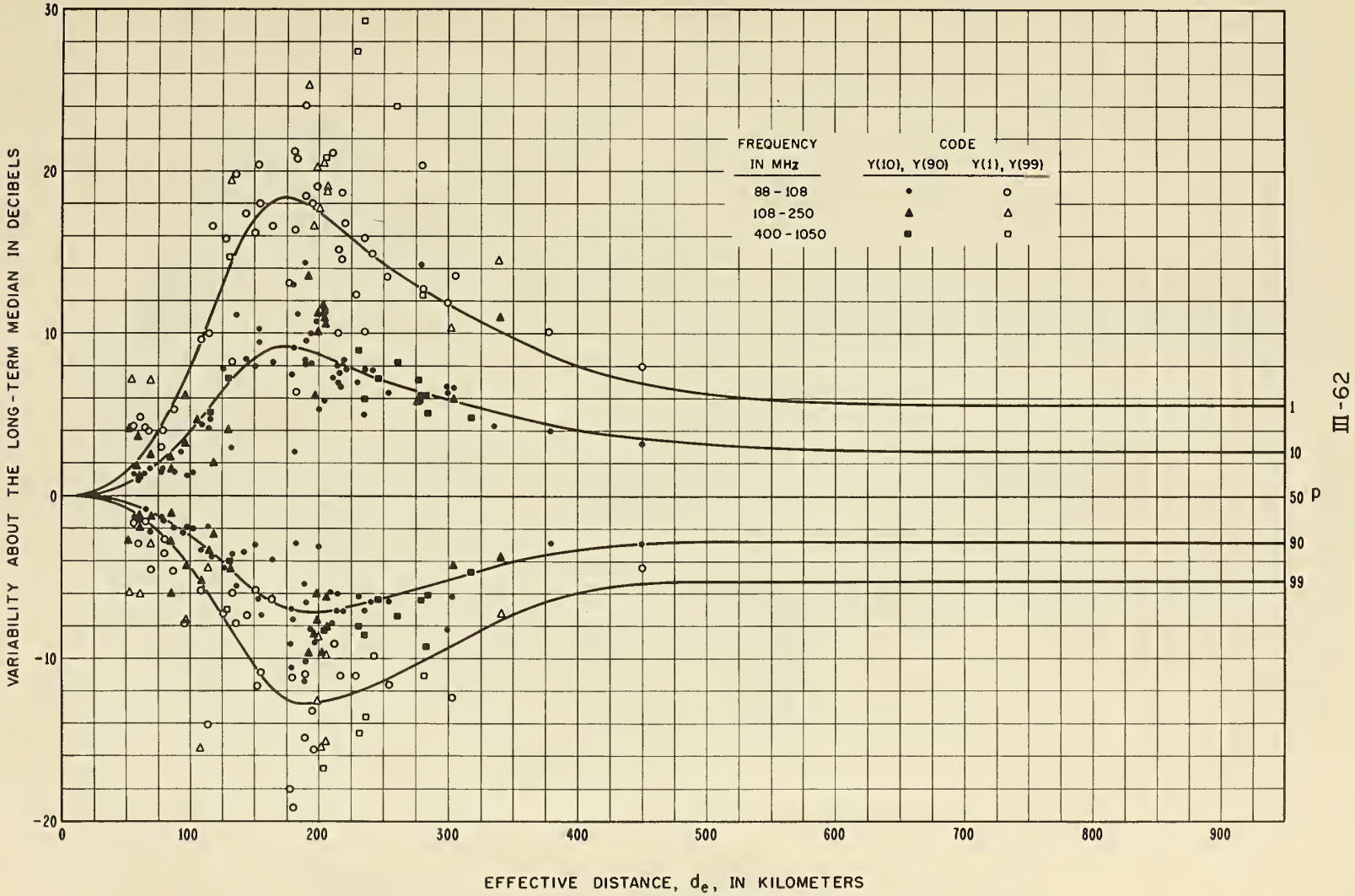

Figure III.36

TIME BLOCK 3, NOV. - APRIL, 1800 - 2400 HRS., U. S. A.
CURVES SHOW Y(p, d_e) FOR THE FREQUENCY RANGE 88 - 108 MHz

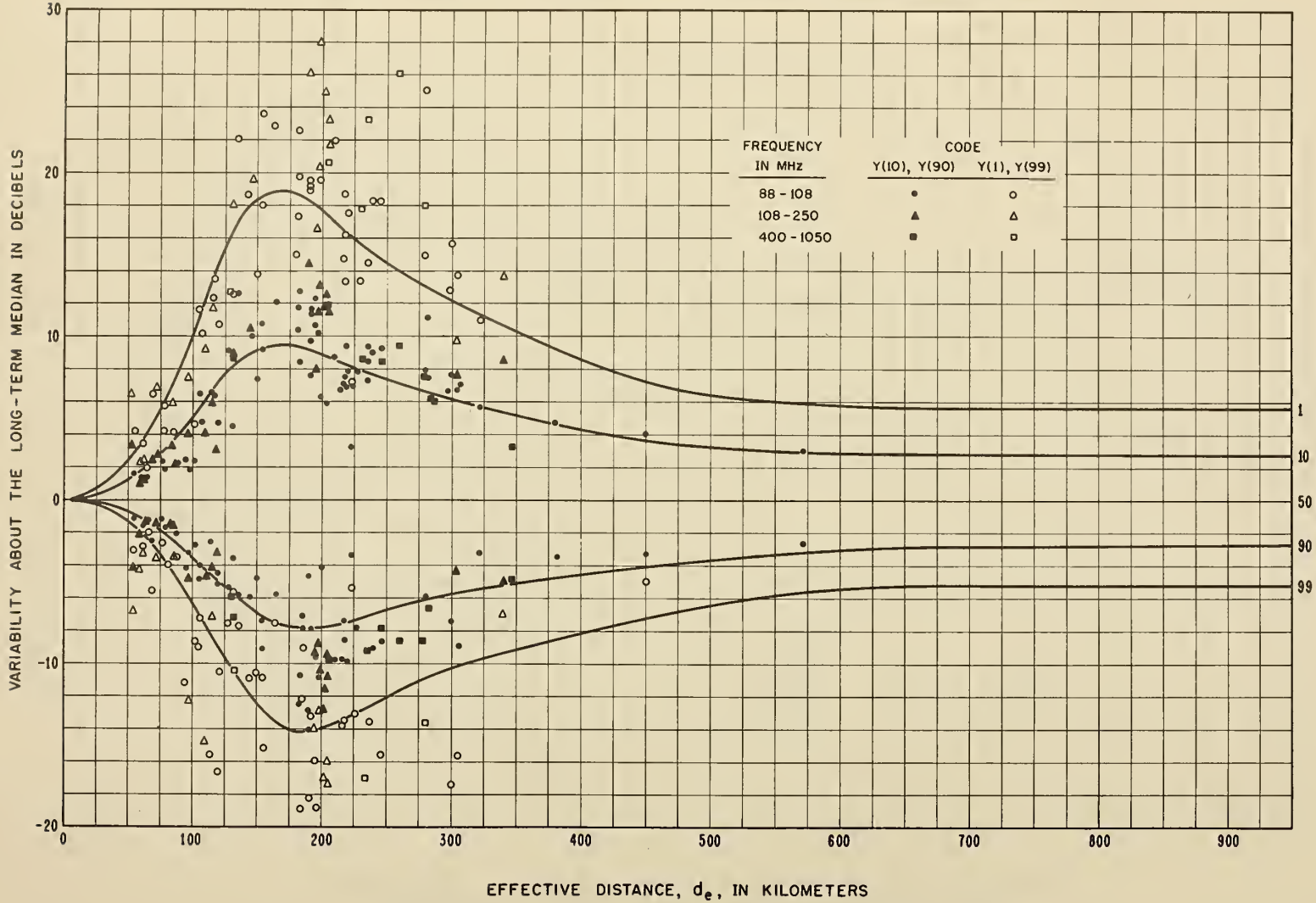

Figure III.37

TIME BLOCK 8, NOV. - APRIL, 0000-0600 HRS., U. S. A.
CURVES SHOW $Y(p, d_e)$ FOR THE FREQUENCY RANGE 88 - 108 MHz

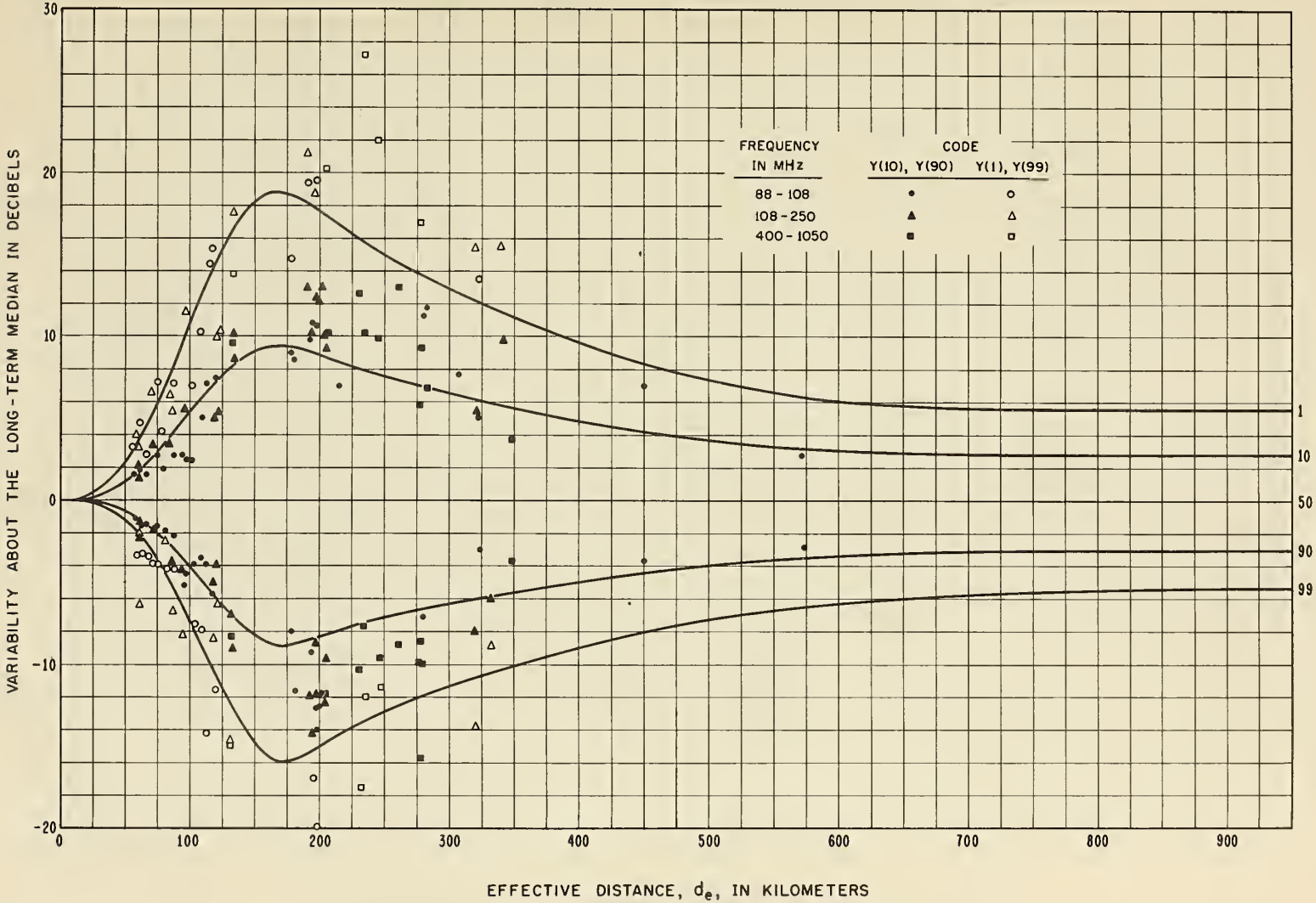

Figure III.38

TIME BLOCK 4, MAY - OCT., 0600-1300 HRS., U. S. A.
CURVES SHOW $Y(p, d_e)$ FOR THE FREQUENCY RANGE 88 - 108 MHz

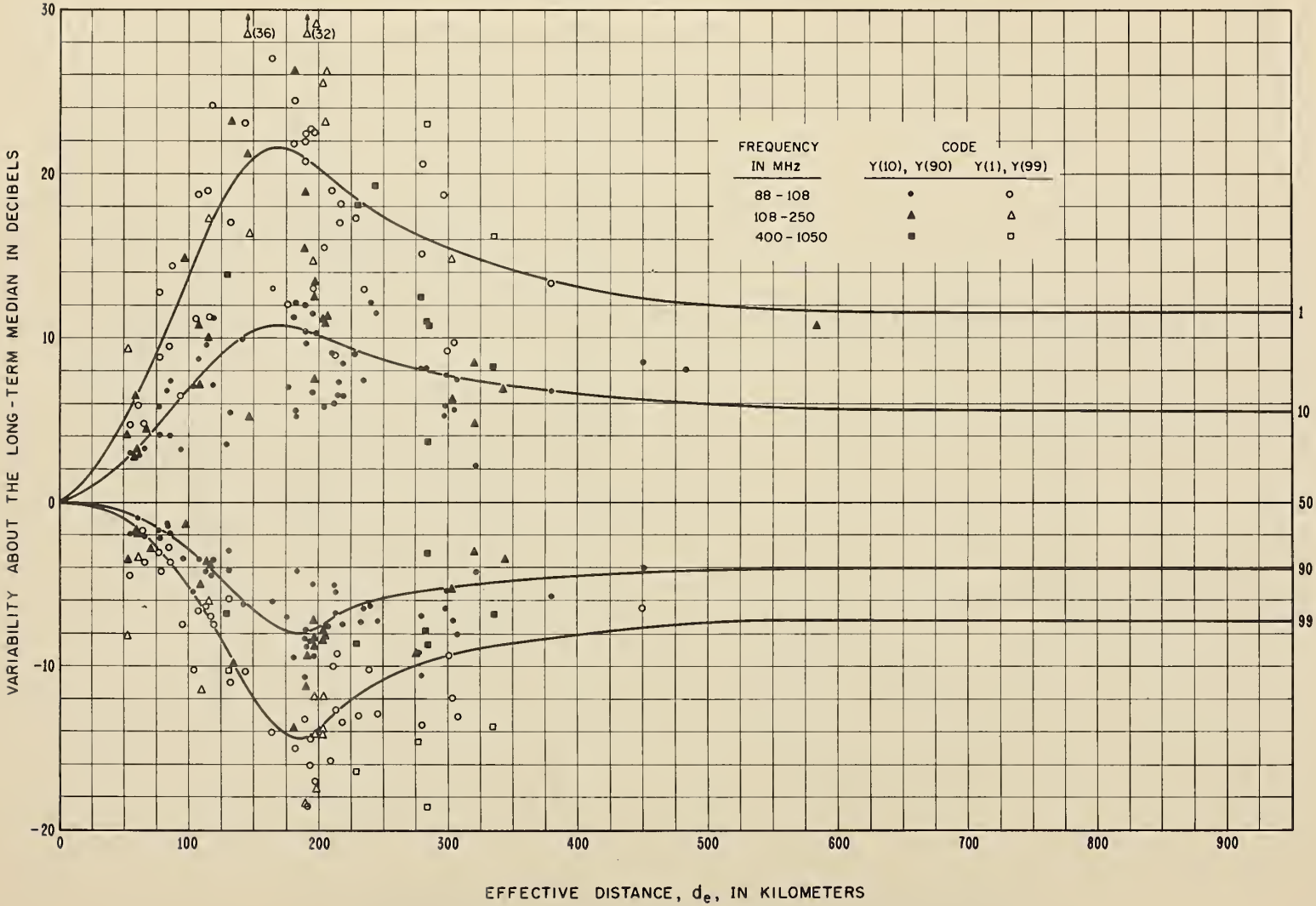

Figure III.39

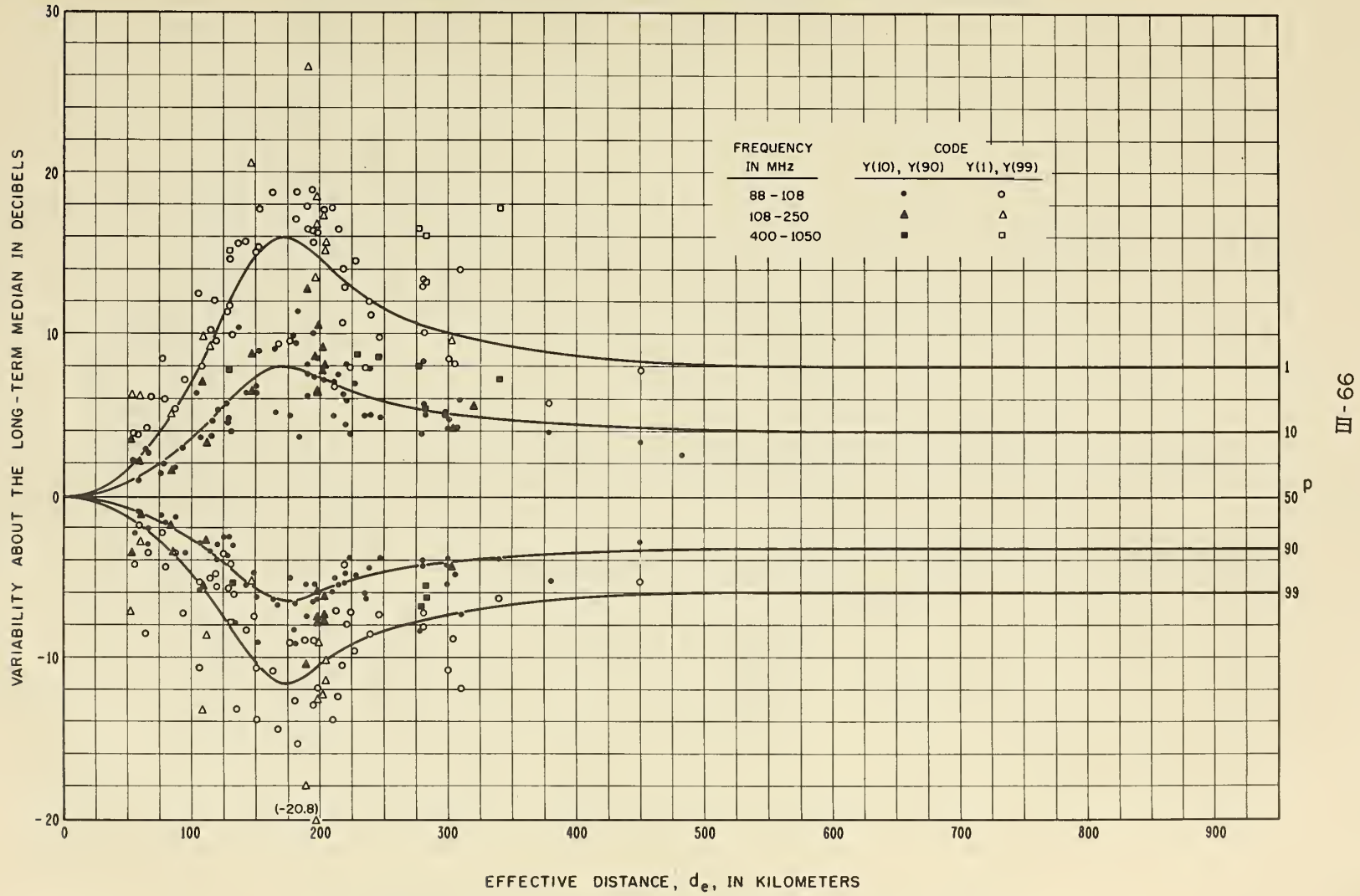

Figure III.40

TIME BLOCK 6, MAY - OCT., 1800 - 2400 HRS., U. S. A.
CURVES SHOW $Y(p, d_e)$ FOR THE FREQUENCY RANGE 88 - 108 MHz

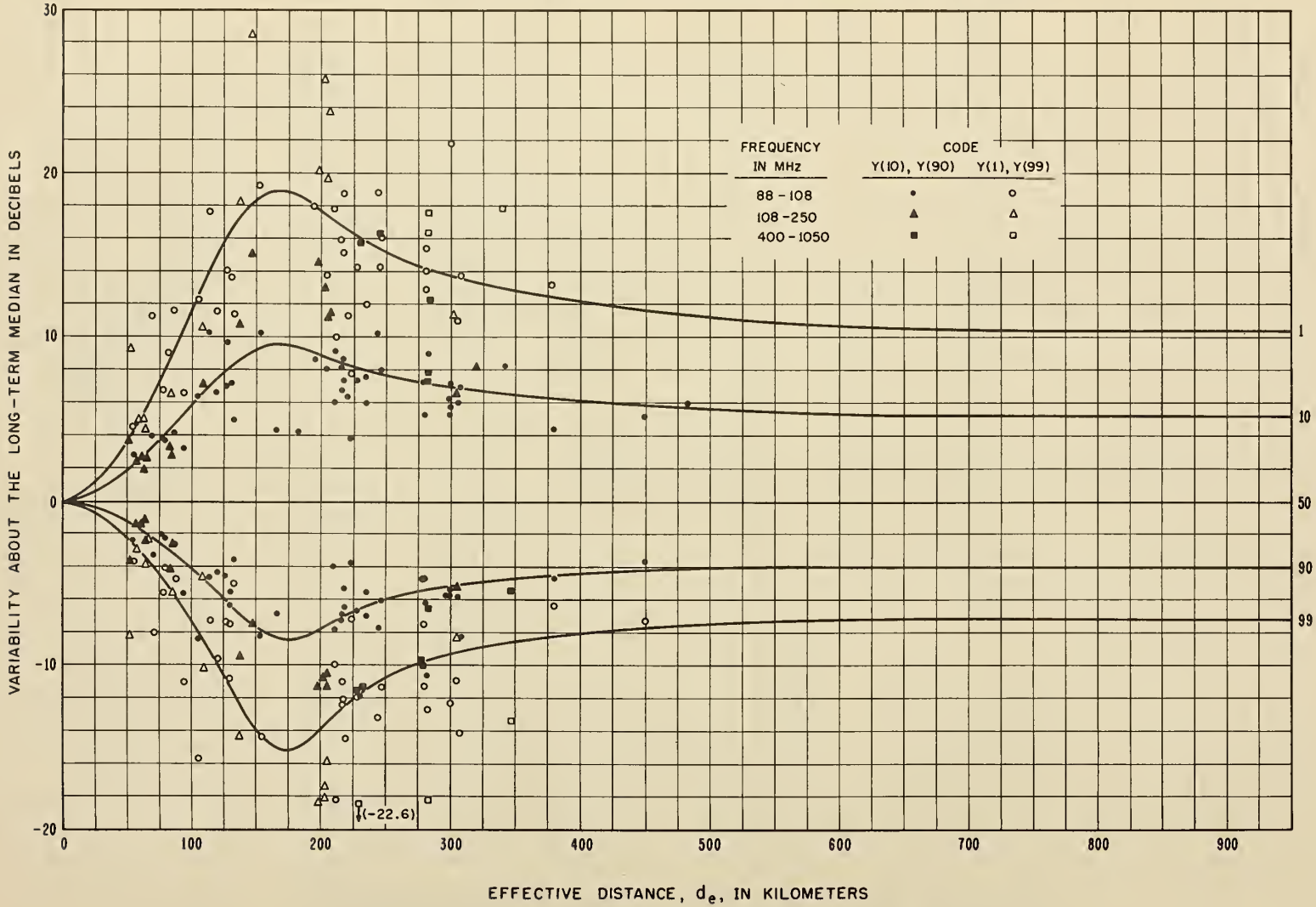

Figure III.41

TIME BLOCK 7, MAY - OCT., 0000 - 0600 HRS., U.S.A.
CURVES SHOW $Y(p, d_e)$ FOR THE FREQUENCY RANGE 88 - 108 MHz

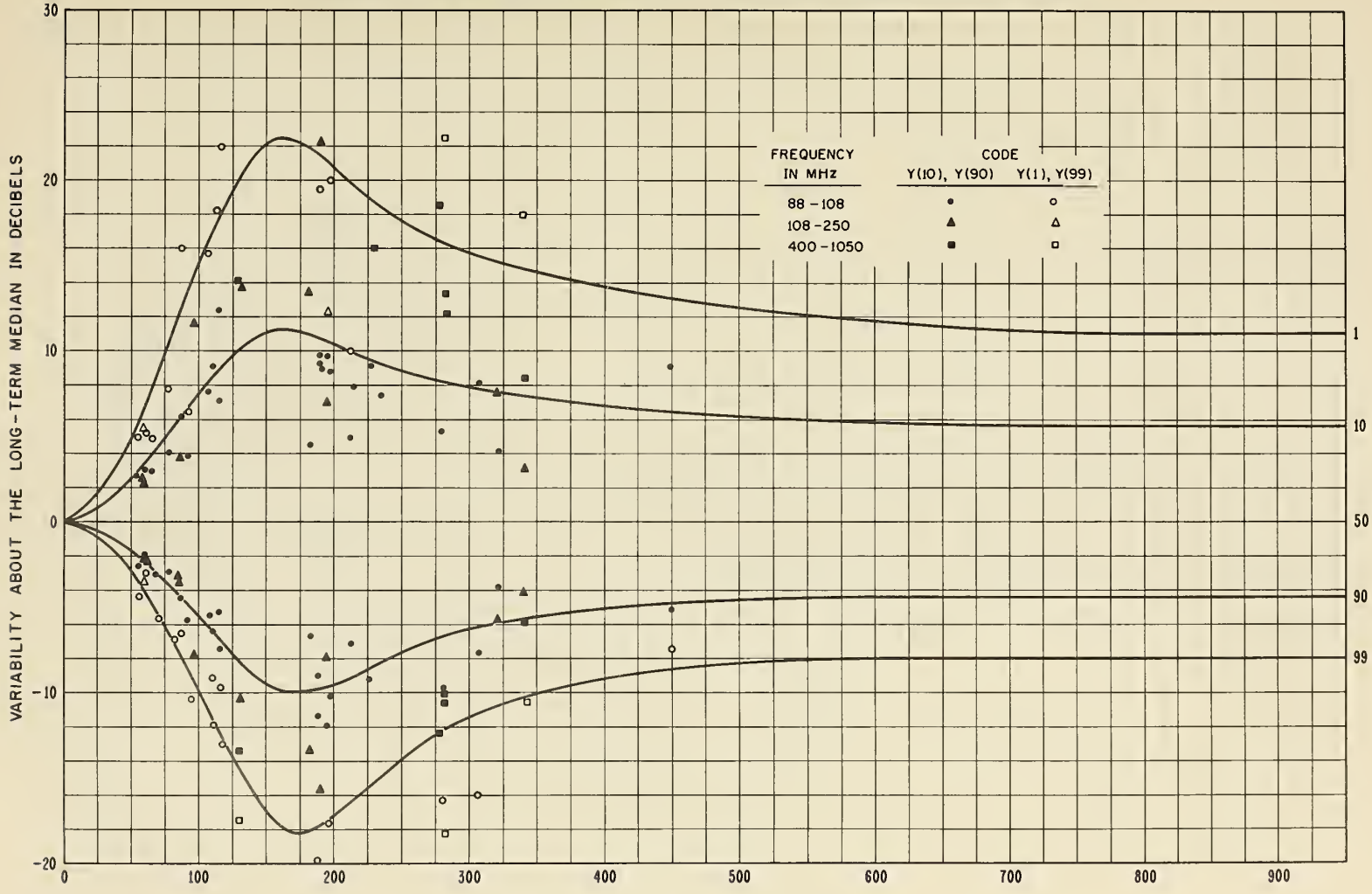

Figure III.42

III.8 Examples

Sample calculations are given here to show the application of the prediction methods described in this report to specific problems. The first example shows predictions for a line-of-sight path over irregular terrain. The second shows predicted transmission loss over a rounded isolated obstacle. The predicted cumulative distribution of hourly median values is compared with measurements over this path. The third example computes predicted scatter and diffraction losses over a transhorizon path and compares the predictions with long-term recordings of data.

III.8.1 Line-of-Sight Predictions

Attenuation relative to free space is predicted for a short line-of-sight path shown in figure III.43. Measurements at a frequency of 100 MHz were made using vertical polarization. The transmitting and receiving antennas are 4 meters and 9 meters, respectively, above ground.

A straight line is fitted by least squares to the terrain visible from both antennas. Terrain near the transmitter is excluded because it is shadowed by high foreground terrain. Twenty-one equidistant points $x_i = x_0, x_1, \ldots x_{20}$ are chosen as shown on figure III.43a, and the corresponding terrain heights, h_i, are read. From (5.15) the average terrain height $\bar{h}$ is 1531.8 m, the average distance $\bar{x}$ is 13.0 km, and the slope m is -6.0 meters per kilometer. The equation for the straight line is then

$$h(x) = 1531.8 - 6(x-13) \text{ m} = 1.5318 - 6(x-13) \cdot 10^{-3} \text{ km}.$$

An effective earth's radius, a, is obtained using figure 4.1 and equations (4.3) and (4.4). For this area in Colorado N_s is 280 and a = 8200 km. From (5.16) the adjustment to allow for the sea level curvature is

$$y(x) = h(x) - x^2/(16,400) \text{ km}$$

Figure III.43b shows the curve y(x) vs x and terrain which has been modified to allow for the sea level curvature.

At the transmitter, x = 0 and h(x = 0) is 1609.5 m. At the receiver, x = d = 19.75 km and h(x = 19.75) is 1491.4 m. From (5.17) the antenna heights above the smooth reflecting plane are then:

$$h'_1 = h_{ts} - h(0) = 1647.1 - 1609.5 = 37.6 \text{ m} = 0.0376 \text{ km},$$

$$h'_2 = h_{rs} - h(d) = 1524.0 - 1491.4 = 32.6 \text{ m} = 0.0326 \text{ km},$$

where $h_{ts} = 1647.1$ m and $h_{rs} = 1524.0$ m are the heights above sea level at the transmitter and receiver respectively. At 100 MHz ($\lambda = 3$ m), the criterion that both h'_1 and h'_2 must

exceed 0.16λ is met. Neither h_1' nor h_2' exceeds one kilometer, so no correction factor, Δh, is required. From (5.6) and (5.7) the distances d_1 and d_2 from each antenna to the point of specular reflection are

$$d_1 = d(1 + h_2'/h_1')^{-1} = 10.58 \text{ km}, \quad d_2 = d(1 + h_1'/h_2')^{-1} = 9.17 \text{ km},$$

and the grazing angle ψ is

$$\tan \psi = h_1'/d_1 = h_2'/d_2 = 0.003554$$

$$\psi = 0.003554 \text{ radians}.$$

From (5.9) the path length difference, Δr, between direct and reflected rays is

$$\Delta r = \left[d^2 + (h_1' + h_2')^2\right]^{\frac{1}{2}} - \left[d^2 + (h_1' - h_2')^2\right]^{\frac{1}{2}} = 1.2413 \times 10^{-4} \text{ km}$$

The approximation

$$\Delta r \simeq 2h_1'h_2'/d = 1.2413 \times 10^{-4} \text{ km} = 0.124 \text{ m} \cong 0.04\lambda$$

is also valid in this case. Note that Δr is less than 0.12λ and optical methods including a divergence factor may underestimate the attenuation.

One should note that important reflections might occur from the high ground near the transmitter. In this case the reflecting plane would correspond to the foreground terrain giving $h_1' = 4$ m, $h_2' = 50$ m, $d_1 = 1.53$ km, $d_2 = 18.22$ km and $\Delta r = 0.02$ m which is much less than 0.16λ. Optical methods would not be applicable here.

The attenuation relative to free space may be estimated using one of the methods described in subsection 5.2. Of these, methods 4 and 5 would apply in this case. Choosing heights $h_1 = 4$ m, $h_2 = 25$ m, as heights above foreground terrain, the theoretical smooth earth curves in the CCIR Atlas [1959] show the predicted field to be about 36 db below the free space value. The "standard" propagation curves on figure I.7, drawn for 100 MHz and $h_1 = h_2 = 30$ meters show the median basic transmission loss to be about 15 db below the free space loss. Greater attenuation would be expected with lower antennas over irregular terrain. Method 5 using the empirical curve through data recorded at random locations in figure I.1 shows the attenuation to be about 20 db below free space. These data were recorded with an average transmitter height of about 250 m, and a receiver height of 10 m.

For the very low antennas used on this Colorado path one would expect the losses to exceed the values shown on figures I.7 and I.1, and also to exceed the theoretical smooth earth value of $A \simeq 36$ db obtained from the CCIR Atlas. Spot measurements yield a value of about 40 db.

If a prediction were desired for transmission over the same path at 300 MHz, $\lambda = 1$ m, then $\Delta r = 0.124$ m is slightly greater than $0.12\,\lambda$ and optical methods may be used. Using the value $\Delta r = 0.124$ m the path length difference in electrical radians is $2\pi\Delta r/\lambda = 0.7805$ radians. As a check, this quantity may be computed using (5.14a):

$$2\pi\Delta r/\lambda = 41.917\, f h'_1 h'_2/d = 0.7805 \text{ radians}$$
$$= 44.7 \text{ degrees}$$

Equation (5.4) shows the attenuation relative to free space assuming a single ground reflection from the smooth curve y(x), figure III.43b. Assuming that free space gains are realized so that $G_p = 10 \log g_{o1} g_{o2}$ the equation may be written

$$A = -10 \log\left[1 + R_e^2 - 2R_e \cos\left(\frac{2\pi\Delta r}{\lambda} - c\right)\right]$$

where R_e is the effective reflection coefficient defined by (5.1):

$$R_e = DR\left(\frac{g_{r1} g_{r2}}{g_{o1} g_{o2}}\right)^{\frac{1}{2}} \exp\left(\frac{-0.6\,\sigma_h \sin\psi}{\lambda}\right)$$

With f = 300 MHz, and $\tan\psi = 0.003554$, figure III.3 shows the theoretical reflection coefficient $R = 0.97$ and the phase shift $c = 0$ for vertical polarization over average ground. The angle between the direct and the reflected ray is small so the ratio of gains in (5.1) may be considered to be unity. The divergence factor D and effective reflection coefficient R_e are

$$D = \left(1 + \frac{2d_1 d_2}{ad \tan\psi}\right)^{-\frac{1}{2}} = 0.865$$

$$R_e = 0.839 \exp\left(\frac{-0.6\,\sigma_h \sin\psi}{\lambda}\right).$$

The terrain roughness factor, σ_h, is the root-mean-square deviation of modified terrain elevations relative to the curve y(x) within the limits of the first Fresnel zone in the horizontal reflecting plane. The first Fresnel ellipse cuts the great circle plane at two points x_a and x_b kilometers from the transmitter. The distances x_a and x_b may be computed using equations (III.18) or (III.19) to (III.21).

$$B = 0.135, \quad x_0 = 10.02, \quad x_1 = 9.12$$

$$x_a = x_0 - x_1 = 0.90 \text{ km}, \quad x_b = x_0 + x_1 = 19.14 \text{ km}$$

The first Fresnel zone cuts the great circle plane at points 0.9 and 19.14 km from the transmitter with an intervening distance of 18.24 km. Equidistant points are chosen at x = 1, 2, . . . 19 and corresponding modified terrain heights and values of y(x) are obtained.

With height differences in kilometers:

$$\sigma_h^2 = \sum_{j=1}^{19} (y_j - h_j)^2 \Big/ 19, \quad \sigma_h = 0.008222$$

The effective reflection coefficient is then

$$R_e = 0.839 \exp - 0.01753 = 0.824$$

which is greater than 0.5 and greater than $\sqrt{\sin \psi}$. The predicted attenuation relative to free space A is then

$$- 10 \log \left[1 + R_e^2 - 2R_e \cos \left(\frac{2\pi \Delta r}{\lambda} - c \right) \right] = - 10 \log \left[1.6793 - 1.6484 \cos 0.7805 \right] \simeq 3 \text{ db}.$$

Due to diffraction effects over irregular terrain, the attenuation A is often observed to be much greater than the values corresponding to the ray theory calculations illustrated in this example. Ray theory is most useful to identify the location and depth of nulls in an interference pattern in the region visible to two antennas. Figure III.44 shows an interference pattern from an aircraft at 10,000 ft., transmitting on 328.2 Mc/s. Measured values compared with theoretical curves based on ray theory are shown on the figure.

III.8.2 Transmission Loss Prediction for a Rounded Isolated Obstacle

The path selected to provide an example of knife-edge diffraction calculations is located in eastern Colorado, extending from a location near Beulah, southwest of Pueblo, to Table Mesa north of Boulder. The common horizon is formed by Pikes Peak, with an elevation 4300 meters above mean sea level. For the purpose of these calculations Pikes Peak is considered to be a single rounded knife edge. The complete path profile is shown in figure III.45. Table III.5 gives all applicable path and equipment parameters and permits a comparison of calculated and actually measured values.

TABLE III.5

Path and Equipment Parameters

Carrier Frequency	751 MHz
Total Great Circle Path Distance	223.3 km
Great Circle Distances from Pikes Peak	
to Transmitter Site	77.3 km
to Receiver Site	146.0 km
Terminal Elevations above Mean Sea Level	
Transmitter Site	1,905 m
Receiver Site	1,666 m
Elevation of Pikes Peak	
Above Mean Sea Level	4,300 m
Above Mean Terminal Elevation	2,507 m
Transmitting Antenna Height Above Ground	7.3 m
Transmitting Antenna Gain Above Isotropic (4.3 m Dish)	26.7 db
Receiving Antenna Height Above Ground	20.0 m
Receiving Antenna Gain Values Above Isotropic (3 m Dish)	23.6 db
Polarization	Horizontal
Modulation	Continuous Wave
Transmitter Power	445 watts

Calculations are given for single-ray diffraction, neglecting possible specular reflections from foreground terrain.

The minimum monthly surface refractivity N_o (referred to mean sea level) from figure 4.1 is 300 N-units. From Table III.5 the terminal elevations are 1905 and 1666 m, respectively. Corresponding surface refractivity values N_s are 245 and 251 N-units (4.3), and the average of these values is $N_s = 248$. In this example, N_s is calculated for the terminals, as the antennas are more than 150 m below their 4300 m radio horizon. Using (4.4) or an extrapolation of figure 4.2, the effective earth radius a for $N_s = 248$ is found to be 7830 km.

The angular distance θ in radians and related parameters are calculated using (6.15) and (6.18a, b): $\theta_{et} = 0.008581$ $\theta_{er} = 0.025953$ $\alpha_{oo} = 0.021827$ $\beta_{oo} = 0.041225$. In this example d_{st} and d_{sr} are negligibly small, and the corrections $\Delta\alpha_o$ and $\Delta\beta_o$ (6.19a, b) can be neglected. Thus, $\alpha_{oo} = \alpha_o$, $\beta_{oo} = \beta_o$, and $\theta = 0.063052$ radians.

The free-space loss and the attenuation relative to free space are computed considering Pikes Peak to be a single isolated rounded obstacle. From a study of large-scale topographic maps, the distance D_s between the radio horizons at the top of the peak is estimated to be 0.040 km. With f = 751 MHz, $d_1 = 146.0$ km, and $d_2 = 77.3$ km, we determine:

$$v = 31.73 \text{ (v is positive, as both } \alpha_o \text{ and } \beta_o \text{ are greater than zero)} \tag{7.1a}$$

$$r = 0.6344 \tag{7.10}$$

$$v\rho = 0.858, \tag{7.9}$$

and therefore

$$\rho = 0.0271$$

The test described in section 7.3 shows that the assumption of an isolated obstacle is applicable. The components of basic transmission loss are then determined as follows:

$$\text{Free-space Loss } L_{bf} = 137.0 \text{ db} \tag{2.31}$$

$$A(v, 0) = 43.0 \text{ db} \tag{7.2}$$

$$A(0, \rho) = 6.0 \text{ db} \tag{7.4}$$

$$U(v, \rho) = 5.1 \text{ db} \tag{7.5}$$

Totals are: $A(v, \rho) = 54.1$ db, and from (7.3), $L_{bd} = L_{bf} + A(v, \rho) = 191.1$ db.

The average atmospheric absorption term, A_a, from figure 3.6 is 0.7 db. The total basic transmission loss value $L_{dr} = 191.8$ db, which is equal to the long-term reference value L_{cr}. This reference value, is strictly applicable only to those hours of the year which are characterized by a surface refractivity of approximately 250 N-units. The expected behavior of the hourly median basic transmission loss for all hours of the year over this path can now be determined in the form of a cumulative distribution by the methods given in section 10.

As this is a knife-edge diffraction path, it will be necessary to calculate cumulative distributions $Y(p, d_e)$ separately for portions of the path on each side of Pikes Peak and to combine the results as described in subsection 10.6. Effective antenna heights are computed as heights above curves fitted to terrain on each side of Pike's Peak using (5.15) and (5.16). The curves are extrapolated to each antenna and to Pike's Peak. The effective heights are then the heights of the antennas and of the Peak above these curves. From Beulah to Pikes

Peak the terrain near the Peak is excluded because it is partially shadowed. Twenty-one evenly spaced points, x_i, from d = 3.3 km to d = 70 km were selected and the corresponding terrain heights x_i were read. From (5.15b) $\bar{h}$ = 2100 m, $\bar{x}$ = 36.6 km, and m = 25.5, and the straight line fitted to terrain is

$$h(x) = 2100 + 25.5(x - 36.6) \text{ meters}$$

At the Beulah antenna, x = 0 and h(x) = 1167 meters, at Pikes Peak x = 75.5 kilometers and h(x) = 3095 meters. The effective antenna heights are then 738 and 1205 meters (5.17). Using (10.1) to (10.3) the distances d_{so} = -187.1 km, d_{s1} = 33.2 km, and the effective distance d_e is 33.2 km.

Similarly on the Table Mesa side much of the terrain is shadowed by the small peak at about 122 km and by the elevated area at about 202 km. The curve fit is therefore computed for the intervening terrain with x_0 = 122.5 km and x_{20} = 200.5 km. Using 21 equidistant terrain heights between these points (5.15b) gives $\bar{h}$ = 2025 m, $\bar{x}$ = 161.5 km, and m = -9.3. From (5.15a) h(x = 75.5) = 2827, h(x = 223.3) = 1448 meters. The effective antenna heights are then 1473 and 218 meters (5.17), d_{so} = -77.7, d_{s1} = 33.2 km, and the effective distance d_e = 74.3 km.

We thus have two paths in tandem where the effective distances are 33.2 and 74.3 km respectively. Cumulative distributions are obtained using figures 10.1, 10.2, 10.3, and equations (10.4) to (10.7). The frequency factors are g(10, f) = 1.33, g(90, f) = 1.29.

	Table Mesa Side	Beulah Side	
$V(50, d_e)$	0.2	0	figure 10.1
$Y_o(10, d_e)$	4.7	1.2	figure 10.2
$Y_o(90, d_e)$	-3.1	-0.6	figure 10.2
Y(10)	6.3	1.6	(10.6)
Y(90)	-4.0	-0.77	(10.6)

Using the reference value L_{cr} = 191.8 db and the ratios given in (10.7) the predicted cumulative distributions for both portions and for the entire path are tabulated below:

$L_b(p)$ in db

percent	Table Mesa	Beulah	Entire Path
0.01	170.6	186.5	170.1
0.1	174.4	187.4	173.8
1	179.0	188.6	178.6
10	185.3	190.2	184.8
50	191.6	191.8	191.3
90	195.6	192.6	195.5
99	198.9	193.2	199.0
99.9	201.2	193.7	201.3
99.99	203.2	194.0	203.2

The cumulative distribution of predicted basic transmission loss for the entire path was obtained by convoluting the distributions for each part of the path, as described in subsection 10.6. This cumulative distribution is shown graphically in figure III.46 together with a distribution derived from measurements over this path, reflecting 1056 hours of data obtained in 1960 and 1962.

The confidence limits on figure III.46 were derived assuming that

$$\sigma_c^2(p) = 16.73 + 0.12\ Y^2(p)$$

where the variance $\sigma_c^2(50) = 12.73\ db^2$ given in (V.40) has been increased by $4\ db^2$ to allow for equipment and reading errors.

III.8.3 Predicted Transmission Loss for a Transhorizon Path

Predicted forward scatter and diffraction losses are computed for a 283 km path from Dallas to Austin, Texas. The prediction is compared with measurements at a frequency of 104.5 MHz. Figure III.47 shows the great circle profile of this path, obtained by the methods of section 6, plotted on a linear scale with allowance for the sea level curvature. The vertical scale in the figure is much exaggerated to show some of the detail of terrain.

The effective earth's radius is determined as described in section 4. From figure 4.1 minimum monthly values of N_o are read at approximate horizon locations. Appropriate terrain heights are used in (4.3) to compute horizon values of N_s, whose average is N_s = 306. From (4.4) the effective earth's radius is then 8580 km.

A reference value, L_{cr}, of basic transmission loss, which corresponds to winter afternoon conditions, is computed as shown below. For each parameter the appropriate equation or figure is referenced.

Path: Dallas to Austin, Texas

d = 283.1 km, f = 104.5 MHz, N_s = 306, a = 8580 km

Parameter	Transmitter	Receiver	Reference
h_{ts}, h_{rs}	280.4 m	243.9 m	figure III.47
h_{te}, h_{re}	135.0 m	9.8 m	(6.11) and (6.12)
h_{Lt}, h_{Lr}	219.5 m	274.3 m	figure III.47
d_{Lt}, d_{Lr}	39.6 km	8.8 km	figure III.47
θ_{et}, θ_{er}	-3.845 mr	+2.933 mr	(6.15)
α_{oo}, β_{oo}	12.777 mr	19.296 mr	(6.18)
θ_{ot}, θ_{or}	0.768 mr	3.961 mr	(6.16)
d_{st}, d_{sr}	130.72 km	103.95 km	(6.20)
$\Delta\alpha_o$, $\Delta\beta_o$	0.057 mr	0.021 mr	figure 6.9
α_o, β_o	12.834 mr	19.317 mr	(6.19)

The angular distance θ = 32.151 mr = 0.032151 radians and the product θd is 9.10. The ratio of α_o/β_o = s = 0.664. Then the function $F(\theta d)$ from figure 9.1 or figures III.12 and III.13 is $F(\theta d)$ = 167.0 db. From (9.3) the height h_o = 2.18 km, and η_s = 1.06. From (9.4) and figure 9.3 the parameters r_1 = 19.01, $H_o(r_1)$ = 0.15 db, r_2 = 1.38, and $H_o(r_2)$ = 13.5 db. From figure 9.4 and (9.5) ΔH_o = 0.61 and H_o = 7.40 db. The correction term F_o defined by (9.7) is negligible. Figure 3.6 shows that in this case the allowance for absorption $A_a \simeq 0.01$ db.

The reference value L_{bsr} of long-term median basic transmission loss due to forward scatter given by (9.1) is then

$30 \log f = 60.573$

$20 \log d = 49.038$

$F(\theta d) = 167.0$ figure 9.1

$F_o = 0$ (9.7)

$H_o = 7.40$ (9.5)

$A_a = 0.01$ figure 3.6

and $L_{bsr} = 186$ db.

Although this is almost certainly a scatter path, the diffraction loss for a transhorizon path is computed as an example. For horizontal polarization over average ground figures 8.1 and 8.2 show $K(a = 8497) = 0.001$ and $b = 93^o$. The following additional parameters are computed:

				Reference
$a_1 = 5808$ km,	$a_2 = 3951$ km,	$a_t = 9179$ km,	$a_r = 5804$	(8.8) and (8.9)
$C_{o1} = 1.135$	$C_{o2} = 1.291$	$C_{ot} = 0.975$	$C_{or} = 1.136$	(8.13)
$K_1 = 0.001135$	$K_2 = 0.001291$	$K_t = 0.000975$	$K_r = 0.001136$	(8.13)
$B_1 = 1.6059$	$B_2 = 1.6058$	$B_t = 1.6062$	$B_r = 1.6059$	figure 8.3
$C_1(K_1) = 20.03$	$C_1(K_2) = 20.03$	$\overline{C}_1(K_{1,2}) = 20.03$		figure 8.4
$x_1 = 385.85$	$x_2 = 112.25$	$x_o = 2452.37$		(8.12) and (8.13)
$F(x_1) = -11.0$	$F(x_2) = -34.5$			figure 8.6
		$G(x_o) = 107.14$		(8.4)

Then from (8.1) the attenuation relative to free space $A = 132.61 + A_a = 132.62$ db. The free space loss from (2.31) is $L_{bf} = 121.87$ db and the long-term median basic transmission loss due to diffraction $L_{bd} = 254.5$ db. As expected this is much more than the predicted scatter loss and the long-term reference value $L_{cr} = L_{bsr} = 186$ db.

In order to predict long-term variability the effective distance d_e is computed using (10.1), (10.2) and (10.3b), $d_{s1} = 64.0$ km, $d_{so} = 220.5$ km, and $d_e = 286.4$ km. From figures 10.2, 10.3, III.32 and from (10.6) the following parameters are:

Parameter	Summer	Winter	All Hours	Reference
$V(50, d_e)$	5.0	1.0	3.0	figure III.32
$Y_o(10, d_e)$	7.75	7.05	7.75	figure 10.2
$Y_o(90, d_e)$	-6.35	-6.35	-6.35	figure 10.2
$g(10, f)$	1.055	1.055	1.055	figure 10.3
$g(90, f)$	1.055	1.055	1.055	figure 10.3
$Y(10)$	8.18	7.44	8.18	(10.6)
$Y(90)$	-6.70	-6.70	-6.70	(10.6)

Using the reference value L_{cr} = 186 db and the ratios given in (10.7) the predicted cumulative distributions for summer, winter and all hours are tabulated below:

	$L_b(p)$ in db		
p	Summer	Winter	All Hours
0.01	153.8	160.2	155.8
0.1	158.7	164.7	160.7
1	164.6	170.1	166.6
10	172.8	177.6	174.8
50	181.0	185.0	183.0
90	187.7	191.7	189.7
99	193.2	197.2	195.2
99.9	197.1	201.1	199.1
99.99	200.4	204.4	202.4

These cumulative distributions are shown graphically on figure III.48 together with distributions derived from measurements over the path. The data represent more than 23,000 hourly medians from measurements over a period of more than 3 years. The arrows on the 0.1 percent values indicate that losses were less than the values plotted while those on the 99 and 99.9 percent values indicate that the losses were greater than the values plotted.

An example may be included here of the method of mixing distributions described in subsection III.7.2. The summer and winter distributions of data may be mixed in order to obtain the distribution of hourly median values for all hours. Several levels of transmission loss from 165 to 195 db are chosen and the value p is read from figure III.48 for each distribution. A weighted average is then obtained at each level to provide the mixed distribution of data corresponding to all hours. The weights are the number of hours of data in each case and the weighted average is $\frac{1}{23,294}\ (p_{\text{winter}} \times 12,160 + p_{\text{summer}} \times 11,134)$.

Level	p_{winter}	p_{summer}	Ave p (all hours)
165	<0.05	1.70	0.84
170	2.1	10.5	6.1
175	8.3	29.2	18.3
180	24.2	59.0	40.8
185	50.0	88.3	68.3
190	86.0	98.7	92.1
195	>99.75	>99.954	>99.85

The weighted averages of p are plotted on figure III.48 at each of these levels of transmission loss and show very good agreement with the distribution obtained directly from the data.

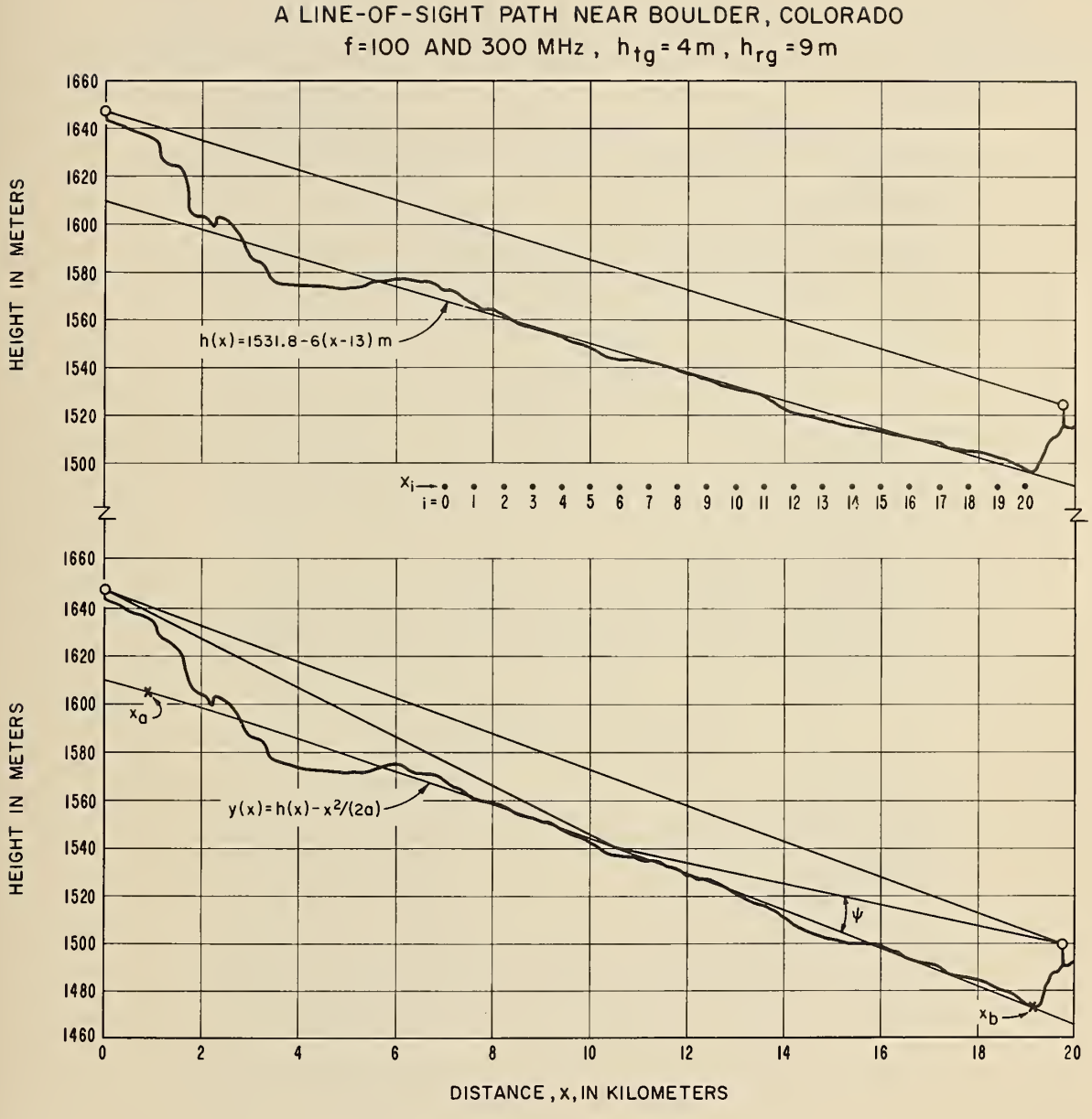

Figure III.43

OBSERVED INPUT VOLTAGE VARIATION AT GROUND STATION RECEIVER FROM AN AIRCRAFT AT 10,000 FEET TRANSMITTING ON 328.2 MC/S

TRANSMITTER POWER: 6 WATTS; TRANSMITTING AND RECEIVING ANTENNA GAIN: 2.15 db (RELATIVE TO AN ISOTROPIC)
GROUND ANTENNA HEIGHT: 75 FEET; TRANSMISSION OVER WATER; 6 db COMMUNICATIONS SYSTEM LOSS ASSUMED FOR THEORETICAL CURVES

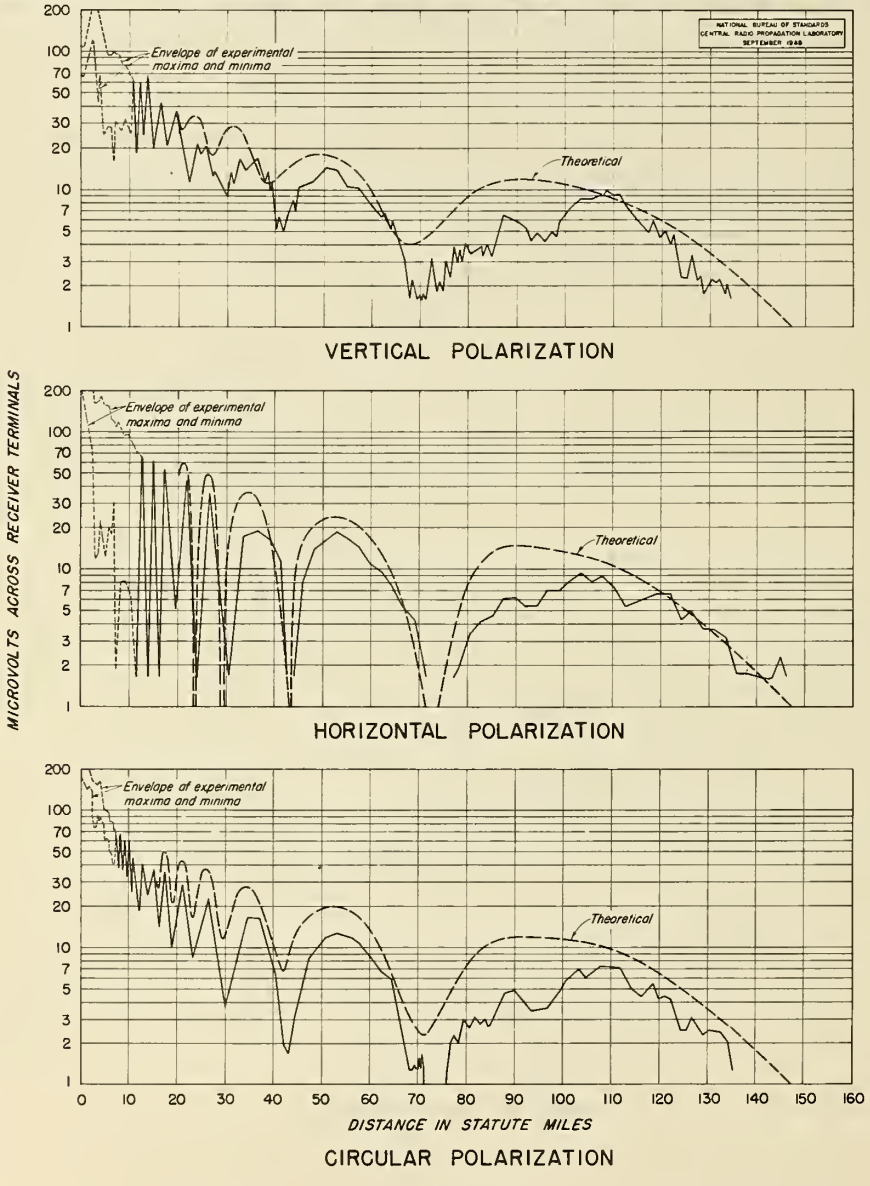

Figure III.44

TERRAIN PROFILE FOR COLORADO KNIFE-EDGE DIFFRACTION PATH

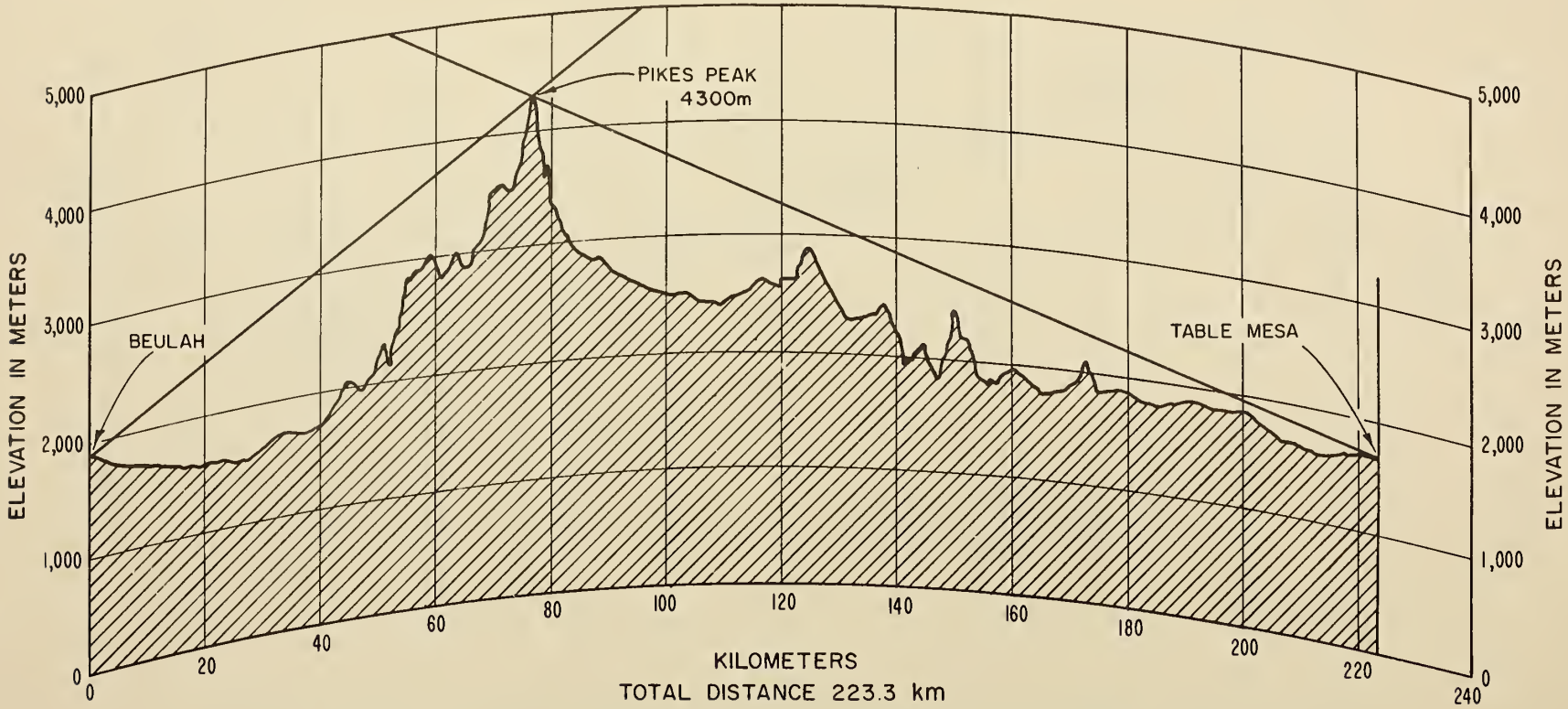

Figure III.45

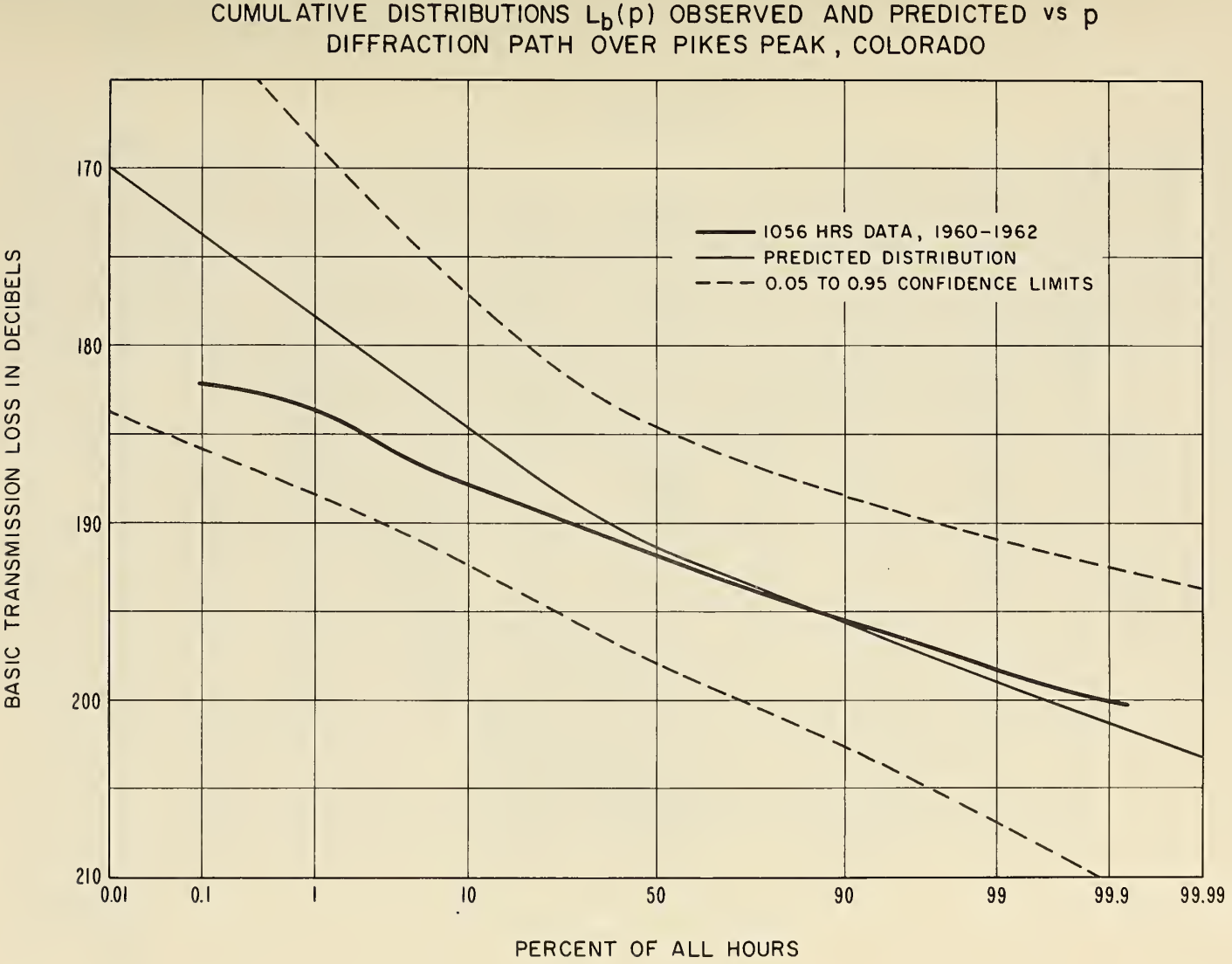

Figure III.46

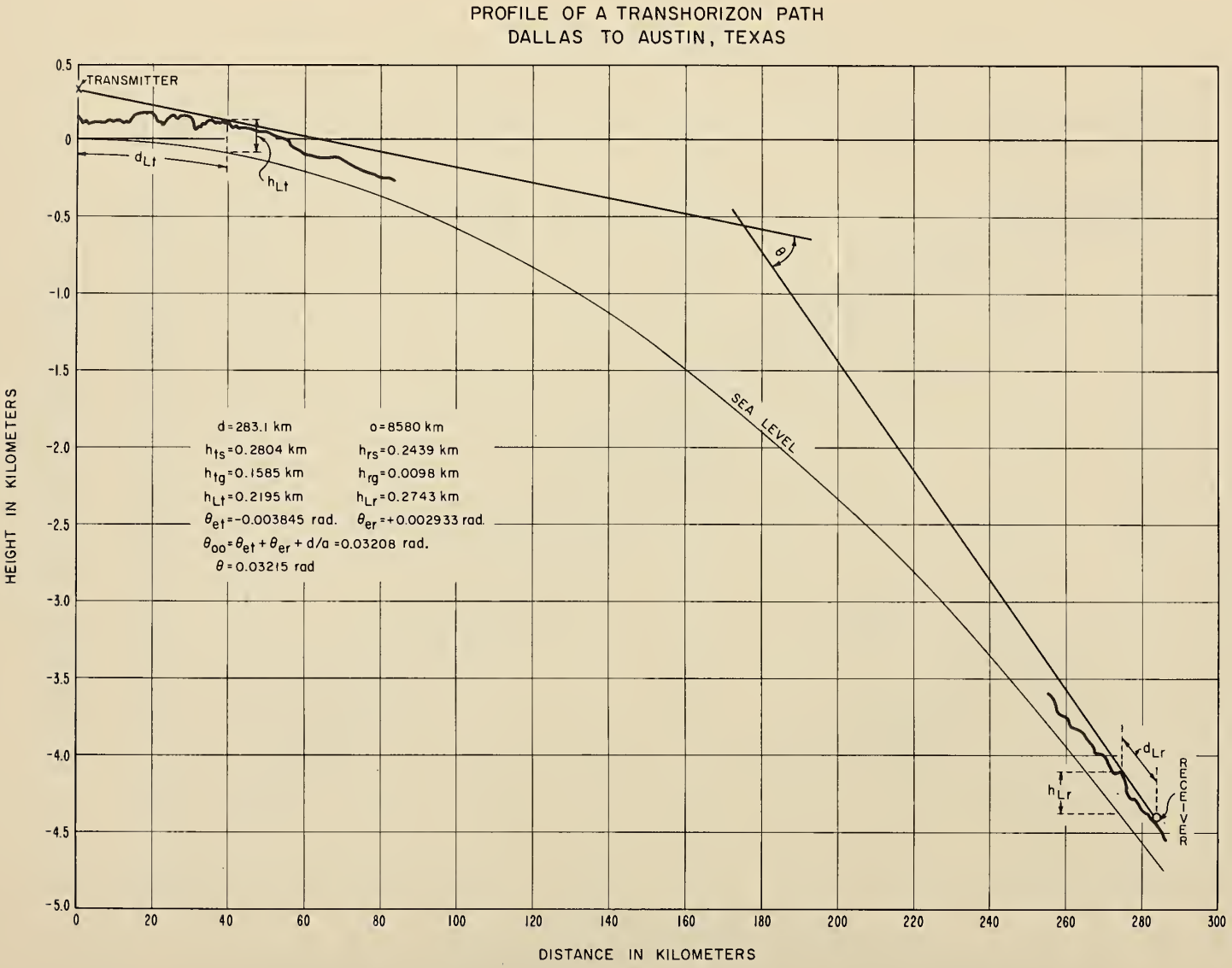

Figure III 47

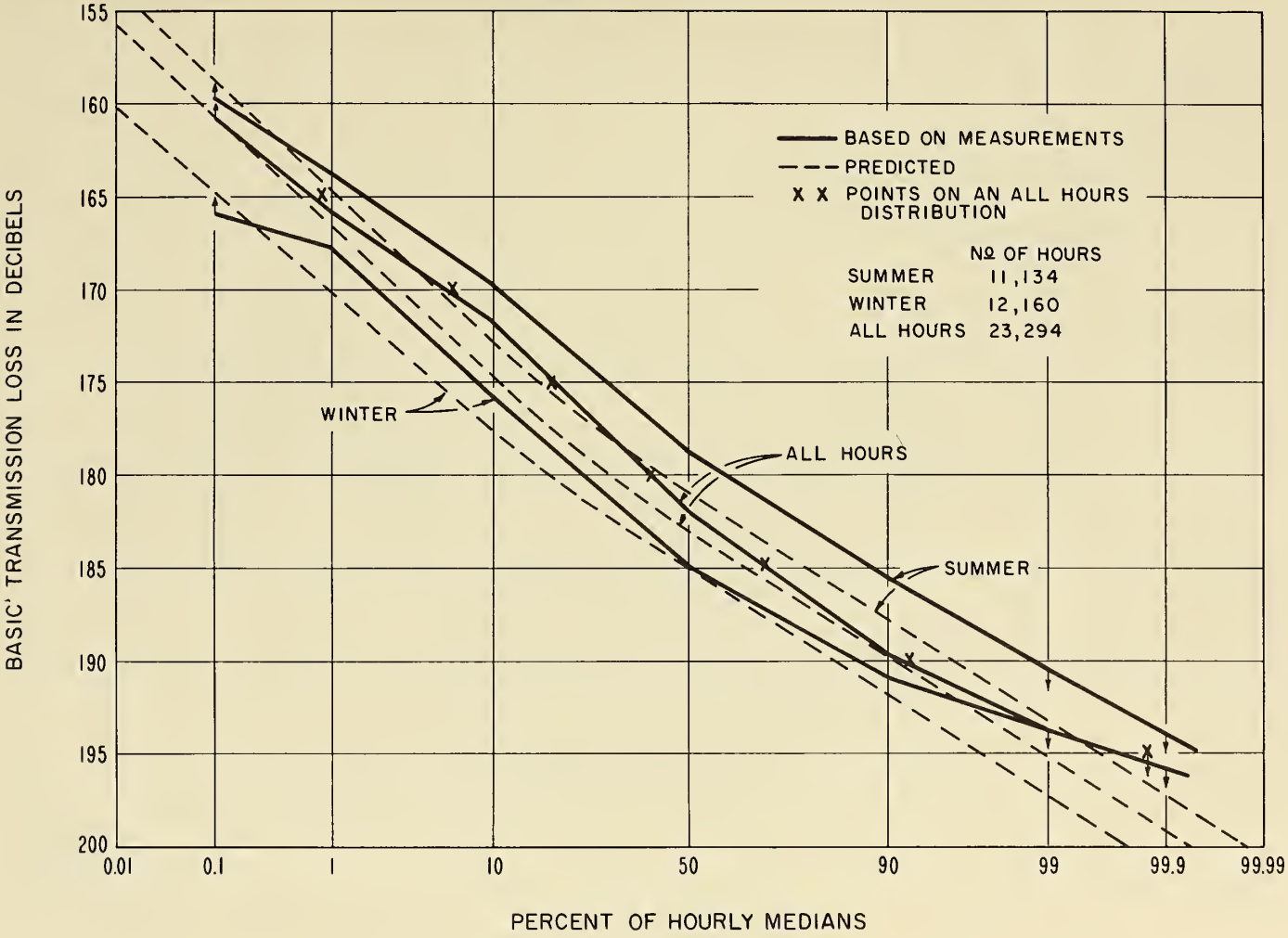

Figure III .48

Annex IV

FORWARD SCATTER

This annex discusses some of the similarities and differences between forward scatter from refractive index turbulence and forward scatter or incoherent reflections from tropospheric layers.

To scatter is to spread at random over a surface or through a space or substance. Scattering which tends to be coherent is more properly called forward scatter, reflection, refraction, focusing, diffraction, or all of these, depending on the circumstances. Modes of scattering as well as mechanisms of propagation bear these names. For example, we may speak of the reflection, refraction, diffraction, focusing, scattering, and absorption of a radio wave by a single spherical hailstone, and all of these modes can be identified in the formal solutions of Maxwell's equations for this problem.

The large volume of beyond-the-horizon radio transmission loss data available in the frequency range 40 to 4000 MHz and corresponding to scattering angles between one and three degrees indicates that the ratio $10^{-A/10}$ corresponding to the transmission loss, A, relative to free space is approximately proportional to the wavelength, λ, or inversely proportional to the radio frequency, f, [Norton, 1960], so that the ratio $10^{-L_b/10}$ corresponding to the forward scatter basic transmission loss is approximately proportional to λ^3 or to f^{-3}. This circumstance is more readily explained in terms of forward scatter from layers [Friis, Crawford, and Hogg, 1957] or in terms of glancing or glinting from brilliant points on randomly disposed "feuillets", [du Castel, Misme, Spizzichino, and Voge, 1962], than in terms of forward scatter from the type of turbulence characterized by the modern Obukhov-Kolmogorov theory [Obukhov, 1941, 1953; Batchelor, 1947, 1953]. There is recent evidence [Norton and Barrows, 1964] that the wavenumber spectrum of refractivity turbulence in a vertical direction has the same form as the more adequately studied spectrum of variations in space in a horizontal direction. Some mechanism other than scatter from refractivity turbulence must be dominant most of the time to explain the observed transmission loss values over a majority of the transhorizon tropospheric paths for which data are available. Scattering from refractivity turbulence and scattering from sharp gradients are mechanisms which coexist at all times in any large scattering volume. Sharp gradients always exist somewhere, and the atmosphere between them is always somewhat turbulent. Power scattered by these mechanisms is occasionally supplemented by diffraction, specular reflection from strong extended layers, and/or ducting.

A tropospheric duct exists, either ground-based or elevated, if a substantial amount of energy is focused toward or defocused away from a receiver as super-refractive gradients of N exceed a critical value called a "ducting gradient." This gradient is about -157 N-units per kilometer at sea level for horizontally launched radio waves. The duct thickness must

exceed about 5062 $f^{-\frac{2}{3}}$ meters with f in MHz [Kerr, 1964] for a duct to completely trap such radio waves. A few useful references in this connection are cited at the end of section 4.

A more or less horizontally homogeneous "kink" in a refractive index profile may indicate the possibility of ducting for very short wavelengths, the presence of a refracting layer for some of the longer waves, and merely a slight and random perturbation of average atmospheric conditions for other frequencies, antenna locations, or antenna beam patterns and elevation angles. The layer that presents a sharp discontinuity for radio frequencies from 30 to 100 MHz (λ = 10 to 3 meters) may represent a relatively gradual change of refractive index at 300 MHz (λ = 1 meter) and higher frequencies. A tropospheric layer or "feuillet" requires a sufficiently abrupt change in refractive index, usually associated with fine weather conditions, to reflect a substantial amount of radio energy at the grazing angles and frequencies of interest. These may be horizontal changes, in thermals, for instance, as well as changes of refractivity, N, with height.

Almost specular reflection from tropospheric layers is often observed between 30 MHz and 200 MHz. At higher frequencies, where focusing, defocusing, and ducting are common, and where extensive layers are not sufficiently abrupt or sufficiently numerous to provide strong reflections, a number of small and randomly oriented surfaces come into play. A recent summary of the role of the layer structure of the troposphere in explaining tropospheric propagation [Saxton, Lane, Meadows, and Matthews, 1964] includes an extensive list of references. Also useful are general discussions of tropospheric propagation by Bullington [1955], du Castel [1960], Crawford, Hogg, and Kummer [1959], Fengler [1964], Fengler, Jeske, and Stilke [1964], Kirby, Rice, and Maloney [1961], Johnson [1958], Rice and Herbstreit [1964], Shkarofsky [1958], and Vvedenskii and Arenberg [1957].

There are at least three distinguishing features in most theories of forward scatter from clouds, precipitation, refractive index turbulence, layers, or feuillets. A calculation is first made of the expected or average forward scattering pattern, reradiation pattern, or diffraction pattern of a scatterer or a group of scatterers, usually located in free space, and usually assuming an incident plane wave and a distant receiver. Second, a decision is made that the relative phases of waves scattered from individual raindrops or subvolumes of refractivity turbulence or feuillets are random, so that we may simply add the power contributions from these elements and ignore the phases. This is an essential feature of a random scatter theory. And third, some way is found to relate the actual terrain, atmosphere, and antenna parameters to the theoretical model so that a comparison may be made between data and theory.

The mechanisms of scattering from refractivity turbulence, reflection from elevated layers, and ducting are much more sensitive to vertical refractivity gradients than to the

horizontal gradients commonly observed. The forward scatter theory used to develop the prediction methods of section 9 assumes that only vertical scales of turbulence or layer thicknesses are important. The radio wave scattered forward by all the scattering subvolumes visible to both antennas or by all the layers of feuillets visible to both antennas is most affected by a particular range of "eddy sizes", ℓ, or by layers of an average thickness $\ell/2$. A stack of eddies of size ℓ must satisfy the Bragg condition that reradiation by adjacent eddies shall add in phase. Reflections from the exterior and interior boundaries of a layer will add in phase if the ray traversing the interior of the layer is an odd number of wavelengths longer than the ray reflected from the exterior boundary. Either the mechanism of forward scatter from refractivity turbulence or the mechanism of reflection from layers or feuillets selects a wavenumber direction $\hat{\kappa}$ that satisfies the specular reflection condition corresponding to Snell's law that angles of incidence and reflection, ψ, are equal. Mathematically, these conditions are represented by the following relations:

$$\ell = \frac{\lambda}{2\sin(\theta/2)} \cong \frac{\lambda}{\theta}, \qquad \hat{\kappa} = \frac{\hat{R}_o + \hat{R}}{|\hat{R}_o + \hat{R}|} \tag{IV.1}$$

where $\hat{R}_o$ and $\hat{R}$ are unit vectors from the centers of radiation of the transmitting and receiving antenna, respectively, towards an elementary scattering volume, or towards the point of geometrical reflection from a layer. The angle between $\hat{R}$ and $\hat{R}_o$ is the scattering angle θ illustrated in figure IV-1 and is thus twice the grazing angle ψ for reflection from a layer:

$$\theta = 2\psi = \cos^{-1}(-\hat{R} \cdot \hat{R}_o) \quad \text{radians} \tag{IV.2}$$

The plane wave Fresnel reflection coefficient q_o for an infinitely extended plane boundary between homogeneous media with refractive indices n_1 and n_2 and for horizontal polarization [Wait, 1962] is

$$q_o = \frac{\sin\psi - \left[2(n_1 - n_2) + (n_1 - n_2)^2 + \sin^2\psi\right]}{\sin\psi + \left[2(n_1 - n_2) + (n_1 - n_2)^2 + \sin^2\psi\right]} \tag{IV.3}$$

The following approximation, valid for $(n_1 - n_2)^2 < \sin^2\psi << 1$ is also good for vertical polarization:

$$q_o \cong \frac{n_2 - n_1}{2\psi^2} \exp\left[-(n_2 - n_1)^2/(2\psi^2)\right] \cong \frac{n_2 - n_1}{2\psi^2} = \frac{2(n_2 - n_1)}{\theta^2} \tag{IV.4}$$

A differential amplitude reflection coefficient dq for a tropospheric layer is next defined as proportional to the difference between two gradients of refractive index, m and m_o, where m is the average refractive index gradient dn/dz across the layer, and m_o is the average refractive index gradient for the region in which the layer is embedded. Let the layer extend in depth from z = 0 to $z = z_o$ in the wavenumber direction $\hat{\kappa}$ defined by (IV. 1), and write the differential reflection coefficient as

$$dq = dz(m - m_o)/(2\psi^2) \tag{IV. 5}$$

A phasor $\exp[-iz(4\pi\psi/\lambda)]$ is associated with dq, and the power reflection coefficient q^2 for a tropospheric layer of thickness z_o is approximated as

$$q^2 = \left| \int_{z=o}^{z=z_o} dq \exp[-iz(4\pi\psi/\lambda)] \right|^2 = (4\pi)^2 \lambda^2 \psi^{-6} M \tag{IV. 6a}$$

$$M = (m - m_o)^2 \left[1 - \cos(4\pi\psi z_o/\lambda)\right]/(4\pi)^4 \tag{IV. 6b}$$

If M is assumed continuous at z = 0 and $z = z_o$, somewhat smaller values of q^2 and m will result [Wait, 1962].

Friis, Crawford, and Hogg [1957] point out that the power received by reflection from a finite layer can be approximated as the diffracted power through an absorbing screen with the dimensions of the layer projection normal to the direction of propagation. They then consider layers of large, small, and medium size compared to

$$2w = 2(\lambda R_o R/d)^{1/2}, \quad d \cong R_o + R \tag{IV. 7}$$

which is the width of a first Fresnel zone. Let b represent the dimensions of a layer or feuillet in any direction perpendicular to $\hat{\kappa}$. Since $\hat{\kappa}$ is usually nearly vertical, b is usually a horizontal dimension. Adopting a notation which conforms to that used elsewhere in this report, the available power p_a at a receiver at a distance d from a transmitting antenna radiating p_t watts is

$$p_a = \frac{4 p_t g_t g_r \lambda^2 q^2}{(4\pi d)^2} \left[C^2(u) + S^2(u)\right] \left[C^2(v) + S^2(v)\right] \tag{IV. 8}$$

in terms of Fresnel integrals given by (III. 33), where

$$u = b\sqrt{2}/w, \quad v = b\psi\sqrt{2}/w \tag{IV. 9}$$

and g_t and g_r are antenna directive gains. For large u and v,

$$C^2(u) = S^2(u) = C^2(v) = S^2(v) = \tfrac{1}{4} ,$$

and for small u and v, $C^2(u) = u^2$, $C^2(v) = v^2$, and $S^2(u) = S^2(v) = 0$.

For large layers, where $b >> 2w$:

$$p_a = p_t g_t g_r \lambda^4 \psi^{-6} d^{-2} M \qquad \text{(IV.10a)}$$

For intermediate layers, where $b \cong 2w$:

$$p_a = p_t g_t g_r \lambda^3 \psi^{-4} (R R_o d)^{-1} b^2 M \qquad \text{(IV.10b)}$$

For small layers, where $b << 2w$:

$$p_a = p_t g_t g_r \lambda^2 \psi^{-4} (R R_o)^{-2} b^4 M \qquad \text{(IV.10c)}$$

Forward scatter from layers depends on the statistics of sharp refractive index gradients in the directions $\hat{\kappa}$ defined by (IV.1). The determination of these statistics from radio and meteorological measurements is only gradually becoming practical. A study of likely statistical averages of the meteorological parameters M, b^2M, and b^4M indicates that these expected values should depend only slightly on the wavelength λ and the grazing angle ψ, as was assumed by Friis, et al [1957]. The expected value of

$$[1 - \cos(4\pi \psi z_o / \lambda)]$$

can vary only between 0 and 2 and is not likely to be either 0 or 2 for any reasonable assumptions about the statistics of z_o.

Available long-term median radio transmission loss data usually show the frequency law given by (IV.10b) for medium-size layers. Long-term cumulative distributions of short-term available power ratios on spaced frequencies rarely show a wavelength law outside the range from λ^2 to λ^4 [Crawford, Hogg, and Kummer, 1959; Norton 1960]. An unreported analysis of 8978 hours of matched simultaneous recordings at 159.5, 599, and 2120 MHz over a 310-km path in Japan shows that this wavelength exponent for transmission loss p_a/p_t is within the range from 2 to 4 ninety-eight percent of the time. This corresponds to a wavelength exponent range from 0 to 2 or a frequency exponent range from 0 to -2 for attenuation relative to free space values, and to corresponding ranges λ^2 to λ^4 or f^{-2} to f^{-4} for values of basic transmission loss, L_b.

Figures IV.1(a) and IV.1(b) illustrate forward scattering from a single small layer and from refractivity turbulence in a single small scattering subvolume of the volume V of space visible to two antennas. Figures IV.1(c) and IV.1(d) illustrate models for the addition of power contributions from large parallel layers, and from scattering or reflection subvolumes, respectively. Contributions from diffraction or ducting are ignored, as well as returns from well-developed layers for which a geometrical reflection point is not visible to both antennas. Combinations of these mechanisms, though sometimes important, are also not considered here.

For each of the cases shown in figure IV.1, coherently scattered or reflected power p_{ai} from the neighborhood of a point $\vec{R}_{oi}$ is conveniently associated with a scattering subvolume $d^3R_o = dv = v_i(\vec{R}_{oi})$, so that the total available forward scattered power at a receiver is

$$p_a = \sum_{i=1}^{N_v} p_{ai} = \sum_{i=1}^{N_v} v_i\, p_{vi} \cong \int_V d^3R_o\, p_v(\vec{R}_o, \vec{R}) \text{ watts} \qquad \text{(IV.11)}$$

where

$$p_{vi} = p_{ai}/v_i = p_v(\vec{R}_o, \vec{R}) \qquad \text{(IV.12)}$$

is the available power per unit scattering volume for the i^{th} scattering subvolume, feuillet, or layer, and it is assumed that only N_v such contributions to p_a are important.

Each of the power contributions p_{ai} is governed by the bistatic radar equation. Omitting the subscript i, this equation may be written as

$$p_a = \left(\frac{p_t g_t}{4\pi R_o^2}\right)\left(\frac{a_s c_p}{4\pi R^2}\right)\left(\frac{\lambda^2 g_r}{4\pi}\right) \text{ watts}, \qquad \text{(IV.13)}$$

where $a_s c_p$ is the effective scattering cross-section of a single scatterer or group of scatterers, including the polarization efficiency c_p of the power transfer from transmitter to receiver. The first set of parentheses in (IV.13) represents the field strength in watts per square kilometer at the point $\vec{R}_o$, the second factor enclosed in parentheses shows what fraction of this field strength is available at the receiver, and $\lambda^2 g_r/(4\pi)$ is the absorbing area of the receiving antenna.

The key to an understanding of scattering from spacecraft, aircraft, rain, hail, snow, refractivity turbulence, or inhomogeneities such as layers or feuillets is the scattering cross-section $a_s c_p$ defined by (IV.13) or the corresponding scattering cross-section per unit volume a_v, defined from (IV.12) and (IV.13) as

$$a_v = (4\pi)^3 (R_o R)^2 p_v/(p_t g_t g_r \lambda^2) \quad \text{per km} \tag{IV.14}$$

This quantity is usually estimated by isolating a small volume of scatterers in free space at large vector distances $\vec{R}_o$ and $\vec{R}$, respectively, from the transmitter and receiver. If both antennas are at the same place, (IV.13) becomes the monostatic radar equation, corresponding to backscatter instead of to forward scatter.

The scattering cross-sections per unit volume for large, medium, and small layers, assuming a density of N_ℓ layers per unit volume, may be obtained by substituting (IV.10a) to (IV.10c) in (IV.14):

For large layers, where $b >> 2w$:

$$a_{v1} = w^4 \psi^{-6} M N_\ell = \lambda^2 \psi^{-6} (R_o R/d)^2 M N_\ell \tag{IV.15}$$

For intermediate layers, where $b \cong 2w$:

$$a_{v2} = w^2 \psi^{-4} b^2 M N_\ell = \lambda \psi^{-4} (R_o R/d) b^2 M N_\ell \tag{IV.16}$$

For small layers, where $b << 2w$:

$$a_{v3} = \psi^{-4} b^2 M N_\ell = \lambda^0 \psi^{-4} b^2 M N_\ell \tag{IV.17}$$

The modern Obukhov-Kolmogorov theory of homogeneous turbulence in a horizontal direction, when extended to apply to the wavenumber spectrum of instantaneous variations of refractive index in a vertical direction, predicts a $\lambda^{-\frac{1}{3}}$ or $f^{\frac{1}{3}}$ law for the variation with wavelength λ or carrier frequency f of either a_v or attenuation relative to free space, or a $\lambda^{5/3}$ or $f^{-5/3}$ law for variations of the transmission loss p_a/p_t. Theoretical studies of multiple scattering by Beckmann [1961a], Bugnolo [1958], Vysokovskii [1957, 1958], and others suggest that single scattering adequately explains observed phenomena. Descriptions of atmospheric turbulence are given by Batchelor [1947, 1953], de Jager [1952], Heisenberg [1948], Kolmogoroff [1941], Merkulov [1957], Norton [1960], Obukhov [1941, 1953], Rice and Herbstreit [1964], Sutton [1955], Taylor [1922], and Wheelon [1957, 1959].

The observed wavelength exponent for the Japanese transmission loss data previously noted was below 5/3 less than two tenths of one percent of the time, and an examination of other data also leads to the conclusion that forward scatter from Obukhov-Kolmogorov turbulence can rarely explain what is observed with frequencies from 40 to 4000 MHz and scattering angles from one to three degrees.

Early recognition of this fact by Norton, Rice, and Vogler [1955] led to the proposal of a mathematical form for the vertical wavenumber spectrum which would achieve agreement between radio data and the theory of forward scatter from refractivity turbulence [Norton, 1960]. Radio data were used to determine the following empirical form for a_v, upon which the predictions of section 9 are based:

$$a_v = \lambda \psi^{-5} M \tag{IV.18}$$

$$M = 3 < (\Delta n)^2 > / (32 \ell_o^2) \tag{IV.19}$$

where

$$\Delta n = n - <\Delta n> \tag{IV.20}$$

is the deviation of refractive index from its expected value $<\Delta n>$, and ℓ_o is a "scale of turbulence" [Rice and Herbstreit, 1964].

Values of the variance $<(\Delta n)^2>$ of refractivity fluctuations and scales of turbulence ℓ_o obtained from meteorological data lead to good agreement between (IV.18) and radio data when an exponential dependence of M on height is assumed, substituting the corresponding value of p_v in (IV.11). It is not yet clear how the estimates of m, m_o, z_o, b, and N_ℓ required by the theory of forward scatter from layers of a given type can be obtained from direct meteorological measurements, nor how these parameters will vary throughout the large volume of space visible to both antennas over a long scatter path. It does seem clear that this needs to be done.

Data from elevated narrow-beam antennas that avoid some of the complex phenomena due to reflection and diffraction by terrain, and which select small scattering volumes, suggest that for scattering angles exceeding ten degrees, reflections from large layers can hardly be dominant over reflection from intermediate and small layers or from refractivity turbulence. Preliminary results indicate that field strengths decrease more slowly at a fixed distance and with scattering angles θ increasing up to fifteen degrees than would be possible with the θ^{-6} dependence of a_v given by (IV.15) added to a probable exponential decay with height of the expected value of the meteorological parameter MN_ℓ for large layers.

The wavelength and angle dependence of forward scatter characterized by the Obukhov-Kolmogorov turbulence theory is nearly the same as that for small layers, given by (IV.17). For scattering from refractivity turbulence:

$$a_{vo} = \lambda^{-1/3} \psi^{-11/3} M_o \tag{IV.21}$$

$$M_o = \frac{\Gamma(11/6) < (\Delta n)^2 >}{4(2\pi)^{13/3} \Gamma(1/3) \ell_o^{2/3}} \tag{IV.22}$$

Although most of the propagation paths which have been studied rarely show this frequency dependence, some occasionally do agree with (IV.21). In general, the radiowave scattering cross-section per unit volume a_v is a weighted average of scattering from all kinds of layers or feuillets and the turbulence between them.

Summarizing the argument:

$$a_v = a_{vo} + a_{v1} + a_{v2} + a_{v3} \cong \lambda \psi^{-5} M \qquad \text{(IV.23)}$$

for $10^{-4} < \lambda < 10^{-2}$ km, $0.01 < \psi < 0.03$ radians, where M has been determined from radio data, subject to the assumption that M decreases exponentially with height above the earth's surface. Equation (IV.23) is intended to indicate the present state of the twin arts of formulating theories of tropospheric forward scatter and comparing these theories with available long-term median transmission loss data. A great deal of available data is not forward scatter data, and it is for this reason that estimates of long-term variability as given in section 10 and annex III are almost entirely empirical.

Also, for this reason, estimates of L_{gp} as given in section 9 are restricted to long-term median forward scatter transmission loss. Available measurements of differences in path antenna gain agree within the limits of experimental error with the values predicted by the method of section 9 whenever the dominant propagation mechanism is forward scatter.

GEOMETRY FOR FORWARD SCATTER

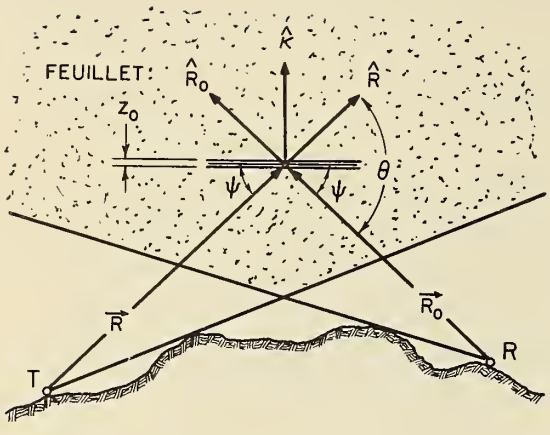

(a)

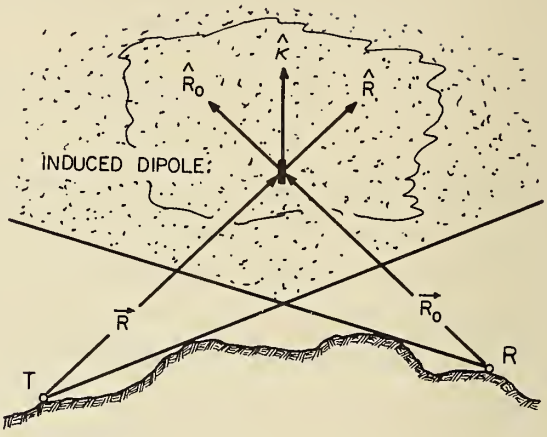

(b)

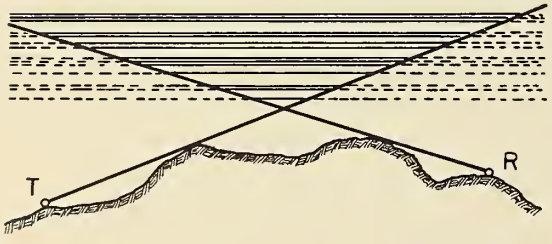

(c)

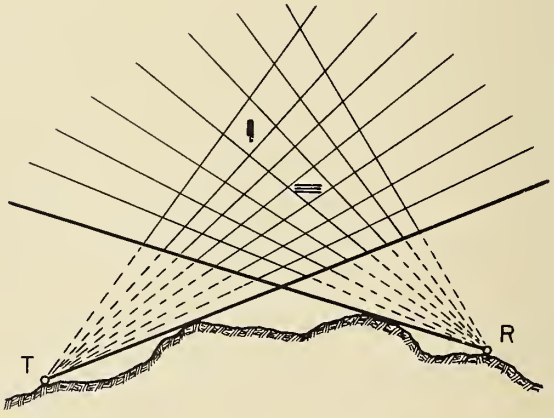

(d)

Figure IV.1

Annex V

PHASE INTERFERENCE FADING AND SERVICE PROBABILITY

As a general rule, adequate service over a radio path requires protection against noise when propagation conditions are poor, and requires protection against interference from cochannel or adjacent channel signals when propagation conditions are good. Optimum use of the radio spectrum requires systems so designed that the reception of wanted signals is protected to the greatest degree practicable from interference by unwanted radio signals and by noise.

The short-term fading of the instantaneous received power within periods of time ranging from a few minutes up to one hour or more is largely associated with random fluctuations in the relative phasing between component waves. These arrive at the receiving antenna after propagation via a multiplicity of propagation paths having electrical lengths that vary from second to second and from minute to minute over a range of a few wavelengths. A small part of this short-term fading and usually all of the long-term variations arise from minute-to-minute changes in the root-sum-square value of the amplitudes of the component waves, i.e., in short-term changes in the mean power available from the receiving antenna. In the analysis of short-term fading, it is convenient to separate the effects of these phase and root-sum-square amplitude changes on the distribution of the instantaneous received power and, for a fixed transmitter power, on the distribution of the instantaneous transmission loss. Multipath or "phase interference fading" among simultaneously occurring modes of propagation usually determines the statistical character of short-term variability.

Over most transhorizon paths, long-term variability is dominated by "power fading", due to slow changes in average atmospheric refraction, in the intensity of refractive index turbulence, or in the degree of atmospheric stratification. The distinction between phase interference fading and power fading is somewhat arbitrary, but is nevertheless extremely useful. Economic considerations, as contrasted to the requirements for spectrum conservation, indicate that radio receiving systems should be designed so that the minimum practicable transmitter power is required for satisfactory reception of the wanted signals in the presence of noise. Fading expected within an hour or other convenient "short" periods of time is allowed for by comparing the median wanted signal power p_m available at the receiver with the median wanted signal power p_{mr} which is required for satisfactory reception in the presence of noise. This operating sensitivity p_{mr} assumes a specified type of fading wanted signal and a specified type of noise, but does not allow for other unwanted signals.

In the presence of a specified unwanted signal, but in the absence of other unwanted signals or appreciable noise, the fidelity of information delivered to a receiver output will increase as the ratio r_u of wanted-to-unwanted signal power increases. The degree of fidelity of the received information may be measured in various ways. For example, voice signals are often measured in terms of their intelligibility, television pictures by subjective

observation, and teletype signals by the percentage of correctly interpreted received characters. A specified grade of service provided by a given wanted signal will guarantee a corresponding degree of fidelity of the information delivered to the receiver output. For example, a Grade A teletype service could be defined as one providing 99.99 percent error-free characters, while a Grade B service could be defined as one providing 99.9 percent error-free characters.

The protection ratio r_{ur} required for a given grade of service will depend upon the nature of the wanted and unwanted signals; i.e., their degree of modulation, their location in the spectrum relative to the principal and spurious response bands of the receiving system, and their phase interference fading characteristics. The use of receiving systems having the smallest values of r_{ur} for the kinds of unwanted signals likely to be encountered will permit the same portions of the spectrum to be used simultaneously by the maximum number of users. For instance, FM with feedback achieves a reduction in r_{ur} for a cochannel unwanted signal by occupying a larger portion of the spectrum. But optimum use of the spectrum requires a careful balance between reductions in r_{ur} on the same channel and on adjacent channels, taking account of other system isolation factors such as separation between channels, geographical separation, antenna directivity, and cross-polarization.

Note that the operating sensitivity p_{mr} is a measure of the required magnitude of the median wanted signal power but r_{ur} involves only the ratio of wanted to unwanted signal powers. For optimum use of the spectrum by the maximum number of simultaneous users, the transmitting and receiving systems of the individual links should be designed with the primary objective of ensuring that the various values of r_u exceed r_{ur} for a large percentage of the time during the intended periods of operation. Then sufficiently high transmitter powers should be used so that the median wanted signal powers p_m exceed p_{mr} for a large percentage of the time during the intended period of reception at each receiving location. This approach to frequency assignment problems will be unrealistic in a few cases, such as the cleared channels required for radio astronomy, but these rare exceptions merely serve to test the otherwise general rule [Norton, 1950, 1962 and Norton and Fine 1954] that optimum use of the spectrum can be achieved only when interference from other signals rather than from noise provides the ineluctable limit to satisfactory reception.

This annex discusses the requirements for service of a given grade g, how to estimate the expected time availability p of acceptable service, and, finally, how to calculate the service probability Q for a given time availability.

In this annex all quantities expressed in decibels are denoted by capital letters; for example, $X = 10 \log x$, where x is usually a power or a power ratio.

V. 1 The Two Components of Fading

Both the wanted signal power p_i and the unwanted signal power p_{ui} available to a receiving system will usually vary from minute to minute in a random or unpredictable fashion. It is convenient to divide the "instantaneous received signal power" $P_i = 10 \log p_i$ into two or three additive components where p_i is defined in the usual way as the average power for a single cycle of the radio frequency, so as to eliminate the variance of power associated with the time factor $\cos^2(\omega t)$:

$$P_i = P_m + Y_i = P_m(50) + Y + Y_i \quad \text{dbw} \tag{V.1}$$

P_m is that component of P_i which is not affected by the usually rapid phase interference fading. P_m is most often identified as the short-term median of the available power P_i at the receiving antenna. $P_m(50)$ is the median of all such values of P_m, and is most often identified as the long-term median of P_i. In terms of the long-term median transmission loss $L_m(50)$ and the total power P_r radiated from the transmitting antenna:

$$P_m(50) = P_r - L_m(50) \quad \text{dbw} \tag{V.2}$$

The characteristics of long-term fading and phase interference fading, respectively, are described in terms of the two fading components Y and Y_i defined by (V. 1):

$$Y = P_m - P_m(50), \qquad Y_i = P_i - P_m \tag{V.3}$$

The long term for which the median power, $P_m(50)$, is defined may be as short as one hour or as long as several years but will, in general, consist of the hours within specified time blocks such as, for example, the hours between 6 PM and midnight in the summer months. However, it will be convenient in the case of most continuously operating services to consider that $P_m(50)$ refers to the median power over a long period of time, including all hours of the day and all seasons of the year for a period of several years.

The observations of long-term variability summarized in section 10 and in annex III show that P_m is a very nearly normally distributed random variable characterized by a standard deviation that may range from one decibel over a period of time of the order of one hour up to ten decibels for periods of the order of several years; these values of standard deviation are representative only of typical beyond-the-horizon propagation paths and vary widely for other propagation conditions.

For periods as short as an hour, the variance of $Y_i = P_i - P_m$ is generally greater than the variance of P_m. The long-term variability of P_m is identified in section 10 with the variability of hourly medians, expressed in terms of

$$Y(p) = P_m(p) - P_m(50) = L_m(50) - L_m(p) \qquad (V.4)$$

where $P_m(p)$ is the hourly median wanted signal power P_m exceeded for p percent of all hours, and $L_m(p)$ is the corresponding transmission loss exceeded for $(100 - p)$ percent of all hours.

Often, data for a path are available in terms of the long-term cumulative distribution of instantaneous power, P_i; that is, we know $P_i(p)$ versus p, but not $P_m(p)$ versus p. Let q represent the probability that P_i will exceed $P_i(q)$ for a given value of P_m; this is the same as the probability that Y_i will exceed $Y_i(q)$. Then an approximation to the cumulative distribution function $L_i(p)$ versus P is given by

$$L_i(p) \cong L_m(50) \pm [Y^2(p) + Y_i^2(q)]^{1/2} \qquad (V.5)$$

where Y_i $(q = p/100)$ is evaluated for the particular type of phase interference fading characteristic of a wanted signal level exceeded p percent of the time. The plus sign in (V.5) is used for $p > 50$ percent, and the minus sign for $p < 50$ percent.

V.2 The Nakagami-Rice Distribution

For studies of the operating sensitivity P_{mr} of a receiver in the presence of a rapidly fading wanted signal, and for studies of the median wanted signal to unwanted signal ratio $R_{ur}(g)$ required for a grade g service, it is helpful to consider a particular statistical model which may be used to describe phase interference fading. Minoru Nakagami [1940] describes a model which depends upon the addition of a constant signal and a Rayleigh-distributed random signal [Rayleigh 1880; Rice, 1945; Norton, Vogler, Mansfield and Short, 1955; Beckmann, 1961a, 1964]. In this model, the root-sum-square value of the amplitudes of the Rayleigh components is K decibels relative to the amplitude of the constant component. $K = -\infty$ corresponds to a constant received signal. For a Rayleigh distribution, $K = +\infty$ and the probability q that the instantaneous power, p_i, will exceed $p_i(q)$ for a given value of the short-term median power, p_m, may be expressed:

$$q[p_i > p_i(q) \mid p_m] = \exp\left[-\frac{p_i(q)\log_e 2}{p_m}\right], \quad [K = +\infty] \tag{V.6a}$$

Alternatively, the above may be expressed in the following forms:

$$q[y_i > y_i(q)] = q[Y_i > Y_i(q)] = \exp[-y_i(q)\log_e 2], \quad [K = +\infty] \tag{V.6b}$$

$$Y_i(q) = 5.21390 + 10\log\{\log(1/q)\}, \quad [K = +\infty] \tag{V.6c}$$

Figure V.1 and Table V.1 show the Nakagami-Rice phase interference fading distribution $Y_i(q)$ as a function of K for particular values of q. It is evident from figure V.1 that the distribution of phase interference fading depends only on K. The utility of this distribution for describing phase interference fading in ionospheric propagation is discussed in CCIR report [1963k] and for tropospheric propagation is demonstrated in papers by Norton, Rice and Vogler [1955], Janes and Wells [1955], and Norton, Rice, Janes, and Barsis [1955]. Bremmer [1959] and Beckmann [1961a] discuss a somewhat more general fading model.

For within-the-horizon tropospheric paths, including either short point-to-point terrestrial paths or paths from an earth station to a satellite, K will tend to have a large negative value throughout the day for all seasons of the year. As the length of the terrestrial propagation path is increased or the elevation angle of a satellite is decreased so that the path has less than first Fresnel zone clearance, the expected values of K will increase until, for some hours of the day, K will be greater than zero and the phase interference fading for signals propagated over the path at these times will tend to be closely represented

by a Rayleigh distribution. For most beyond-the-horizon paths K will be greater than zero most of the time. For knife-edge diffraction paths K is often much less than zero. When signals arrive at the receiving antenna via ducts or elevated layers, the values of K may decrease to values much less than zero even for transhorizon propagation paths. For a given beyond-the-horizon path, K will tend to be negatively correlated with the median power level P_m; i.e., large values of K are expected with small values of P_m. For some within-the-horizon paths, K and P_m tend to be possitively correlated.

Discussions of fading rate and the distribution of the duration of fading are given in CCIR Report No. 242 for tropospheric propagation [1963k] and in CCIR Report No. 266 for ionospheric propagation [1963ℓ].

It is assumed in this report that a particular value of K may always be associated with any time availability, p. However, few data analyses of this kind are presently available. A program of data analysis is clearly desirable to provide empirical estimates of K versus p for particular climates, seasons, times of day, lengths of recording, frequencies, and propagation path characteristics. It should be noted that K versus p expresses an assumed functional relationship. The percentage p is the time availability associated with the cumulative distribution $L_m(p)$ versus p.

An analysis of data for a single day's recording at 1046 MHz over a 364-kilometer path is presented here to illustrate how a relationship between K and p may be established. Figure V.2 shows for a single day the observed interdecile range $P_i(0.1) - P_i(0.9) = L_i(0.9) - L_i(0.1)$ for each five-minute period plotted against the median transmission loss L_m for the five-minute period. Figure V.1 associates a value of K with each value of $L_i(0.9) - L_i(0.1)$, and the cumulative distribution of L_m associates a time availability p with each value of L_m. In figure V.2, K appears to decrease with increasing L_m for the hours 0000 - 1700, although the usual tendency over long periods is for K to increase with L_m. The straight line in the figure is drawn through medians for the periods 0000 - 1700 and 1700 - 2400 hours, with linear scales for K and L_m, as shown by the inset for figure V.2. The corresponding curve of K versus p is compared with the data in the main figure.

Figure V.3 shows for f = 2 GHz and 30-meter antenna heights over a smooth earth a possible estimate of K versus distance and time availability. These crude and quite speculative estimates are given here only to provide an example of how such information with (V. 5) may be used to obtain curves of $L_i(p)$ versus p. The solid curves in the lower part of figure V.3 show how $L_i(p)$ varies with distance for p = 0.01, 1, 50, 99, and 99.99 percent, where L_i is the transmission loss associated with the instantaneous power, P_i.

Table V.1 Characteristics of the Nakagami-Rice Phase Interference Fading Distribution $Y_i(q)$

$Y_i > Y_i(q)$ with Probability q; $Y_i(0.5) \equiv 0$

K	$\overline{Y}_i$	σ_{Yi}	$Y_i(0.01)$	$Y_i(0.1)$	$Y_i(0.9)$	$Y_i(0.99)$	$Y_i(0.1) - Y_i(0.9)$	$Y_i(0.005)$	$Y_i(0.02)$	$Y_i(0.05)$	$Y_i(0.95)$	$Y_i(0.98)$	$Y_i(0.995)$
db	db	db	db	db	db	db	db	db	db	db	db	db	db
-40	-0.0002	0.061	0.1417	0.0784	-0.0790	- 0.1440	0.1574	0.1568	0.1252	0.1004	- 0.1016	- 0.1270	- 0.1596
-35	-0.0007	0.109	0.2504	0.1352	-0.1411	- 0.2579	0.2763	0.2768	0.2214	0.1778	- 0.1815	- 0.2272	- 0.2860
-30	-0.0022	0.194	0.4403	0.2453	-0.2525	- 0.4638	0.4978	0.4862	0.3898	0.3136	- 0.3254	- 0.4082	- 0.5151
-25	-0.0069	0.346	0.7676	0.4312	-0.4538	- 0.8421	0.8850	0.8460	0.6811	0.5496	- 0.5868	- 0.7391	- 0.9374
-20	-0.0217	0.616	1.3184	0.7508	-0.8218	- 1.5544	1.5726	1.4486	1.1738	0.9524	- 1.0696	- 1.3572	- 1.7389
-18	-0.0343	0.776	1.6264	0.9332	-1.0453	- 2.0014	1.9785	1.7840	1.4508	1.1846	- 1.3660	- 1.7416	- 2.2461
-16	-0.0543	0.980	1.9963	1.1558	-1.3326	- 2.5931	2.4884	2.1856	1.7847	1.4573	- 1.7506	- 2.2463	- 2.9231
-14	-0.0859	1.238	2.4355	1.4247	-1.7028	- 3.3872	3.1275	2.6605	2.1829	1.7896	- 2.2526	- 2.9156	- 3.8422
-12	-0.136	1.569	2.9491	1.7455	-2.1808	- 4.4715	3.9263	3.2136	2.6507	2.1831	- 2.9119	- 3.8143	- 5.1188
-10	-0.214	1.999	3.5384	2.1218	-2.7975	- 5.9833	4.9193	3.8453	3.1902	2.6408	- 3.7820	- 5.0372	- 6.9452
- 8	-0.334	2.565	4.1980	2.5528	-3.5861	- 8.1418	6.1389	4.5493	3.7975	3.1602	- 4.9287	- 6.7171	- 9.6386
- 6	-0.507	3.279	4.9132	3.0307	-4.5714	-11.0972	7.6021	5.3093	4.4591	3.7313	- 6.4059	- 8.9732	-13.4194
- 4	-0.706	4.036	5.6559	3.5366	-5.7101	-14.2546	9.2467	6.0955	5.1494	4.3315	- 8.1216	-11.5185	-17.1017
- 2	-0.866	4.667	6.3811	4.0366	-6.7874	-16.4258	10.8240	6.8613	5.8252	4.9219	- 9.6278	-13.4690	-19.4073
0	-0.941	5.094	7.0246	4.4782	-7.5267	-17.5512	12.0049	7.5411	6.4248	5.4449	-10.5553	-14.5401	-20.5618
2	-0.953	5.340	7.5228	4.8088	-8.0074	-18.0527	12.8162	8.0697	6.8861	5.8423	-11.0005	-15.0271	-21.0706
4	-0.942	5.465	7.8525	5.0137	-8.0732	-18.2573	13.0869	8.4231	7.1873	6.0956	-11.1876	-15.2273	-21.2774
6	-0.929	5.525	8.0435	5.1233	-8.1386	-18.3361	13.2619	8.6309	7.3588	6.2354	-11.2606	-15.3046	-21.3565
8	-0.922	5.551	8.1417	5.1749	-8.1646	-18.3669	13.3395	8.7394	7.4451	6.3034	-11.2893	-15.3349	-21.3880
10	-0.918	5.562	8.1881	5.1976	-8.1753	-18.3788	13.3729	8.7918	7.4857	6.3341	-11.3005	-15.3466	-21.4000
12	-0.916	5.567	8.2090	5.2071	-8.1792	-18.3834	13.3863	8.8155	7.5031	6.3474	-11.3048	-15.3512	-21.4046
14	-0.916	5.569	8.2179	5.2112	-8.1804	-18.3852	13.3916	8.8258	7.5106	6.3531	-11.3065	-15.3529	-21.4064
16	-0.915	5.570	8.2216	5.2128	-8.1811	-18.3860	13.3929	8.8301	7.5136	6.3552	-11.3072	-15.3537	-21.4072
18	-0.915	5.570	8.2232	5.2135	-8.1813	-18.3863	13.3948	8.8319	7.5149	6.3561	-11.3075	-15.3540	-21.4075
20	-0.915	5.570	8.2238	5.2137	-8.1814	-18.3864	13.3951	8.8326	7.5154	6.3565	-11.3076	-15.3541	-21.4076
∞	-0.915	5.570	8.2242	5.2139	-8.1815	-18.3865	13.3954	8.8331	7.5158	6.3567	-11.3077	-15.3542	-21.4077

THE NAKAGAMI-RICE PROBABILITY DISTRIBUTION OF THE INSTANTANEOUS FADING ASSOCIATED WITH PHASE INTERFERENCE

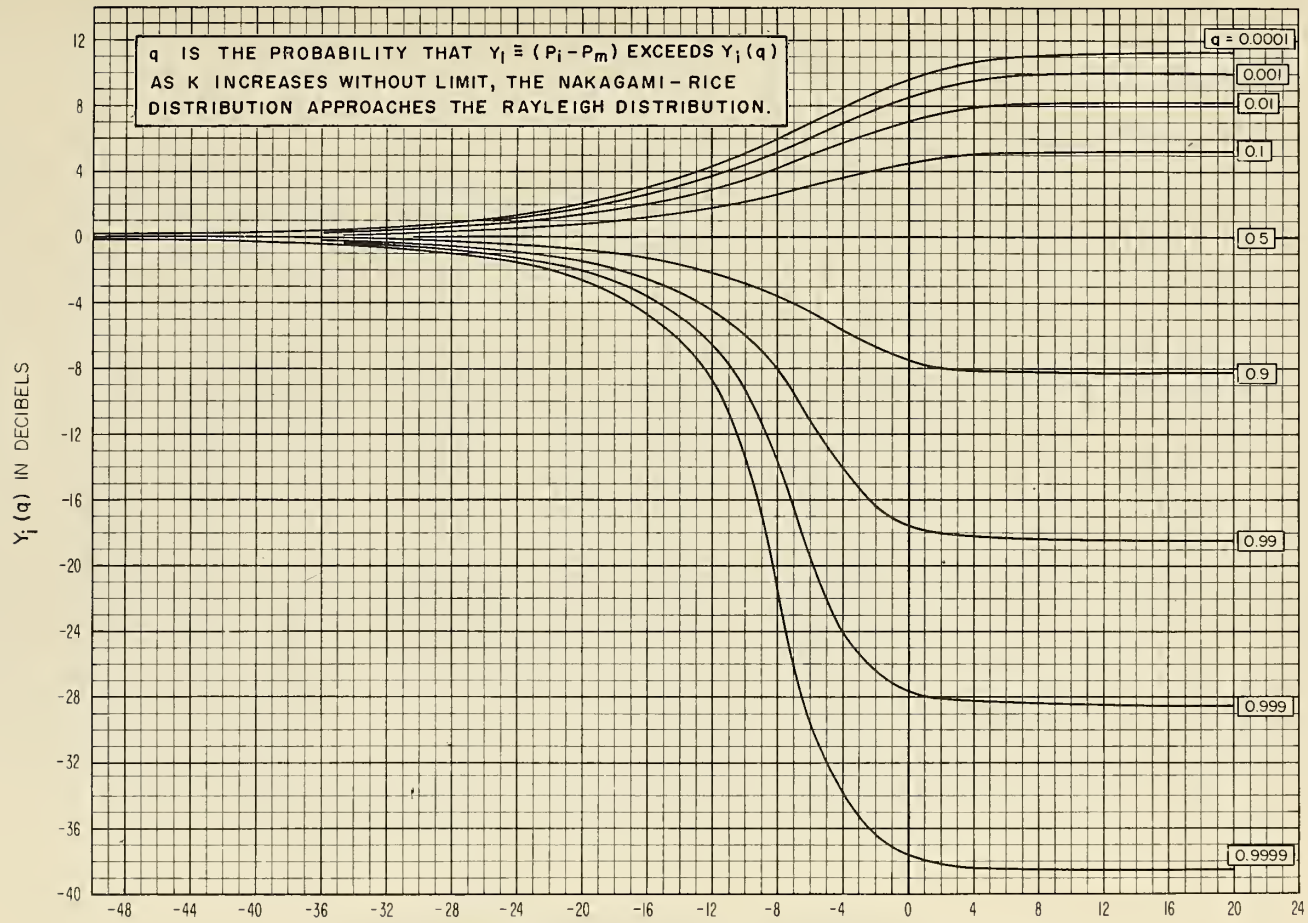

K = RATIO IN DECIBELS BETWEEN THE ROOT-SUM-SQUARE OF THE AMPLITUDES OF THE RAYLEIGH FADING COMPONENT AND THE AMPLITUDE OF THE STEADY COMPONENT OF THE RECEIVED SIGNAL

Figure V.1

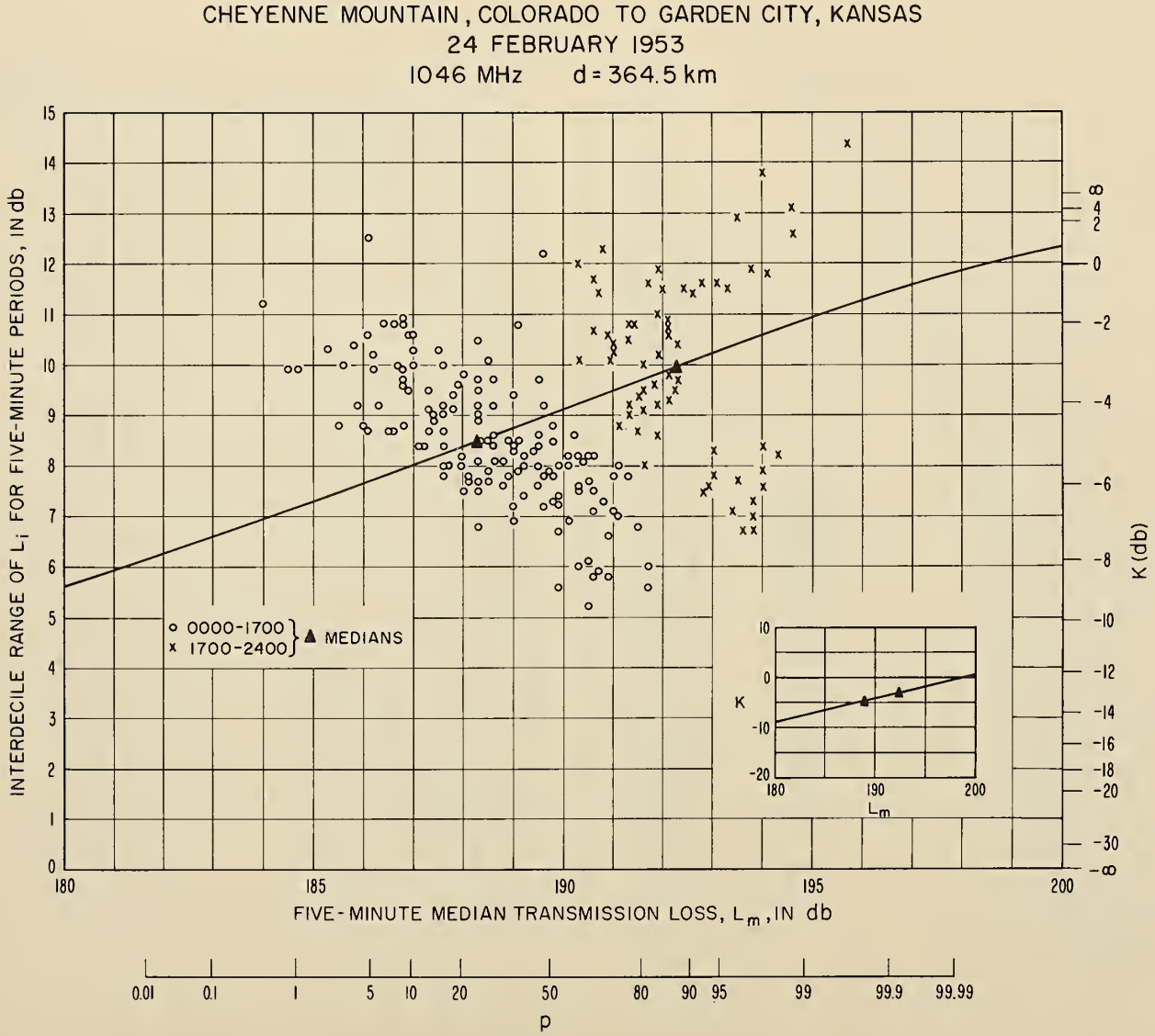
CHEYENNE MOUNTAIN, COLORADO TO GARDEN CITY, KANSAS
24 FEBRUARY 1953
1046 MHz d = 364.5 km
INTERDECILE RANGE OF L_i FOR FIVE-MINUTE PERIODS, IN db
FIVE-MINUTE MEDIAN TRANSMISSION LOSS, L_m, IN db
K (db)
o 0000-1700
x 1700-2400
▲ MEDIANS
K
L_m
p
0.01
0.1
1
5
10
20
50
80
90
95
99
99.9
99.99

Figure V.2

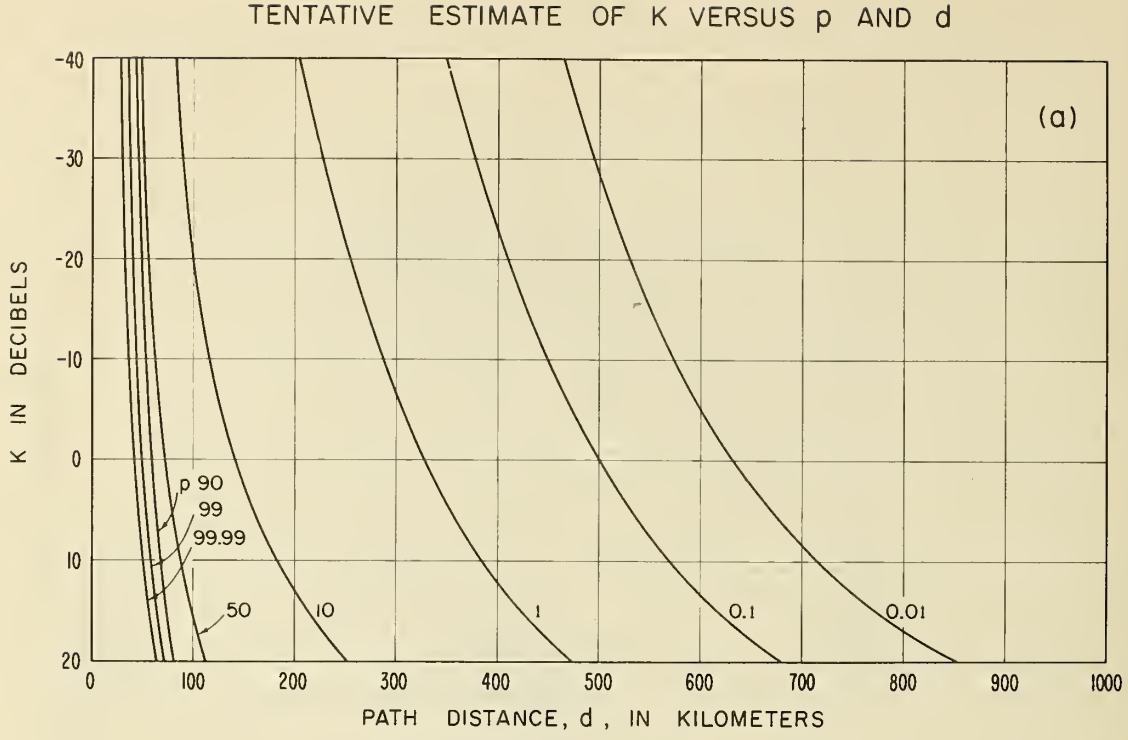
TENTATIVE ESTIMATE OF K VERSUS p AND d
(a)
K IN DECIBELS
-40
-30
-20
-10
0
10
20
p 90
99
99.99
50
10
1
0.1
0.01
0
100
200
300
400
500
600
700
800
900
1000
PATH DISTANCE, d, IN KILOMETERS

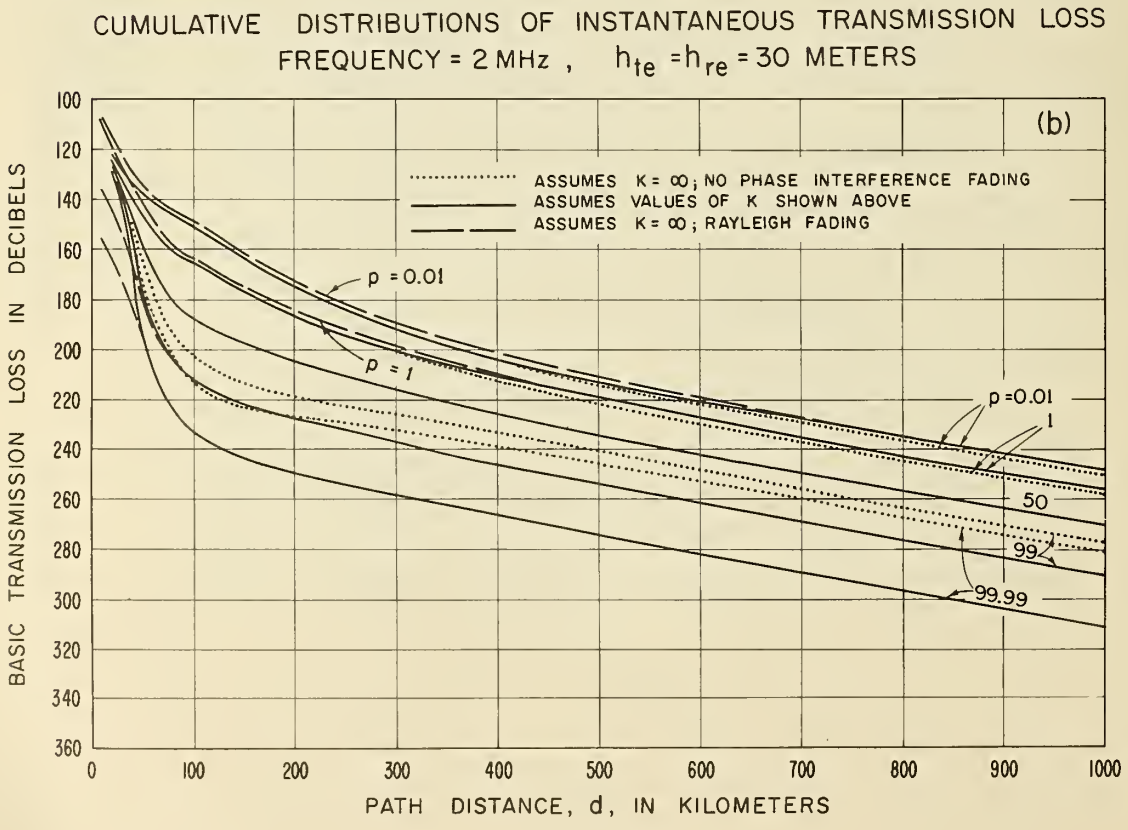
CUMULATIVE DISTRIBUTIONS OF INSTANTANEOUS TRANSMISSION LOSS
FREQUENCY = 2 MHz , $h_{te} = h_{re} = 30$ METERS
(b)
ASSUMES K = ∞; NO PHASE INTERFERENCE FADING
ASSUMES VALUES OF K SHOWN ABOVE
ASSUMES K = ∞; RAYLEIGH FADING
BASIC TRANSMISSION LOSS IN DECIBELS
100
120
140
160
180
200
220
240
260
280
300
320
340
360
p = 0.01
p = 1
p =0.01
1
50
99
99.99
0
100
200
300
400
500
600
700
800
900
1000
PATH DISTANCE, d, IN KILOMETERS

Figure V.3

Let $P_m = 10 \log p_m$ dbw represent the median of that component of available wanted signal power which is associated with phase interference fading at the terminals of an equivalent loss-free receiving antenna, and let $P_{mr}(g)$, the "operating sensitivity" expressed in dbw, represent the minimum value of P_m which will provide a grade g service in the presence of noise alone. This operating sensitivity P_{mr} assumes a specified type of fading wanted signal and a specified type of noise, but does not allow for other unwanted signals. A detailed discussion of the effective noise bandwidth, the operating noise factor, and the operating sensitivity of a receiving system will be found in a recent report, "Optimum Use of the Radio Frequency Spectrum," prepared under Resolution 1 of the CCIR [Geneva, 1963c].

The median value p_{mn} of the total noise power in watts in a bandwidth b cycles per second at the output load of the linear portion of a receiving system includes external noise accepted by the antenna as well as noise generated within the receiving system, including both principal and spurious responses of the antenna and transmission line as well as the receiver itself. This total noise power delivered to the pre-detection receiver output may be referred to the terminals of an equivalent loss-free antenna (as if there were only external noise sources) by dividing p_{mn} by g_o, the maximum value of the operating gain of the pre-detection receiving system.

The operating noise factor of the pre-detection receiving system, f_{op}, may be expressed as the ratio of the "equivalent available noise power" p_{mn}/g_o to the Johnson noise power kT_ob that would be available in the band b from a resistance at a reference absolute temperature $T_o = 288.37$ degrees Kelvin, where $k = 1.28054 \times 10^{-23}$ joules per degree is Boltzmann's constant:

$$f_{op} = \frac{p_{mn}/g_o}{k T_o b} \qquad (V.7)$$

or in decibels:

$$F_{op} = (P_{mn} - G_o) - (B - 204) \quad \text{db} \qquad (V.8)$$

The constant 204 in (V.8) is $-10 \log (kT_o)$.

Note that the available power from the antenna as defined in section 2 has the desired property of being independent of the receiver input load impedance, making this concept especially useful for the definition and measurement of the operating noise factor f_{op} as defined under CCIR Resolution 1 [Geneva, 1963c].

At frequencies above 100 MHz, where receiver noise rather than external noise usually limits reception, f_{op} is essentially independent of external noise. In general, f_{op} is proportional to the total noise p_{mn} delivered to the pre-detection receiver output and so measures the degree to which the entire system, including the antenna, is able to discriminate against both external noise and receiver noise.

Compared to the total range of their long-term variability, it is assumed that P_m and $P_{mr}(g)$ are hourly median values; i.e., that long-term power fading is negligible over such a short period of time. Let G_{ms} represent the hourly median operating signal gain of a pre-detection receiving system, expressed in db so that $P_m + G_{ms}$ very closely approximates the hourly median value of that component of available wanted signal power delivered to the pre-detection receiver output and associated with phase interference fading. Let P_{mn} represent the hourly median value of the total noise power delivered to the pre-detection receiver output. The median wanted signal to median noise ratio available at the pre-detection receiver output is then

$$R_m = [P_m + G_{ms}] - P_{mn} \quad \text{db} \tag{V.9a}$$

and the minimum value of R_m which will provide a desired grade of service in the presence of noise alone is

$$R_{mr}(g) = [P_{mr}(g) + G_{ms}] - P_{mn} \quad \text{db} \tag{V.9b}$$

V.4 Interference-Limited Service

Only the short-term variations of the wanted signal power p_i and the unwanted signal power p_{ui} associated with phase interference fading are used in determining $r_{ur}(g)$, the ratio of the median wanted signal power p_m to the median unwanted signal power p_{um} required to provide a specified grade of service g. Separate account is taken of the variations with time of the median power levels $P_m = 10 \log p_m$ and $P_{um} = 10 \log p_{um}$. This separation of the total fading into a phase interference component Y_i and the more slowly varying component Y appears to be desirable for several reasons: (1) those variations of that component of the instantaneous received power Y_i which are associated with phase interference alone may be expected to occur completely independently for the wanted and unwanted signals, and this facilitates making a more precise determination of the proper value for $R_{ur}(g)$, (2) the random variable Y_i follows the Nakagami-Rice distribution, as illustrated on figure V.1, while variations with time of the remaining component Y are approximately normally distributed, (3) the variations with time of P_m and of P_{um} tend to be correlated for most wanted and unwanted propagation paths, and an accurate allowance for this correlation is facilitated by separating the instantaneous fading into the two additive components Y and Y_i, and (4) most of the contribution to the variance of P_m with time occurs at low fluctuation frequencies ranging from one cycle per year to about one cycle per hour, whereas most of the contribution to the variance of Y_i occurs at the higher fluctuation frequencies greater than about one cycle per hour.

Let R_{ui} denote the instantaneous ratio between the instantaneous wanted signal power $P_m + Y_i$ and the instantaneous unwanted signal power $P_{um} + Y_{ui}$:

$$R_{ui} = P_m + Y_i - P_{um} - Y_{ui} = R_u + Z_i \tag{V.10}$$

where

$$Z_i \equiv Y_i - Y_{ui}, \text{ and } R_u = P_m - P_{um} \tag{V.11}$$

Note that the cumulative distribution function $Y_i(q, K)$ for Y_i will usually be different from the cumulative distribution function $Y_i(q, K_u)$ for Y_{ui} since the wanted signal propagation path will differ from the propagation path for the unwanted signal. Let $Z_i > Z_i(q, K, K_u)$ with probability q; then the approximate cumulative distribution function of Z_i is given by:

$$Z_{ia}(q, K, K_u) = \pm \sqrt{Y_i^2(q, K) + Y_i^2(1-q, K_u)} \tag{V.12}$$

In the above, the plus sign is to be used when $q < 0.5$ and the minus sign when $q > 0.5$; note that $-Z_{ia}(1-q, K, K_u) = Z_{ia}(q, K, K_u)$. This method of approximation is suggested by two observations: (1) service may be limited for $100\,q$ percent of a short period of time either by downfades of the wanted signal corresponding to a level exceeded with a probability q or by

upfades of an unwanted signal corresponding to a level exceeded with a probability 1-q, and (2) the standard deviation of the difference of two uncorrelated random variables Y_i and Y_{ui} equals the square root of the sum of their variances, and under fairly general conditions $Z_i^2(q)$ is very nearly equal to $Y_i^2(q) + Y_{ui}^2(100-q)$. Equation (V.11) is based on the reasonable assumption that Y_i and Y_{ui} are independent random variables and, for this case, (V.11) would be exact if Y_i and Y_{ui} were normally distributed. The departure from normality of the distribution of Y_i is greatest in the limiting case of a Rayleigh distribution, and for this special case, the following exact expression is available [Siddiqui, 1962]:

$$Z_i(q, \infty, \infty) = 10 \log \left(\frac{1}{q} - 1\right) \qquad (V.13)$$

Table V.2 compares the above exact expression $Z_i(q, \infty, \infty)$ with the approximate expression $Z_{ia}(q, \infty, \infty)$. Note that the two expressions differ by less than 0.2 db for any value of q and, since this difference may be expected to be even smaller for finite values of K, it appears that (V.12) should be a satisfactory approximation for most applications and for any values of K and q.

Table V.2

The Cumulative Distribution Function $Z_i(q, \infty, \infty)$ for the Special Case of the Ratio of Two Rayleigh-Distributed Variables

q	$Z_i(q, \infty, \infty)$	$Z_{ia}(q, \infty, \infty)$	$Z_i - Z_{ia}$
	db	db	db
0.0001	39.99957	40.0178	-0.01823
0.0002	36.98883	37.0362	-0.04737
0.0005	33.00813	33.0757	-0.06757
0.001	29.99566	30.1099	-0.11424
0.002	26.98101	27.1216	-0.14059
0.005	22.98853	23.1584	-0.16987
0.01	19.95635	20.1420	-0.18565
0.02	16.90196	17.0949	-0.19294
0.05	12.78754	12.9719	-0.18436
0.1	9.54243	9.7016	-0.15917
0.2	6.02060	6.1331	-0.11250
0.5	0	0	0

Let $R_{uro}(g)$ denote the required value of R_u for non-fading wanted and unwanted signals and it follows from (V.10) that the instantaneous ratio for fading signals will exceed $R_{uro}(g)$ with a probability at least equal to q or for a percentage of time at least equal to $100\,q$ provided that:

$$R_u > R_{ur}(g, q, K, K_u) = R_{uro}(g) - Z_i(q, K, K_u) \qquad (V.14)$$

The use of (V.14) for determining an allowance for phase interference fading will almost always provide a larger allowance than will actually be necessary since (V.14) was derived on the assumption that $R_{uro}(g)$ is constant. For most services, $R_{uro}(g)$ will not have a fixed value for non-fading signals and will instead have either a probability distribution or a grade of service distribution; in such cases $R_{ur}(g)$ should be determined for a given q by a convolution of the distributions of $R_{uro}(g)$ and $-Z_i$. In still other cases the mean duration of the fading below the level $Z_i(q, K, K_u)$ will be comparable to the mean duration of the individual message elements and a different allowance should then be made. In some cases it may be practical to determine R_{ur} as a function of g, q, K, and K_u in the laboratory by generating wanted and unwanted signals that vary with time the same as Y_i and Y_{ui}. This latter procedure will be successful only to the extent that the fading signal generators properly simulate natural phase interference fading both as regards their amplitude distributions and their fading duration distributions. Since the present report is intended to deal only with general definitions and procedures, functions $R_{ur}(g)$ applicable to particular kinds of wanted and unwanted signals and which include an appropriate phase interference fading allowance should be developed by other CCIR working groups with members having a greater familiarity with the requirements of the wanted service and the nature of the phase interference fading of the wanted and unwanted signals likely to be encountered, and the nature of any diversity system which may be used.

The ratio R_u will also vary with time since it has been defined as an hourly median equal to the difference between $P_m(50) + Y$ and $P_{um}(50) + Y_u$:

$$R_u \equiv P_m - P_{um} = P_m(50) - P_{um}(50) + Z \qquad (V.15)$$

$$Z \equiv Y - Y_u \qquad (V.16)$$

The random variables Y and Y_u tend to be approximately normally distributed with a positive correlation coefficient ρ which will vary considerably with the propagation paths

and the particular time block involved. For the usual time block involving all hours of the day for several years preliminary analyses of data indicate that ρ will usually exceed 0.4 even for propagation paths in opposite directions from the receiving point. Z will exceed a value $Z_a(p)$ for a percentage of time p where the approximate cumulative distribution function $Z_a(p)$ of Z is given by

$$Z_a(p) = \pm\sqrt{Y^2(p) + Y_u^2(100-p) + 2\rho\, Y(p)\, Y_u(100-p)} \qquad \text{(V.17)}$$

In the above the plus sign is to be used for $p < 50\%$ and the minus sign for $p > 50\%$, while $Z_a(50) \equiv 0$. It follows from (V.15) and (V.17) that R_u will exceed $R_{ur}(g)$ for at least a percentage of time p provided that

$$P_m(50) - P_{um}(50) > R_{ur}(g) - Z_a(p) \qquad \text{(V.18)}$$

In some cases it may be considered impractical to determine the function $R_{ur}(g)$ by adding an appropriate phase interference fading allowance to $R_{uro}(g)$; in such cases it may be useful to use the following approximate relation which will ensure that the instantaneous ratio $R_{ui} > R_{uro}(g)$ for at least a percentage of time p:

$$P_m(50) - P_{um}(50) > R_{uro}(g) \pm\sqrt{Z_a^2(p) + Z_i^2(0.01\,p, K, K_u)} \qquad \text{(V.19)}$$

In the above, the minus sign is to be used for $p < 50\%$ and the plus sign for $p > 50\%$. Although (V.19), or its equivalent, has often been used in past allocation studies, this usage is deprecated since it does not provide a solution which is as well adapted to the actual nature of the problem as the separation of the fading into its two components Y_i and Y and the separate use of (V.14) and (V.18). Note that (V.19) provides a fading allowance which is too small compared with that estimated using (V.14) and (V.18) separately. The recommended method makes more appropriate allowance for the fact that communications at particular times of the day or for particular seasons of the year are more difficult than at other times.

V.5 The Joint Effect of Several Sources of Interference Present Simultaneously

The effects of interference from unwanted signals and from noise have so far been considered in this report as though each affected the fidelity of reception of the wanted signal independently. Let $p_{mr}(g)$ and $r_{ur}(g)p_{um}$ denote power levels which the wanted median signal power p_m must exceed in order to achieve a specified grade of service when each of these sources of interference is present alone. To the extent that the various sources of interference have a character approximating that of white noise, this same grade of service may be expected from a wanted signal with median level

$$p_m = p_{mr}(g) + \sum r_{ur}(g)\, p_{um}$$

when these sources are present simultaneously.

An approximate method has been developed [Norton, Staras, and Blum, 1952] for determining for a broadcasting service the distribution with time and receiving location of the ratio

$$p_m / \left[p_{mr}(g) + \sum r_{ur}(g)\, p_{um} \right]$$

Although this approach to the problem of adding the effects of interference will probably always provide a good upper bound to the interference, this assumption that the interference power is additive is often not strictly valid. For example, when intelligible cross-talk from another channel is present in the receiver output circuit, the addition of some white noise will actually reduce the nuisance value of this cross-talk.

Frequently, however, both $p_{mr}(g)$ and p_{um} will be found to vary more or less independently over wide ranges with time and a good approximation to the percentage of time that objectionable interference is present at a particular receiving location may then be obtained [Barsis, et al, 1961] by adding the percentage of time that p_m is less than $p_{mr}(g)$ to the percentages of time that p_m is less than each of the values of $r_{ur}(g)\, p_{um}$. When this total time of interference is small, say less than 10%, this will represent a satisfactory estimate of the joint influence of several sources of interference which are present simultaneously. Thus, when the fading ranges of the various sources of interference are sufficiently large so that this latter method of analysis is applicable, the various values of $p_{mr}(g)$ and of $r_{ur}(g)\, p_{um}$ will have comparable magnitudes for negligible percentages of the time so that one may, in effect, assume that the various sources of interference occur essentially independently in time.

Minimum acceptable wanted-to-unwanted signal ratios r_{ur} may sometimes be a function of r_m, the available wanted signal-to-noise ratio. When r_{ur} is within 3 db of r_{mr}, an unwanted signal may be treated the same as external noise, and, in a similar fashion, long-term distributions of available wanted-to-unwanted signal ratios may be determined for each class of unwanted signals for which r_{ur} is nearly the same.

V.6 The System Equation for Noise-Limited Service

Essential elements of a noise-limited communication circuit are summarized in the following system equation. The transmitter output $P_{\ell t}$ dbw which will provide $P_t = P_{\ell t} - L_{\ell t}$ dbw of total radiated power in the presence of transmission line and matching network losses $L_{\ell t}$ db, and which will provide a median delivered signal at the pre-detection receiver output which is R_m db above the median noise power P_{mn} delivered to the pre-detection receiver output is given by

$$(P_{\ell t} - L_{\ell t}) = L_m + R_m + (P_{mn} - G_{ms}) \quad \text{dbw} \tag{V.20}$$

in the presence of a median transmission loss L_m and a median operating receiving system signal gain G_{ms}. The operating signal gain is the ratio of the power delivered to the pre-detection receiver output to the power available at the terminals of an equivalent loss-free antenna. G_o is its maximum value for c.w. frequencies in the receiver pass band, and G_{ms} is its median value for all signal frequencies in the pass band. $(P_{mn} - G_{ms})$ in (V.20) is the equivalent median noise power at the antenna terminals, as defined in section V.3.

It is appropriate to express the system equation (V.20) in terms of the operating noise factor F_{op} defined by (V.8), rather than in terms of P_{mn} or $(P_{mn} - G_{ms})$ in order to separate studies of receiving system characteristics from studies of propagation. For this reason all predicted power levels are referred to the terminals of an equivalent loss-free antenna, and receiving system characteristics such as F_{op}, G_o, G_{ms}, and $B = 10 \log b$ are separated from transmission loss and available power in the formulas.

Rearranging terms of (V.8), the equivalent median noise power $P_{mn} - G_{ms}$ delivered to the antenna terminals may be expressed as

$$P_{mn} - G_{ms} = F_{op} + (G_o - G_{ms}) + (B - 204) \tag{V.21}$$

where G_o and G_{ms} are usually nearly equal. Assuming that $L_{\ell t}$, G_o, G_{ms}, and B are constant, it is convenient to combine these parameters into an arbitrary constant K_o:

$$K_o = L_{\ell t} + G_o - G_{ms} + B - 204 \quad \text{dbw} \tag{V.22}$$

and then write the system equation as:

$$P_{\ell t} = K_o + L_m + R_m + F_{op} \quad \text{dbw} \tag{V.23}$$

In general, if unwanted signals other than noise may be disregarded, service exists whenever $R_m(p)$ exceeds $R_{mr}(g)$, where $R_m(p)$ is the value of R_m exceeded p percent of all hours. With G_{ms} and P_{mn} assumed constant, so that

$$R_m(p) = P_m(p) + G_{ms} - P_{mn} \tag{V.24}$$

service exists whenever $P_m(p)$ exceeds P_{mr}, or whenever $L_m(p)$ is less than the maximum allowable transmission loss $L_{mo}(g) = P_t - P_{mr}(g)$. An equivalent statement may be made in terms of the system equation. The transmitter power $P_{\ell t}(p)$ which will provide for p percent of all hours at least the grade g service defined by the required signal-to-noise ratio $R_{mr}(g)$ is

$$P_{\ell t}(p) = K_o + L_m(p) + F_{op} + R_{mr}(g) \tag{V.25}$$

where $L_m(p)$ is the hourly median transmission loss exceeded $(100 - p)$ percent of all hours, or not exceeded p percent of all hours.

For a fixed transmitter power P_o dbw, the signal-to-noise ratio exceeded p percent of all hours is

$$R_m(p) = P_o - K_o - F_{op} - L_m(p) \quad \text{db} \tag{V.26}$$

for an "average" or "median" propagation path.

The maximum allowable transmission loss

$$L_{mo}(g) = P_o - K_o - F_{op} - R_{mr}(g) \tag{V.27}$$

is set equal to the loss $L_m(p, Q)$ exceeded $(100 - p)$ percent of all hours with a probability Q. This value is fixed when P_o, K_o, and $R_{mr}(g)$ have been determined, and for each time availability p there is a corresponding service probability, Q(p). Section V.9 will explain how to calculate Q(p).

When external noise is both variable and not negligible, the long-term variability of F_{op} must be considered, and the following relationships may be used to satisfy the condition

$$R_m(p) > R_{mr}(g) \tag{V.28}$$

$$R_m(p) \equiv R_m(50) + Y_m(p) \tag{V.29}$$

$$R_m(50) \cong P_o - K_o - F_{op}(50) - L_m(50) \tag{V.30}$$

$$Y_m^2(p) \cong Y^2(p) + Y_n^2(100 - p) - 2\rho_{tn}\, Y(p)\, Y_n(100 - p) \tag{V.31}$$

$$Y(p) \equiv L_m(50) - L_m(p), \qquad Y_n(p) \equiv F_{op}(p) - F_{op}(50) \tag{V.32}$$

where ρ_{tn} is the long-term correlation between P_m and F_{op}. Though ρ_{tn} could theoretically have any value between -1 and 1, it is usually zero.

V.7 The Time Availability of Interference-Limited Service

Let ρ_{tu} denote the long-term correlation between P_m and P_{um}, the power expected to be available at least p percent of all hours at the terminals of an equivalent loss-free receiving antenna from wanted and unwanted stations radiating p_o and p_u watts, respectively:

$$P_m(p) = P_o - L_m(p) \quad \text{dbw}, \qquad P_{um}(p) = P_u - L_{um}(p) \quad \text{dbw} \tag{V.33}$$

$$P_o = 10 \log p_o \quad \text{dbw}, \qquad P_u = 10 \log p_u \quad \text{dbw} \tag{V.34}$$

The criterion for service of at least grade g in the presence of a single unwanted signal and in the absence of other unwanted signals or appreciable noise is

$$R_u(p) > R_{ur}(g, p) \tag{V.35}$$

where

$$R_u(p) = R_u(50) + Y_R(p) \tag{V.36}$$

$$R_u(50) \cong P_m(50) - P_{um}(50) \tag{V.37}$$

$$Y_R^2(p) \cong Y^2(p) + Y_u^2(100-p) - 2\rho_{tu}\, Y(p)\, Y_u(100-p) \tag{V.38}$$

$$Y_u(p) = P_{um}(p) - P_{um}(50) = L_{um}(50) - L_{um}(p) \tag{V.39}$$

If P_m, P_{um}, and F_{op} were exactly normally distributed, (V.31) and (V.38) would be exact, and they represent excellent approximations in practice.

V.8 The Estimation of Prediction Errors

Consider the calculation of the power $P_m(p)$ available at the terminals of an equivalent loss-free receiving antenna during p percent of all hours. $P_m(p)$ refers to hourly median values expressed in dbw. For a specific propagation path it is calculated in accordance with the methods given in sections 2-10 using a given set of path parameters (d, f, θ, h_{te}, etc.). Denote by $P_{mo}(p)$ observations made over a large number of randomly different propagation paths, which, however, can all be characterized by the same set of prediction parameters. Values of $P_{mo}(p)$ will be very nearly normally distributed with a mean (and median) equal to $P_m(p)$, and a variance denoted by $\sigma_c^2(p)$. This path-to-path variability is illustrated in Fig. V.4 for a hypothetical situation which assumes a random distribution of all parameters which are not taken into account in the prediction method.

The variance σ_c^2 of deviations of observation from prediction depends on available data and the prediction method itself. The most sophisticated of the methods given in this report for predicting transmission loss as a function of carrier frequency, climate, time block, antenna gains, and path geometry have been adjusted to show no bias, on the average, for the data discussed in subsections 10.3 and 10.4 and in Annex I.

Most of these data are concentrated in the 40-1000 MHz frequency range, and were obtained primarily for transhorizon paths in climates 1, 2, and 3. Normally, one antenna was on the order of 10 meters above ground and the other one was higher, near 200 meters. Even the low receiving antennas were either on high ground or in clear areas well removed from hills and terrain clutter. Few of the data were obtained with narrow-beam antennas. An attempt has been made to estimate cumulative distributions of hourly transmission loss medians for accurately specified time blocks, including estimates of year-to-year variability.

A prediction for some situation that is adequately characterized by the prediction parameters chosen here requires only interpolation between values of these parameters for which data are available. In such a case, $\sigma_c(p)$ represents the standard error of prediction. The mean square error of prediction, referred to a situation for which data are not available, is $\sigma_c^2(p)$ plus the square of the bias of the prediction method relative to the new situation.

Based on an analysis of presently available transhorizon transmission loss data, the variance $\sigma_c^2(p)$ is estimated as

$$\sigma_c^2(p) = 12.73 + 0.12\, Y^2(p) \quad db^2 \tag{V.40}$$

where $Y(p)$ is defined in section 10. Since $Y(50) \equiv 0$, the variance $\sigma_c^2(50)$ of the difference between observed and predicted long-term medians is $12.73\ db^2$, with a corresponding standard deviation $\sigma_c(50) = 3.57$ db.

It is occasionally very difficult to estimate the prediction error $\sigma_c(p)$ and the service probability Q. Where only a small amount of data is available there is no adequate way of estimating the bias of a prediction. One may, however, assign weights to the curves of $V(50, d_e)$ in figure 10.1 for climates 1-7 based on the amount of supporting data available:

Climate Number	Weight
1	300
2	120
3	60
4	2
5	1
6	5
7	5

As an example, for $d_e = 600$ km, the average $V(50)$ weighted in accordance with the above is -0.4 db, and the corresponding climate-to-climate variance of $V(50)$ is $3.7\ db^2$.

If the variance of $V(50)$ is $12.7\ db^2$ within any given climate, the standard error of prediction $L(50) = L_{cr} + 0.4$ db, given by (10.4), will be $\sqrt{12.7 + 3.7} = 4.0$ db if a random sampling of these climates is desired or applicable. If there is doubt as to which of two climates i and j should be chosen, the best prediction of $L_b(p)$ might depend on the average of $V_i(50, d_e)$ and $V_j(50, d_e)$ and the root-mean square of $Y_i(p, d_e)$ and $Y_j(p, d_e)$:

$$L(p) = L_{cr} - 0.5\left[V_i(50, d_e) + V_j(50, d_e)\right] - Y(p, d_e) \quad db, \tag{V.41}$$

$$Y(p, d_e) = \left[0.5\, Y_i^2(p, d_e) + 0.5\, Y_j^2(p, d_e)\right]^{\frac{1}{2}} \quad db \tag{V.42}$$

The bias of this prediction may be as large as $0.5\left[V_i(50, d_e) - V_j(50, d_e)\right]$ db. The root-mean square prediction error may therefore be estimated as the square root of the sum of $\sigma_c^2(50) = 12.7\ db^2$, the square of the bias, and $0.12\, Y(p, d_e)^2$, or:

$$\left\{12.7 + 0.25\left[V_i(50, d_e) - V_j(50, d_e)\right]^2 + 0.12\, Y^2(p, d_e)\right\}^{\frac{1}{2}} \quad db,$$

with $Y(p, d_e)$ obtained from (V.42) above.

According to figure 10.1, $V(50, d_e)$ is expected to be the same for climates 1 and 8. This conclusion and the estimate for $Y(p, d_e)$ shown in figure III.55 for climate 8 are based solely on meteorological data. In order to obtain these estimates, the percentages of time for which surface-based ducts existed in the two regions were matched with the same value of $Y(p, d_e)$ for both climates. In this way, $Y_8(p, d_e)$ was derived from $Y_1(p, d_e)$ by relating p_8 to p_1 for a given Y instead of relating Y_8 to Y_1 for a given p.

V.9 The Calculation of Service Probability Q for a Given Time Availability p

For noise-limited service of at least grade g and a time availability p, the service probability Q is the probability that

$$L_{mo}(g) - L_m(p) > 0 \qquad (V.43)$$

if external noise is negligible. $L_{mo}(g)$ is defined by (V.27). The criterion for service limited by external noise, where F_{op} as given by (V.8) is variable, is

$$R_m(p) - R_{mr}(g) > 0 \quad \text{(from equation V.28)}$$

For service limited only by interference from a single unwanted signal,

$$R_u(p) - R_{ur}(g, p) > 0 \quad \text{(from equation V.35)}$$

Combining (V.22) and (V.27), (V.43) may be rewritten as

$$P_o - L_{lt} - G_o + G_{ms} - B + 204 - F_{op} - R_{mr}(g) - L_m(p) > 0 \qquad (V.44)$$

where (V.8), (V.9), or section V.6 may be referred to for a definition of the terms in (V.44). Assuming that the error of estimation of these terms from system to system is negligible except for the path-to-path variance $\sigma_c^2(p)$ given by (V.40) for the last term, it is convenient to represent the service probability Q as a function of the standard normal deviate

$$z_{mo} = \frac{L_{mo} - L_m(p)}{\sigma_c(p)} \qquad (V.45)$$

which has a mean of zero and a variance of unity. L_{mo} is identified as the transmission loss exceeded (100 - p) percent of the time with a probability Q, which is expressed in terms of the error function erf x as

$$Q(z_{mo}) = \tfrac{1}{2} + \tfrac{1}{2}\,\mathrm{erf}(z_{mo}/\sqrt{2}) \qquad (V.46)$$

Figure V.5 is a graph of Q versus z_{mo}.

For the method described here, the condition

$$0.12\,Y(p)\,z_{mo}(Q) < -\sigma_c(p) \qquad (V.47)$$

is sufficient to insure that the service probability Q increases as the time availability p is decreased. A less restrictive condition is

$$Y(p)[L_{mo} - L_m(50)] < 106 \quad db^2 \qquad (V.48)$$

An example is shown in figure V.6, with p versus Q for radiated powers $P_o = 30$ dbw and $P_o = 40$ dbw, and $L_m(p, Q) = P_o + 140$ db. Here,

$$p = 50 + 50 \text{ erf} \left[\frac{L_m(p) - 140}{10\sqrt{2}} \right] , \tag{V.49}$$

corresponding to a normal distribution with a mean $L_m(50) = 140$ db and a standard deviation $Y(15.8) = 10$ db. [Note that $L_m(p)$ versus p as estimated by the methods of section 10 is usually not normally distributed].

To obtain the time availability versus service probability curves of figure V.6, $L_m(p)$ was obtained from p, Y(p) from (V.4), $\sigma_c^2(p)$ from (V.40), z_{mo} from (V.45), and Q from figure V.5. This same method of calculation may be used when there are additional sources of prediction error by adding variances to $\sigma_c^2(p)$. Examining possible trade-offs between time availability and service probability shown in figure V.5, note the increase from $p = 96.5\%$ to $p = 99.3\%$ for $Q = 0.95$, or the increase from $Q = 0.78$ to $Q = 0.97$ for $p = 99\%$, as the radiated power is increased from one to ten kilowatts.

For the case of service limited by external noise (V.28) to (V.30) may be rewritten as

$$P_o - K_o - F_{op}(50) - L_m(50) + Y_m(p) - R_{mr}(g) > 0 \tag{V.50}$$

One may ignore any error of estimation of P_o, K_o, and $R_{mr}(g)$ as negligible and assume no path-to-path correlation between $F_{op}(50)$ and $L_m(50)$. The variance $\sigma_{op}^2(p)$ of $F_{op}(50) + L_m(50) - Y_m(p)$ in (V.48) may then be written as a sum of component variances σ_F^2 and $\sigma_c^2(p)$:

$$\sigma_{op}^2(p) = \sigma_F^2 + 12.73 + 0.12\, Y_m^2(p) \quad \text{db}^2 \tag{V.51}$$

Very little is known about values for the variance σ_F^2 of $F_{op}(50)$, but it is probably on the order of 20 db^2.

The corresponding standard normal deviate is given by

$$z_{op} = \frac{R_m(p) - R_{mr}(g)}{\sigma_{op}(p)} \tag{V.52}$$

and the service probability Q(p) is given by (V.46) with z_{mo} replaced by z_{op}. The restriction (V.47) still holds with z_{mo} and σ_c replaced by z_{op} and σ_{op}. A less restrictive condition equivalent to (V.48) can be stated only if a specific value of σ_F^2 is assumed.

For the case of service limited only by interference from a single unwanted radio signal (V.35) to (V.39) may be rewritten as

$$L_{um}(50) - L_m(50) + Y_R(p) - R_{ur}(g, p) > 0 \qquad \text{(V.53)}$$

Let $\rho_{\ell u}$ denote the normalized correlation or covariance between path-to-path variations of $P_m(50)$ and $P_{um}(50)$. Then assuming a variance of $25.5(1 - \rho_{\ell u}) + 0.12\ Y_u^2(p)\ db^2$ for the first three terms of (V.53) and a variance σ_{ur}^2 for the estimate of $R_{ur}(g, p)$, the total variance $\sigma_{uc}^2(p)$ of any estimate of the service criterion given by (V.53) may be written as

$$\sigma_{uc}^2(p) = 25.5(1 - \rho_{\ell u}) + 0.12\ Y_R^2(p) + \sigma_{ur}^2 \qquad \text{(V.54)}$$

for this case, corresponding to a standard normal deviate

$$z_{uc} = \frac{R_u(p) - R_{ur}(p, g)}{\sigma_{uc}(p)} \qquad \text{(V.55)}$$

and a service probability $Q(p)$ given by (V.46) with z_{mo} replaced by z_{uc}. The variance σ_{ur}^2 may range from $10\ db^2$ to very much higher values. The restrictions (V.47) and (V.48) apply with z_{mo} and σ_c replaced by z_{uc} and σ_{uc} and with 106 db in (V.48) replaced by $(212 + \sigma_{ur}^2)\ db^2$.

TYPICAL PATH-TO-PATH VARIATION OF INFINITE-TIME DISTRIBUTIONS
FOR A SINGLE SET OF VALUES OF THE PREDICTION PARAMETERS

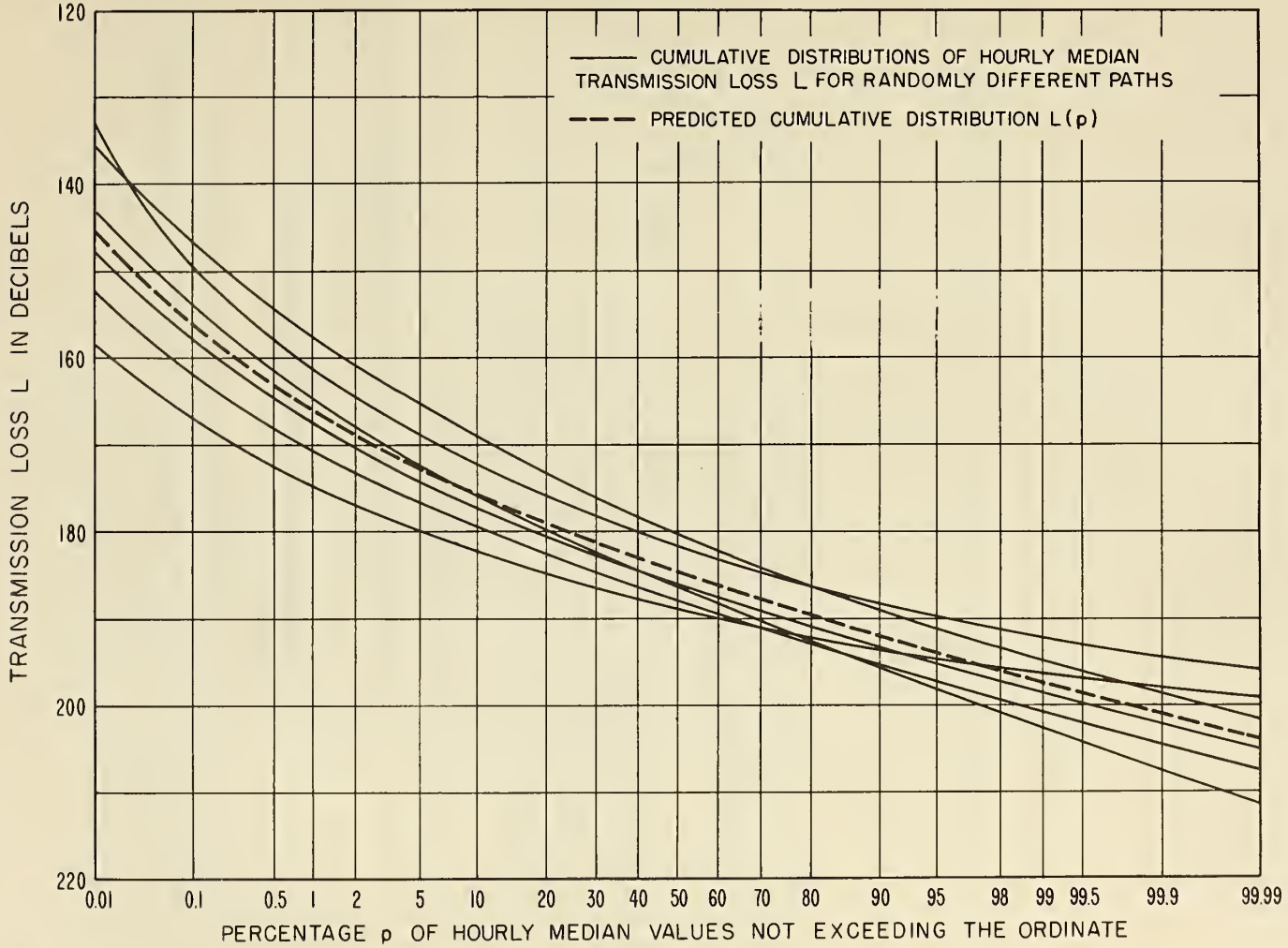

Figure V.4

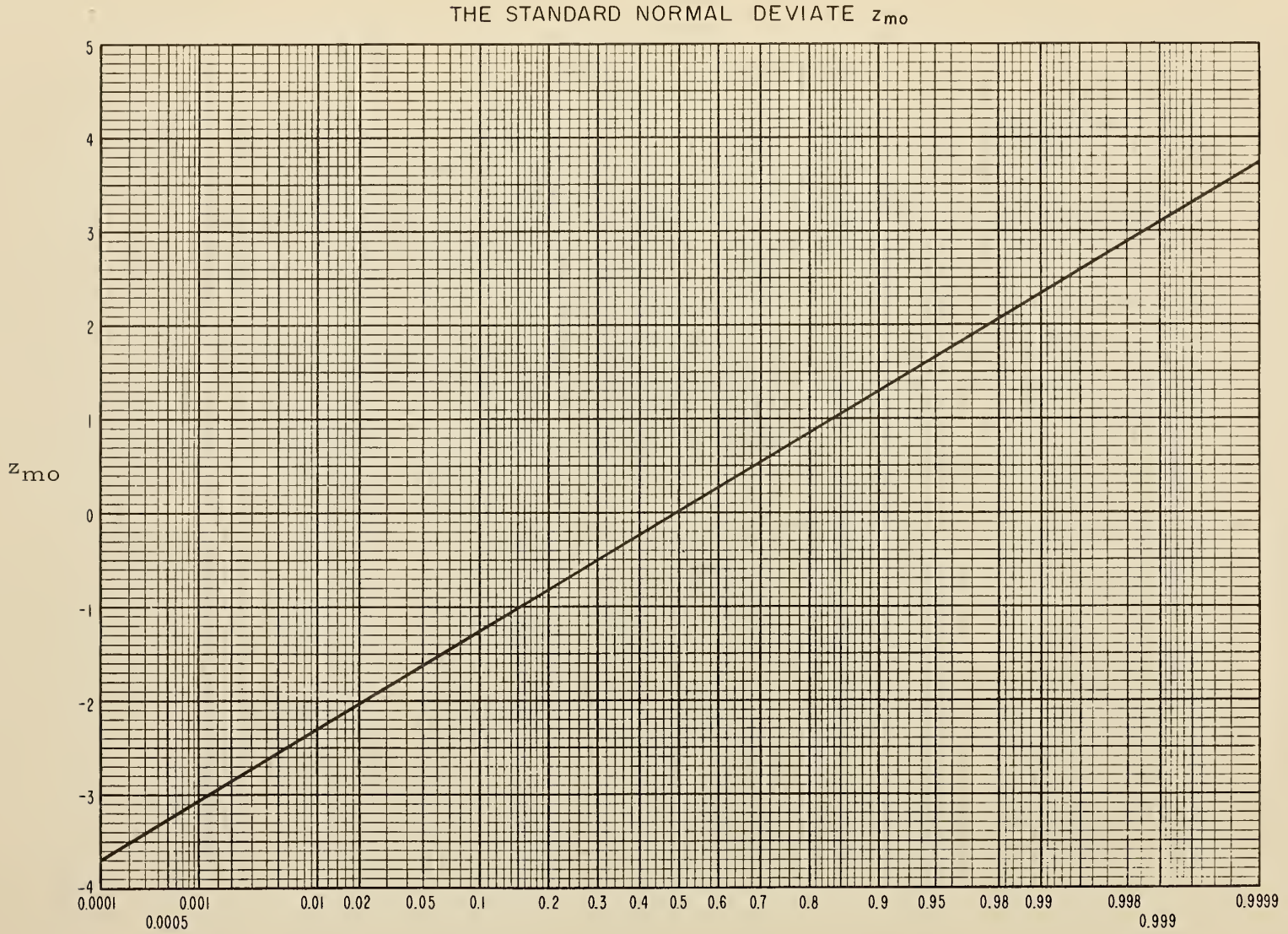
THE STANDARD NORMAL DEVIATE z_{mo}
z_{mo}
5
4
3
2
1
0
-1
-2
-3
-4
0.0001
0.0005
0.001
0.01
0.02
0.05
0.1
0.2
0.3
0.4
0.5
0.6
0.7
0.8
0.9
0.95
0.98
0.99
0.998
0.999
0.9999
SERVICE PROBABILITY, Q

Figure V.5

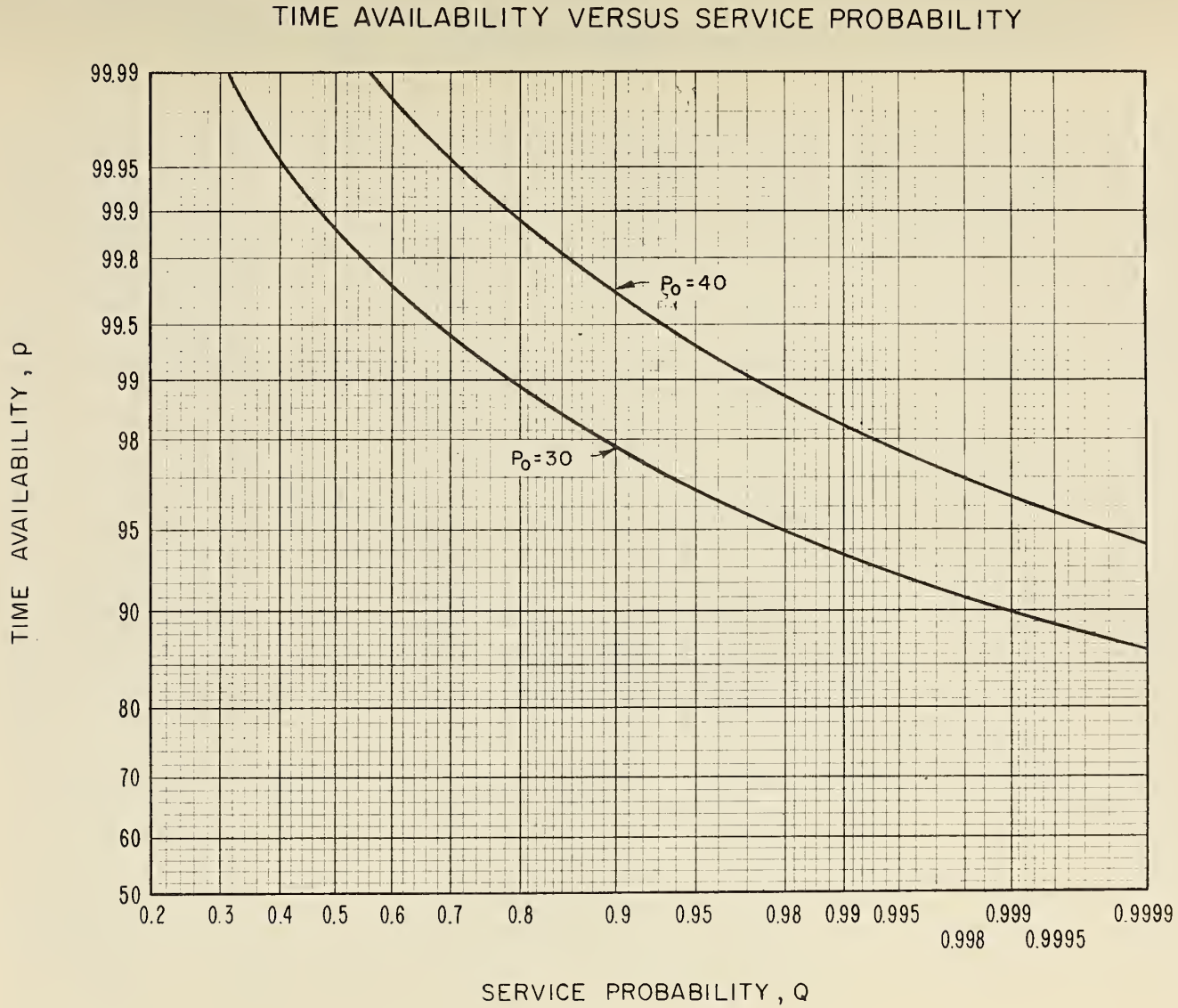
TIME AVAILABILITY VERSUS SERVICE PROBABILITY
TIME AVAILABILITY , p
99.99
99.95
99.9
99.8
99.5
99
98
95
90
80
70
60
50
P_0=40
P_0=30
0.2
0.3
0.4
0.5
0.6
0.7
0.8
0.9
0.95
0.98
0.99
0.995
0.998
0.999
0.9995
0.9999
SERVICE PROBABILITY , Q

Figure V.6

V.10 Optimum Use of the Radio Frequency Spectrum

The business of the radio engineer is to develop efficient radio systems, and the principal tool for improving efficiency is to adjust the various parameters to their optimum values. For example, it is usually more economical to use lower effective radiated powers from the transmitting systems by reducing the operating sensitivities of the receiving systems. Receiving system sensitivities can be reduced by (a) reducing the level of internally generated noise, (b) the use of antenna directivity to reduce the effects of external noise, (c) the reduction of man-made noise levels by the use of suppressors on noise generators such as ignition systems, relays, power transmission systems, etc., and (d) the use of space or time diversity and coding. The use of more spectrum in a wide band FM system or in a frequency diversity system can also reduce the receiving system operating sensitivity as well as reduce the acceptance ratios against unwanted signals other than noise.

Unfortunately, unlike other natural resources such as land, minerals, oil, and water, there is currently no valid method for placing a monetary value on each hertz of the radio spectrum. Thus, in the absence of a common unit of exchange, these tradeoffs are often made unrealistically at the present time. It is now generally recognized that the use of large capacity computers is essential for optimizing the assignment of frequencies to various classes of service including the development of optimum channelization schemes. Typical inputs to such computers are:

1. Nominal frequency assignments.
2. Transmitting system locations, including the antenna heights.
3. Transmitting system signatures; i.e., the radiated emission spectrum characteristics including any spurious emission spectrums.
4. Transmitting antenna characteristics.
5. Receiving system locations, including the antenna heights.
6. Spurious emission spectrums of the receiving systems.
7. Operating sensitivities of the receiving systems in their actual environments which thus make appropriate allowance for the effects of both man-made and natural noise.
8. Required values of wanted-to-unwanted phase interference median signal powers for all unwanted signals which could potentially cause harmful interference to the wanted signal; these acceptance ratios include appropriate allowances for reductions in the effects of fading achieved by the use of diversity reception and coding.

9. Long-term median reference values of basic transmission loss and path antenna gain for the wanted path and all of the unwanted signal propagation paths; these path antenna gains include allowances for antenna orientation, polarization, and multipath phase mismatch coupling losses.

10. Distributions with time of the transmission loss for the wanted signal path and all of the unwanted signal paths.

11. Correlations between the transmission losses on the wanted and on each of the unwanted propagation paths.

12. Transmission line and antenna circuit losses.

13. The spurious emission spectrum of any unwanted signals arising from unlicensed sources such as diathermy machines, electronic heaters, welders, garage door openers, etc.

14. Assigned hours of operation of each wanted and each unwanted emission.

The output of the computer indicates simply the identity and nature of the cases of harmful interference encountered. Harmful interference is defined as a failure to achieve the specified grade of service for more than the required percentage of time during the assigned hours of operation. Changing some of the inputs to the computer, an iterative process can be defined which may lead to an assignment plan with no cases of harmful interference.

It is assumed that a given band of radio frequencies has been assigned to the kind of radio service under consideration and that the nature of the services occupying the adjacent frequency bands is also known. Furthermore, it is assumed that the geographical locations of each of the transmitting and receiving antennas are specified in advance, together with the relative values of the radiated powers from each transmitting antenna and the widths and spacings of the radio frequency channels. In the case of a broadcasting service the specification of the intended receiving locations can be in terms of proposed service areas. With this information given, use may be made of the following procedures in order to achieve optimum use of the spectrum by this particular service:

(a) The system loss for each of the wanted signal propagation paths should be minimized and for each of the unwanted signal propagation paths should be maximized; this may be accomplished by maximizing the path antenna power gains for each of the wanted signal propagation paths, minimizing the path antenna gains for each of the unwanted propagation paths, and in exceptional cases, by appropriate antenna siting. The path antenna gains for the unwanted signal propagation paths may be minimized

by the use of high-gain transmitting and receiving antennas with optimum side lobe suppression and front-to-back ratios and, in some cases, by the use of alternate polarizations for geographically adjacent stations or by appropriate shielding.

(b) The required protection ratios $r_{ur}(g)$ should be minimized by (1) appropriate radio system design, (2) the use of stable transmitting and receiving oscillators, (3) the use of linear transmitting and receiving equipment, (4) the use of wanted and unwanted signal propagation paths having the minimum practicable phase interference fading ranges; from band 6 to band 9 (0.3 to 3000 MHz), minimum phase interference fading may be achieved by the use of the maximum practicable transmitting and receiving antenna heights, and (5) the use of space diversity, time diversity, and coding.

(c) Wanted signal propagation paths should be employed having the minimum practicable long-term power fading ranges. In bands 8 and 9, minimum fading may be achieved by the use of the maximum practicable transmitting and receiving antenna heights.

The above procedures should be carried out with various choices of transmitting and receiving locations, relative transmitter powers, and channel spacings until a plan is developed which provides the required service with a minimum total spectrum usage. After the unwanted signal interference has been suppressed to the maximum practicable extent by the above methods so that, at each receiving location each of the values of r_u exceeds the corresponding protection ratio $r_{ur}(g)$ for a sufficiently large percentage of the time, then the following additional procedures should be adopted in order to essentially eliminate interference from noise:

(d) The system loss on each of the wanted signal propagation paths should be minimized; this may be accomplished by (1) the use of the highest practicable transmitting and receiving antenna heights in bands 8 and 9, and (2) maximizing the path antenna power gains for each of the wanted signal propagation paths. The path antenna power gains of the wanted signal propagation paths may be maximized by using the maximum practicable transmitting and receiving antenna gains and by minimizing the antenna circuit and polarization coupling losses. The minimization of the system loss on each of the wanted signal propagation paths will already have been achieved to a large extent in connection with procedures (a), (b), and (c) above.

(e) In general, receiving systems should be employed which have the lowest practicable values of operating sensitivity $p_{mr}(g)$.

(f) Finally, sufficiently high transmitter powers should be used [keeping the relative powers at the optimum relative values determined by procedures (a), (b), and (c)] so that the wanted signal power p_m will exceed the operating sensitivity $p_{mr}(g)$ for a sufficiently large percentage of the time during the intended period of operation at every receiving location.

Although it might at first seem impracticable, serious consideration should be given to the use of auxiliary channels from wanted receivers to wanted transmitters. The provision of such channels might well be feasible in those cases where two-way transmissions are involved and might lead to important economies in both power and spectrum occupancy [Hitchcock and Morris, 1961].

Ultimately, when optimum use of the spectrum has been achieved, it will not be possible to find a single receiving location at which radio noise rather than either wanted or unwanted signals can be observed for a large percentage of the time throughout the usable portions of the radio spectrum not devoted to the study of radio noise sources, as is the radio astronomy service. Although everyone will agree that the attainment of this ideal goal of interference-free spectrum usage by the maximum number of simultaneous users can be achieved only over a very long period of time because of the large investments in radio systems currently in operation, nevertheless it seems desirable to have a clear statement of the procedures which should be employed in the future in order to move in the direction of meeting this ultimately desirable goal whenever appropriate opportunities arise.

GPO 849-641


DEPARTMENT OF COMMERCE
NATIONAL BUREAU OF STANDARDS